AD-A139 227 INVESTIGATION OF NONLINEAR OPTICAL PROPERTIES OF SEMICONDUCTORS(U) NORTH TEXAS STATE UNIV DENTON CENTER FOR APPLIED QUANTUM ELECTRONICS D G SEILER 23 FEB 84 1/2

UNCLASSIFIED N00014-82-C-0545 F/G 20/12 NL

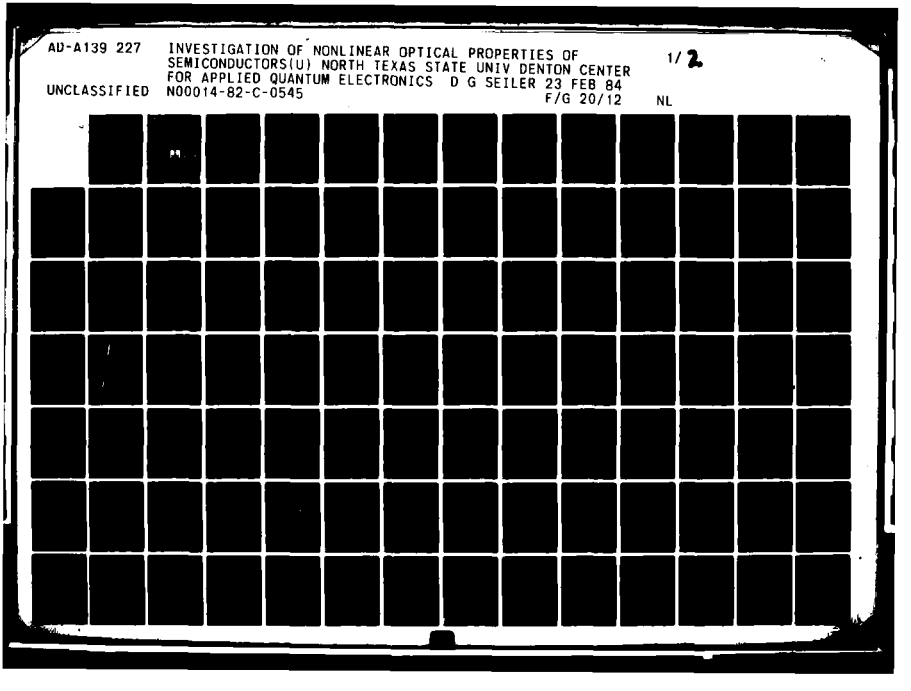

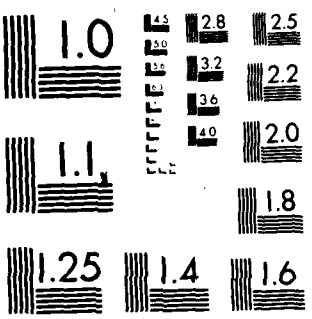

(12)

INVESTIGATION OF NONLINEAR OPTICAL PROPERTIES OF SEMICONDUCTORS

FINAL REPORT

Contract Number: N00014-82-C-0545

David G. Seiler
Center for Applied Quantum Electronics
Department of Physics
North Texas State University
Denton, Texas 76203

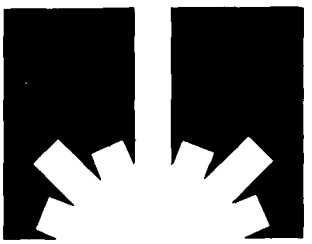

CAQE

Prepared for

Office of Naval Research
Department of the Navy
Arlington, Virginia 22217

SECURITY CLASSIFICATION OF THIS PAGE (When Data Entered)

REPORT DOCUMENTATION PAGE

READ INSTRUCTIONS BEFORE COMPLETING FORM

1. REPORT NUMBER	2. GOVT ACCESSION NO. AD-A139227 / 3. RECIPIENT'S CATALOG NUMBER
4. TITLE (and Subtitle) INVESTIGATION OF NONLINEAR OPTICAL PROPERTIES OF SEMICONDUCTORS	5. TYPE OF REPORT & PERIOD COVERED Final Oct. 1, 1981 - Sept. 30, 1983
	6. PERFORMING ORG. REPORT NUMBER N/A
7. AUTHOR(s) David George Seiler	8. CONTRACT OR GRANT NUMBER(s) N00014-82-C-0545
9. PERFORMING ORGANIZATION NAME AND ADDRESS Department of Physics North Texas State University Denton, TX 76203	10. PROGRAM ELEMENT, PROJECT, TASK AREA & WORK UNIT NUMBERS NR 318-039
11. CONTROLLING OFFICE NAME AND ADDRESS Office of Naval Research 800 N. Quincy Street Arlington, VA 22217	12. REPORT DATE February 23, 1984 / 13. NUMBER OF PAGES 135
14. MONITORING AGENCY NAME & ADDRESS (if different from Controlling Office) Office of Naval Research Resident Representative Room 582 - Federal Building 300 East 8th Street Austin, Texas 78701	15. SECURITY CLASS. (of this report) UNCLASSIFIED / 15a. DECLASSIFICATION/DOWNGRADING SCHEDULE N/A

16. DISTRIBUTION STATEMENT (of this Report)

Approved for Public Release: Distribution Unlimited

17. DISTRIBUTION STATEMENT (of the abstract entered in Block 20, if different from Report)

18. SUPPLEMENTARY NOTES

19. KEY WORDS (Continue on reverse side if necessary and identify by block number)

Nonlinear Optical Properties, Semiconductors, p-InSb, n-InSb, CdS, GaAs, Excitons, Deep Level Absorption, Free Carrier Absorption, Acceptor Impurity Levels, Photoelectronic Effects, Photoconductivity, Two-Photon Absorption, Zeeman Splittings, Diamagnetic Shifts, Band Parameters

20. ABSTRACT (Continue on reverse side if necessary and identify by block number)

Nonlinear optics is an increasingly interesting and exciting area of physics. Many nonlinear optical effects have been discovered and various nonlinear optical devices constructed from a wide variety of materials. In particular, small band gap semiconductors like InSb can have unique optical properties because of their small effective masses and direct band gaps. Unusual and often unexpected results are found in their nonlinear behavior--optical bistability, nonlinear refraction, laser pulse limiting and shaping effects, optical transistor action, etc. These effects can be

DD FORM 1 JAN 73 1473 EDITION OF 1 NOV 65 IS OBSOLETE

UNCLASSIFIED

SECURITY CLASSIFICATION OF THIS PAGE (When Data Entered)

described in terms of a third order susceptibility $\chi^{(3)}$ and are associated with the creation of free carriers by the light. The creation of even a small number of free electrons or holes can strongly effect the "dynamic" nonlinear optical properties of the material. In this project we used sensitive photoelectronic methods to investigate the nonlinear generation of electrons in InSb, CdS, and GaAs induced by two-photon absorption of light.

A wide variety of photoelectronic effects are initiated by the creation of free carriers from the absorption of light in a semiconductor or insulator. These include the photo-Hall effect, photoconductivity, recombination, trapping, lifetimes, all of which are important for understanding devices such as light detectors, light emitters, or energy converters. On the other hand these photoelectronic effects can also be exploited to investigate the nonlinear absorption of light in solids and thus gain an enhanced understanding of their material properties. In this project we have shown that the photoconductive response of semiconductor samples can sensitively detect two-photon absorption processes.

Two-photon absorption processes have been studied in n-InSb using a tunable cw CO_2 laser and high magnetic fields. This work represents the first time two-photon absorption was observed in solids using only cw lasers. Various theoretical and experimental aspects of two-photon absorption spectra in a magnetic field were investigated: (1) selection rule dependence, (2) energy band parameters needed to describe the data, (3) intensity dependence, (4) lattice temperature dependence of the energy gap, (5) two-photon absorption coefficients, and (6) transition energies.

Other absorption processes besides two-photon absorption were observed and investigated in InSb. These include free carrier and deep level transitions in n type samples, and free and bound hole transitions in p-type samples.

High-resolution spectra were obtained for the free A- and B-excitons in CdS by two-photon absorption using photoconductivity techniques. Anisotropy splittings were observed and interpreted with an anisotropic effective-mass Hamiltonian. Zeeman splittings and diamagnetic interactions were observed and analyzed. Variational calculations which take into account the interaction of states through the diamagnetic term in the Hamiltonian describe the data quite well. Exciton and band parameter values were determined along with the temperature dependence of the A energy gap. The anisotropy splitting of the B (2P) exciton state was observed for the first time and the B (3P) exciton state was also observed for the first time.

Two-photon absorption spectra of high purity GaAs were obtained at 1.8 K using a tunable dye laser and hydrogen filled Raman cell. Resonant structure is seen at high magnetic fields and shown to be related to exciton and Landau-level behavior.

INVESTIGATION OF NONLINEAR OPTICAL PROPERTIES OF SEMICONDUCTORS

David G. Seiler
Center for Applied Quantum Electronics
Department of Physics
North Texas State University
Denton, Texas 76203

FINAL REPORT

Contract Number: N00014-82-C-0545

Prepared for

Office of Naval Research
Department of the Navy
Arlington, Virginia 22217

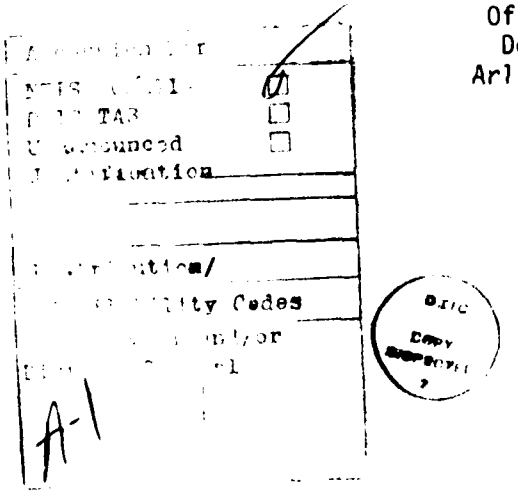

TABLE OF CONTENTS

SUMMARY

Nonlinear optics is an increasingly interesting and exciting area of physics. Many nonlinear optical effects have been discovered and various nonlinear optical devices constructed from a wide variety of materials. In particular, small band gap semiconductors like InSb can have unique optical properties because of their small effective masses and direct band gaps. Unusual and often unexpected results are found in their nonlinear behavior--optical bistability, nonlinear refraction, laser pulse limiting and shaping effects, optical transistor action, etc. These effects can be described in terms of a third order susceptibility $\chi^{(3)}$ and are associated with the creation of free carriers by the light. The creation of even a small number of free electrons or holes can strongly effect the "dynamic" nonlinear optical properties of the material. In this project we used sensitive photoelectronic methods to investigate the nonlinear generation of electrons in InSb, CdS, and GaAs induced by two-photon absorption of light.

A wide variety of photoelectronic effects are initiated by the creation of free carriers from the absorption of light in a semiconductor or insulator. These include the photo-Hall effect, photoconductivity, recombination, trapping, lifetimes, all of which are important for understanding devices such as light detectors, light emitters, or energy converters. On the other hand these photoelectronic effects can also be exploited to investigate the nonlinear absorption of light in solids and thus gain an enhanced understanding of their material properties. In this project we have shown that the photoconductive response of semiconductor samples can sensitively detect two-photon absorption processes.

Two-photon absorption processes have been studied in n-InSb using a tunable cw CO_2 laser and high magnetic fields. This work represents the first time two-

photon absorption was observed in solids using only cw lasers. Various theoretical and experimental aspects of two-photon absorption spectra in a magnetic field were investigated: (1) selection rule dependence, (2) energy band parameters needed to describe the data, (3) intensity dependence, (4) lattice temperature dependence of the energy gap, (5) two-photon absorption coefficients, and (6) transition energies.

Other absorption processes besides two-photon absorption were observed and investigated in InSb. These include free carrier and deep level transitions in n type samples, and free and bound hole transitions in p-type samples.

High-resolution spectra were obtained for the free A- and B-excitons in CdS by two-photon absorption using photoconductivity techniques. Anisotropy splittings were observed and interpreted with an anisotropic effective-mass Hamiltonian. Zeeman splittings and diamagnetic interactions were observed and analyzed. Variational calculations which take into account the interaction of states through the diamagnetic term in the Hamiltonian describe the data quite well. Exciton and band parameter values were determined along with the temperature dependence of the A energy gap. The anisotropy splitting of the B (2P) exciton state was observed for the first time and the B (3P) exciton state was also observed for the first time.

Two-photon absorption spectra of high purity GaAs were obtained at 1.8 K using a tunable dye laser and a hydrogen filled Raman cell. Resonant structure is seen at high magnetic fields and shown to be related to exciton and Landau-level behavior.

FOREWORD AND ACKNOWLEDGEMENTS

This report is the final report on contract N00014-82-C-0545 for the Office of Naval Research.

The technical work of the contracts has been carried out by graduate students who used certain phases of this work for a Ph.D. or M.S. thesis. Graduate students who obtained advanced degrees while associated with this work (their present affiliation is given in parentheses) have been:

Mike Goodwin	(Texas Instruments, Inc.)
Larry Hanes	(Raytheon)
Kay Hansen Littler	(Denton)
Chris Littler	(continuing Ph.D. work)

Technical support was provided by the NTSU Machine Shop and the NTSU Electronics laboratory (Dwight Maxson). Finally we acknowledge the many helpful discussions with colleagues at NTSU.

LIST OF FIGURES

LIST OF TABLES

I. INTRODUCTION

The realm of "linear optics" present in one photon spectroscopy has provided much of the basic information about semiconductor properties such as energy gaps, effective masses, g-factors, impurity levels, band symmetries, relaxation times, etc. Because of the very high absorption coefficients ($10^4 cm^{-1}$) usually dealt with, light only penetrates 0.1 micron into the sample. Consequently, thin films or thin crystals are needed. Reflectivity measurements over a wide spectral range followed by a Kramer's-Kronig analysis does not give great accuracy. In contrast to the major disadvantages of the one photon case, two-photon spectroscopy can provide uniform absorption throughout the bulk of the sample because of the much smaller two-photon absorption cross-sections. This part of the realm of "nonlinear optics" has proven to be quite important and useful in probing the eigenstates of not only solids, but of gasses too. Transitions which are forbidden in conventional one-photon spectroscopy are now possible to observe using two-photon techniques. In fact, it becomes possible to uniquely identify the symmetry of the eigenstates. Practically speaking, it is important to understand the role of two-photon processes in windows damaged by high power lasers. There are several good review articles[1-3] on two-photon spectroscopy that can be consulted.

Experimentally, the task is to detect the simultaneous absorption of two photons. The same techniques used for detecting one-photon transitions in linear spectroscopy can be used: (1) absorption spectroscopy, (2) fluorescence or luminescence spectroscopy, (3) Photo-emission or photoconductivity, (4) Photochemical reactions, and (5) Photoacoustic spectroscopy. A simple two-photon absorption experiment occurs when two beams of light are incident on a sample. The sample is transparent to each of the two beams, but when both beams are present at the same time and when $\hbar\omega_1 + \hbar\omega_2$ is equal to an allowed transi-

tion energy, the sample absorbs simultaneously one photon from each beam. One beam might be a laser and the other a wide frequency band, or continuum. It is also possible to use two lasers, one or both being tunable. Even simpler would be the use of only one laser beam to provide the two-photons.

Two-photon spectroscopy in a magnetic field was demonstrated in this project to be a valuable technique for investigating semiconductors. Seiler and co-workers have shown that TPA in n-InSb is even observable with the milliwatt powers available from a cw CO_2 laser.[4] These studies represented the first time that TPA experiments in solids were ever carried out using only cw lasers. The high resolution permitted observation of many new TPA lines not previously seen. The report of these results at a recent international conference in France was one reason Laser Focus recently printed an interesting news report:[5] "New experimental results are challenging established theory in nonlinear optics. It had been widely assumed that second-order effects (proportional to the square of the electromagnetic field) generally would be weaker than effects proportional to higher powers of the field. But high-order nonlinear effects in semiconductors have been showing up with surprising magnitudes in laboratories in Britain and the United States. Milliwatt lasers have produced effects which it had been thought would require much higher laser intensities. Some specialists are even coming to the conclusion that the distinction between "low-order" and "high-order" nonlinear phenomena and some of the underlying theory may not be relevant for certain materials, in particular gallium arsenide and indium antimonide."

A wide variety of photoelectronic effects are initiated by the creation of free carriers from the absorption of light in a semiconductor or insulator. These effects involve the Hall effect, photoconductivity, recombination, trapping, lifetimes, etc., and are important for understanding materials used as light detectors, light emitters, or energy converters. On the other hand, these photoelectronic effects can be exploited to investigate the absorption of light

in solids.

Photoconductivity can be a complex process involving several successive or simultaneous mechanisms: optical absorption, charge carrier transport, hot carrier relaxation, and radiative and/or nonradiative recombination. It covers all phenomena by which an increase or decrease in conductivity can take place following the absorption of light in the semiconductor. The presence of non-equilibrium carriers generated by the light alters the conductivity of a semiconductor. The general form of the conductivity can be written as

$$\sigma = e[\mu_n(n_o + \Delta n) + \mu p(P_o + \Delta P) + n_o \Delta\mu_n + P_o \Delta\mu_p]$$

or

$$\sigma = \sigma_o + \Delta\sigma$$

where e is the electronic charge, $n_o(P_o)$ is the concentration of electrons (holes) at thermal equilibrium in the dark, $n(P)$ is the excess electron (hole) concentration induced by the light, $\mu_n(\mu_p)$ is the electron (hole) mobility, $\Delta\mu_n(\Delta\mu_p)$ is the change in the electron (hole) mobility caused by the light, $\sigma_o = e(\mu_n n_o + \mu_p P_o)$ and $\Delta\sigma = e[\mu_n \Delta n + \mu_p \Delta P + n_o \Delta\mu_n + P_o \Delta\mu_p]$. Thus in general the conductivity can change if the carrier concentration or the mobility changes. Some detector materials (Putley or hot electron detectors) make use of this mobility change which can be quite large in the far infrared region. Here we shall be primarily concerned with the changes in concentration produced by the nonlinear absorption of light. Since in many semiconductors $\mu_p << \mu_n$, the change in conductivity arising from nonlinearly produced electro-hole pairs can be written simply as

$$\Delta\sigma = e\mu_n \Delta n$$

Thus measurements of the photoconductivity are directly related to changes in electron concentration. It is a very sensitive indicator of small changes in n,

particularly in n_0 is small. Thus if $n_0 \gtrsim 10^{14}cm^{-3}$, $\Delta n/n_0$ changes of $\gtrsim 0.001$ (or $\Delta n \gtrsim 10^{11}cm^{-3}$) can easily be detected.

Two-photon absorption spectra were obtained using photoconductivity techniques in InSb[4,6] and CdS.[7-9] We have shown that photoconductivity studies are very powerful for investigating semiconductors. InSb is a narrow gap semiconductor with an energy band gap of $\gtrsim$ 235 meV at 4 K. Thus a CO_2 laser can be tuned so that $2\hbar\omega$ is both below and above this energy. Seiler and co-workers [4] have used the photoconductivity technique to detect two-photon absorption in InSb using only cw CO_2 lasers. Application of a magnetic field allowed the study of two-photon magneto absorption (TPMA) structure. Derivative TPMA spectroscopy using sampling oscilloscope and magnetic field modulation techniques applied to the photoconductivity signal allowed the observation of numerous weak transitions. Various theoretical and experimental aspects of the two-photon spectra were investigated including (1) selection rule dependence, (2) energy band parameters needed to describe the data, (3) intensity dependence, (4) lattice temperature dependence of the energy gap, (5) TPMA coefficients, and (6) transition energies.

Two-photon spectroscopy measurements have also been carried out by Seiler, et. al.[7-9] on CdS samples using a visible dye laser in conjunction with the output from a H_2 filled Raman cell. Free exciton spectra dominated the absorption which was monitored by measuring the increase in sample conductivity as a function of photon energy. This represented the first time that the photoconductivity technique was used to obtain the two-photon absorption spectra of free excitons in semiconductors. High resolution spectra of both the A- and B-free excitons were obtained. Anisotropy splitting of the 2P and 3P exciton states was observed, along with Zeeman splitting and diamagnetic shifts. Experimental results were interpreted with an anisotropic effective mass Hamil-

tonian and variational calculations taking into account the interaction of states through the diamagnetic term. These studies allowed accurate characterization of the A and B exciton and band properties of CdS.

II. INTERACTION OF CO_2 LASER RADIATION WITH p-InSb

In this section we present the results of a collaborative effort in the study of the interaction of CO_2 laser radiation with samples of p-InSb. High magnetic field studies (fields $\gtrapprox$ 10 T) were carried out at the U.S. Naval Research Laboratory in conjunction with Dr. R. Kaplan and Dr. R. J. Waqner. Lower field (< 2 T) studies were carried with the facilities at NTSU. In what follows in this section we reproduce several of our published papers. More extensive details will be contained in a future Ph.D. thesis of Mr. C. L. Littler.

Solid State Communications, Vol.37, pp.783-788.
Pergamon Press Ltd. 1981. Printed in Great Britain.

0038-1098/81/100783-06$02.00/0

HIGH RESOLUTION MAGNETO-OPTICAL STUDIES OF p-InSb*

C.L. Littler

Department of Physics, North Texas State University
Denton, Texas 76203 USA

and

D.G. Seiler**

Francis Bitter National Magnet Laboratory
Massachusetts Institute of Technology
Cambridge, Massachusetts 02139 USA

and

R. Kaplan and R.J. Wagner

Naval Research Laboratory
Washington, D.C. 20390 USA

and

W. Zawadzki

Institute of Physics, Polish Academy of Science
Warsaw, Poland

(Received 1 December 1980 by J. Tauc)

High resolution photoconductivity and transmission spectra in p-InSb are obtained over a wide temperature range at magnetic fields from 9 to 100 kG using a CO_2 laser. The low temperature results are described in terms of hole transitions from the acceptor ground state to excited states associated with free light-hole Landau states.

In this communication we will present the results of magneto-optical experiments on acceptor excitations in InSb, and discuss their relevance to the determination of valence band parameters. The latter are not known with nearly the accuracy of the InSb conduction band parameters. In part, this is due to the greater complexity of the valence bands. Additionally, there is a relative lack of hole intraband data, as compared with numerous conduction electron studies involving cyclotron, spin, and combined resonance, and harmonic and phonon-assisted variants of these. Currently available valence band parameters have been determined mainly from interband and cyclotron resonance magneto-optical experiments. However, exciton effects must be taken into account in analyzing the interband data, leading to some ambiguity in the determination of the band parameters. Cyclotron resonance experiments are also difficult to interpret because of k_z-dependent energy terms, and complex spectra are observed due to the valence band degeneracy. Ranvaud[1] has shown that application of uniaxial stress simplifies the hole cyclotron resonance spectra of InSb; the results were later used by Ranvaud, Trebin et al.[2] to obtain the valence band parameters. However, the HCN laser spectrometer used in this study only allowed the observation of transitions very close to the band edge. The band parameters thus determined differ strongly from those obtained by analysis[3] of interband and intra-conduction band data. Recently, Grisar et al.[4] obtained photoconductive spectra for p-type InSb at 12 K for two CO_2 laser wavelengths. These spectra were interpreted as LO phonon-assisted spin-conserving free carrier transitions between light hole Landau levels, and a new set of valence band parameters was thus derived. However, similar spectra obtained by Kaplan[5] were instead described as excitations of bound holes from the ground state acceptor to excited states associated with light hole levels. It appears that a definitive determination of the InSb valence

*Work supported in part by the Office of Naval Research.
**Permanent Address: Department of Physics, North Texas State University, Denton, Texas 76203

band parameters has yet to be achieved.

The specific goals of the present work are: (1) To obtain more detailed intraband data for the transitions reported in Ref. 4 and 5 through the use of high-resolution, high sensitivity techniques; (2) To determine the process responsible for these transitions; (3) If this process indeed involves acceptor excitations, to search for additional free hole transitions. By these means we hope to obtain new intraband data sufficient for the accurate determination of valence band parameters.

The experiments were performed on InSb crystals grown by Cominco and by E.M. Swiggard at N.R.L. Values of N_A-N_D were in the range of 0.5 - 1.5 x 10^{14} cm^{-3}, with Zn or Cd the acceptor used for doping. Typical sample thicknesses were 3 mm for transmission and 0.1 mm for photoconductivity studies. For the high field experiments described here, the magnetic field and direction of light propagation were along a <111> crystal axis. Low magnetic field measurements were performed with an iron-core magnet using magnetic field modulation and sampling oscilloscope techniques,[6] while the high field studies utilized a Bitter solenoid of the NRL High Magnetic Field Facility and ratioing techniques.[7] The CO_2 lasers were grating tunable, providing single line outputs of several watts.

Figure 1 shows a comparison of transmission and photoconductive data at 9.57 μm. A one-to-one correspondence between the photoconductive peaks and the transmission minima is evident. The photoconductive measurements clearly provide a more sensitive means of determining the small changes in absorption due to the resonant processes. An apparent doublet structure is resolved at higher magnetic fields as previously reported.[4,5] This structure is not simply due to the appearance of spin splitting. Rather it is a consequence of the ordering of light hole Landau levels of differing principle quantum number and effective "spin," the latter designation being accurate only for more energetic states where the wave function mixing is small. The photoconductive spectral response has been determined at several CO_2 laser wavelengths, as shown in Fig. 2. Resonant structure is resolved down to fields as low as 10 kG. No polarization dependence was observed for the Voigt configuration for either $\vec{e} \parallel \vec{B}$ or $\vec{e} \perp \vec{B}$ where $\vec{e}$ is the direction of the electric field of the light. The magnetic field dependence of these peak positions is plotted in Fig. 3. No attempt has been made to correct for the slightly decreased separation of the observed apparent doublet components due to the overlap of the peaks.

In order to identify the charge carriers responsible for the observed transitions, the temperature dependence of the Hall voltage and the magneto-optical spectra were investigated for several samples. The Hall measurements indicated that hole freezeout occurs largely between 12 and 20 K. Transmission spectra remained unchanged between 4.2 and 14 K (see

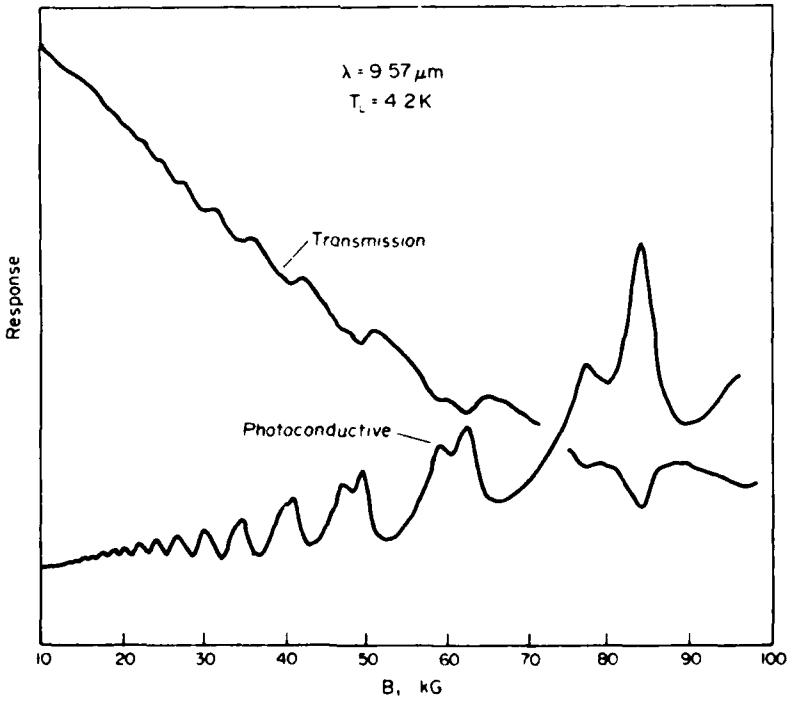

Fig. 1 Photoconductivity and transmission spectra for p-InSb at 9.57 μm and a lattice temperature of 4.2 K. The change in transmission from the monotonic background to the resonance position at ~83 kG is approximately 7%.

Fig. II.1

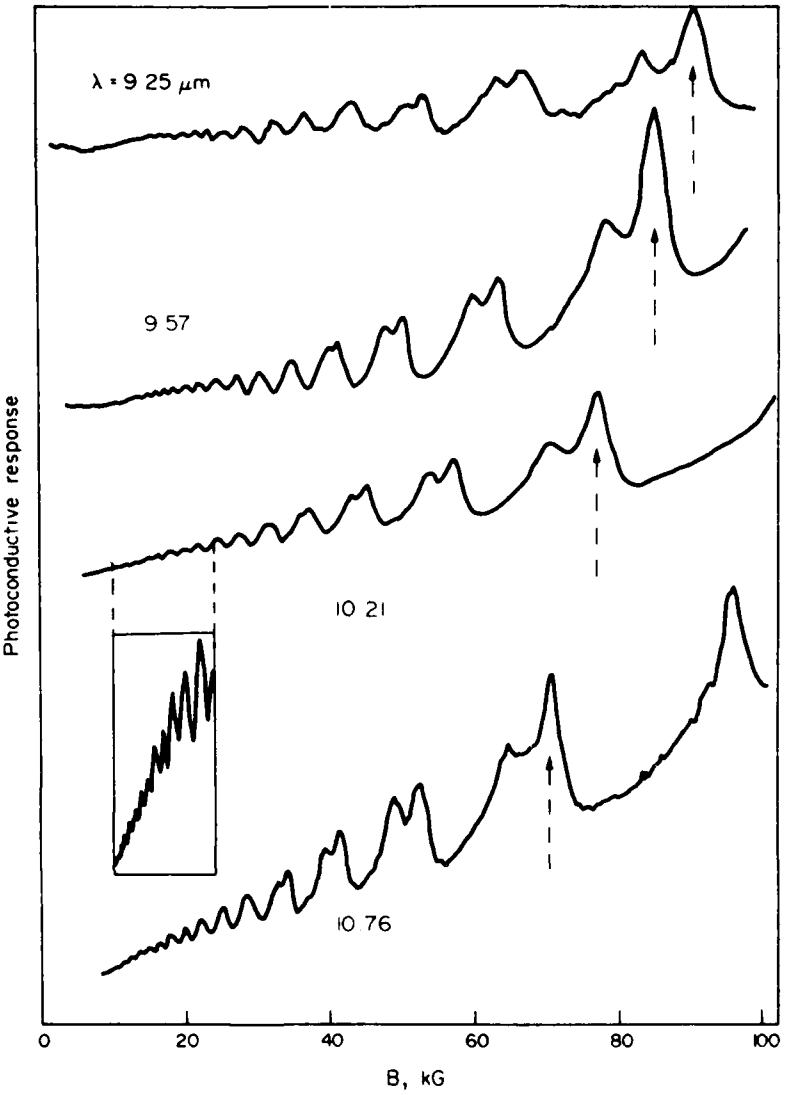

Fig. 2 Photoconductive spectra at four different wavelengths. Inset shows the high resolution of the data with increased gain. Arrows show how a given peak tracks with photon energy.

Fig II. 2

Fig. 4), and only began to show strong new features, and weakening of the old, above 14 K.

Both of the observations involving temperature dependence cited above, indicate that the optical spectra obtained at 14 K and below represent excitations of holes bound at acceptors. In Ref. 5 it was argued that the final states of the transitions are excited acceptor states bound to light hole levels split off by the magnetic field. That such levels and transitions exist and are strongly allowed, has been demonstrated by the theory of Lin-Chung and Henvis.[8] In this interpretation an interesting situation exists, in which the acceptor ground state is in the "low effective field" regime, $E_{gs} >> h\nu_c$, for all field strengths, while the excited levels are "high effective field" states, $E_{es} << h\nu_c$, for fields above several kilogauss. Here E_{gs} and E_{es} are the binding energies of the ground and excited states, relative to the valence band edge and any light hole Landau level, respectively, and ν_c is the cyclotron energy $eB/2\pi m^* c$. This behavior occurs because the light hole mass responsible for the small value of E_{es}, is some 30 times smaller than the heavy hole mass at the band edge, which largely determines E_{gs}.

In order to compare the transition energy data with a band model, it is necessary to examine the field dependence of all contri-

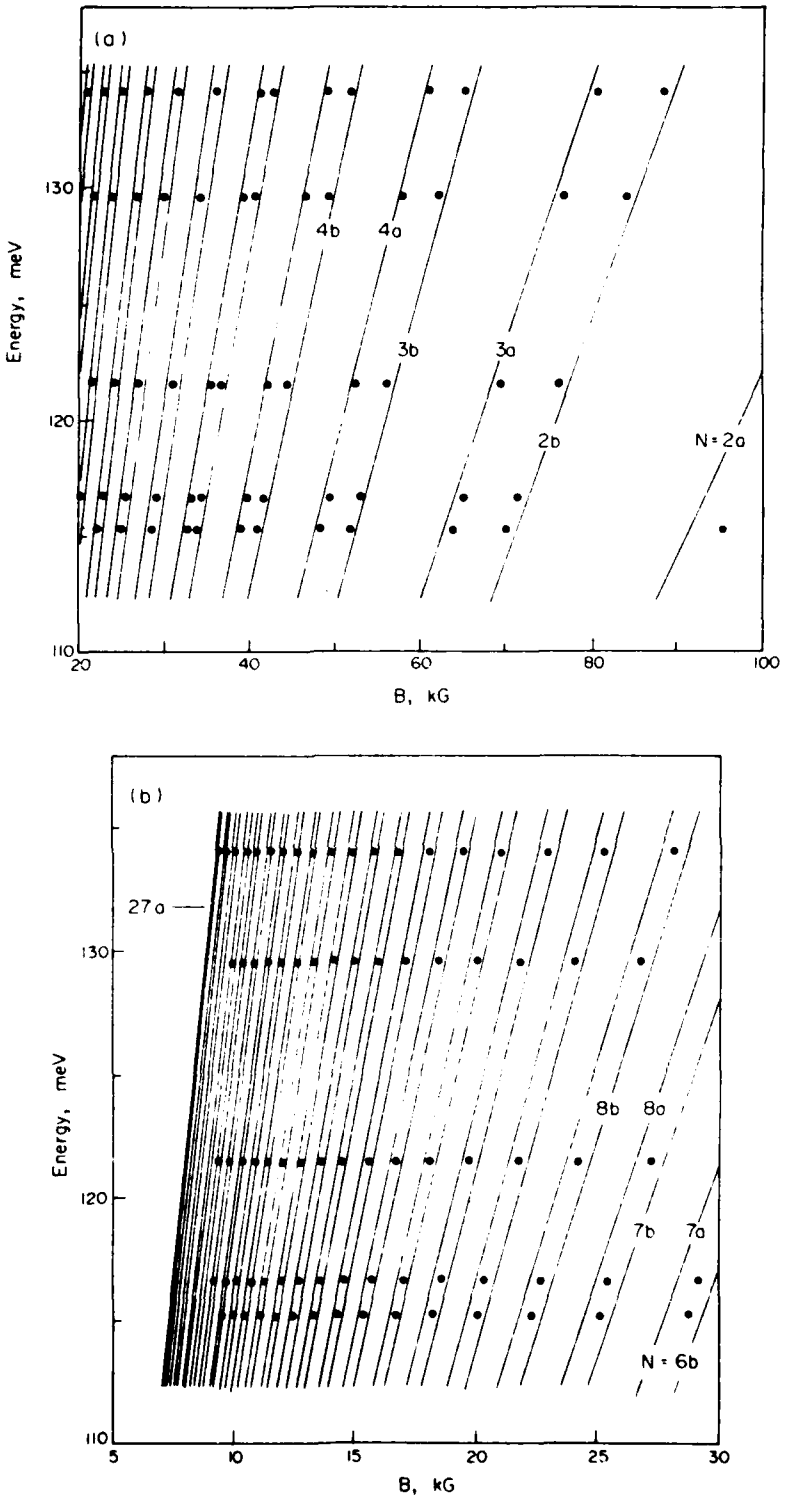

Fig. 3 Field dependence of the transition energies. Lines indicate results of three-level theory fit to data points: (a) magnetic fields above 20 kG and (b) fields below 30 kG. The numbers indicate the light hole Landau levels and a or b the spin state to which the hole transitions occur.

Fig. II.3

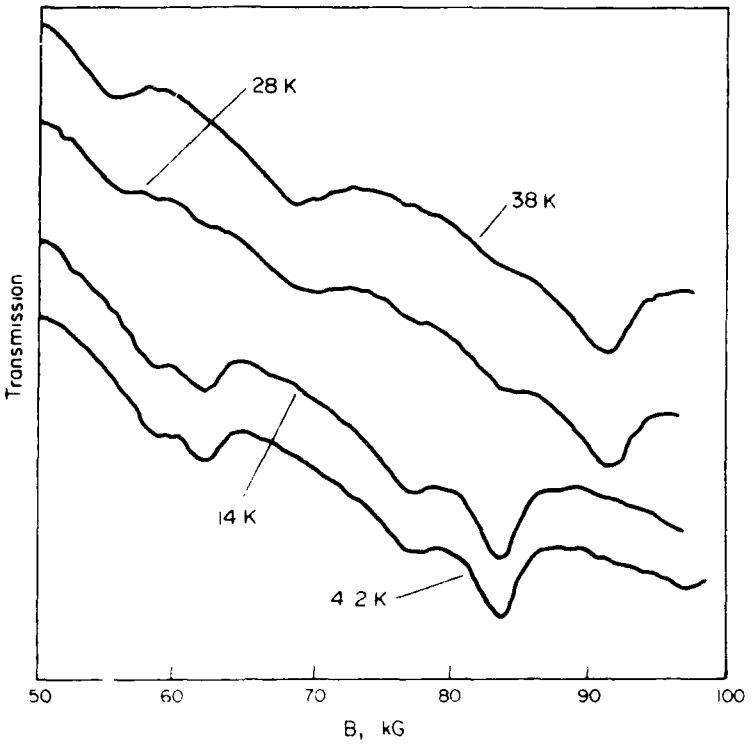

Fig. 4 Comparison of the transmission spectra of a single sample obtained at 9.57 μm for four different temperatures.

Fig. II.4

butions to the transition energy hν:

$$h\nu = E_{gs}(o) + \Delta E_{gs}(B) + \epsilon_{LH}^{a,b}(N,B) - E_{es}(B). \quad (1)$$

$\epsilon_{LH}^{a,b}(N,B)$ is the energy of the N^{th} light hole Landau level in ladder a or b, and $\Delta E_{gs}(B)$ is the field-induced shift of the acceptor ground state energy from its zero-field value $E_{gs}(o)$. At present, $\Delta E_{gs}(B)$ and $E_{es}(B)$ are not accurately known, but they are small quantities of comparable magnitude and opposite sign. (At a 10 micrometer wavelength, their magnitudes are ≤0.01 hν.) Thus in the present approach we write

$$h\nu = E_{gs}(o) + \epsilon_{LH}^{a,b}(N,B) \quad (2)$$

and fit the transition energies using a three band model,[9] with energy gap 236.7 meV and spin-orbit splitting 803 meV. Below 30 kG the apparent doublets are no longer resolved, and a single point representing the average field position of the two unsplit components is plotted. A best fit to the data, shown in Fig. 3a,b, yields $E_{gs}(o) = 9.0$ meV, and the band parameter value $P^2 = 0.46$ a.u. corresponding to $E_P = 25.1$ eV. Excellent agreement between theory and experiment is achieved over the entire range of light hole quantum numbers 2 to 27. Values of $E_{gs}(o)$ and E_P determined in the fit are in good agreement with corresponding values in the literature, e.g. for $E_{gs}(o)$, 8.5±0.5,[10] 8,[11] and 9.3 0.6[5] meV, and for E_P, 26.1,[7] 23.5±0.5,[3] 24,[12] 21.2,[13] 23.7,[14] and 24[15] eV.

The excellent fit of the three band model calculations to the low temperature data attests to the correctness of the interpretation based on acceptor excitations. In order to fully exploit the data for determination of valence band structure, it will be necessary to determine the magnetic field dependence of the ground and excited state acceptor binding energies, and to apply an eight band model including anisotropy. We are presently pursuing this direction. In addition, we have examined the spectra obtained for sample temperatures above 20 K. Our preliminary results indicate that these spectra are due to harmonic cyclotron resonance and combined resonance of free holes. Analysis of these free hole transitions should provide an additional means for determining the valence band structure, in this case free from complications due to acceptor level binding energies.

We are pleased to acknowledge helpful discussions with M.H. Weiler and the support of the staff of the High Magnetic Field Facility at NRL.

REFERENCES

1. R.D. RANVAUD, Ph.D. Thesis, Brown University, 1973, available from University Microfilms Order No. 74-3064.
2. R. RANVAUD, H.R. TREBIN, Ü. ROSSLER and F.H. POLLAK, Physical Review B 20, 701 (1979); and H.R. TREBIN, Ü. ROSSLER and R. RANVAUD, Physical Review B 20, 686 (1979).
3. M.H. WEILER, Journal of Magnetism and Magnetic Materials 11, 131 (1979).
4. R. GRISAR, H. WACHERNIG, G. BAUER, J. WLASAK, J. KOWALSKI and W. ZAWADZKI, Physical Review B 18, 4355 (1978).
5. R. KAPLAN, Physical Review Letters 20, 329 (1968); and R. KAPLAN, S.G. BISHOP and B.D. McCOMBE, in Proceedings of the Ninth International Conference on the Physics of Semiconductors, Moscow, 1968, edited by S.M. Ryvkin (Nauka, Lenningrad, 1968), p. 317.
6. H. KAHLERT and D.G. SEILER, Review of Scientific Instruments 48, 1017 (1977).
7. R.J. WAGNER and G.A. PRINZ, Applied Optics 10, 2060 (1971).
8. P.J. LIN-CHUNG and B.W. HENVIS, Physical Review B 12, 630 (1975).
9. W. ZAWADZKI, New Developments in Semiconductors, edited by P.R. Wallace et al. (Noordhoff, Leyden, 1973), p. 441.
10. E.J. JOHNSON and H.Y. FAN, Physical Review 139, 1991 (1965).
11. E.H. PUTLEY, Proceedings of the Physical Society of London 73, 128 (1959).
12. E.O. KANE, Journal of Physical and Chemical Solids 1, 249 (1957).
13. C.R. PIDGEON and R.N. BROWN, Physical Review 146, 575 (1966).
14. R.L. BELL and K.T. ROGERS, Physical Review 152, 746 (1966).
15. E.J. JOHNSON and D.H. DICKEY, Physical Review B 1, 2676 (1969).

II -8

Magneto-optical detection of deep acceptor impurities in p-InSb

C. L. Littler and D. G. Seiler
Center for Applied Quantum Electronics, Department of Physics, North Texas State University, Denton, Texas 76203

R. Kaplan and R. J. Wagner
Naval Research Laboratory, Washington, D.C. 20390

(Received 23 July 1982; accepted for publication 24 August 1982)

We report the first magneto-optical experiments on Au-doped p-InSb and show how they can be used to detect and identify impurities in semiconductor materials. A ground state binding energy of 42.5 ± 0.5 meV has been determined for the lower level of the Au double acceptor in InSb. The technique also provides information about the magnetic field dependence of the excited states associated with a deep acceptor level.

PACS numbers: 71.55.Fr, 78.20.Ls, 72.40. + w, 78.50.Ge

Detection and identification of impurities in semiconductor materials has long been a topic of technological importance. Of particular interest is the location of the impurity states within the forbidden energy gap region and their behavior in the presence of an external magnetic field. As a result there have been many theoretical[1-5] and experimental[6-13] investigations in InSb designed to probe the magnetic field dependence of shallow donor[1,2,4,5,7-9] and acceptor[2,3,6,10-13] impurities. In addition, oscillatory photoconductivity[14,15] and transmission[16] studies at zero-magnetic field as well as Hall measurements[15,17] have given information about ground and excited state binding energies of shallow[16] and deep acceptor[14-17] impurities in InSb. However, none of these studies[14-17] were extended to include the effect of a magnetic field on the observed deep acceptor levels.

In this letter we report the results of magneto-optical experiments on Au-doped InSb. To our knowledge these are the first magneto-optical studies on Au-InSb. We have analyzed the high resolution photoconductive spectra using a modified Pidgeon and Brown 8×8 band model[18] and have obtained a ground state binding energy of 42.5 ± 0.5 meV for the lower level of the Au double acceptor (intentionally present in the crystal). In addition, weaker structures visible in the spectra due to the presence of Cd (or Zn) monoacceptors (unintentionally present) have also been identified. We are also able to show from the analysis that the excited impurity states associated with the deep Au acceptor in InSb are similar in nature to those associated with the excited states of the the shallow Zn or Cd acceptors.

The experiments reported here were performed on a single crystal of InSb intentionally doped with Au impurities. The impurity concentration was no more than 10^{14} cm^{-3} at 77 K. The sample thickness was approximately 0.1 mm and the magnetic field and direction of light propagation were along a ⟨111⟩ crystal axis. A Bitter solenoid of the NRL high magnetic field facility was used to obtain fields up to 105 kG (10.5 T) and signal ratioing techniques[19] were employed to obtain the high resolution spectra. The CO_2 laser used was grating tunable, providing single line outputs of several watts.

Figure 1 shows the photoconductive spectral response observed at three CO_2 laser wavelengths. The spectra are complicated, containing many strong and weak resonant peaks. The maxima in the detector response corresponds to a maxima in the conductivity, where the resonant increase in absorption has given rise to an increase in the number of holes. The peaks are labelled according to which acceptor (Au or Cd) the excitation peak has been identified with and to which light hole Landau level the excited acceptor states are associated. We see that the stronger photoconductive peaks result from the excitation of the Au impurities. In addition, weaker resonant peaks are seen which, upon analysis, were found to result from excitation of (Cd or Zn) impurities unintentionally introduced during crystal growth.

Figure 2 is a diagram of possible hole transitions at 70 kG (7.0 T) which are allowed between ground and excited acceptor states of Au or Cd. It has been previously shown for shallow acceptors[2,13] that the most strongly allowed transitions occur between the s-like acceptor ground state and the

Fig. II.5

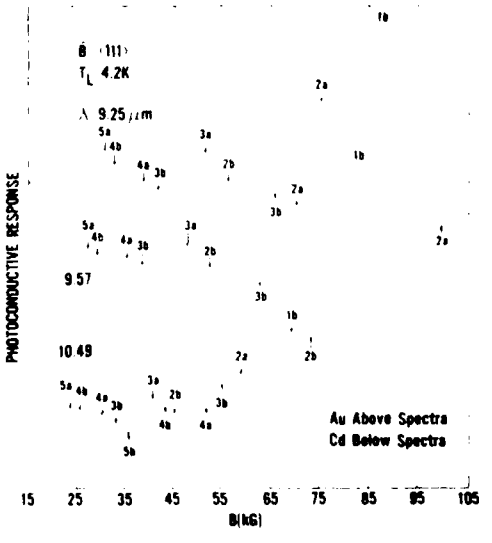

FIG. 1. High resolution photoconductive spectra obtained for three CO_2 laser wavelengths for B‖⟨111⟩. The peaks are labelled according to which light-hole Landau levels the excited acceptor states are associated. The strong Au resonances are indicated by the labels appearing above each spectra and the weaker Cd peaks are indicated by the labels appearing below each spectra.

 0003-6951/82/090880-03$01.00

II - 7

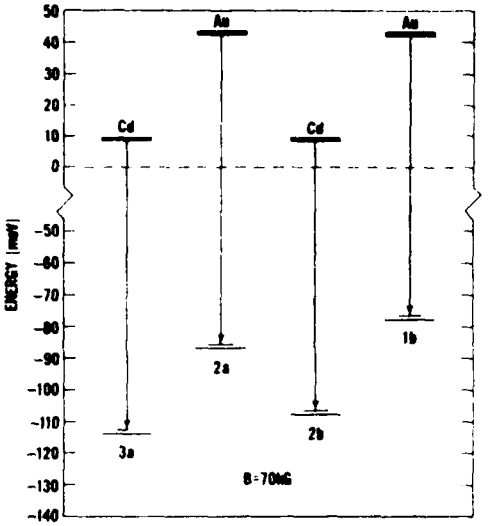

FIG. 2. Diagram of allowed transitions at $B = 70$ kG (7.0 T). Transitions indicated are from the acceptor ground state of the Au and Cd acceptors to excited states associated with the light-hole Landau levels 1b and 2a for Au, and 2a and 3b for Cd.

Fig. II.6

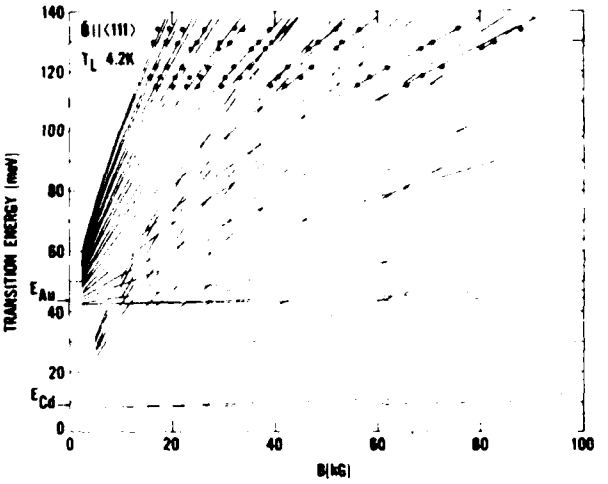

FIG. 3. Calculated transition energies for B||⟨111⟩. Dashed lines indicate calculated transition energies for Cd and the solid lines show the calculated Au transition energies. The solid dots and open dots represent the observed transition energies for the Au and Cd acceptors, respectively. The ground state binding energies for the Au and Cd acceptors are indicated by the zero field intercepts $E_{Au} = 42.5$ meV and $E_{Cd} = 8.1$ meV.

Fig. II.7

p-like excited states, which lie close in energy to the light hole Landau levels. Impurity photoionization[5] is ruled out since it is expected to be much weaker than bound hole transitions and is predicted to disappear in the high field limit.[20]

In order to compare the transition energy data obtained from the photoconductive spectra to a band model it is necessary to examine all contributions to the transition energy. Since the light-hole excited-state binding energies and the field-induced shift of the acceptor ground state are considered to be small, we have found that[6,11-13] it is sufficient to add the ground state binding energy to the light hole Landau level energies in order to accurately describe the observed transitions. We have used a modified Pidgeon and Brown 8×8 band model to calculate the light hole Landau level energies and adjusted the value of the ground state binding energy in order to obtain a fit of theory to data. The band model parameters $E_g = 0.2352$ eV, $E_p = 23.2$ eV, $\Delta = 0.803$ eV, $\gamma_1 = 3.25$, $\gamma_2 = -0.20$, $\gamma_3 = 0.90$, $\kappa = -1.30$, $F = -0.20$, $q = 0.0$, and $N_1 = -0.55$, were chosen for the analysis since this set of parameters has been previously shown[13,21,22] to describe well an extensive set of conduction-band cyclotron and combined resonance, phonon-assisted cyclotron resonance, two-photon magneto-absorption, intravalence band combined resonance, and acceptor-excitation data.

A best fit to the data using this model is shown in Fig. 3. The dashed and solid lines represent calculated transition energies for the Cd (or Zn) and Au impurities, respectively, using the procedure discussed above. The solid dots represent Au transition energy data and the open dots are Cd (or Zn) excitation data. The zero-field intercepts indicated by E_{Cd} and E_{Au} thus represent the ground state binding energy for the Cd and Au acceptors. We see that by adjusting two sets of calculated transition energies (dashed and solid line) until a fit is obtained, we can explain well the complex spectra of Fig. 1 as a superposition of the strong Au and weak Cd resonances. From the analysis we extract a ground state binding energy of 42.5 ± 0.5 eV for the lower level of the Au double acceptor. We see that the weaker resonances are indeed due to the presence of Cd (or Zn) monoacceptors since the use of 8.1 meV for the binding energy, consistent with the binding energy for Cd (or Zn),[13,23] explained well the transition energies observed for the weak resonances. The value for the Au binding energy is in excellent agreement with oscillatory photoconductivity measurements,[15,16] where the long wavelength threshold was obtained.

The excellent fit to the Au transition data seen in Fig. 3 (solid dots and lines) shows that the excited state energies of the Au acceptor must be very close to the calculated light hole Landau level energies. The same is seen for the Cd data (dashed lines—open dots). This indicates that the excited states (excluding s states) of single and double acceptors do not significantly differ from one another. This feature agrees with predictions for single and double acceptors in Ge[24] and has been seen for Cd and Ag acceptors in InSb[16] at zero-magnetic field, and for Cd acceptors in InSb in the presence of a magnetic field.[13] This is the first time, however, that this feature has been observed for Au acceptors in InSb using magneto-optical techniques.

In summary, we have shown that high resolution magneto-optical techniques can be used to detect and identify deep acceptor impurities in InSb. This technique also provides information about the behavior of acceptor impurities in the presence of an external magnetic field and allows extraction of ground state binding energies. In principle, if the acceptor cross section is measured or known then one could also develop this technique into a tool for determining the number of acceptors present in the semiconductor crystal. Thus, high resolution magnetospectroscopy is a valuable method for the characterization of semiconductor materials.

This work was supported in part by the Office of Naval Research.

[1]Y. Yafet, R. W. Keyes, and E. N. Adams, J. Phys. Chem. Solids **1**, 137 (1956).
[2]P. J. Lin-Chung and B. W. Henvis, Phys. Rev. B **12**, 630 (1975).
[3]N. O. Lipari and A. Baldereschi, Phys. Rev. Lett. **25**, 1660 (1970).
[4]W. Zawadzki and J. Wlasak, Int. Phys. Conf. Ser. **43**, 413 (1979).
[5]R. F. Wallis and H. J. Bowlden, J. Phys. Chem. Solids **7**, 78 (1958).
[6]R. Kaplan, Phys. Rev. Lett. **20**, 329 (1968).
[7]R. Kaplan, Phys. Rev. **181**, 1154 (1969).
[8]R. Kaplan and R. F. Wallis, Phys. Rev. Lett. **20**, 1499 (1968).
[9]B. D. McCombe and R. Kaplan, Phys. Rev. Lett. **21**, 756 (1968).
[10]R. Kaplan, K. L. Ngai, and B. W. Henvis, Phys. Rev. Lett. **28**, 1044 (1972).
[11]C. L. Littler, D. G. Seiler, R. Kaplan, R. J. Wagner, and W. Zawadzki, Solid State Commun. **37**, 783 (1981).
[12]R. Kaplan, R. J. Wagner, D. G. Seiler, C. L. Littler, M. H. Weiler, and W. Zawadzki, in *Proceedings of the Physics of Narrow Gap Semiconductors, Linz, Austria, 1981* edited by E. Gornik, H. Heinrich, and L. Palmetshofer (Springer, New York, 1982), p. 188.
[13]C. L. Littler, D. G. Seiler, R. Kaplan, and R. J. Wagner (unpublished).
[14]W. Engeler, H. Levinstein, and C. Stannard, Jr., Phys. Rev. Lett. **7**, 62 (1961).
[15]W. Engeler, H. Levenstein, and C. Stannard, Jr., J. Phys. Chem. Solids **22**, 249 (1961).
[16]R. Kaplan, Solid State Commun. **12**, 191 (1973).
[17]R. F. Blunt, Bull. Am. Phys. Soc. II **3**, 115 (1958).
[18]M. H. Weiler, R. L. Aggarwal, and B. Lax, Phys. Rev. B **17**, 3269 (1978).
[19]R. J. Wagner and G. A. Prinz, Appl. Opt. **10**, 2060 (1971).
[20]H. Hasegawa and R. E. Howard, J. Phys. Chem. Solids **21**, 179 (1961).
[21]M. W. Goodwin, D. G. Seiler, and M. H. Weiler, Phys. Rev. B **25**, 6300 (1982).
[22]M. W. Goodwin and D. G. Seiler (unpublished).
[23]A. G. Milnes, *Deep Impurities in Semiconductors* (Wiley, New York, 1973), p. 72.
[24]W. J. Moore, J. Phys. Chem. Solids **32**, 93 (1971).

PHYSICAL REVIEW B VOLUME 27, NUMBER 12 15 JUNE 1983

High-resolution magneto-optical studies of free and bound holes in *p*-type InSb

C. L. Littler and D. G. Seiler
Center for Applied Quantum Electronics, Department of Physics, North Texas State University, Denton, Texas 76203

R. Kaplan and R. J. Wagner
Naval Research Laboratory, Washington, D. C. 20375

(Received 4 October 1982)

High-resolution magneto-optical experiments on *p*-type InSb have been performed over a wide range of temperatures and photon energies for the sample orientations $\vec{B} \parallel \langle 111 \rangle$ and $\vec{B} \parallel \langle 100 \rangle$. The spectra obtained at temperatures greater than ~20 K result from combined-resonance transitions of free holes between heavy- and light-hole Landau levels, while bound-hole transitions between ground heavy-hole-like and excited light-hole-like acceptor states are observed at lower temperatures. The high resolution of the low-temperature spectra has allowed observation of bound-hole transitions originating from heavy-hole-like ground states to final excited acceptor states associated with light-hole Landau levels with quantum numbers $n = -1$ to 27. Polarization and Hall-coefficient measurements have confirmed the origin of both the bound- and free-hole spectra. Analysis of the high-temperature free-hole combined-resonance data along with extensive intra-conduction-band and two-photon interband data using a modified Pidgeon and Brown 8×8 band model has allowed the determination of a single set of band parameters for InSb that quantitatively describes these different sets of data. In addition, a ground-state binding energy of 8.1 ± 0.3 meV for Cd acceptors has been extracted from analysis of the bound-hole spectra. The energy-band parameters determined from this work are $E_g = 0.2352$ eV, $E_p = 23.2$ eV, $\Delta = 0.803$ eV, $\gamma_1 = 3.25$, $\gamma_2 = -0.2$, $\gamma_3 = 0.9$, $\kappa = -1.3$, $F = -0.2$, $q = 0.0$, and $N_1 = -0.55$.

I. INTRODUCTION

In the past the determination of band parameters for InSb has depended largely on the results of intra-conduction-band and one-photon interband experiments. Owing to substantial disagreement between the parameters adjusted to fit the conduction band and the interband data, some doubt arose as to the validity of the quasi-Ge model for InSb proposed by Pidgeon and Brown.[1] However, it has been shown by Weiler[2] and more recently by Efros *et al.*[3] that exciton effects must be included in order to properly describe the one-photon interband results. Also, intra-conduction-band experiments are relatively insensitive to the nature of the valence bands and are thus not particularly suited to the determination of valence-band parameters. Therefore it is not surprising that there is some disagreement between published sets of band parameters which have been obtained by separate analyses of either conduction-band or interband data.

Another reason for the discrepancy between band parameters is the relative lack of hole-intraband data,[4-12] in contrast to the numerous conduction electron studies reported, and the added difficulty in interpretation of these results due to the greater complexity of the valence bands in InSb. Specifically, Suzuki and Hensel[13] have shown that the degeneracy of the valence bands at the center of the Brillouin zone introduces k_z-dependent energy differences in most observable intraband transitions that take place near the band edge. Earlier hole-cyclotron-resonance studies[4-6] met these difficulties in the interpretation of their results. Ranvaud[7] showed that the application of uniaxial stress simplifies the hole-cyclotron-resonance spectra by destroying the cubic symmetry responsible for the degeneracy of the valence bands, and later Ranvaud *et al.*[8] investigated both hole-cyclotron and combined resonance as a function of applied stress. However, the hydrogen cyanide (HCN) laser spectrometer used only allowed observation of transitions near the band edge; therefore it is not unexpected that the parameters determined differed significantly from those obtained by analysis of interband and intra-conduction-band data.

II-12

Only one attempt has been made to include hole-intraband data along with one-photon interband and conduction-band data in order to obtain a single set of band parameters for InSb. Grisar *et al.*[9] obtained photoconductive spectra for *p*-type InSb at 12 K for two CO_2 laser wavelengths. These spectra were interpreted as LO phonon-assisted spin-conserving free-carrier transitions between light-hole Landau levels and, by analyzing this data along with the interband and conduction-band data, a new set of band parameters were supposedly obtained. However, similar spectra in the same temperature regime first obtained by Kaplan,[10] and later by Littler *et al.*[11] using a CO_2 laser, were instead described in terms of hole transitions from a Cd acceptor ground state to excited acceptor states closely associated in energy with the light-hole Landau levels. Additional verification for the identification of the spectra came from temperature-dependent Hall-coefficient measurements. Littler *et al.*[11] explained their acceptor excitation spectra using a three-band model[14] to calculate the transition energies, and a good fit of theory to data was obtained. However, the three-band model used does not describe accurately all band features. Clearly, a definitive determination of the band parameters for InSb has yet to be achieved.

In this paper we present extensive high-resolution hole-intraband data which must be used for the proper determination of band parameters for InSb. New low- and high-temperature spectra obtained for $\vec{B}||\langle 111\rangle$ and $\vec{B}||\langle 100\rangle$ through the use of CO_2 and optically-pumped far-infrared (far-ir) lasers and conventional grating monochromators is presented. The low-temperature ($T_L < 20$ K) spectra are described in terms of bound-hole transitions between heavy-hole-like ground and light-hole-like excited acceptor states; the high-temperature ($T_L > 20$ K) spectra result from combined resonance of free holes between different spin states of the heavy- and light-hole Landau levels. The high resolution of the low-temperature spectra has allowed identification of bound-hole transitions with final excited acceptor states associated with the light-hole Landau level quantum numbers $n = -1$ to 27. Anisotropy effects seen in both the combined-resonance and bound-hole spectra have provided additional constraints necessary for determining the final set of band parameters. We have used a modified version[15] of the Pidgeon and Brown quasi-Ge model for InSb to analyze our results and, along with the use of extensive conduction-band and two-photon interband data, have been able to determine a set of band parameters for InSb. This new set of parameters explains well not only the valence-band results presented here but also those of a number of other experiments: two-photon interband,[16,17] conduction-band cyclotron[18–20] and combined[9,18–21] resonance, conduction-band cyclotron[9,20–22] and combined[9,21]-resonance harmonics, electron-spin resonance[23–25] and phonon-assisted cyclotron-resonance harmonics.[9,20,21,26–29]

In addition to the band parameters obtained we show that the high-resolution magneto-optical techniques employed in this study are useful for sensitively detecting the presence and determining the location of acceptor impurity states in the forbidden energy-gap region. Until now, other studies designed to investigate acceptor impurities in InSb have consisted largely of oscillatory photoconductivity,[30,31] negative photoconductivity,[32] and transmission[33] studies at zero magnetic field, and Hall measurements.[30,34,35] From the analysis of the low-temperature bound-hole spectra, a value of 8.1 ± 0.3 meV has been determined for the Cd ground-state binding energy. Also from the analysis we are able to obtain information about the magnetic field dependence of the Cd ground and excited acceptor impurity states.

II. THEORY

In this study extensive use was made of a modified Pidgeon and Brown 8×8 quasi-Ge band model. We have adopted the version presented by Weiler *et al.*,[15] which was used to describe warping and inversion-asymmetry-induced cyclotron-harmonic transitions in InSb. In this version the complete InSb $\vec{k}\cdot\vec{p}$ Hamiltonian is obtained to first order in $\vec{B}$ and second order in $\vec{k}$, and the quasi-Ge model is described for the magnetic field lying in the $(1\bar{1}0)$ plane of the crystal. The energies of the conduction band, and the light-hole, heavy-hole, and split-off valence bands are calculated in an approximate coupled-band scheme which includes nonparabolic, warping, and "quantum" effects in such a manner that only 4×4 matrices corresponding to the *a* and *b* Landau ladders need to be diagonalized for each Landau quantum number *n*. The model uses a group-theoretical treatment to obtain all allowed matrix elements of $\vec{k}$ and $\vec{k}\times\vec{k}$ among the valence-band states transforming as the Γ_8 representation of the double group. The results give a complete set of adjustable parameters for the coupled Γ_6, Γ_7, and Γ_8 bands. The set of basis functions used by Weiler are slightly different from other sets found in the literature.

The strongest allowed transitions are those proportional to the interband matrix element *P*, and the selection rules for both intraband and interband transitions are given by[15]

$$a_n \rightarrow a_{n-1},\ b_n \rightarrow b_{n-1},$$
$$a_n \rightarrow a_{n+1},\ b_n \rightarrow b_{n+1}, \quad (1)$$
$$a_n \rightarrow b_{n+1},\ b_n \rightarrow a_{n-1}$$

for σ_R, σ_L, and π, respectively. For intraband transitions, the π transition occurs at $\omega = \omega_c + \omega_s$ or the "combined-resonance" frequency, where ω_c is the cyclotron frequency and ω_s is the spin-flip frequency, and the σ_L transition occurs at $\omega = \omega_c$. Also, in this approach the valence-band states are not renumbered $n \rightarrow n+1$ as was done by Pidgeon and Brown.

Free-hole transitions between valence-band Landau levels obeying the selection rules given in Eq. (1) should be observable in p-type InSb following thermal ionization of the acceptors present in the material. The selection rules apply equally well for free-hole transitions from heavy- to heavy-hole, heavy- to light-hole, and light- to light-hole Landau levels and thus the particular transitions observed depend on the thermal population of the initial states and the range of photon energies employed. Since relative strengths and field positions of allowed transitions are directly obtainable from band-model calculations, they provide a straightforward method for identifying observed transitions.

At low temperatures holes are frozen out onto acceptor sites, and another class of excitations involving transitions between acceptor impurity states then becomes possible. A standard approach to the treatment of acceptor impurity states in the presence of an external magnetic field is to use the effective-mass approximation.[36] This approach was used by Lin-Chung and Henvis[37] to describe high-field donor and acceptor states associated with the Landau levels by extending the effective-mass approximation to include the details of the InSb band structure. From this analysis we note several features characteristic of bound-hole states. First, unlike free holes, bound holes possess unique states. Also because of the degeneracy of the valence bands, the acceptor states in a magnetic field exist in association with both heavy-hole and light-hole Landau levels. At low temperatures it is expected that the excited acceptor states would be the final states of hole transitions originating from a ground acceptor state. Transitions to the continuum levels are not expected to dominate since transition probabilities to states in the continuum decrease with increasing field.[38] The selection rules between acceptor states are expected to be the same as that given for donor states; i.e., for π polarization or $\vec{e} \| \vec{B}$, the selection rule is $\Delta N = 0$, $\Delta M = 0$, $\Delta\lambda$ odd, and for circularly polarized radiation the selection rule is $\Delta N = 0$ or ± 1, $\Delta M = \pm 1$, and $\Delta\lambda$ even (M is positive for σ_L and negative for σ_R).

III. EXPERIMENTAL METHOD

The experiments described in this work were performed on p-type InSb crystals grown either by Cominco or by E. M. Swiggard of Naval Research Laboratory (NRL). Cd was the acceptor used for doping, with the values of $N_A - N_D$ in the range $(0.5-1.5)\times 10^{14}$ cm^{-3}. Sample thicknesses were typically 3–5 mm for transmission and 0.1 mm for photoconductivity studies. For high-magnetic-field measurements a Bitter solenoid of the NRL High Magnetic Field Facility and signal ratioing techniques were employed.[39] At lower fields, measurements were performed using either an iron core magnet along with magnetic field modulation and sampling oscilloscope techniques,[40] or a superconducting solenoid and signal ratioing.

The wide range of fixed photon energies used in the experiments were provided by CO_2 and optically pumped far-ir lasers, a grating monochromator, and an interferometric spectrometer. Measurements were conducted on samples in both Faraday and Voigt configurations, with either $\vec{B} \| \langle 111 \rangle$ or $\vec{B} \perp \langle 100 \rangle$. The low-field facility at North Texas State University (NTSU) had light polarization capabilities, whereas the high-field facility at NRL did not; therefore, except where indicated, the light incident on the sample was unpolarized, containing both σ and π components.

In order to achieve the wide range of temperatures used, the sample was situated in a cryogenic optical Dewar and was either immersed in liquid helium or nitrogen, surrounded by flowing helium gas, or immersed in a static helium exchange gas on a heated sample block in a tube immersed in liquid helium. Temperatures between 4.2 and 77 K were monitored by either a calibrated thermocouple or a Lake Shore Cryotronics carbon-glass resistor located nearby the sample.

IV. RESULTS

Figure 1 shows a comparison of the transmission spectra obtained for a single sample of p-InSb at four different temperatures. Resonant minima in the transmission are seen in the spectra at various magnetic fields. The change in transmission in the 4.2-K spectra from the monotonic background to the resonance position at 83 kG is approximately 7%. Clearly, a substantial change in the spectra is seen in going from 4.2 to 38 K. The doublet feature, resolved at fields above 40 kG in the low-temperature spectra, is seen to die out as the temperature is increased and a new set of resonances appear. Also, the linewidths of the low-temperature minima are significantly narrower than that of the

II - 14

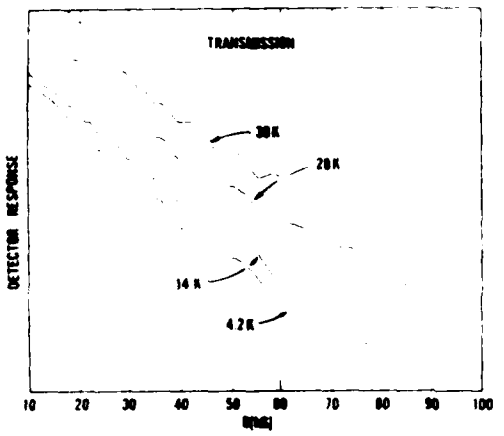

FIG. 1. Comparison of the transmission spectra obtained from a sample of Cd-doped p-type InSb at 9.57 μm for four different temperatures. The observed transmission minima result from absorption resonances corresponding to high-temperature free-hole transitions between heavy- and light-hole Landau levels and low-temperature bound-hole transitions between ground and excited acceptor impurity states.

Fig. II.8

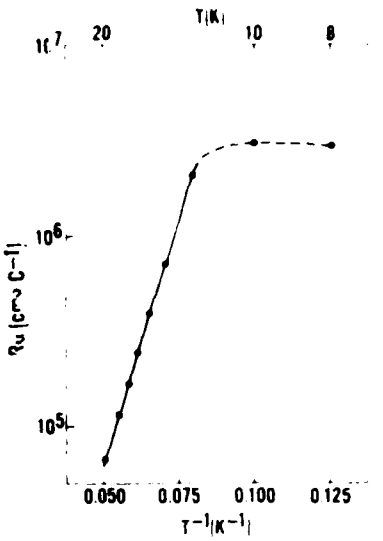

FIG. 2. Temperature dependence of the Hall coefficient for Cd-doped InSb. From the semilogarithmic plot it is seen that hole freezout has occurred at temperatures below ~ 12 K.

Fig. II.9

high-temperature minima. These differences suggest that two different types of transitions are responsible for the spectra observed at low and high temperatures. To aid in determining the origin of the observed transitions, the Hall coefficient was measured at various temperatures in order to help identify the contribution of free holes in the observed transitions. The results of this study are presented in Fig. 2. These measurements indicate that free-hole generation starts to occur at approximately 12–14 K, thus indicating that bound-hole (i.e., acceptor) transitions are responsible for the low-temperature spectra and free-hole transitions are responsible for the high-temperature spectra. In addition, the narrower linewidth of the low-temperature spectra indicates that the transitions observed at low temperatures are to discrete states rather than continuum levels, in agreement with the bound-hole transition model. Therefore, the data and hence our results and discussion will be separated into two categories, free- and bound-hole spectra, respectively.

A. Free-hole spectra

The spectral region investigated in this work includes many possible transitions, due to the mixed character of the wave functions and the thermal population of numerous low-lying levels. These transitions tend to group around the closely spaced pairs of light-hole Landau levels. Figure 3 shows a diagram of the six possible free-hole transitions allowed at 60 kG for the light-hole energy range 120–130 meV. The transitions satisfy the selection rules given by Eq. (1) of Sec. II. The energies were obtained using the band parameters cited in Table I for the sample orientation $\vec{B}\|\langle 111\rangle$. Also shown are transitions, labeled A, corresponding to bound-hole transitions that are present at low temperatures ($T_L < 20$ K). These transitions will be discussed later.

Since most of the high-field spectra was obtained using unpolarized light, containing both σ and π components, the observed free-hole spectra is assumed to contain contributions from all six possible transitions. Figure 4 shows the wavelength dependence of the free-hole spectra obtained for $\vec{B}\|\langle 111\rangle$. The arrows show how a given peak tracks with photon energy. The identification of the transitions responsible for the transmission minima observed was arrived at by calculating the positions and relative strengths of all six allowed transitions, and comparing these results with the data. An example of this can be seen in Fig. 5. The transition strengths (directly proportional to the absorption coefficient) were determined by calculating the square of the matrix elements, for σ_L (transition 1), σ_R (transition 2), and π (transition 3) polarizations. These relative transition strengths were plotted as a

II-15

Table II.1

TABLE I. Comparison of band parameters

	One-photon interband						Hole cyclotron and combined resonance			Intraconduction band		Others		
	Zwerdling *et al.*[a]	Pidgeon and Brown[b]	Pidgeon and Groves[c]	Weiler[d]	Roth and Fortin[e]	Efros *et al.*[f]	Bagguley *et al.*[g]	Robinson[h]	Ranvaud *et al.*[i]	Johnson and Dickey[j]	Isaacson[k] Summers[n] *et al.*	Grisar *et al.*[l]	Lawaetz theory[m]	This work
E_g (eV)	0.2357 ±0.0005	0.2355 ±0.0005	0.2366	0.2329	0.235 ±0.0001	0.2368	0.236		0.235	0.2367 ±0.0002		0.2355	0.237	0.2352
E_p (eV)		21.9	21.2	23.5 ±0.5	21.53 ±0.25	23.42	16.0		26.1	24.0±1		21.6	23.1	23.2
Δ (eV)		0.9	0.9	0.81	0.81		0.9		0.803	0.81±0.01		0.803	0.81	0.803
γ_1		1.5	3.64	3.4	1.86	3.44			3.1			0.5	2.59	3.25
γ_2		−1.2	−0.45	−0.3	−0.97	−0.54			0.4			−1.0	0.60	0.20
γ_3		−0.1	0.72	0.9	0.13	0.51			0.7			0.1	0.66	0.90
κ		−2.1	−1.47	−1.2		−1.26			1.5			−1.4	1.48	−1.3
F		0.0	0.0	0.0	0.0 ±0.1	−1.18							0.0	0.2
q		0.0	0.39	0.0		0.31			0.39			0.0	0.15	0.0
N_1		0.0	0.0	−0.3		−0.33							0.0	0.55
m_c/m_0	0.0145 ±0.0003	0.0144	0.0149	0.0136	0.0145 ±0.0001	0.0139			0.012	0.0139 ±0.0001	0.0137[n] ±0.0001	0.0146	0.014	0.0136
g_c^*	−48.0	−47.1	−45.3	−51.4	−45 ±0.2	−51.9			−55.3	−51.3	51.3[k]	−47.8	48.4	−51.1
m^+/m_0	0.0149	0.0160	0.0157	0.0141	0.0160 ±0.0002	0.0144	0.021 ±0.005		0.013			0.0164	0.015	0.0143
$m^-([111])/m_0$		0.44	0.36	0.44	0.44	0.34	0.45 ±0.03	0.45 ±0.02	0.44			1.18	0.53	0.50
$m^-([110])/m_0$		0.41	0.33	0.40	0.41	0.32	0.42 ±0.03	0.42 ±0.02	0.41			0.95	0.47	0.45
$m^-([100])/m_0$		0.32	0.27	0.31	0.032	0.27	0.34	0.34 ±0.03	0.32			0.60	0.35	0.35

[a]Reference 49.
[b]Reference 1.
[c]Reference 42.
[d]Reference 2.
[e]Reference 50.
[f]Reference 3.
[g]Reference 5.
[h]Reference 4.
[i]Reference 8.
[j]Reference 20.
[k]Reference 51.
[l]Reference 9.
[m]Reference 46.
[n]Reference 52.

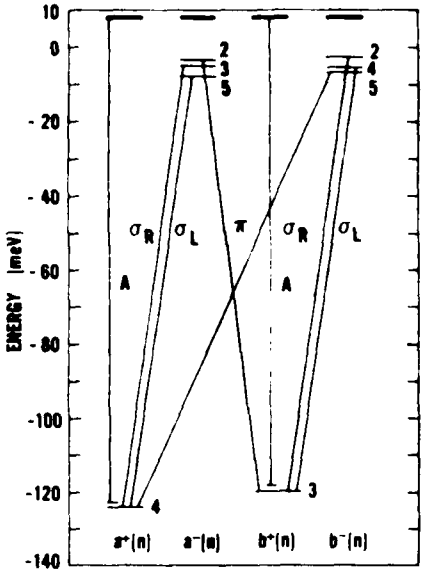

FIG. 3. Diagram showing allowed free- and bound-hole transitions involving the $a^+(4)$ and $b^+(3)$ light-hole Landau levels at $B=60$ kG for $\vec{B}||\langle 111\rangle$. At low temperatures, the bound-hole transitions (labeled A) originate from the Cd ground-state acceptor level shown. At high temperatures free-hole transitions are observed between heavy- and light-hole Landau levels.

Fig. II .10

function of magnetic field, as seen in the lower half of Fig. 5. It can be seen that the strongest allowed transitions, by a factor of ~ 3, are those corresponding to combined resonance of free holes $[b^-(n+1)\rightarrow a^+(n)$ and $a^-(n-1)\rightarrow b^+(n)]$ requiring π polarization, rather than the cyclotron-resonance transitions predicted for σ_L and σ_R light polarizations. Figure 5 also shows the experimental spectra obtained with the same transition energy, 118.15 meV ($\lambda=10.49$ μm), that was used in calculating the field positions of the relative transition strengths. A one-to-one correspondence of the transmission minima with the average position of the combined-resonance transitions, indicated by the arrows, can be seen throughout the entire spectra.

Figure 6 shows the results of a transmission experiment carried out at low magnetic fields and high sample temperatures using linearly polarized light to determine the selection-rule dependence of the observed transitions. The spectra presented was taken using field-modulation techniques, and they represent the second derivative of the transmission. Owing to the low signal-to-noise ratio in this field range, the experiment was repeated several times

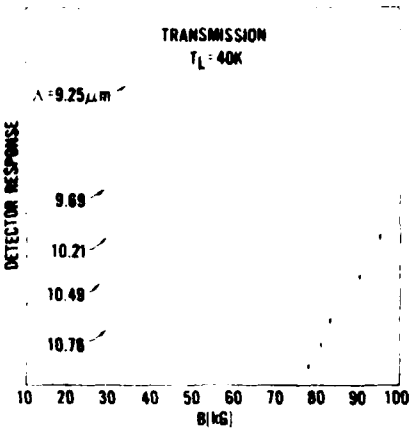

FIG. 4. Wavelength dependence of the high-temperature free-hole transmission spectra for $\vec{B}||\langle 111\rangle$. Arrows indicate how a given peak tracks with photon energy.

Fig. II .11

and the same results were obtained. It is seen that the transmission minima using $\pi(\vec{e}||\vec{B})$ polarization are $2\frac{1}{2}-3$ times larger than those observed using $(\vec{e}\perp\vec{B})$ polarization, consistent with the calculated transition strengths presented in Fig. 5. Also, the observed transmission minima for $\vec{e}\perp\vec{B}$ occur at slightly higher fields than the minima observed for $\vec{e}||\vec{B}$. This seems to be a result of the stronger σ_L transition, also seen from Fig. 5. Thus we conclude that the transmission minima obtained with unpolarized light originate predominantly from unresolved closely spaced pairs of combined-resonance transitions, and the average calculated positions were used to fit the spectra.

Experiments were also performed for the magnetic field oriented parallel to the $\langle 100\rangle$ crystallographic direction in order to observe any effects of hole anisotropy on the transition energies. We indeed do see a striking effect on the observed spectra due to hole anisotropy by comparing the spectra obtained for $\vec{B}||\langle 111\rangle$ and $\vec{B}||\langle 100\rangle$: such a comparison is shown in Fig. 7. To our knowledge, this is the first time that this anisotropy has been observed in combined resonance free-hole spectra. It is seen that the minima observed in the $\vec{B}||\langle 100\rangle$ spectra occur at higher magnetic field than the minima observed in the $\vec{B}||\langle 111\rangle$ spectra. Also, the relative shift between the corresponding minima is seen to decrease with increasing field. These features can be explained by looking more closely at the anisotropy of the light- and heavy-hole Landau-level energies for the a and b ladders. As will be discussed later

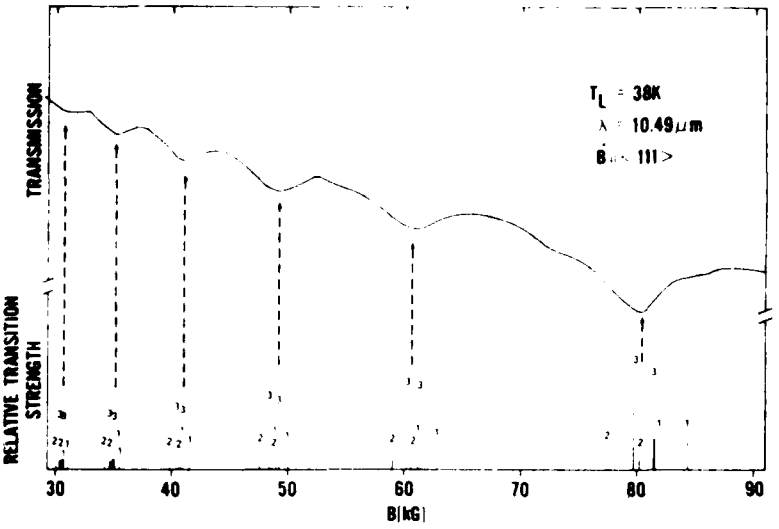

FIG. 5. Comparison of free-hole transmission spectra obtained at 10.49 μm with theoretically calculated field positions and relative transition strengths for different light polarizations. The numbers indicate the light polarization: $\sigma_L = 1$, $\sigma_R = 2$, $\pi = 3$. The arrowed dashed lines show the one-to-one correspondence between the average field position of the combined resonance (π) transitions and the observed resonant transmission minima.

Fig. II . 12

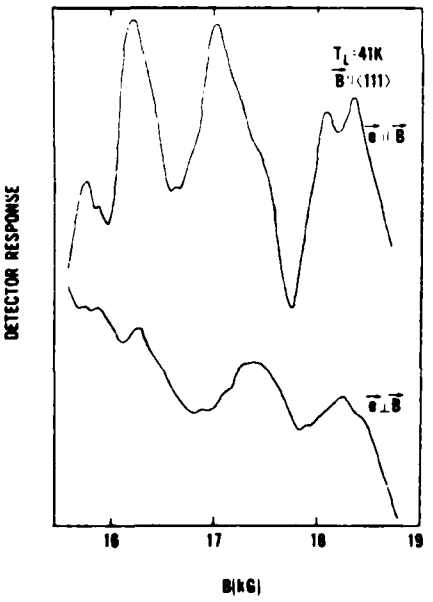

FIG. 6. Polarization dependence of the free-hole transmission spectra at low fields for the Voigt configuration. The amplitude of the spectra obtained for $\vec{\epsilon} \parallel \vec{B}$ (π polarization) is $2\frac{1}{2}-3$ times that obtained for $\vec{\epsilon} \perp \vec{B}$, in agreement with theoretical predictions of the relative transition strengths.

Fig. II . 13

(see Fig. 15 and corresponding discussion) it is seen that only the *b* set of the light-hole Landau levels displays any significant effects due to the hole anisotropy. In contrast, both the *a* and *b* heavy-hole Landau ladders show effects of hole anisotropy. Thus for the transitions obeying the selection rule $b^-(n)$

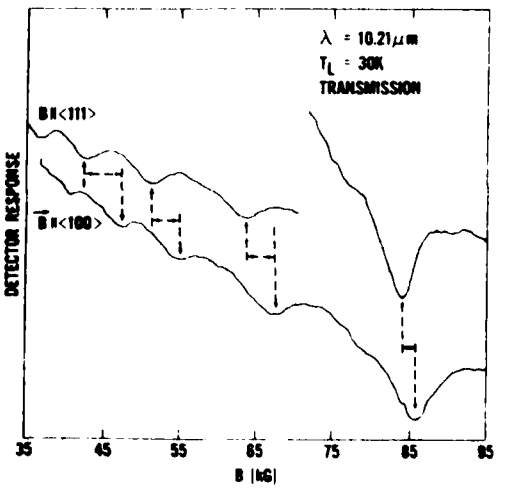

FIG. 7. Free-hole transmission spectra obtained at 10.21 μm for $\vec{B} \parallel \langle 111 \rangle$ and $\vec{B} \parallel \langle 100 \rangle$. Arrowed-dashed lines show the shift in resonant minima field positions due to the effects of heavy- and light-hole anisotropy.

Fig. II . 14

II - 18

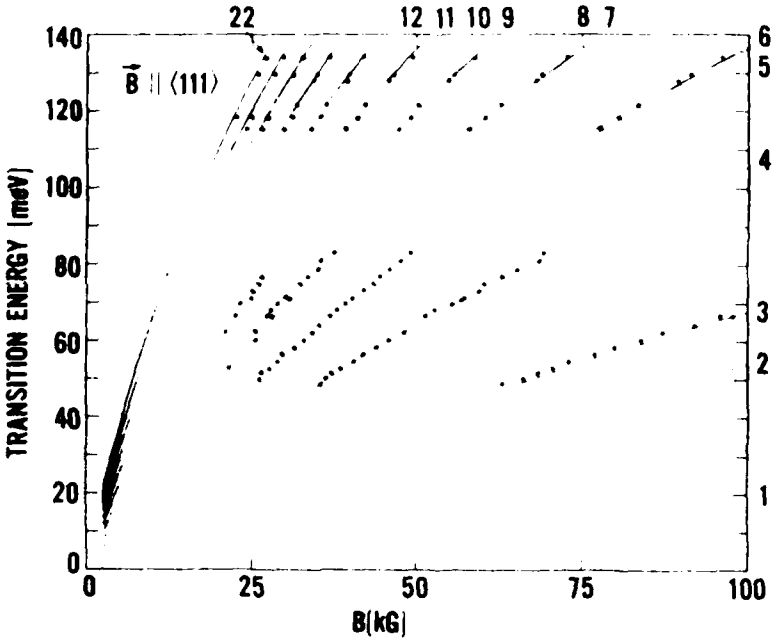

FIG. 8. Combined-resonance transition energies calculated from the 8×8 band model (solid lines) and the observed free-hole transitions (dots) for $\vec{B}\parallel\langle 111\rangle$. The numbers correspond to the following transition assignments: 1, $b^-(1)\rightarrow a^+(0)$; 2, $a^+(-1)\rightarrow b^+(0)$; 3, $b^-(2)\rightarrow a^+(1)$; 4, $b^-(3)\rightarrow a^+(2)$; 5, $a^-(1)\rightarrow b^+(2)$; 6, $b^-(4)\rightarrow a^+(3)$; 7, $a^-(2)\rightarrow b^+(3)$; 8, $b^-(5)\rightarrow a^+(4)$; 9, $a^-(3)\rightarrow b^+(4)$; 10, $b^-(6)\rightarrow a^+(5)$; 11, $a^-(4)\rightarrow b^+(5)$; 12, $b^-(7)\rightarrow a^+(6)$; 13, $a^-(5)\rightarrow b^+(6)$; 14, $b^-(8)\rightarrow a^+(7)$; 15, $a^-(6)\rightarrow b^+(7)$; 16, $b^-(9)\rightarrow a^+(8)$; 17, $a^-(7)\rightarrow b^+(8)$; 18, $b^-(10)\rightarrow a^+(9)$; 19, $a^-(8)\rightarrow b^+(9)$; 20, $b^-(11)\rightarrow a^+(10)$; 21, $a^-(9)\rightarrow b^+(10)$; 22, $b^-(12)\rightarrow a^+(11)$.

Fig. II .15

$\rightarrow a^+(n-1)$ the shift in corresponding minima is predominantly due to the anisotropy in the energies of the heavy-hole b ladder, while for transitions obeying $a^-(n)\rightarrow b^+(n+1)$ contributions to the observed shift come about equally from both the a heavy-hole and b light-hole ladders.

Determination of the band parameters obtained in this study was accomplished in several steps. First, extensive intra-conduction-band and two-photon interband data, reported elsewhere,[9,16–29] were fitted using the modified Pidgeon and Brown 8×8 band model. In order that correct effective masses would result, equations of constraint were used to constrain the values of $\gamma_2-\gamma_3$ and the heavy hole m^- ($\langle 111\rangle$) at -1.1 and $0.45m_0$, respectively. These values were chosen to agree with previous major studies (see Table I). The value of Δ was also held fixed at 0.803 eV, as determined from the stress-modulated magnetoreflectance results of Aggarwal.[41] Then, using the combined-resonance free-hole data presented here, adjustments were made to the set of parameters in order to best describe all data. It was seen that the anisotropy of the free-hole data provided additional constraints necessary to determine the final values for the band parameters; in particular, the values of the valence-band parameters, γ_1, γ_2, γ_3, κ, and E_p. The resulting set of parameters are listed in Table I, along with other published parameter sets for comparison. From the comparison it is seen that, with the exception of E_g, our set of parameters agree most closely with those of Weiler,[2] who included exciton effects in analyzing her one-photon interband results. In addition, some similar agreement is seen with the very recent results of Efros *et al.*[3] (in particular, the values of E_p and γ_1), who also analyzed one-photon interband data using exciton corrections.

Figures 8 and 9 show the results obtained by using our set of parameters to calculate the transition energies for $\vec{B}\parallel\langle 111\rangle$ and $\vec{B}\parallel\langle 100\rangle$. Since the data was taken over a large range of temperatures ranging from 20 to 77 K, a value of 233 meV for E_g was used for free-hole results. This value for E_g is approximately the value of the band gap at $T_L=40$ K,

II - 19

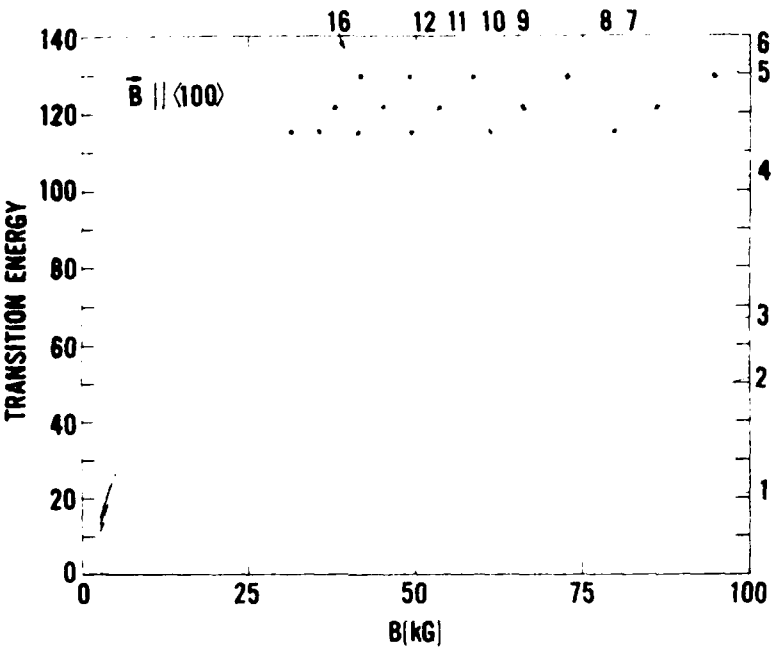

FIG. 9. Theoretically calculated combined-resonance transition energies (solid lines) and observed free-hole transitions (dots) for $\vec{B} \| \langle 100 \rangle$. The numbers correspond to the transition assignments listed in the caption for Fig. 8.

Fig. II.16

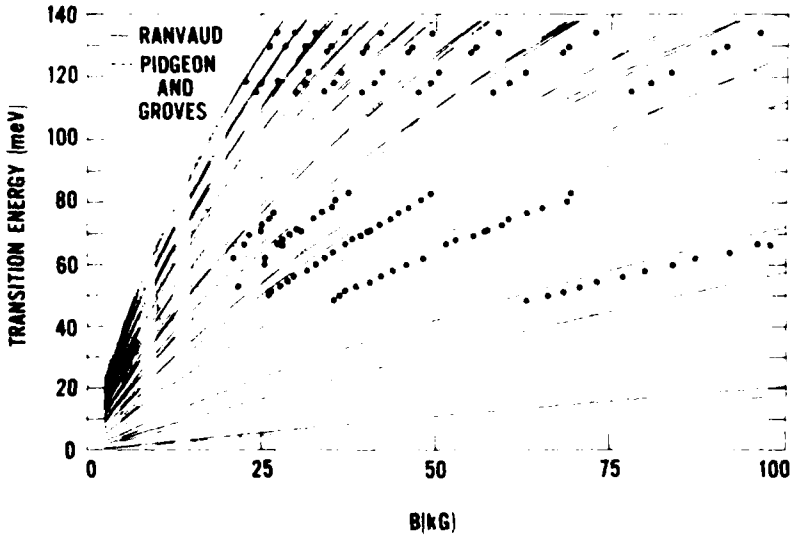

FIG. 10. Comparison of our observed free-hole transitions for $\vec{B} \| \langle 111 \rangle$ (dots) with the theoretically calculated transition energies using the band parameters of Ranvaud *et al.* (Ref. 8) (solid lines) and Pidgeon and Groves (Ref. 42) (dashed lines). Neither set of parameters is seen to describe our combined resonance free-hole spectra.

Fig. II.17

as determined from two-photon studies.[17] The final fit for our combined-resonance data is, however, not very sensitive to small changes in E_g. An excellent fit is obtained which explains well all observed features of the combined-resonance data. From Table I we see that the effective masses and g-factor calculated using this new set of band parameters compares favorably to other sets of published values.

A preliminary study of the free-hole spectra, reported earlier,[12] obtained a fit similar to that shown in Figs. 8 and 9. This fit, however, was obtained without the benefit of the intra-conduction-band data as a constraint. The energies of the combined-resonance transitions calculated for the $\vec{B}\|\langle 100\rangle$ orientation using this set of band parameters displayed a separation approximately 3 times larger than that seen in Fig. 9. With this large a separation, doublets would have been easily resolved. But, as is seen in Figs. 4, 5, and 7, this doublet feature is not present. Also, calculations made using this set of parameters gave heavy-hole effective masses 30% larger than what would be expected. Thus we see that it is important to include data from all regions in the analysis in order to obtain a correct set of parameters.

We recalculated the transition energies for $\vec{B}\|\langle 111\rangle$ using other published sets of band parameters and found relatively poor agreement with our data, as is shown in Fig. 10. This figure shows the transition energies obtained using parameters obtained by Ranvaud *et al.*[8] (solid lines) and Pidgeon and Groves[42] (dashed lines). It is seen that neither set describes the combined-resonance data presented here. Thus is it is evident that our new set of free-hole data must be included in order to determine a proper set of band parameters for InSb.

B. Bound-hole spectra

As was previously discussed, at sample temperatures below ~14 K holes are frozen out onto acceptor sites, and bound-hole transitions should then be observed in the transmission or photoconductive spectra. Figure 11 shows a comparison of photoconductive and transmission spectra obtained at 4.2 K for 9.57 μm. A one-to-one correspondence between the transmission minima and the photoconductive peaks is evident. As indicated by the arrows, there is no shift seen in peak positions between the transmission and photoconductive spectra. However, the photoconductive spectra provides much better resolution than does the transmission spectra. Clearly, the photoconductive measurements provide a more sensitive means of determining small changes in absorption due to resonant processes.

The inset of Fig. 11 shows transmission data taken using magnetic field modulation and sampling oscilloscope techniques and indicates the high resolution possible at low field using these techniques. From Fig. 11 it is noted that, unlike the free-hole spectra, an apparent doublet is resolved at higher fields. This feature has been previously reported in the literature.[9-12] The doublet is a consequence of the ordering of the light-hole Landau levels such that a and b spin states differing in quantum number n by unity [i.e., $1b(b^+(1))$--$2a(a^+(2))$, etc.] lie close together in energy. This ordering is due to the large spin splitting in the valence band of InSb, shown qualitatively in Fig. 3.

As discussed in Sec. II, transitions between acceptor impurity states should follow the same selection rules that are predicted for donor states. Also, the observed acceptor excitations should be equally allowed for σ or π polarization. Owing to the near degeneracy of the initial heavy-hole-like acceptor states, the observed transitions for both polarizations should occur at nearly the same field positions. To check this, a polarization study was conducted at low fields using magnetic field modulation and sampling oscilloscope techniques, the results of which are displayed in Fig. 12. For each polarization the same intensity was incident on the sample. Little difference in either amplitude or field position of the transmission spectra were detected, in agreement with the predictions of the bound-hole model.

Figure 13 shows photoconductive and transmis-

Fig. II.18

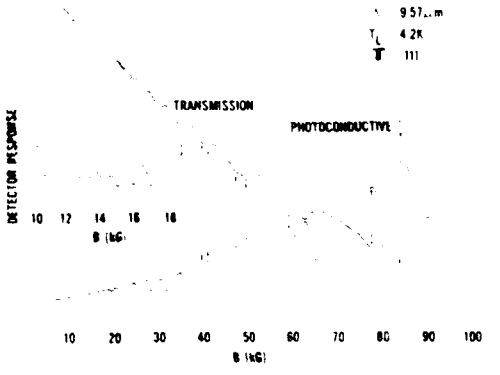

FIG. 11. Comparison of photoconductive and transmission spectra obtained at 4.2 K for $\vec{B}\|\langle 111\rangle$. Arrows indicate the one-to-one correspondence between the photoconductive peaks and the transmission minima. The inset shows the high resolution possible at lower magnetic fields using magnetic field modulation and sampling oscilloscope techniques. The detector response shown in the inset is proportional to the second derivative of the transmission signal.

II - 21

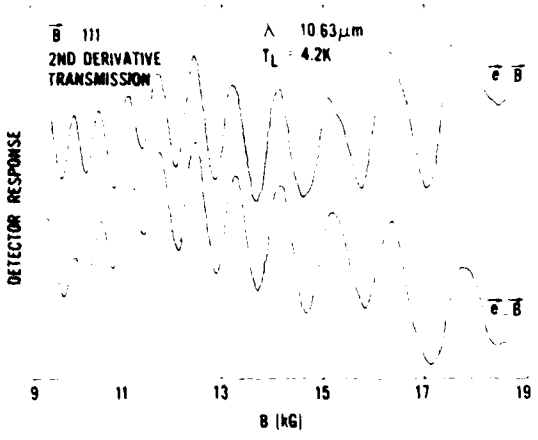

FIG. 12. Polarization dependence of the bound-hole spectra for $\vec{B}\|\langle 111\rangle$ and in the Voigt configuration. No significant differences in either the amplitude or field positions of the resonant minima are seen.

Fig. II.19

sion spectra obtained at three different widely spaced wavelengths. The numbers used to identify the individual transmission minima (or photoconductive peaks) refer to the light-hole Landau level to which the excited acceptor states are associated. Note that the high resolution of the spectra allows individual transitions to be studied over a broad range of photon energies. The unlabeled peak at ~22 kG and the even smaller one at ~33 kG in the photoconductive spectra obtained at 70.6 μm have been identified as the free-hole combined-resonance transitions whose assignments are $b^-(2) \rightarrow a^+(1)$ and $a^+(-1) \rightarrow b^+(0)$. The free holes in this case are generated by the photoexcitation process itself and the other free-hole transitions possible at this energy and field range are obscured by the observed bound-hole spectra.

A remarkable crystallographic-dependent anisotropy of the transition energies is observed in the bound-hole spectra, as can be seen in Fig. 14. Over a large portion of the spectrum, the high-field component of the doublet structure is seen to shift to higher field values upon changing sample orientation from $\vec{B}\|\langle 111\rangle$ to $\vec{B}\|\langle 100\rangle$, while the low-field component remains virtually stationary. This behavior is a direct consequence of the anisotropy of the light-hole Landau-level energies, assuming that the binding energies of the excited light-hole acceptor states themselves do not show significant effects of anisotropy. An example of this light-hole anisotropy can be seen in Fig. 15, which shows the energies of the light- and heavy-hole a and b Landau

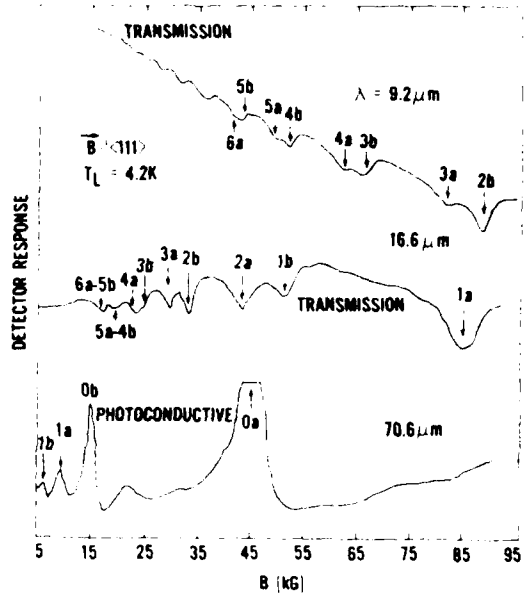

FIG. 13. Wavelength dependence of the bound-hole spectra for $\vec{B}\|\langle 111\rangle$. The high resolution of the spectra allows individual transitions to be tracked over a broad range of photon energies. The numbers refer to the light-hole Landau levels to which the excited impurity states are associated.

Fig. II.20

Fig. II.21

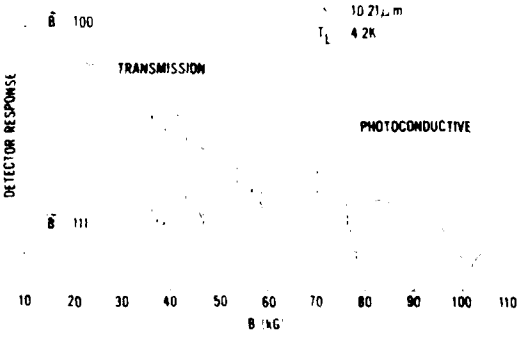

FIG. 14. Bound-hole photoconductive and transmission spectra obtained at 10.21 μm for $\vec{B}\|\langle 111\rangle$ and $\vec{B}\|\langle 100\rangle$. The dashed arrowed lines show how a shift in resonant field position is seen for the higher field component of each doublet, while no shift is evident for the lower field component.

II - 22

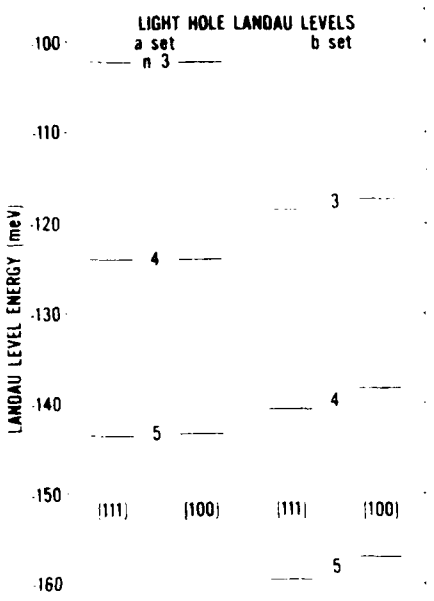

FIG. 15. Diagram of the calculated Landau-level energies using our set of band parameters for $\vec{B} \parallel \langle 111 \rangle$ and $\vec{B} \parallel \langle 100 \rangle$ and for the $n = 3$, 4, and 5 levels showing the effects of light-hole anisotropy. The b set of levels, corresponding to the high-field component of each observed doublet, is seen to show an anisotropy in the transition energy, while the a-set energies for $\vec{B} \parallel \langle 111 \rangle$ and $\vec{B} \parallel \langle 100 \rangle$ remain virtually identical.

Fig. II. 22

ladders for $\vec{B} \parallel \langle 111 \rangle$ and $\vec{B} \parallel \langle 100 \rangle$ at 60 kG. These energies were calculated from the 8×8 band model using the set of band parameters determined in this work (see Table I). It is seen that the b set of light-hole levels corresponds to the high-field (low-energy) component of each doublet and is most sensitive to the effects of anisotropy. It might also be noted that the prediction of this behavior by theory is sensitive to the choice of band parameters and therefore provides another useful constraint in the determination of the band parameters.

A useful method for extracting the zero-field acceptor ground-state binding energy from the low-temperature data is to consider all field contributions to the bound-hole transition energy $\hbar\omega$. This is given by[9,11]

$$\hbar\omega = E_{gs}(0) + \Delta E_{gs}(B) + \epsilon_{lh}^{a,b}(n,B) - E_{es}(B) , \quad (2)$$

where $E_{gs}(0)$ is the zero-field acceptor ground-state binding energy, $\Delta E_{gs}(B)$ is the field-induced shift of the ground state, $\epsilon_{lh}^{a,b}(n,B)$ refers to the energy of the nth light-hole Landau level in ladder a or b, and $E_{es}(B)$ is the binding energy of the excited light-hole acceptor state (final state for the transition). Since values of $\Delta E_{gs}(B)$ and $E_{es}(B)$ are considered to be small, and their difference even smaller, to a first approximation we may neglect their contributions to the transition energy and write

$$\hbar\omega = E_{gs}(0) + \epsilon_{lh}^{a,b}(n,B) \quad (3)$$

Thus the observed transitions can be theoretically fit by simply adding the zero-field binding energy to the light-hole energies calculated using the 8×8 band model.

Figure 16 shows the results obtained by calculating the transition energies for $\vec{B} \parallel \langle 111 \rangle$. We see that excellent agreement between the theoretical predictions of Eq. (3) and our data is achieved over the range of light-hole quantum numbers $n = -1$ to 27 for an extremely large number of data points taken over a wide range of photon energies ($\sim 12-135$ meV) and magnetic fields ($\sim 7-110$ kG). In order to more clearly see the high resolution of the bound-hole spectra, Fig. 17 shows an expanded view of Fig. 16 for $\vec{B} \parallel \langle 111 \rangle$, with $B = 0-20$ kG. From this figure we see that we are able to resolve transitions down to the excited states associated with the $n = 26b$ $27a$ light-hole Landau levels. Figure 18 shows the excellent agreement of the theory to our data (solid dots) for $\vec{B} \parallel \langle 100 \rangle$. In addition it shows the agreement of the theory using our set of band parameters with the only other bound-hole transition data, taken by Grisar *et al.*[9] (open triangles). Here the agreement of theory to data indicates that Cd (or Zn) impurities were evidently present in the sample of Grisar *et al.* since their data fits the transition energies calculated for the impurity transitions. From our analysis, a value of 8.1 ± 0.3 meV was obtained for the ground-state binding energy of the Cd acceptor [$E_{gs}(0)$]. This energy is in general agreement with the values 8.5 ± 0.5 meV (Ref. 43) and 8 meV (Ref. 44) found in the literature. Other values found in the literature are as follows: 9.3 ± 0.6,[10] 9.86,[33] 7,[45] 8.55,[46] and 9.1 meV.[47]

The above analysis assumed that $E_{es}(B)$ and $\Delta E_{gs}(B)$ were negligible compared to the transition energies. This assumption is particularly valid for low magnetic fields and large light-hole quantum number n. However, as suggested by the theoretical analysis of Lin-Chung and Henvis,[17] the binding energies of the p-like excited states increase monotonically with increasing B and decreasing n. Therefore, the fit of the bound-hole data to theory discussed above was accomplished by adjusting $E_{gs}(0)$ such that the low-field, high-energy data fit best, as seen in Fig. 17. Any deviation seen between theory and data at high field and low Landau quantum num-

II-23

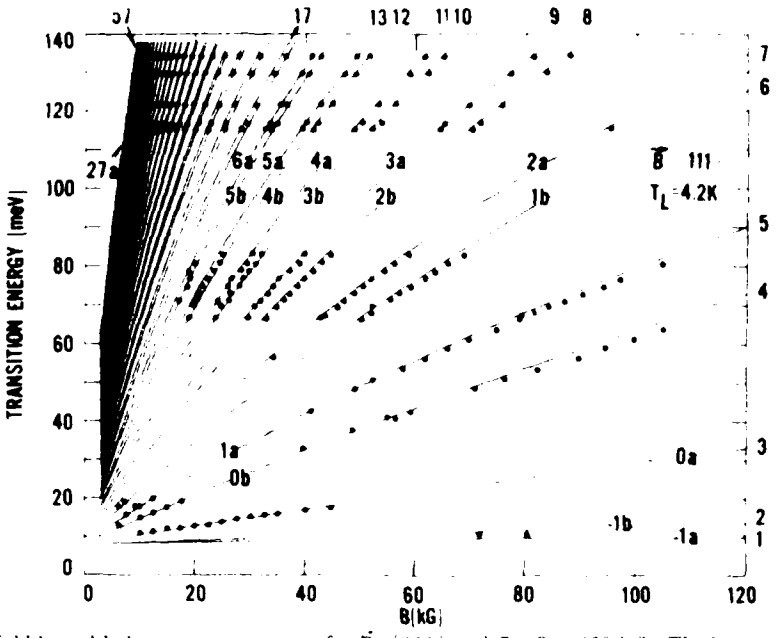

Fig. II.23

FIG. 16. Low-field bound-hole transition energies for $\vec{B}$ (111) and $B = 0$ to 120 kG. The lines represent energies calculated using the 8×8 band model and a zero-field intercept [$E_{g_c}(0)$] of 8.1 meV. Dots represent observed bound-hole transition energies. The numbers on the lines identify the light-hole Landau levels and the numbers on the borders refer to bound-hole transition assignments (e.g., 1, ground acceptor level to $a^+(-1)$; 2, ground acceptor level to $b^+(-1)$, etc.).

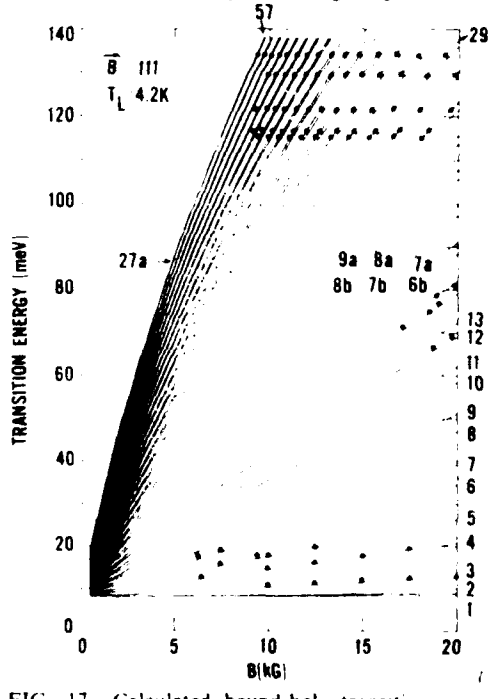

FIG. 17. Calculated bound-hole transition energies, $\vec{B}$ (111) and $B = 0$ to 20 kG (solid lines) and observed bound-hole transitions (dots). The numbers on the lines identify the light-hole Landau levels and the numbers on the borders refer to bound-hole transition assignments (see Fig. 16).

Fig. II.24

bers would then be a consequence of the non-negligible value for E_{c_c} or ΔE_{g_c}. A deviation is indeed observed, as seen in Fig. 16. At magnetic fields greater than 50 kG, we can see slight energy differences between theory and data of 1–3 meV for transitions to excited states identified by light-hole quantum numbers $-1a(a^+(-1))$ to $1a(a^+(1))$. Since the difference is observable, we might be able to determine the final states of the bound-hole transitions. Figure 19 shows an energy-level diagram for the light-hole acceptor states associated with the light-hole Landau levels $0b(b^+(0))$ and $1a(a^+(1))$ in InSb at $B = 100$ kG. The energies of the excited states were calculated in a manner similar to that presented by Lin-Chung and Henvis[37,48] and the energies of the light-hole continuum levels were calculated using our band parameters and the 8×8 band model. The arrows show allowed transitions between the *s*-like acceptor ground states and *p*-like impurity excited states associated with the light-hole Landau ladders *a* and *b*. Since unpolarized light was used, containing both σ and π components, and the sample was mounted in the Voigt configuration for the monochromator measurements, contributions from the $\Delta\lambda$ odd and $\Delta\lambda$ even transitions would be expected. This appears to be the case; Table II lists a comparison of theoretically calculated and experimentally observed transition energies for high-field data. In this calculation the value of

II - 24

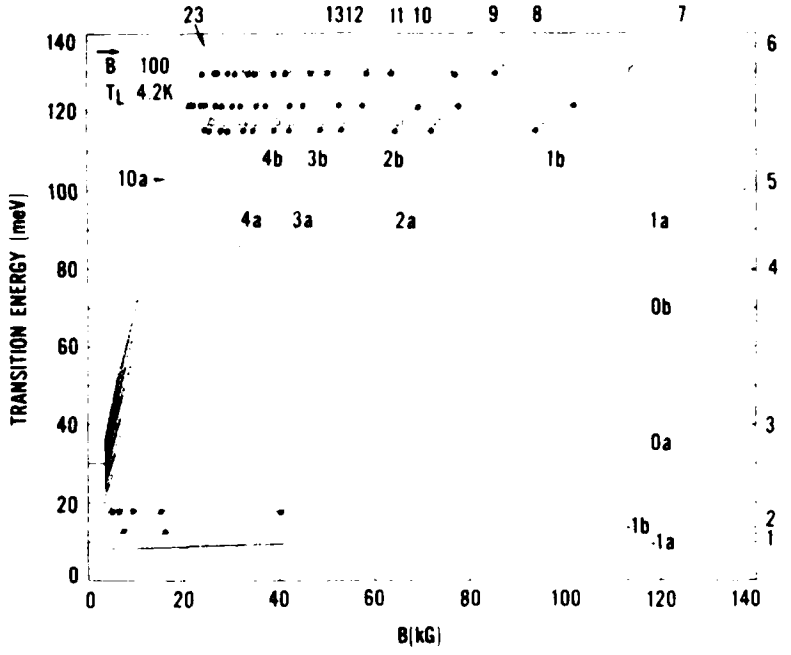

FIG. 18. Calculated bound-hole transition energies $\vec{B} \parallel \langle 100 \rangle$ and $B = 0$ to 140 kG (solid lines) and our observed bound-hole transitions (dots). The open triangles represent the data of Grisar *et al.* (Ref. 9) obtained at 12 K. The numbers on the lines identify the light-hole Landau levels and the numbers on the borders refer to bound-hole transition assignments (see Fig. 16).

Fig. II.25

ΔE_{gs} was still assumed to be negligible. From the comparison we see that the observed transition energies always fall in the energy range between the transitions to the two excited p states, indicating that the observed spectra is probably due to unresolved transitions between the ground-state acceptor level and the two excited p states.

V. CONCLUSIONS

High-resolution magneto-optical techniques have now been extended to the study of valence-band transitions in p-type InSb, yielding new information necessary to the determination of band model parameters for InSb. New free-hole combined-resonance and bound-hole acceptor transitions are observed for $\vec{B} \parallel \langle 111 \rangle$ and $\vec{B} \parallel \langle 100 \rangle$, clearly displaying the effects of the valence-band anisotropy. The free-hole data has been analyzed along with extensive conduction band and two-photon interband data using a modified Pidgeon and Brown band model, resulting in a set of band parameters for InSb that describes a wide variety of experiments. In particular, the set of band parameters obtained in this study has recently been used by Goodwin and Seiler[29] to describe an extensive set of intra-conduction-band data.

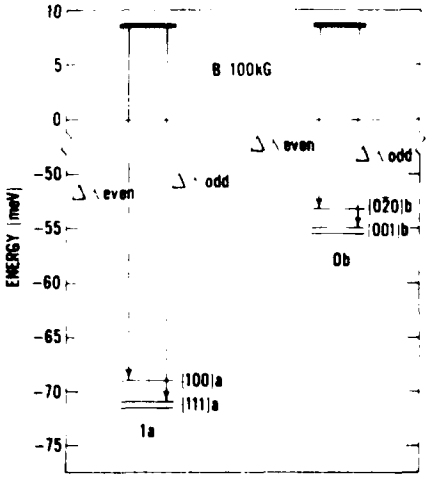

FIG. 19. Diagram of allowed transitions between the heavy-hole (s-like) acceptor ground state and the light-hole (p-like) excited impurity states for $n = 0b$ and $1a$ at $B = 100$ kG. The notation and selection rules are those of Lin-Chung and Henvis (Ref. 37). The energies of the excited states were calculated in a manner similar to that given by the theory of Lin-Chung and Henvis, and the energies of the light-hole continuum levels were calculated using the 8×8 band model. The transitions shown correspond to bound-hole transitions 4 and 5 (see Fig. 16).

Fig. II.26

II - 25

TABLE II. Comparison of bound-hole transition energies calculated using Eq. (2) [assuming $\Delta E_{gs}(B) \simeq 0$] and E_{∞} values obtained from Lin-Chung (Ref. 48) with experimentally observed transition energies.

B (T)	E_{gs} (meV)	$E_{th}^{a,b}$ (meV)	(020)b	$E_{gs} + E_{th}^{a,b}$ (001)b	E_{∞} (meV) (111)a	(100)a	Experimental (meV)
7.09	8.1	41.1	47.2	48.7			48.4
8.24	8.1	46.9	52.8	54.5			53.5
8.95	8.1	50.5	56.3	58.6			56.4
9.02	8.1	66.1			71.7	73.6	72.9
9.40	8.1	68.2			73.8	75.8	74.7
9.45	8.1	52.9	58.7	60.8			58.9
9.67	8.1	69.7			75.3	77.3	76.6
9.95	8.1	55.3	60.8	62.6			61.3
10.45	8.1	74.1			79.5	82.1	80.7

Table II.2

The high resolution of the bound-hole spectra has allowed determination of the Cd acceptor ground-state binding energy in InSb as well as provided experimental evidence suitable for studying the behavior of excited acceptor states in the presence of a magnetic field. High-field data has been compared to theoretical calculations for the excited states, resulting in a qualitative agreement between theory and experiment. In addition, recent measurements[53] on Au-doped p-type InSb using the same high-resolution magneto-optical techniques have shown directly that the methods developed in this study can be used to detect and identify impurities in semiconductor materials.

ACKNOWLEDGMENTS

We wish to express our gratitude to Dr. Margaret H. Weiler of Massachusetts Institute of Technology for her assistance with the band-model calculations and to Dr. P. J. Lin-Chung of Naval Research Laboratory for helpful discussions. This work has been supported in part by the U. S. Office of Naval Research.

[1]C. R. Pidgeon and R. N. Brown, Phys. Rev. 146, 575 (1966).
[2]M. W. Weiler, J. Magn. Magn. Mater. 11, 131 (1979).
[3]Al. L. Efros, L. M. Kanskaya, S. I. Kokhanovskii, and R. P. Seysyan, Solid State Commun. 43, 613 (1982).
[4]M. L. A. Robinson, Phys. Rev. Lett. 17, 963 (1966).
[5]D. M. S. Bagguley, M. L. A. Robinson, and R. A. Stradling, Phys. Lett. 6, 143 (1963).
[6]K. J. Button, B. Lax, and C. C. Bradley, Phys. Rev. Lett. 21, 250 (1968).
[7]R. Ranvaud, Ph.D. Dissertation, Brown University, 1973 (unpublished), available from University Microfilms, P. O. Box 1764, Ann Arbor, MI 48106, order No. 74-3064.
[8]R. Ranvaud, H. R. Trebin, U. Rossler, and F. H. Pollak, Phys. Rev. B 20, 701 (1979); and H. R. Trebin, U. Rossler, and R. Ranvaud, *ibid.* 20, 686 (1979).
[9]R. Grisar, H. Wachernig, G. Bauer, J. Wlasak, J. Kowalski, and W. Zawadzki, Phys. Rev. B 18, 4355 (1978).
[10]R. Kaplan, Phys. Rev. Lett. 20, 329 (1968).
[11]C. L. Littler, D. G. Seiler, R. Kaplan, R. J. Wagner, and W. Zawadzki, Solid State Commun. 37, 783 (1981).
[12]R. Kaplan, R. J. Wagner, D. G. Seiler, C. L. Littler, and M. H. Weiler, in *Proceedings of the Physics of Narrow Gap Semiconductors, Linz, Austria, 1981*, edited by E. Gornik, H. Heinrich, and L. Palmetschofer (Springer, New York, 1982), p. 188.
[13]K. Suzuki and J. C. Hensel, Phys. Rev. B 9, 4184 (1974).
[14]W. Zawadzki, *New Developments in Semiconductors*, edited by P. R. Wallace, R. Harris and M. J. Zuckermann (Noordhoff, Heyden, 1973), p. 441.
[15]M. H. Weiler, R. L. Aggarwal, and B. Lax, Phys. Rev. B 17, 3269 (1978).
[16]D. G. Seiler, M. W. Goodwin, and M. H. Weiler, Phys. Rev. B 23, 6806 (1981).
[17]M. W. Goodwin, D. G. Seiler, and M. H. Weiler, Phys. Rev. B 25, 6300 (1982).
[18]B. D. McCombe, S. G. Bishop, and R. Kaplan, Phys. Rev. Lett. 18, 748 (1967).
[19]B. D. McCombe, Phys. Rev. 181, 1206 (1969).
[20]E. J. Johnson and D. H. Dickey, Phys. Rev. B 1, 2676 (1970).
[21]K. Lee, B.S. thesis, Massachusetts Institute of Technology, 1976 (unpublished).
[22]M. H. Weiler, R. L. Aggarwal, and B. Lax, Solid State Commun. 14, 229 (1974).

II - 26

[23]B. D. McCombe and R. J. Wagner, Phys. Rev. B 4, 1285 (1971).
[24]F. Kucher, R. Meisels, and M. Kriechbaum, in *Proceedings of the Physics of Narrow Gap Semiconductors, Linz, Austria, 1981*, edited by E. Gornik, H. Heinrich, and L. Palmetschofer (Springer, New York, 1982), p. 197.
[25]G. Bemski, Phys. Rev. Lett. 4, 62 (1960).
[26]R. C. Enck, A. L. Saleh, and H. F. Fan, Phys. Rev. 182, 790 (1969).
[27]S. Morita, S. Takano, H. Kawamura, J. Phys. Soc. Jpn. 39, 1040 (1975).
[28]V. I. Ivanov-Omskii, K. I. Korovin, E. M. Shereghii, Phys. Status Solidi (B) 90, 11 (1978).
[29]M. W. Goodwin and D. G. Seiler, Phys. Rev. B 27, 3451 (1983).
[30]W. Engeler, H. Levinstein, and C. Stannard, Jr., Phys. Rev. Lett. 7, 62 (1961).
[31]W. Engeler, H. Levinstein, and C. Stannard, Jr., J. Phys. Chem. Solids, 22, 249 (1961).
[32]I. Ismailov, D. N. Nasledov, M. A. Sipouskaya, and Yu. S. Smetannikova, Fiz. Tekh. Poluprovdn. 3, 1386 (1969) [Sov. Phys.—Semicond. 3, 1154 (1970)].
[33]R. Kaplan, Solid State Commun. 12, 191 (1973).
[34]R. F. Blunt, Bull. Am. Phys. Soc. II 3, 115 (1958).
[35]I. N. Kurilenko, L. B. Lituak-Gorskaya, and G. E. Lugovaya, Fiz. Tekh. Poluprovdn. 13, 1556 (1979) [Sov. Phys.—Semicond. 13, 906 (1979)].
[36]N. O. Lipari and A. Baldereschi, Phys. Rev. Lett. 25, 1660 (1970).
[37]P. J. Lin-Chung and B. W. Henvis, Phys. Rev. B 12, 630 (1975).
[38]H. Hasegawa and R. E. Howard, J. Phys. Chem. Solids 21, 179 (1961).
[39]R. J. Wagner and G. A. Prinz, Appl. Opt. 10, 2060 (1971).
[40]H. Kahlert and D. G. Seiler, Rev. Sci. Instrum. 48, 1017 (1977).
[41]R. L. Aggarwal, in *Semiconductors and Semimetals*, edited by R. K. Willardson and A. C. Beer (Academic, New York, 1972), Vol. 9, p. 151.
[42]C. R. Pidgeon and S. H. Groves, Phys. Rev. 186, 824 (1969).
[43]E. J. Johnson and H. Y. Fan, Phys. Rev. 139, 1991 (1965).
[44]I. M. Ismailov, D. N. Nasledov, and Yu. S. Smetannikova, Fiz. Tekh. Poluprovdn. 2, 901 (1967) [Sov. Phys.—Semicond. 2, 754 (1968)].
[45]H. J. Hrostowski, F. J. Morin, T. H. Geballe, and G. H. Wheatley, Phys. Rev. 100, 1672 (1965).
[46]P. Lawaetz, Phys. Rev. B 4, 3460 (1971).
[47]V. N. Murzin, A. I. Demeshina, and L. M. Umarov, Fiz. Tekh. Poluprovdn. 6, 488 (1971) [Sov. Phys.—Semicond. 3, 367 (1969)]; 3, 434 (1968) [6, 419 (1972)].
[48]P. J. Lin-Chung (private communication).
[49]S. Zwerdling, W. H. Kleiner, and J. P. Theriault, J. Appl. Phys. 32, 2118 (1961).
[50]A. P. Roth, and E. Fortin, Phys. Rev. B 18, 4200 (1978).
[51]R. A. Isaacson, Phys. Rev. 169, 312 (1969).
[52]C. J. Summers, R. B. Dennis, B. S. Wherrett, P. G. Harper, and S. D. Smith, Phys. Rev. 170, 755 (1968).
[53]C. L. Littler, D. G. Seiler, R. Kaplan, and R. J. Wagner, Appl. Phys. Lett. 41, 880 (1982).

III. INTERACTION OF CO_2 LASER RADIATION WITH n-InSb - DEEP LEVEL AND FREE CARRIER EFFECTS

In this section we present the results of a study involving optical transitions from deep levels to the conduction band Landau levels. A new experimental technique is presented for the detection of deep levels which should help in semiconductor characterization using laser spectroscopy methods. Intraconduction band transitions were also seen in the photoconductive spectra and extensive investigations carried out. In what follows two major papers are reproduced. More extensive details can be seen in Dr. M. W. Goodwin's Ph.D. thesis.

III -2

Laser-induced magneto-optical transitions from deep levels in *n*-InSb

D. G. Seiler and M. W. Goodwin[a)]
Center for Applied Quantum Electronics, Department of Physics, North Texas State University, Denton, Texas 76203

(Received 15 June 1982; accepted for publication 23 July 1982)

We present a novel means for detecting and studying deep levels in high purity *n*-InSb with extremely sensitive magneto-optical techniques, combining sampling oscilloscope and lock-in amplifier methods. Oscillatory photoconductivity behavior in InSb has been investigated previously under a variety of conditions and in both *n*- and *p*-type samples. However, to our knowledge, no evidence has ever been presented for oscillatory magnetophotoconductivity (MPC) in *n*-InSb (or in any other semiconductor) caused by electron transitions from deep levels to the conduction band Landau levels. These studies allow a more precise determination and sensitive detection of deep levels through a more direct means than has been previously possible. We observe a resonant structure in the CO_2 laser-induced MPC at liquid helium temperatures in *n*-InSb which is periodic in the inverse magnetic field and whose amplitude increases with the magnetic field. This behavior is typical for resonances involving Landau levels. The effect of lattice temperature, laser intensity, photon energy, and light polarization on the MPC is studied. The amplitude of this resonant structure saturates at moderate intensities (~ 30 W/cm^2) and shows no polarization dependence (for $\mathbf{e}\perp\mathbf{B}$ and $\mathbf{e}\parallel\mathbf{B}$). These and other results indicate the presence of a deep level $\simeq 74$ meV below the conduction band edge ($E_g \simeq 235$ meV). Using a CO laser, a resonant structure is also observed from another deep level, $\simeq 170$ meV below the band edge. These deep levels could be caused by either lattice defects or residual impurities. Other structures observed with the CO_2 laser are identified with LO phonon-assisted cyclotron resonance harmonic transitions within the conduction band, and two-photon magnetoabsorption interband transitions.

PACS numbers: 78.20.Ls, 72.40. + w, 78.50.Ge, 71.55.Fr

I. INTRODUCTION AND BACKGROUND

The properties of deep levels in semiconductors are receiving a great deal of attention, in part because they are now a major limiting factor affecting device performance and reliability. Unfortunately, deep levels are rather poorly understood. These deep levels are associated with a potential that is short range in nature and, hence, effective mass theory becomes inadequate in describing them. There are also many difficulties in the detection and identification of deep levels. Consequently, it is highly desirable to develop new experimental techniques for the detection and study of deep levels which could aid in their characterization and theoretical understanding. In this paper we present a novel method of studying deep levels in *n*-InSb using high resolution and extremely sensitive magneto-optical techniques.

Evidence is presented for two deep levels in high purity *n*-InSb (band gap $\simeq 235$ meV at 4 K): (1) using a CO_2 laser a level $\simeq 74$ meV below the conduction band edge has been identified; (2) using a CO laser another level $\simeq 170$ meV below the conduction band has also been observed.

Photoconductivity oscillations in InSb have been investigated previously under a variety of conditions and samples. In *p*-type InSb at a zero magnetic field, extrinsic behavior has been observed due to the excitation of a hole from the impurity state to the valence band with the emission of one or more LO phonons.[1,2] With the application of a magnetic field to *p*-InSb it has been possible to more precisely investigate bound hole excitations,[3,4] and, in addition, to observe and study free hole transitions.[5,6] Intrinsic photoconductivity oscillations have also been observed in *p*-InSb due to valence-band to conduction-band transitions.[7] For *n*-type InSb most photoconductive work in a magnetic field has centered on the shallow donor levels that are nearly degenerate with the conduction band or on free carrier properties. Intrinsic photoconductivity has also been observed in *n*-InSb due to band to band transitions.[8,9] However, to our knowledge, no one has previously presented evidence for oscillatory photoconductivity in *n*-InSb caused by electron transitions from deep levels to the conduction band. These magneto-optical studies thus allow a more precise determination and detection of deep levels through a more direct means than has previously been possible.

The effects of deep levels usually show up most predominantly in samples with low carrier concentrations. It is just this experimental condition that makes photoconductivity measurements extremely powerful in the detection of weak magneto-optical transitions. Because of the originally low number of thermal equilibrium electrons in the conduction band, it is rather easy to detect a small percentage of photoexcited carriers. In addition, at low temperatures electrons excited high into the conduction band give rise to an enhanced mobility. Free carrier absorption, which can mask transitions from the deep levels, is also minimized by the low concentrations. Figure 1 shows the magneto-optical transitions originating from deep levels within the forbidden gap

a) Present address: Texas Instruments, Inc., Dallas, Texas 75265

 0021-8979/82/117505-11$02.40

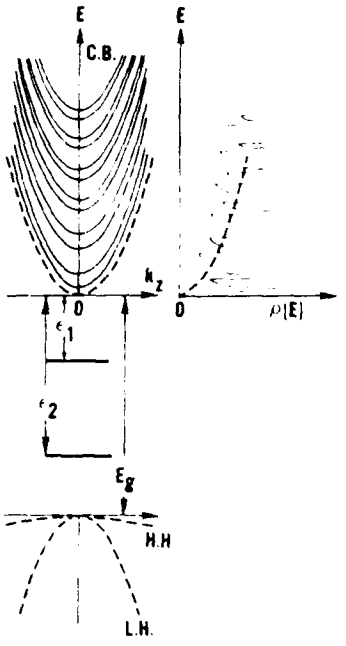

FIG. 1. Schematic representation of the origin of the resonant magneto-optical transitions from two deep levels in InSb. At zero magnetic field the dashed lines show the E vs k behavior of the light and heavy holes and the conduction band, as well as the variation of the density of states $\rho(E)$. Upon application of a magnetic field, the density of states exhibits the well-known singularities due to the Landau levels.

Fig. III.1

region. At $B = 0$ direct transitions from these deep levels at the CO_2 ($\sim$115–135 meV) and CO (215–225 meV) laser energies can not take place. Nonresonant transitions from these levels with the assistance of phonons or impurities, free carrier absorption, or even two-photon absorption effects may be present in some combination. However, the application of a magnetic field creates the well known Landau-level structure and opens up the possibility of direct transitions from the deep to Landau levels. The resonant photoconductivity structure would be expected to follow the final electron density of states which has singularities at the energies corresponding to the bottom of each Landau level. Energy level broadening removes these singularities but still leaves peaks in the density of states. Consequently, for a fixed photon energy, the number of carriers and/or the mobility and hence conductivity resonantly increases as the magnetic field is increased.

II. EXPERIMENTAL WORK

The samples used were cut from bulk grown n-type InSb having a concentration of 9×10^{13} cm^{-3} and a Hall mobility of 400 000 cm^2/V s at 77 K. The front surface was optically polished with 0.3 μm Al_2O_3 polishing grit. The rear surface was left rough to eliminate multiple reflections and etalon effects. The sample dimensions were $5.5\times1.5\times0.2$ mm thick. Two current contacts and two potential contacts were made using pure indium. The sample was illuminated with a 20-μs wide pulse produced by mechanically chopping a beam from either a cw CO_2 or a CO laser at a repetition rate of 1700 Hz. The 3% duty cycle prevents lattice heating by the laser. The grating-tuned CO_2 laser is a flowing gas, electric discharge cw laser capable of single line outputs of several watts on many lines between 9.20 to 10.8 μm.

The cw CO laser is a sealed off, electric discharge laser capable of up to 2 W on a number of lines between 5.15 and 5.8 μm. The beam is focused onto the sample so that the region between the potential probes is as uniformly illuminated as possible. A He-Ne laser is used with a silicon PIN photodiode to produce a trigger pulse for the sampling oscilloscope. Calibrated filters are used along with an absorption cell filled with propylene of variable pressure to attenuate the laser power. Simultaneous use of both sampling oscilloscope and lock-in amplifier techniques provided an enhanced signal-to-noise ratio in observing the weak magneto-optical structure. A constant dc current is applied to the sample while an ac magnetic field of 150 G modulates the sample conductivity at 43 Hz. The signal at the sample potential contacts, produced by the laser pulse and the field modulation is fed through a high impedance differential amplifier into a sampling oscilloscope. The output of the sampling oscilloscope is then fed into a lock-in amplifier tuned to 86 Hz which results in a lock-in detector response proportional to the second derivative of the photoconductive signal.

III. RESULTS

A portion of our studies with the CO_2 laser is shown in Fig. 2 for various wavelengths. The detector response is proportional to the second derivative of the photoinduced change in magnetoresistance. The numbers correspond to distinct resonances for each wavelength. Doublets, labeled with plus and minus symbols, are resolved at the higher magnetic fields. The minima positions correspond to minima in the resistance or maxima in the conductivity and are seen to

Fig. III.2

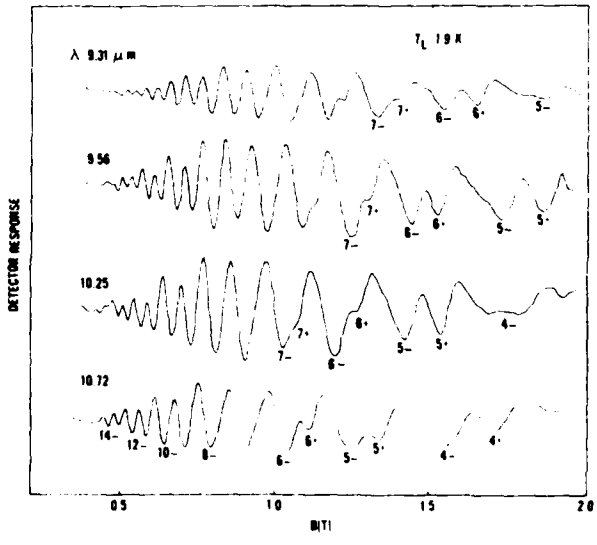

FIG. 2. Wavelength dependence of the DLCRH (arising from level E_1 shown in Table I) structure for e||B. The numbers correspond to the final state conduction band Landau level and + and − are the spin-up and spin-down states, respectively. The applied electric field is $\simeq$1 V/cm.

shift to higher magnetic fields as the photon energy increases. The envelope of the resonant structure depends upon the ac magnetic field modulation technique; the actual amplitudes of the resonant structure increase with magnetic field. The magnetic field positions of the structure are periodic in inverse magnetic field. These facts suggest some type of resonance behavior involving Landau levels. A two-photon magnetoabsorption (TPMA) structure[10,11] is absent in the spectra because the data was taken with low laser powers ($\simeq$30 mW) where TMPA effects are weak, and for **e**$\|$**B** where TPMA is approximately a factor of 4 weaker than for **e**$\perp$**B**. Phonon-assisted cyclotron resonance harmonic transitions[12-18] (PACRH) within the conduction band are also absent because of the **e**$\|$**B** polarization configuration where they are not allowed. This resonant structure shown in Fig. 2 has not been extensively studied since it is a weak magneto-optical effect, observable with only the best high-resolution signal processing techniques. It is our purpose to show that the structure shown in Fig. 2 arises from deep level cyclotron resonance harmonic (DLCRH) transitions originating from a deep level within the band gap of InSb.

There is a distinct contrast between the TPMA structure and the DLCRH structure, as shown in Fig. 3 for **e**$\|$**B** polarization. Here, reproductions of the lock-in detector output versus inverse magnetic field are given for various relative peak incident laser powers at 9.56 μm. The laser power was attenuated with calibrated filters and an absorption cell filled with propylene of variable pressures. The top trace has a peak incident power of $\simeq$1.4 W, while the lower traces were taken with successively smaller values of P_R. The bottom trace was recorded with the laser beam physically blocked. As P_R is increased a series of weak resonant resistivity minima develop which is the same structure as that presented in Fig. 2. The photoconductive amplitude of this series saturates with increasing laser power. With continued increasing laser power another series of very sharply defined resonant resistivity minima develops, which has been shown to arise from TPMA,[10] and at the higher laser powers this structure clearly dominates the photoconductive spectra. Both sets of resonant structures are periodic in inverse magnetic field. The envelope of the resonant structure depends upon the ac field modulation technique, as mentioned previously.

Fig. III.3

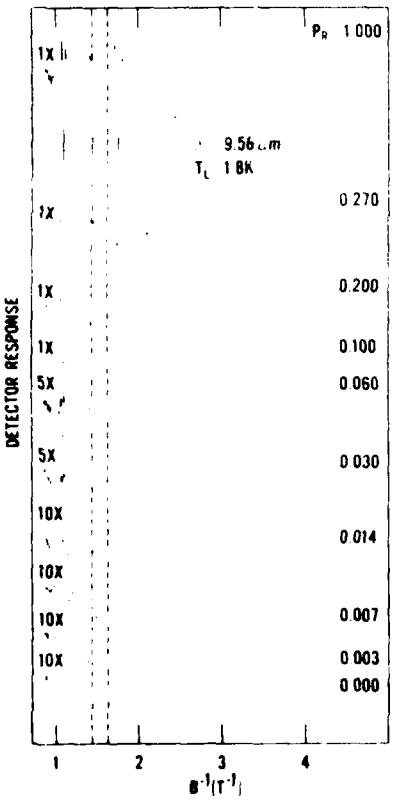

FIG. 3. Photoconductive spectra for different relative peak incident CO_2 laser powers P_R. Note the gain setting on the left. For P_R = 1, the peak incident power is $\sim$1.4 W with a beam of 1.5-mm 1/e^2 intensity diameter. The dashed vertical lines are drawn at the magnetic field positions of a TPMA (high powers) and a DLCRH (lower powers) resonance as discussed in the text and illustrate the fact that the magnetic field positions are independent of laser power.

A DLCRH structure exists for the entire spectral range of the CO_2 laser, while a TPMA structure has a definite threshold at about 10.33 μm. Therefore, most of the experiments on DLCRH were done using wavelengths above 10.33 μm to avoid confusing the spectra with the TPMA structure.

The power dependence of a particular transition in the DLCRH structure is shown in Fig. 4 for the wavelength λ = 10.53 μm. The amplitude A was normalized to the highest power amplitude A_0. As shown, the amplitude of the structure increases approximately linearly to a peak incident power of about 0.15 W. With greater powers the amplitude saturates ($\simeq$0.20 W) and decreases in size. The same type of behavior is also characteristic of the other transitions in the DLCRH spectra. The TPMA spectra exhibits a different power dependence in that the amplitude has a parabolic dependence at low powers and does not show a saturation and decrease in size with increasing powers available from the cw laser. The amplitude of the DLCRH structure also rises fas-

Fig. III.4

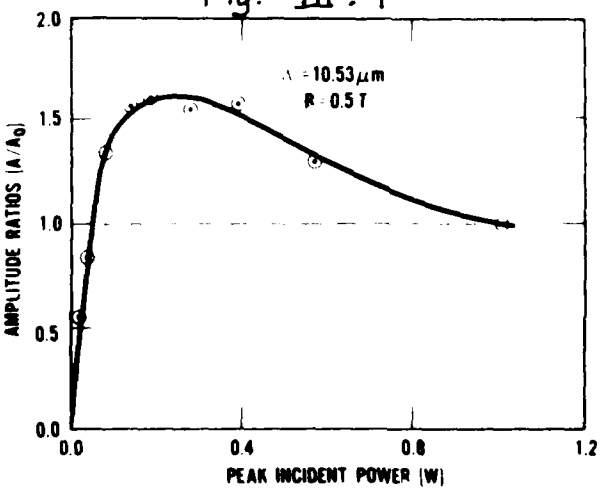

FIG. 4. Relative power dependence of the amplitude of a DLCRH transitions at $B \sim 0.5$ T and for **e**$\|$**B** and λ = 10.53 μm. The amplitude is normalized to the highest power amplitude. Note the initial linear behavior.

ter with power than the TPMA structure until saturation occurs. The rise and saturation of the amplitude with power can be easily described by a simple rate equation analysis of a two-level system. However, the two-level analysis can not predict which model of the two presented here is correct. The rise of the amplitude would be due to the generation of photoexcited carriers by the absorption of the incident light. In a quasi-steady-state condition the saturation would be due to the fact that the generation rate of carriers into the final state would be equal to the recombination or scattering rate out.

This DLCRH structure was apparently first observed in n-InSb by Morita *et al.*[19] for only one photon energy (117 meV) of the CO_2 laser. They observed resonances in the magnetophotoconductivity for samples ($n \simeq 10^{14}$ cm^{-3}) at liquid helium temperaures. They attributed this structure to a photoinduced sum of the normal, spin-flip, and two-phonon magnetophonon effect. The magnetophonon effect in n-InSb is usually only observable at temperatures near or above that of liquid nitrogen. Under hot electron conditions it can be seen at liquid helium lattice temperatures. The presence of these resonances at 4.2 K was then attributed to photoinduced hot electron magnetophonon effects. The exact mechanism which caused the spin-flip and two-phonon resonances was not clear. The magnetophonon model of Morita *et al.* cannot predict the observed shift of the structure with incident photon energy, because the magnetic field positions of the magnetophonon resonances essentially depend only upon the energy of the LO phonons, which is independent of the photon energy. We thus have to look for other explanations of this resonant behavior. The only possibilities are that these effects arise from some kind of intraconduction band processes (model I) or from transitions originating from deep levels within the forbidden gap (model II). Specifically, we now look at Model I, which we have previously used to explain these effects.[20,21]

Model I: Three-phonon assisted cyclotron and combined resonance harmonic transitions

Figure 5 shows how the resonance positions shift in magnetic field as the photon energy of the laser is varied. As

Fig. III.5

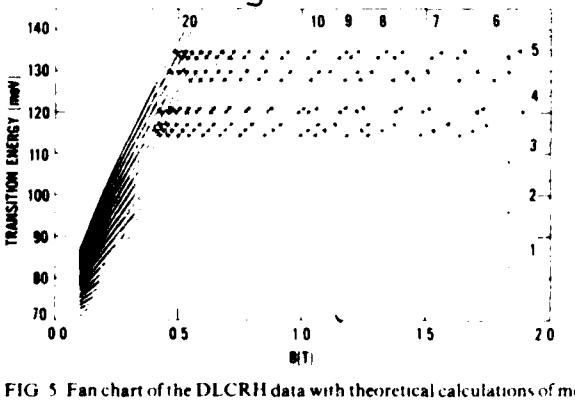

FIG. 5. Fan chart of the DLCRH data with theoretical calculations of model I discussed in the text. The intercept was adjusted to 70 meV. The numbers are the final state Landau level and + and − are the spin-up and spin-down states, respectively.

seen in this "fan chart," and in the raw data shown in Fig. 2, the structure shifts toward higher magnetic fields as the photon energy increases. The lines represent theoretical calculations from a model in which the electrons in the lowest spin-up $n = 0$ Landau level are excited by photon absorption to some other higher energy Landau level, either the spin-up (cyclotron harmonic) or spin-down (combined harmonic) state. This could be a probable absorption mechanism, because at these low electric fields most of the electrons reside in the lowest Landau level.[22] The energies of the conduction band Landau levels were calculated with a modified Pidgeon-Brown 8×8 band model using the following set of band parameters: $E_g = 0.2352$ eV; $E_p = 23.2$ eV; $\Delta = 0.803$ eV; $\gamma_1 = 3.24$, $\gamma_2 = 0.20$, $\gamma_3 = 0.90$; $\kappa = -1.3$; $F = -0.20$; $q = 0$; $N_1 = -0.55$. This same set describes a wide variety of other magneto-optical experiments: intravalence band, intraconduction band, and two-photon interband.

With the period and magnetic field positions of the resonant structure shown in Fig. 5, a fit of the transition energies to the data was not possible with a model in which the electron is simply photoexcited from the lowest energy state to some other state at a photon energy $\hbar\omega$ higher. However, a fairly good fit was found when the energy intercept at $B = 0$ was adjusted to be 70 instead of 0 meV, and when the transition energies were calculated with known band parameters for InSb. Since PACRH in InSb is well known for one LO phonon-assisted transition, the energy intercept (70 meV) could be interpreted as the amount of energy lost to a multiple emission of LO phonons by the photoexcited electrons. The dominant electron-phonon interaction is polar optical scattering. From energy conservation this can be written as

$$\hbar\omega = E^{+}_{\pm}(n) - E^{+}_{\pm}(0) + m\hbar\omega_0, \tag{1}$$

where $E^{+}_{\pm}(n)$ is the energy of either the spin-up (+) or spin-down (−) state of the n_{th} Landau level of the conduction band and m the number of LO phonons emitted in the transition. The energy of the LO phonon is known to be approximately 24.4 meV, thus making the number m of emitted LO phonons from the equation $m\hbar\omega_0 = 70$ meV to be nearest three. The calculated LO phonon energy would therefore be 23.3 meV, which is outside the uncertainty of 24.4 ± 0.3 meV of Johnson and Dickey[14] and the 24.4 ± 0.2 meV determination from our PACRH studies.[18]

Multiple phonon interactions have been observed in "pinning" or level crossing effects in InSb.[17] Several combinations of two-phonon, optical, and acoustic interactions were used to model a variety of pinning processes.[15] A very weak two-LO phonon-assisted cyclotron resonance harmonic transition was also reported by Morita *et al.*[16] However, only one small peak in the photoresponse of a sample of InSb was observed at one photon energy (117 meV) by Morita *et al.*

The three-phonon assisted cyclotron and combined harmonic transitions proposed by model I can be described by a transition rate which is proportional to the square of fourth-order perturbation theory matrix elements.[20] Such a matrix element can be written as

III - 6

$$M_n = \sum_{\alpha,\beta,\gamma} \frac{\langle f|H_L|\gamma\rangle\langle\gamma|H_L|\beta\rangle\langle\beta|H_L|\alpha\rangle\langle\alpha|H_R|i\rangle}{(E_i - \epsilon_\gamma - 2\hbar\omega_0)(E_i - \epsilon_\beta - \hbar\omega_0)(E_i - \epsilon_\alpha)}, \quad (2)$$

where the sum is over all intermediate states α,β,γ, and $E_i = \epsilon_i + \hbar\omega$. The energy of the electron in state α is ϵ_α, etc. There are three other terms similar to Eq. (2) in which one or more phonons are emitted before the photon is absorbed. This type of process is expected to be extremely weak, certainly in comparison to one-phonon assisted cyclotron resonance harmonic transitions (PACRH).

Athough there is good overall agreement between theory and data, closer examination of Fig. 5 shows that for low and high magnetic fields the theory does not agree completely with the data. An improvement to the model may be made by including an energy shift in the resonance positions due to polaron and broadening effects.[16] Thus, Eq. (1) could be modified by the following equation:

$$\hbar\omega = E^+_{n,s}(n) - E^-_{n,s}(0) + 3\hbar\omega_0 + \Delta, \quad (3)$$

where Δ takes into account possible shifts in resonance positions due to polaron and broadening effects. No attempt was made to include the term Δ in the calculations shown in Fig. 5.

There are some important aspects which do suggest that model I (a three-phonon assisted cyclotron and combined resonance harmonic effect) may not be adequate in describing the observed resonant structure. The transition matrix element of Eq. (2) predicts an extremely weak resonance effect, much smaller than PACRH and smaller than a two-phonon assisted cyclotron resonance effect. Furthermore, Eq. (2) would predict resonances at energies in which the denominator goes to zero or with broadening considered, becomes very small. No evidence for these resonances in the matrix elements can be seen in the data. The resonance structure does, instead, seem to be described by the final density of states in the conduction band. At no time in the course of this study were two-phonon assisted transitions ever observed. At present, there is no physical reason why one-phonon (PACRH) and three-phonon assisted transitions should occur while two-phonon assisted processes should not. Morita *et al.*[23] much later reinterpreted the DLCRH structure which they originally called a photoinduced magneto-phonon structure with a three-LO-phonon assisted cyclotron and combined resonance harmonic effect similar to model I of this section. However, they could only fit their data with a model in which electrons initially in the higher energy spin-down ($s = -1/2$) state of the $n = 0$ Landau level were photoexcited with the simultaneous emission of three LO phonons to a final state Landau level n of either the spin-up or spin-down state. They could not explain why the transitions should originate from the $n = 0, s = -1/2$ spin state instead of the lower energy $n = 0, s = +1/2$ spin or ground state where a majority of the electrons exist.

As will be shown in the next section, further experiments give results in which a new model must be used for the proper understanding of this resonance data. This new model, model II, appears to be much more consistent with all results presented here and results of previous PACRH experiments.

Model II: Transitions from a deep level

Model I suggests that properties of the DLCRH structure should be similar to those of PACRH, because (1) the electrons which are excited are initially in the same state ($n = 0$ spin-up state) and (2) both mechanisms involve the interaction with phonons. Therefore, a series of experiments was designed and carried out to check the similarity, if any, between the two processes. Morita and Mikoshiba[24] reported that they observed a drastic change in the photoresponse of a sample of *n*-InSb from the DLCRH structure to the PACRH structure after the sample had been exposed to the atmosphere for 40 days. They attributed the change in the photoresponse to a formation of an accumulation layer on the surface, but did not explain the actual mechanism. They also reported that they observed a change when a strong electric field was applied to the sample, but again no specific details were given. We have not observed any of the changes reported by Morita *et al.*

In Fig. 6 the change of the resonant structure from PACRH to DLCRH with increasing current I or electric field is shown for $\mathbf{e}\perp\mathbf{B}$ polarization at a wavelength of 10.65 μm. At ohmic or near ohmic electric fields of 100 mV/cm ($I = 1$ mA in top trace), the observed resonant structure arises from PACRH. For much higher currents and nonohmic electric fields DLCRH is dominant and the PACRH structure has disappeared. The DLCRH structure is clearly present for lower magnetic fields. Traces with $I = 10$ and 20 mA ($\simeq 1.5$ V/cm) show essentially the same DLCRH structure. Thus the DLCRH structure shows essentially no current dependence. This is in sharp contrast to PACRH which is present at low currents but not at high currents where the electric field is nonohmic. Thus, a major difference exists between the PACRH and DLCRH structure with respect to the magnitude of an applied electric field.

One consequence of high or nonohmic electric fields is the heating of the electrons in the conduction band. The electrons initially in the ground state at low fields are redistributed to higher energy states because of changes in the

Fig. III.6

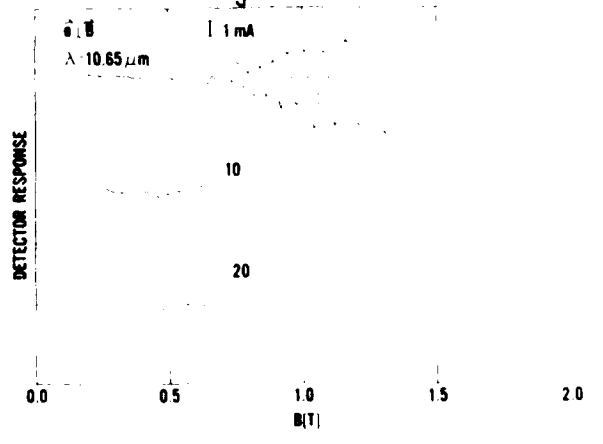

FIG. 6. Current dependence of PACRH and DLCRH showing the transition of the PACRH structure at low currents to DLCRH structure at higher currents. For $I = 1$ and 10 mA the electric field in the sample is ~ 100 and 1 V/cm, respectively.

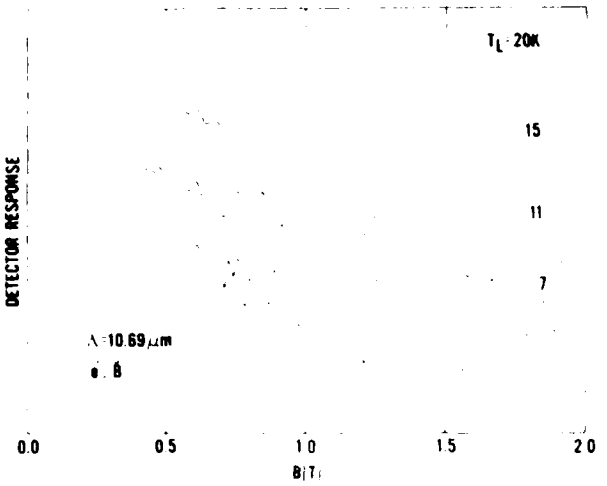

FIG. 7. Lattice temperature dependence of the PACRH structure. The applied electric field is ~200 mV/cm.

Fig. III.7

Boltzmann distribution with applied field. This would explain the decrease in amplitude of the PACRH structure with higher currents or higher electric fields. As the electric field is increased, the carrier distribution is broadened in energy, because of the higher temperatures, and thus causes a redistribution of electrons in the ground state. This also depletes or broadens the initial occupied states for PACRH, thus causing an apparent decrease in the amplitude of the PACRH structure. With higher currents causing even higher electron temperatures, the PACRH structure would disappear below observable levels, as shown in Fig. 6.

The decrease in amplitude of the PACRH structure can be seen more directly from a lattice temperature study. Figure 7 illustrates the dramatic temperature dependence of the PACRH amplitudes. Traces were taken with four different lattice temperatures between 7 and 20 K. The PACRH amplitudes are large at 7 K, but become progressively smaller as the temperature is raised. At 20 K the PACRH structure is so weak that it can hardly be seen. Thus, even over a short temperature range, the distribution of carriers can be changed enough to cause PACRH to become hardly observable. This is in agreement with the current dependence of PACRH shown in Fig. 6. However, the current or electric field dependence of the DLCRH structure shown in Fig. 6 does not appear to agree with the interpretation of a three-phonon assisted cyclotron resonance harmonic effect in model I because at high electron temperatures it is still present. This would suggest that the initial state electrons of DLCRH occupy a different state from that of PACRH.

There is also a marked contrast between the polarization dependence of the PACRH and DLCRH structures. The polarization dependence of PACRH is shown in Fig. 8 for $\mathbf{e}\perp\mathbf{B}$ and $\mathbf{e}\parallel\mathbf{B}$. The bottom trace with $\mathbf{e}\perp\mathbf{B}$ shows the usual PACRH structure. However, in addition there appears to be another resonant structure present. For $\mathbf{e}\parallel\mathbf{B}$, top trace, there are definite differences in the observed spectra. The PACRH structure is absent for $\mathbf{e}\parallel\mathbf{B}$, but a new and different structure which we have identified as DLCRH is now clearly observa-

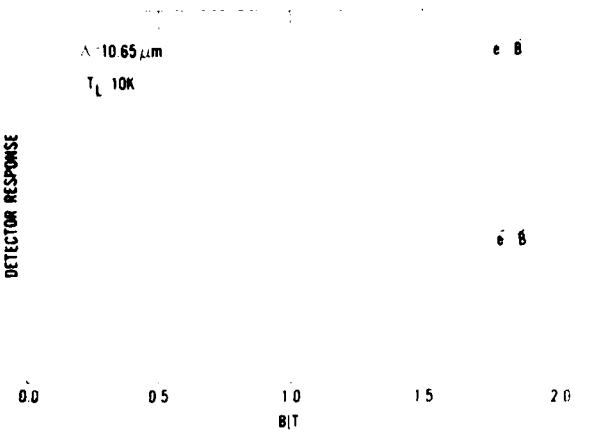

FIG. 8. Polarization dependence of PACRH. The bottom trace for e⊥B shows the usual PACRH structure. The top trace shows an absence of PACRH but shows the DLCRH structure quite clearly. The applied electric field is ~200 mV/cm. Note the strong admixture of PACRH for e⊥B.

Fig. III.8

ble. This DLCRH structure is also present for $\mathbf{e}\perp\mathbf{B}$ and adds to the normal PACRH structure, producing the observed bottom spectra. The purpose of this figure is to show that PACRH is present for $\mathbf{e}\perp\mathbf{B}$, but not for $\mathbf{e}\parallel\mathbf{B}$, in agreement with the photon matrix element selection rules for cyclotron resonance transitions.

The polarization dependence of DLCRH is shown in Fig. 9 for $\mathbf{e}\perp\mathbf{B}$ and $\mathbf{e}\parallel\mathbf{B}$ and for high currents (nonohmic electric fields ~1 V/cm). As can be seen, in contrast to PACRH, DLCRH is present for both polarizations, and does not show any significant difference between them. The small differences in amplitude of the structure is due to slight differences in incident power between the two traces. Thus, DLCRH does not appear to obey any specific selection rules for the optical matrix element part of the transition. Many transitions to all levels of the conduction band seem to be possible. The polarization dependence (or independence) of the DLCRH structure is surprising, if DLCRH is an intraconduction band process. Every known intraconduction band process exhibits some form of polarization dependence, certainly between $\mathbf{e}\perp\mathbf{B}$ and $\mathbf{e}\parallel\mathbf{B}$ where the optically

Fig. III.9

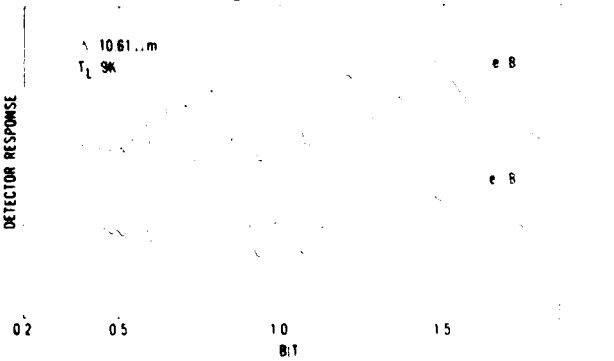

FIG. 9. Polarization dependence of the DLCRH structure. The applied electric field is ~1 V/cm.

III - 9

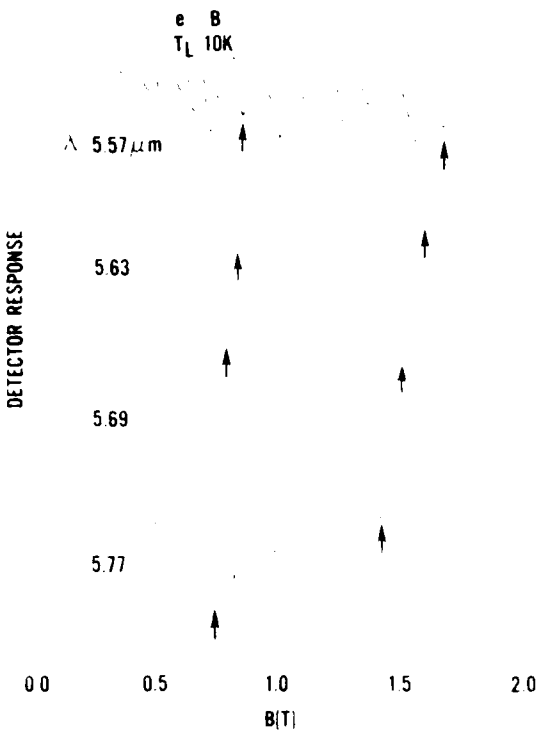

FIG. 10. Wavelength dependence of the CO laser induced deep level transitions. The arrows show the shift of the structure to higher magnetic fields with higher photon energies.

Fig. III.10

allowed selection rules are completely different. Therefore, one might conclude that this is not an intraconduction band process where both the initial and final states are conduction band states (i.e., model I).

In general, the results of the experiments discussed for DLCRH do not agree with the results of PACRH. The electric field, polarization, and temperature dependence all show signifnicant differences, which point to the fact that the initial states for the two processes must be different. These conclusions therefore suggest that model I (in which the initial states for both processes are the same) does not adequately describe the experimental results. Although there is fairly good agreement between the theory and data in Fig. 5 with model I, the good fit must only be coincidental.

The independence of the DLCRH structure on the polarization of the laser with respect to the magnetic field indicates that the initial state is not a state in the conduction band. If it were, the transitions would show some polarization dependence because of optically allowed selection rules. Because of known impurity or defect levels in InSb, it is reasonable to assume that the initial state might be some deep level within the band gap. Photoconductivity and photoelectromagnetic measurements have indicated a midgap donor-like flaw intrinsic to the InSb lattice.[25-27] Several deep impurities, such as gold and silver, have also been found within the band gap of InSb.[28] Thus, an electron in some deep impurity or defect level in the band gap would be photoexcited out of that level into some conduction band Landau level or shallow impurity state attached to the conduction band Landau levels. This would increase the conductivity of the sample just like a mobility increase would (i.e., model I), because the total number of conduction band electrons is increased. Also, since electrons are deposited at high energies in the conduction band, the electron mobility may also increase.

Spectroscopic measurements of a sample from the same lot of *n*-InSb used in this investigation have also revealed an additional deep level in the band gap of InSb. With a continuous wave CO laser (photon energies of between 215 and 240 meV) we have also observed transitions from another deep level into the conduction band. Figure 10 shows the CO laser-induced photoconductivity results of those experiments obtained with the sampling and lock-in technique. These traces were taken with small powers ($\lesssim 500$ mW) and show a smaller signal-to-noise ratio than the DLCRH structure taken with the CO_2 laser. The four wavelengths in Fig. 10 are such that their photon energy is below the band gap of InSb.

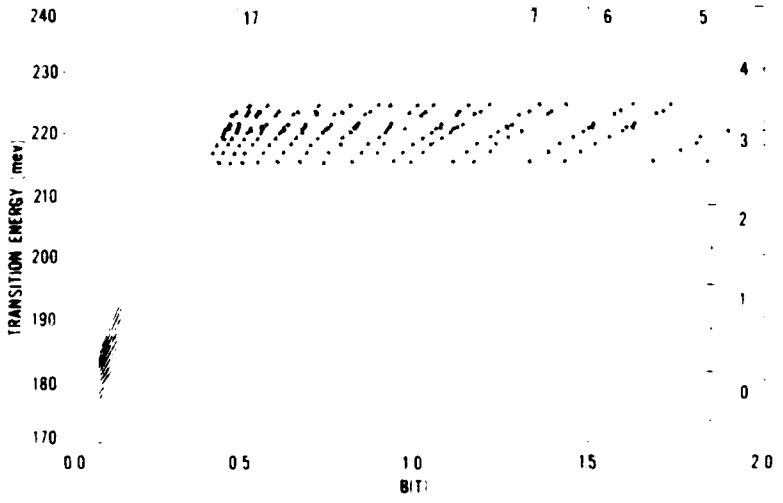

Fig. III.11

FIG. 11. Fan chart of the CO laser-induced deep level transitions with theoretical calculations of a deep level model discussed in the text. The intercept at $B = 0$ is 170 meV.

Thus, interband transitions from the valence band to the conduction band are not possible. Traces with higher photon energies (greater than the band gap) do show the usual one-photon interband transitions.[29] As indicated by the arrows, the structure shifts towards higher magnetic fields with higher photon energies in agreement with Landau level related resonances. Again, the minima of the structure correspond to conductivity maxima. Although the signal-to-noise is less, there are clearly indicated some important similarities to the CO_2 laser induced DLCRH structure (Fig. 2). That is, the doublet structure to the minima are present at the higher magnetic field and become much more pronounced with field. This is clearly shown for $\lambda = 5.77\ \mu$m (bottom trace) and qualitatively agrees with the behavior of the structure seen in Fig. 2. The amplitude of the structure in Fig. 10 is of the same relative size for both polarizations $\mathbf{e}\|\mathbf{B}$ and $\mathbf{e}\perp\mathbf{B}$ in agreement with the polarization independent results shown in Fig. 9.

The minimum positions of this CO laser-induced structure are plotted in Fig. 11 for each CO laser photon energy used. The theoretical lines were calculated with a model in which an electron is photoexcited from some deep level that is independent of magnetic field to some conduction band Landau level, either spin up or spin down, in the conduction band. This is a one-photon absorption process with no phonon emission or absorption. The band calculations were made with a set of band parameters that explains a wide variety of intraconduction, intravalence band, and two-photon interband data.[6,11,18] The energy intercept at $B = 0$ was adjusted to best fit the data. The best fit resulted from an energy intercept of $E_I = 170 \pm 2$ meV. That is, the impurity state for this process is located $\simeq 170$ meV below the bottom of the conduction band or $\sim 65 \pm 2$ meV above the top of the valence band (with an energy band gap of 235.2 meV for InSb). In a simple energy conservation equation

$$\hbar\omega = E_{+,-}(n) + E_I, \tag{4}$$

where the zero of energy is located at the bottom of the conduction band at zero magnetic field and E_I is the magnitude of the binding energy of the deep level.

The theory of this model Eq. (4) agrees well for most of the data shown in Fig. 11. There are some noticeable differences, however, at the low and high magnetic fields. The data at low fields lie slightly below the theoretical lines, while the high field data are just slightly above the theory. The data at low fields should also be a convolution or a mixture of the two spin states of the Landau levels; the experiment can not resolve the two spin states because they are too close together in magnetic field. In this model the impurity level activation energy was assumed to have no magnetic field dependence and hence remained fixed at all magnetic fields. Zawadzki[30] has shown that shallow donor levels can be approximated by a hydrogen-like model and do have a magnetic field dependence which closely follows the Landau levels of the conduction band. Although very little information exists on the magnetic field properties of deep levels, it is not too unreasonable to conclude that, at least, a small magnetic field dependence of the impurity level should be included. However, since no adequate theory exists for description of the deep

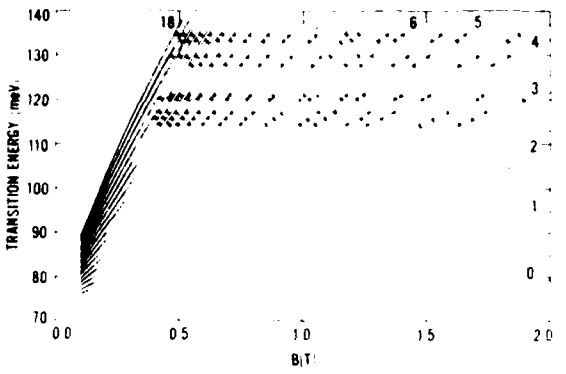

FIG. 12. Fan chart of the DLCRH transitions with theoretical calculations of model II (deep level transitions). The intercept at $B = 0$ is 74 meV.

Fig. III.12

levels, no attempt was made to include this slight field dependence in the deep level model.

Since the structure for the impurity transitions caused by the CO laser have qualitatively the same appearance and behavior as the DLCRH structure observed with the CO_2 laser (same doublet structure and polarization independence), a fit to the CO_2 laser-induced DLCRH resonance in Fig. 12 was also made using a photoexcited deep level model. That is, Eq. (4) was fit to the minimum positions of the DLCRH resonance structure of Fig. 2 for each photon energy of the CO_2 laser used. The energy intercept was again adjusted to best fit the data and was determined to be 74 ± 2 meV. Thus, the data could be represented by a model in which electrons are photoexcited out of an impurity level 74 meV below the bottom of the conduction band, to some Landau level, either spin-up or spin-down state, of the conduction band. The DLCRH data of Fig. 12 shows the same qualitative behavior as the transitions of Fig. 11. The data at low fields are slightly lower than the theoretical energies while the high field data is at a slightly higher energy than the theoretical curve. An accurate model for the magnetic field dependence of the deep level might possibly improve the fit. It should be noted that the observed doublet structure can only be described by a splitting of the final state, rather than the initial state. This is because the energy separation of the two parts of the doublet structure at a constant magnetic field decreases for higher Landau level numbers. If the observed splitting were a result of the initial deep level splitting, the separation of the doublet structure would remain constant.

Further evidence of a deep level approximately 70 meV below the bottom of the conduction band comes from the temperature dependence of the DLCRH structure. Figure 13 illustrates the decrease in amplitude of the DLCRH structure with temperature. The traces are plotted in the inverse magnetic field for five temperatures between 2 and 32 K. The amplitude of the resonant structure is largest at 2 K and remains relatively constant with temperature until temperatures of 20–26 K are reached. At those temperatures the amplitudes decrease dramatically and at 32 K the DLCRH structure seems to have disappeared completely.

The sharp decrease in amplitude of the DLCRH reso-

III - 10

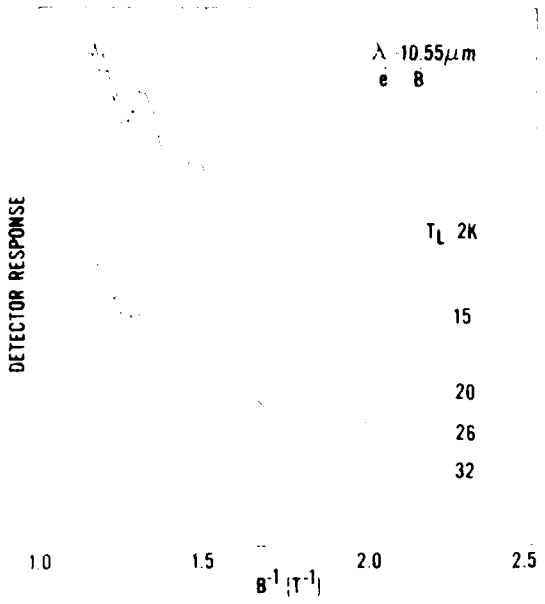

FIG. 13. Temperature dependence of the DLCRH structure. The applied electric field is ~1 V/cm. The data is plotted in units of the inverse magnetic field.

Fig. III.13

nant structure at approximately 26 K can be explained by thermal ionization of the 74 meV impurity level and decreases in the detector response of the sample. Thermal excitation of electrons from the valence band to the conduction band across the band gap (235.2 meV) starts occurring at temperatures of about 120 K (demonstrated in Hall coefficient measurements and in magnetophonon effect measurements). Thus, thermal ionization of a 74-meV level could start occurring in the neighborhood of 25–30 K, because of the tail of the Maxwell-Boltzmann distribution. The CO_2 laser-induced photoconductive response of the sample also depends quite dramatically upon temperature, becoming very small at the higher temperatures. From the results of the experiments discussed here it would appear that model II, in which electrons are photoexcited from a deep level, 74 meV below the bottom of the conduction band into some conduction band Landau level, is the correct model for the interpretation of the DLCRH structure. Model I would predict some similar result for DLCRH as compared to PACRH, yet polarization and electric field studies show definite differences between the two effects. In addition, the photoconductive results obtained with CO laser-induced deep level transitions show the same general shape of the structure and polarization independence as with the CO_2 laser-induced impurity transitions. Polarization indepen-

Table III.1

TABLE I. Summary of various deep level measurements in InSb and their energies below the conduction band.

Year published	Type of measurement	Temperature (K)	n- or p-type concentration (cm^{-3} at 77 K)	E_1 (meV)	E_2 (meV)	E_3 (meV)	References
1959	Lifetime	77–300	p, 10^{15}–10^{16}	170–180			Zitter *et al*
1961	Lifetime	15–200	n and p, 10^{14}–10^{15}	175	110		Laff and Fan
1962	Lifetime	90–180	n and p, 10^{13}–10^{14}	170–180	100–110	70–80	Nasledov and Smetannikova
1962	Hall coefficient, mobility	77–300	p, 10^{13}–10^{15}		106		Cunningham *et al*
1966	Hall coefficient, Transmission	55–300	p, 10^{14}		120		Baryshev *et al*
1967	Hall coefficient, Lifetime	< 150	n and p, 10^{13}–10^{17}	159	120		Hollis *et al*
1967	Lifetime	77	n, 10^{13}–10^{15}	165	110	40	Abduvakhidov *et al*
1969	Hall coefficient	78–250	p, 10^{13}–10^{15}		120		Galavanov and Oding
1969	Hall coefficient Conductivity, mobility Electric field dependence	4.2–200	n, 10^{13}–10^{14}			18, 67	Ismailov *et al*
1970	Noise	77–200	n, 10^{13}–10^{14}		100	30–40	Heyke *et al*
1971	Hall coefficient, Mobility	4.2–200	n, 10^{13}–10^{15}		100–128		Trifonov and Yaremenko
1972	Lifetime	4.2–77	n, 10^{14}		125		Guseinov *et al*
1973	Noise	77	p, 10^{15}	165 ± 5	110 ± 3		Galavanov *et al*
1973	Absorption	1.6	n and p, 10^{13}–10^{15}	168, 187	103		Valyashko and Pleskacheva
1975	Lifetime	77–200	n, 10^{14}			10–20	Blaut-Blachev, Ightsyn *et al*
1975	Hall coefficient Stress dependence	77	p, 10^{15}		140		Mackey *et al*
1975	Lifetime	77–200	n, 10^{14}	180	120		Blaut-Blachev, Ivleva *et al*
1975	Lifetime, noise	77	p, 10^{14}	165 ± 5	110 ± 5		Galavanov and Oding
1976	Lifetime	30–200	n, 10^{13}–10^{14}	163	130	22	Korotin *et al*
1982	Magneto-optical	4.2	n, 10^{14}	170 ± 2		74 ± 2	Present work

dence has also been observed in acceptor impurity transitions in p-InSb.[31] In our case, transitions from the deep levels for both polarizations would be possible if the wave function for the deep level state is some mixture or linear combination of the Bloch states used for the other bands. Then the optical matrix element between the initial and final states would probably be nonzero if the deep level wave function was a large enough linear combination of other band wave functions. Since detailed information about deep levels is very limited, knowledge of the wave functions for these states is minimal. Perhaps a careful analysis of these results would yield some information on the wave function. The intensity dependence observed in Fig. 4 can also be explained by optical depletion of the deep levels.

IV. CONCLUSIONS

Deep levels in InSb have been studied by a wide variety of experimental techniques over the last several decades.[25-28,32-44] These measurements include lifetime,[25-27,32-33,40,43,46,47] Hall coefficient, conductivity or mobility,[26,34,36,37,39,44] transmission or absorption,[35,42] and noise.[38,41,45] A summary of the results of these experiments are given in Table I where we also present a comparison with our determinations of the deep level positions. As can be seen from the table, there is quite good agreement on the location of level E_1, located 170 meV below the conduction band. In contrast, the values for level E_2 are in rather poor agreement. Possibly, there might actually be two different levels involved as indicated by Ismailov *et al.*[37] As noted in most of the previous publications, centers with deep levels (E_2) are always present in InSb independent of the method and time of crystal growth, and also independent of the doping level. Thus, these E_2 levels seem to be caused by lattice defects characteristics of the crystal. Their concentration may be about 10^{14} cm^{-3}. Their position is located approximately in the midgap region and most of the experimental results shown in Table I are consistent with each other.

In summary, we have shown that magneto-optical techniques are capable of being used to study deep levels in high purity InSb. Using a CO_2 laser, a level ~ 74 meV below the conduction band has been identified, a level ~ 170 meV below has been found with a CO laser. These values are in good agreement with previous results obtained over the last two decades. It is not clear whether these two levels are caused by lattice defects or residual impurities. We can also conclude that thes magneto-optical techniques should be valuable in the investigation of deep levels in other semiconductors.

ACKNOWLEDGMENTS

We gratefully acknowledge the help of K.E.H. Littler in helping to take the experimental data. This work was supported in part by the Office of Naval Research and a Faculty Research Grant from North Texas State University.

[1] W. Engler, H. Levinstein, and C. Stannard, Jr., Phys. Rev. Lett. **7**, 62 (1961).
[2] H. J. Stocker, H. Levinstein, and C. R. Stannard, Jr., Phys. Rev. **150**, 613 (1966).
[3] R. Kaplan, Phys. Rev. Lett. **20**, 329 (1969).
[4] R. Kaplan, S. G. Bishop, and B. D. McCombe, in *Proceedings of the Ninth International Conference on the Physics of Semiconductors, Moscow, 1968*, edited by S. M. Ryvkin (Nauka, Leningrad, 1968), p. 317.
[5] C. L. Littler, D. G. Seiler, R. Kaplan, R. J. Wagner, and W. Zawadzki, Solid State Commun. **37**, 783 (1981).
[6] R. Kaplan, R. J. Wagner, D. G. Seiler, C. L. Littler, M. H. Weiler, and W. Zawadzki, in the *Proceedings of the Physics of Narrow Gap Semiconductors, Linz, Austria, 1981*, edited by E. Gornik, H. Heinrich, and L. Palmetshofer (Springer, New York, 1982), p. 188.
[7] M. A. Habeggar and H. Y. Fan, Phys. Rev. Lett. **12**, 99 (1964).
[8] D. N. Nasledov, Y. G. Popov, and Y. S. Smetannikova, Fiz. Tverd. Tela **6**, 3728 (1964) [Sov. Phys. Solid State **6**, 2989 (1965)].
[9] V. J. Mazurczyk, G. V. Ilmenkov, and H. Y. Fan, Phys. Lett. **21**, 251 (1966).
[10] D. G. Seiler, M. W. Goodwin, and M. H. Weiler, Phys. Rev. B **23**, 6806 (1981).
[11] M. W. Goodwin, D. G. Seiler, and M. H. Weiler, Phys. Rev. B **25**, 6300 (1982).
[12] F. G. Bass and I. B. Levinson, Zh. Eksp. Teor. Fiz. **49**, 914 (1965) [Sov. Phys. JETP **22**, 635 (1966).]
[13] R. C. Enck, A. S. Saleh, and H. Y. Fan, Phys. Rev. **182**, 790 (1969).
[14] E. J. Johnson and D. H. Dickey, Phys. Rev. B **1**, 2676 (1970).
[15] V. I. Ivanov-Omskii and E. M. Shereghii, Fiz. Tverd. Tela **16**, 3379 (1974) [Sov. Phys. Solid State **16**, 2189 (1975)].
[16] S. Morita, S. Takano, and H. Kawamura, J. Phys. Soc. Jpn. **39**, 1040 (1975).
[17] V. I. Ivanov-Omskii, L. I. Korovin, and E. M. Shereghii, Phys. Status Solidi B **90**, 11 (1978).
[18] M. W. Goodwin and D. G. Seiler (unpublished).
[19] S. Morita, S. Takano, and H. Kawamura, Solid State Commun. **12**, 175 (1973).
[20] M. W. Goodwin, D. G. Seiler, and D. H. Kobe, Solid State Commun. **33**, 489 (1980).
[21] D. G. Seiler, M. W. Goodwin, and A. Miller, Phys. Rev. Lett. **44**, 807 (1980).
[22] K. I. I. Kobayashi and E. Otsuka, J. Phys. Chem. Solids **35**, 559 (1974).
[23] S. Morita, S. Takano, and N. Mikoshiba, J. Phys. Soc. Jpn. **49**, 573 (1980).
[24] S. Morita and N. Mikoshiba, J. Phys. Soc. Jpn. Lett. **48**, 1401 (1980).
[25] R. A. Laff and H. Y. Fan, Phys. Rev. **121**, 53 (1961).
[26] J. E. L. Hollis, S. C. Choo, and E. L. Heasell, J. Appl. Phys. **38**, 1626 (1967).
[27] A. N. Blaut-Blachev, V. S. Iveleva, V. G. Korotin, S. N. Krivonogov, V. I. Selyanina, and Yu. S. Smetannikova, Fiz. Tekh. Poluprovod. **9**, 2176 (1975) [Sov. Phys. Semicond. **9**, 1414 (1976)].
[28] A. G. Milnes, in *Deep Impurities in Semiconductors* (Wiley, New York, 1973), p. 72.
[29] C. R. Pidgeon and R. N. Brown, Phys. Rev. **146**, 575 (1966).
[30] W. Zawadzki and J. Wlasak, in *Proceedings of the 14th International Conference on the Physics of Semiconductors, Edinburgh, 1978*, edited by B. L. H. Wilson (Institute of Physics, London, 1979), p. 413.
[31] C. L. Littler, D. G. Seiler, R. Kaplan, and R. J. Wagner (unpublished).
[32] R. N. Zitter, A. J. Strauss, and A. E. Attard, Phys. Rev. **115**, 266 (1959).
[33] D. N. Nasledov and Y. S. Smetannikova, Fiz. Tverd. Tela **4**, 110 (1962) [Sov. Phys. Solid State **4**, 78 (1962)].
[34] R. W. Cunningham, E. E. Harp, and W. M. Bullis, in *Proceedings of the International Conference on the Physics of Semiconductors, Exeter, 1962* (Institute of Physics and Physical Society, London, 1962), p. 732.
[35] N. S. Baryshev, E. E. Vdovkina, A. P. Martynovich, I. M. Nesmelova, N. P. Tsitsina, and I. S. Aver'yanov, Fiz. Tverd. Tela **8**, 2258 (1966) [Sov. Phys. Solid State **8**, 1800 (1967)].
[36] Kh. M. Abduvakhidov, A. S. Volkov, and V. V. Galavanov, Fiz. Tekh. Poluprov. **6**, 945 (1966) [Sov. Phys. Semicond. **1**, 788 (1967)].
[37] V. V. Galavanov and V. G. Oding, Fiz. Tekh. Poluprovod. **3**, 284 (1969) [Sov. Phys. Semicond. **3**, 238 (1969)].
[38] I. M. Ismailov, D. N. Nasledov, Y. S. Smetannikova, and V. R. Felitsiant, Phys. Status Solidi **36**, 747 (1969).
[39] K. Heyke, G. Lautz, and H. Schumny, Phys. Status Solidi A **1**, 459 (1970).
[40] V. I. Trifonov and N. G. Yaremenko, Fiz. Tekh. Poluprovod. **5**, 953 (1971) [Sov. Phys. Semicond. **5**, 839 (1971)].
[41] E. K. Guseinov, R. I. Ibragimov, V. G. Korotin, D. N. Nasledov, and Y. G. Popov, Fiz. Tekh. Poluprovod. **5**, 1776 (1971) [Sov. Phys. Semicond. **5** 1549 (1972)].
[42] V. V. Galavanov, E. L. Ivchenko, and V. G. Oding, Fiz. Tekh. Poluprovod.

vod. 7, 798 (1973) [Sov. Phys. Semicond. 7, 547 (1973)].
[43]E. G. Valyashko and T. B. Pleskacheva, Fiz. Tekh. Poluprovod. 7, 836 (1973) [Sov. Phys. Semicond. 7 573 (1973)].
[44]A. N. Blaut-Blachev, M. I. Ightsyn, V. S. Ivleva, and V. I. Selyanina, Fiz. Tekh. Poluprovod. 9, 374 (1974) [Sov. Phys. Semicond. 9, 247 (1975)].
[45]H. J. Mackey, B. J. Vaughn, L. M. Rater, and D. G. Seiler, Solid State Commun. 16, 997 (1975).
[46]V. V. Galavanov and V. G. Oding, Fiz. Tekh. Poluprovod. 9, 2013 (1975) [Sov. Phys. Semicond. 1317 (1976)].
[47]V. G. Korotin, S. N. Krivonogov, D. N. Nasledov, and Y. S. Smetannikova, Fiz. Tekh. Poluprovod. 10, 20 (1976) [Sov. Phys. Semicond. 10, 10 (1976)].

III -13

PHYSICAL REVIEW B VOLUME 27, NUMBER 6 15 MARCH 1983

Intra-conduction-band magneto-optical studies of InSb

M. W. Goodwin* and D. G. Seiler
Center for Applied Quantum Electronics, Department of Physics, North Texas State University, Denton, Texas 76203
(Received 3 September 1982)

CO_2-laser- induced phonon-assisted cyclotron-resonance harmonics (PACRH) in *n*-type InSb are investigated at low magnetic fields with photoconductivity techniques. The high resolution allowed transitions up to the 23rd harmonic to be seen. Polarization studies of PACRH show that strong resonances are present for $\vec{\epsilon} \perp \vec{B}$ (but not for $\vec{\epsilon} \parallel \vec{B}$) in the Voigt geometry. In the Faraday geometry, the resonances were found to be of approximately equal amplitude for both σ_R and σ_L circularly polarized light. A large variety of intra-conduction-band magneto-optical experimental work has been unified and explained using a modified Pidgeon-Brown energy-band model and only one set of band parameters. These include cyclotron resonance, combined resonance, cyclotron-resonance harmonics, combined resonance harmonics, electron-spin resonance, and PACRH data from a wide variety of authors. The resulting set of energy-band parameters are $E_g = 235.2$ meV, $E_p = 23.2$ eV, $\Delta = 0.803$ eV, $\gamma_1 = 3.25$, $\gamma_2 = 0.2$, $\gamma_3 = 0.9$, $\kappa = -1.3$, $F = -0.2$, $q = 0.0$, $N_1 = -0.55$. These parameters are also shown to explain the variation of the effective g factor with magnetic field. In addition, these parameters also quantitatively explain recent two-photon magnetoabsorption data and recent intra-valence-band data.

INTRODUCTION

Over the past several decades magneto-optical studies in semiconductors have proven capable of determining energy-band parameters because of the optical transitions that occur between magnetically quantized electronic or impurity states. The conduction band of InSb, in particular, has been extensively studied with a wide variety of techniques. In part this is because high-quality InSb material can be grown with a small number of impurities and excellent homogeneity characteristics. It is thus not surprising to find that a great many intra-conduction-band processes have been observed and studied in InSb. However, there have been few attempts to quantitatively characterize all these processes with theoretical models using the same set of energy-band parameters.

One purpose of this investigation is to unify the experimental work on the conduction band of InSb into a more logical and complete study. With a simplified 8×8 Pidgeon-Brown model[1] of the bands, we simultaneously explain a wide variety of conduction-band data: cyclotron resonance,[2-4] combined resonance,[2-4] cyclotron-resonance harmonics,[4-9] combined resonance harmonics,[4-9] electron-spin resonance,[10-12] and phonon-assisted cyclotron-resonance harmonics[4-7,13-15] (PACRH) using only one set of band parameters.

In past studies there has been limited success in explaining the magnetic field dependence of the conduction-band *g* factor of McCombe and Wagner[10] or the more recent results of Kuchar *et al.*[11] However, our new set of band parameters and calculations obtained here are shown to explain this magnetic field dependence extremely well. In addition we present new experimental work on PACRH. With a high-resolution CO_2-laser- induced photoconductivity technique, transitions up to the 23rd harmonic at very low magnetic fields ($\sim$ 6 kG) are resolved. From a polarization study of PACRH we find for the first time that the absorption strengths for the circularly polarized light configrations σ_R and σ_L are approximately equal in magnitude for the range of photon energies and magnetic fields in this study.

EXPERIMENTAL WORK

The method to obtain the new low-field data presented here on PACRH used the sensitive photoconductive response of the sample itself in conjunction with sampling oscilloscope and magnetic field modulation techniques. The source of incident radiation was a continuous-wave CO_2 laser with a tunable grating providing variable photon energies. The

III-14

laser beam was mechanically chopped, producing optical and hence photoconductivity pulses approximately 20 μsec wide at a repetition of 1200 Hz. The sample was mounted in an optical variable temperature Dewar between the pole faces of a 20-kG electromagnet. Helmholtz coils wrapped around the pole faces produced a 43-Hz, 400-G, peak-to-peak magnetic field modulation. A sampling oscilloscope and lock-in amplifier were used to process the photoconductivity pulses produced in the sample by the chopped laser beam and the ac magnetic field. The data were recorded as the second derivative of the photoinduced magnetoresistance (y axis) as a function of magnetic field (x axis).

The samples of n-type InSb were obtained from Cominco American, Inc. and had a net carrier concentration of $\sim 9\times10^{13}$ cm^{-3} and an electron mobility of 700 000 cm/V sec at 77 K. The dimensions of the samples after cutting were approximately $6\times2\times0.2$ mm^3. After polishing on both sides with 3-μm alumina polishing grit, the samples were then etched in a bromine-methanol solution for about 1 min. Contacts to the samples were made by first fluxing the surface and then soldering small indium dots with small gold wires to the samples. Two end current contacts and two side voltage contacts formed a standard four-contact potential measuring geometry.

DISCUSSION OF THEORETICAL PROCESSES AND RESULTS

The theory of the Landau-level energies used in this study was based upon an 8×8 Pidgeon-Brown energy-band model developed by Pidgeon and Groves[16] and more recently[9,17] by Weiler *et al.* Weiler has reduced the full 8×8 Hamiltonian containing warping and inversion asymmetry effects to two 4×4 matrices (one each for the spin-up and spin-down Landau levels) which contain only warping effects along the diagonal part of the matrices. The reduced 4×4 Hamiltonians contain ten parameters which must be adjusted to fit the theoretical transition energies to a set of experimental data. Of these ten parameters a new one, Λ_1, was introduced by Weiler to include the spin-orbit splitting of higher bands of Γ_8 symmetry. The 4×4 matrices, which are solved numerically by a computer, give the energy eigenvalues for the conduction, valence (light and heavy hole), and spin-orbit split-off bands for both spin-up and spin-down Landau levels. The transition energies for the different magneto-optical processes are then calculated by combining the Landau-level energies with specific selection rules. In the following sections the selection rules for these different processes are given.

Cyclotron, combined, harmonics, and electron-spin resonances

Cyclotron resonance was first used by Dresselhaus *et al.*[18] to investigate the band structure of silicon and germanium. In simple terms, cyclotron resonance occurs when the energy between the $n=0$ and $n=1$ spin-up conduction-band Landau levels equals the incident photon energy. That is

$$\hbar\omega = E_a^c(1) - E_a^c(0), \tag{1}$$

where $\hbar\omega$ is the photon energy and $E_a^c(n)$ is the energy of the nth spin-up conduction-band Landau level. The defining equation for the cyclotron-resonance effective mass m_c^* is

$$\hbar\omega = \hbar\omega_c, \tag{2}$$

where $\omega_c = eB/m_c^*$, B is the magnetic field strength, and m_c^* is an effective mass which for conduction-band cyclotron resonance is an electron effective mass. This equation has been traditionally used for cyclotron resonance even for bands that are nonparabolic. Cyclotron resonance is a result of the selection rules $\Delta n = +1$; $\Delta s = 0$ for $\vec{\epsilon}\perp\vec{B}$ (σ_l polarization) and can be derived from one-photon absorption processes with the use of the usual spherical approximation.[9] When the magnetic field B is such that a resonance occurs, then electrons in the $n=0$ spin-up conduction-band Landau level will absorb photons from the optical flux and be excited to the $n=1$ spin-up conduction-band Landau level.

Cyclotron resonance in InSb was first observed in transmission studies by Dresselhaus *et al.*[19] using microwave radiation and later by Burstein *et al.*[20] using infrared radiation. Cyclotron resonance was also observed by a number of other investigators.[21–23] In addition to cyclotron resonance, McCombe and co-workers[2,3] studied other types of intra-conduction-band processes such as combined resonance, spin-down cyclotron resonance, and PACRH which will be discussed in the next section. Combined resonance is a process in which an electron initially in the $n=0$ spin-up conduction-band Landau level makes a transition by photon absorption to the $n=1$ spin-down Landau level. That is, at resonance

$$\hbar\omega = \hbar\omega_c + \hbar\omega_s = E_b^c(1) - E_a^c(0), \tag{3}$$

where $\hbar\omega_s$ is the energy between a spin-up and spin-down Landau level and

$$\hbar\omega_s = g_c^*\mu_B B, \tag{4}$$

where g_c^* is the Lande g factor and μ_B is the Bohr magneton. The selection rule for this process is again derived from the spherical approximation

III - 15

treatment for one-photon absorption and is $\Delta n = +1$; $\Delta s = 1$ for $\hat{e} \perp \hat{B}$ (π polarization).[9] This process is not allowed for $\hat{e} \perp \hat{B}$ in the spherical approximation. Spin-down cyclotron resonance obeys Eq. (2) except electron transitions occur between the spin-down ($s = -\frac{1}{2}$) levels of the $n=0$ and $n=1$ Landau levels. This effect is usually observed[2] at the higher temperatures (~ 77 K), where the tail of the probability distribution of carriers is long enough to significantly populate the higher-energy spin-down $n=0$ Landau level.

Another comprehensive study of conduction-band processes in InSb was performed by Johnson and Dickey.[4] In addition to those processes studied by McCombe, they observed resonant structure in transmission spectra which were caused by harmonics of cyclotron resonance. Harmonics of cyclotron resonance are the result of electrons in the spin-up $n=0$ Landau level being photoexcited to the spin-up state of some $n>1$ Landau level. Thus when a resonance condition occurs

$$\hbar\omega = n\hbar\omega_c = E_a^c(n) - E_a^c(0), \tag{5}$$

where $n=1$ is the condition for cyclotron resonance. It should be pointed out that because of nonparabolicity and quantum effects, the "harmonic" transitions $n\hbar\omega_c$ do not occur exactly at the energy n times $\hbar\omega_c$. Therefore, the notation $n\hbar\omega_c$ is used merely for labeling purposes. The origin of these processes in terms of selection rules cannot be derived in the usual spherical approximation. However, there have been extensive theoretical investigations[9,16,24] of these processes. Other processes which have also been observed in studies of the spin-flip Raman laser[25,26] are spin-flip with the harmonics of the cyclotron resonance or

$$\hbar\omega = n\hbar\omega_c + \hbar\omega_s = E_b^c(n) - E_a^c(0). \tag{6}$$

Electron-spin resonance associated with spin-flip processes can be described by

$$\hbar\omega = \hbar\omega_s = E_b^c(0) - E_a^c(0), \tag{7}$$

where electrons in the spin-up ($s = +\frac{1}{2}$) state are photoexcited to the spin-down ($s = -\frac{1}{2}$) state of the $n=0$ Landau level. Isaacson[27] and McCombe and Wagner[10] investigated this process in order to obtain the conduction-band g factor g_c^*, Eq. (4). More recently Kuchar *et al.*[11] found that the strength of the spin-resonance line depended upon the amount of uniaxial stress applied to the sample. However, the magnetic field positions of the resonances are not measurably effected. The magnitude of the observed g factor and its variation with magnetic field will be discussed in more detail later.

The band parameters used in this study were obtained by numerically fitting the theoretical transition energies to a large set of magneto-optical data. In addition to the intra-conduction-band data just discussed and PACRH data to be discussed later in this paper, a set of two-photon interband[28] and one-photon intra-valence-band[29] data were also used to numerically obtain the band-parameter set reported here. With all these processes the resulting band parameters reported here should be more uniquely determined than in previous studies.

Figure 1 shows the fit of the theoretical transition energies to the intra-conduction-band processes that have been described so far. The band parameters determined from the fit are $E_g = 235.2$ meV, $E_p = 23.2$ eV, $\Delta = 0.803$ eV, $\gamma_1 = 3.25$, $\gamma_2 = -0.2$, $\gamma_3 = 0.9$, $\kappa = 1.3$, $F = -0.2$, $q = 0.0$, and $N_1 = 0.55$. The definitions of these parameters are given by Weiler *et al.*[9] and a comparison with other work is reported by Littler *et al.*[29] It must be pointed out that our measurements could not satisfactorily determine the spin-orbit splitting energy Δ. We therefore used the value obtained by Aggarwal ($\Delta = 0.803$ eV).[30]

In Fig. 1 are plotted the transition energy versus magnetic field data of several authors.[3-8] The data should represent most of the important work on the conduction band of InSb, but is not an exhaustive set. However, the data of other works[31,32] do agree with those results presented here. The labels correspond to the final state of the transition; the initial state for all the transitions is the spin-up $n=0$ or $a(0)$ Landau level. With this set of band parameters, a good fit to all the data is very apparent even to the high magnetic fields of 20.0 T (200 kG). At energies below 120 meV there is an excellent fit of the theoretical lines with the data. Above 120 meV for the $a(2)$, $b(2)$, and $a(3)$ transitions there does appear, however, to be a slight shift of the theory from the data. This may be the result of the energy-band model's failure to predict accurate transition energies at the higher energies. Another possibility might be that small adjustments in the band parameter set are needed to improve the fit. However, this deviation does not significantly detract from the good overall agreement of the theory with a large amount of data.

The data in Fig. 1 is a mixture of data obtained with B parallel to the (111) and (100) crystal directions. The theoretical lines were calculated for $\hat{B}$ (100) crystal direction. The data for the two crystal directions agree within experimental error, indicating no major differences between them. Figure 2 illustrates the differences in the theoretically calculated transition energies between the two directions with the band-parameter set given previously.

III -16

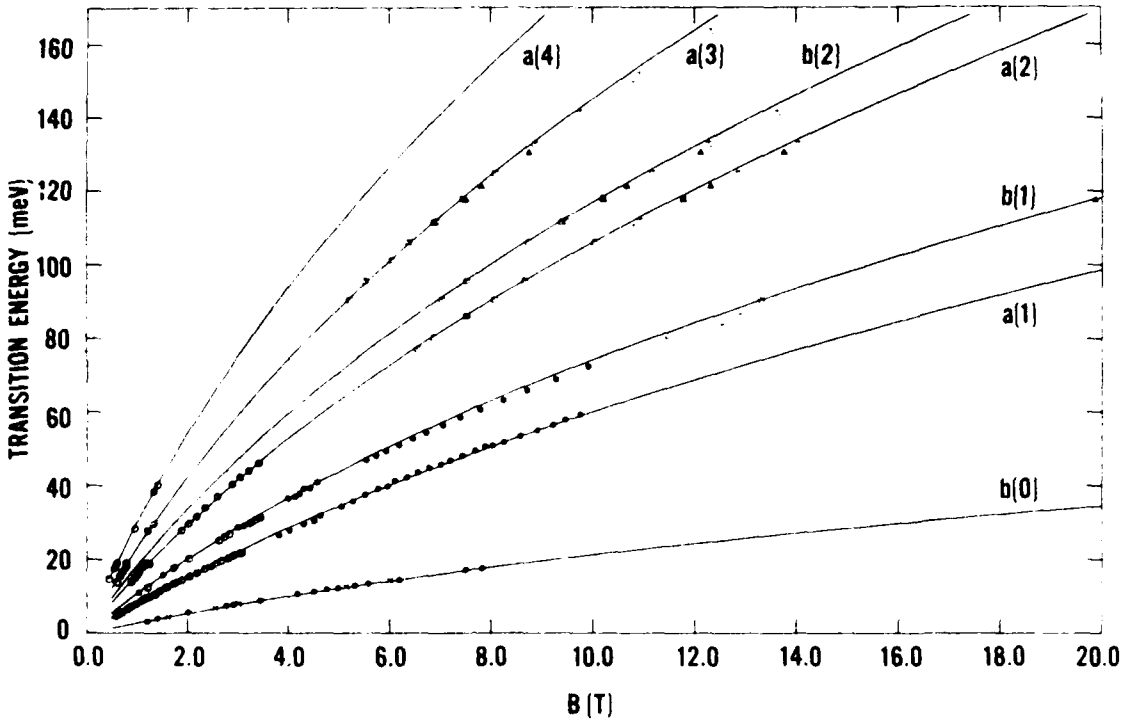

FIG. 1. Fan chart of various intraconduction processes used to determine the band parameter set of this study. The notation $a(n)$ or $b(n)$ refer to the final-state spin-up or spin-down level, respectively, of the nth Landau level. The data points are as follows. ●, Refs. 2 and 3; ×, Ref. 11; ○, Ref. 4; □, Ref. 5; ▲, Ref. 6; +, Ref. 8. The labels by the line represent electron spin resonances [$b(0)$], cyclotron resonance, [$a(1)$], combined resonance [$b(1)$], cyclotron resonance harmonics [$a(2)$, $a(3)$, $a(4)$], and combined resonance harmonics [$b(2)$].

Fig. III.14

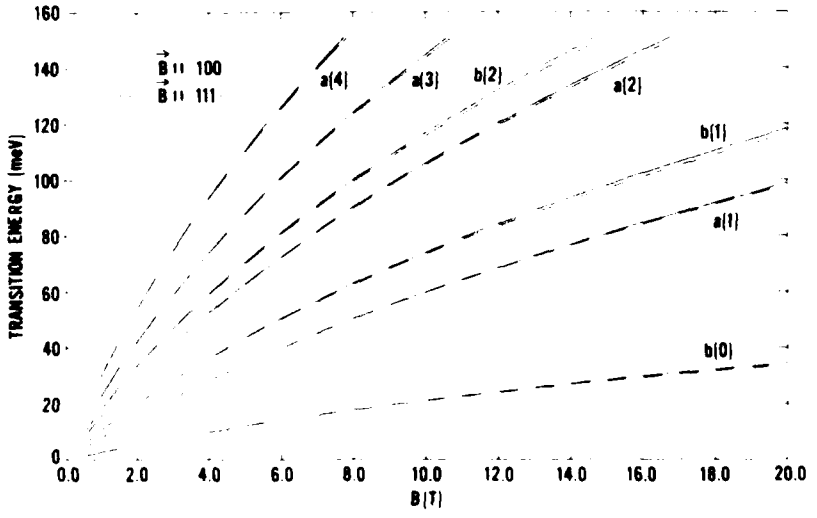

FIG. 2. Anisotropy differences for B ⟨111⟩ and ⟨100⟩ for the transitions in Fig. 1.

Fig. III.15

III - 17

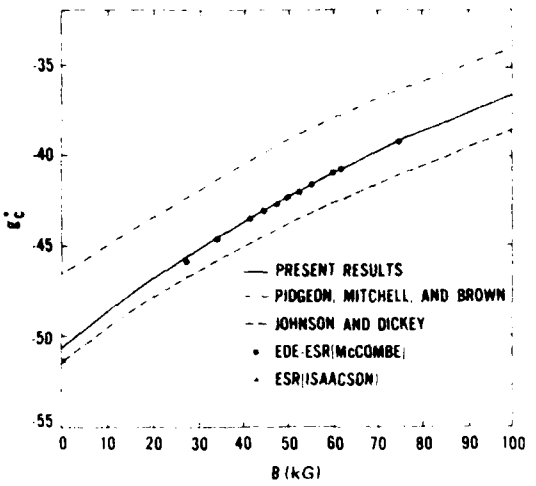

FIG. 3. Extrapolated magnetic field dependence of the conduction-band g_c^* factor showing the excellent fit of our theoretical calculations to the data of Refs. 3 and 27.

Fig. III.16

The $\vec{B}\parallel\langle 111\rangle$ transition energies are only slightly lower in energy than the $\vec{B}\parallel\langle 100\rangle$ transition energies, in agreement with the anisotropy measurements of McCombe.[33] The deviation is more pronounced for transitions at high energy and high magnetic fields. The high-field and high-energy data of Fig. 1 (□,▲) were obtained with $\vec{B}\parallel\langle 100\rangle$, as were the theoretical lines, thus no discrepancy should exist because of the differences in the two crystal-field directions. There remain only the low-energy, low magnetic field data, which is a mixture of $\vec{B}\parallel\langle 111\rangle$ and $\langle 100\rangle$ data and for which there should be no noticeable differences in energy as shown in Fig. 2.

As was mentioned previously, McCombe and Wagner[10] experimentally determined the conduction-band g factor g_c^* from Eq. (4) as a function of magnetic field from spin-resonance measurements. In Fig. 3 their values for $g_c^*(B)$ are plotted along with theoretical results of other work[4,34] and of this study. The theoretical calculation of $g_c^*(B)$ was obtained by finding the theoretical energy difference $\hbar\omega_c(B)$ between the $a(0)$ and $b(0)$ Landau levels of the different theories and then using Eq. (4) to determine $g_c^*(B)$. As shown, the theoretical lines of Pidgeon *et al.*[34] and Johnson and Dickey[4] underestimate and overestimate the data, respectively. The band parameters of this study were adjusted to fit g_c^* to McCombe and Wagner's data.[10] Thus there is good agreement between theory and data even for Isaacson's[27] $B=0$ value of -51.3. The higher band parameter which influences $g_c^*(B)$ the most is N_p, which is -0.55 from these measurements. At $B=0$ our value of $g_c^*(0)$ is -50.6, while Johnson and Dickey's result is $g_c^*(0)=-51.3$. The excellent fit of the theory to $g_c^*(B)$ is also apparent in Fig. 1 where the same good agreement of the transition energies to the spin-resonance line $b(0)$ also occurs. In the same manner Weiler[35] also explained the magnetic field dependence of the spin-flip frequency (ω_s),[10] but with a slightly different set of band parameters.

Phonon-assisted cyclotron-resonance harmonic transitions

Another major magneto-optical effect which is certainly relevant to any discussion of intraconduction processes is that of PACRH. The basic theory for this process was first published by Bass and Levinson.[36] In addition to an electron-photon interaction which causes the processes described in the preceding section, a longitudinal-optical (LO) polar phonon also interacts with the electron-photon system to create absorption resonances. Specifically, an electron in the $a(0)$, spin-up $n=0$, Landau level will absorb a photon, while simultaneously emitting an LO phonon of energy $\hbar\omega_0$, and thus make a transition to some higher n spin-up $a(n)$ Landau level. The simple energy conservation equation for this process is

$$\hbar\omega = n\hbar\omega_c + \hbar\omega_0 = E_a^c(n) - E_a^c(0) + \hbar\omega_0, \tag{8}$$

where $\hbar\omega_0$ is the LO-phonon energy. The transition rate for this process is usually described by second-order perturbation theory[36,37] and can be written as

$$T_{if} = \frac{2\pi}{\hbar}\sum_t \left| \frac{\langle f|H_L|t\rangle\langle t|H_R|i\rangle}{E_t - E_a^c(0) - \hbar\omega} + \sum_{t'} \frac{\langle f|H_R|t'\rangle\langle t'|H_L|i\rangle}{E_{t'} - E_a^c(0) - \hbar\omega_0} \right|^2 \times \delta(E_a^c(n) - E_a^c(0) - \hbar\omega + \hbar\omega_0), \tag{9}$$

where H_R and H_L are the electron-photon and electron-phonon interactions, respectively, and $E_a(0)$, E_t, and $E_a(n)$ are the energies of the initial, intermediate, and final states (i,t,f), respectively. The δ function is a statement of the energy conservation, Eq. (8), and the sum is over all possible intermediate states. For the light polarization σ_L in the electron-photon interaction H_R, the Landau-level number n changes to $n+1$ from the initial to the intermediate states (first term) or intermediate to final states (second term) for the same spin. The electron-phonon interaction H_L allows a transition from a state n to any state n', but is strongly spin conserving. Thus, although there are definite selection rules for the electron-photon interaction, transi-

III - 18

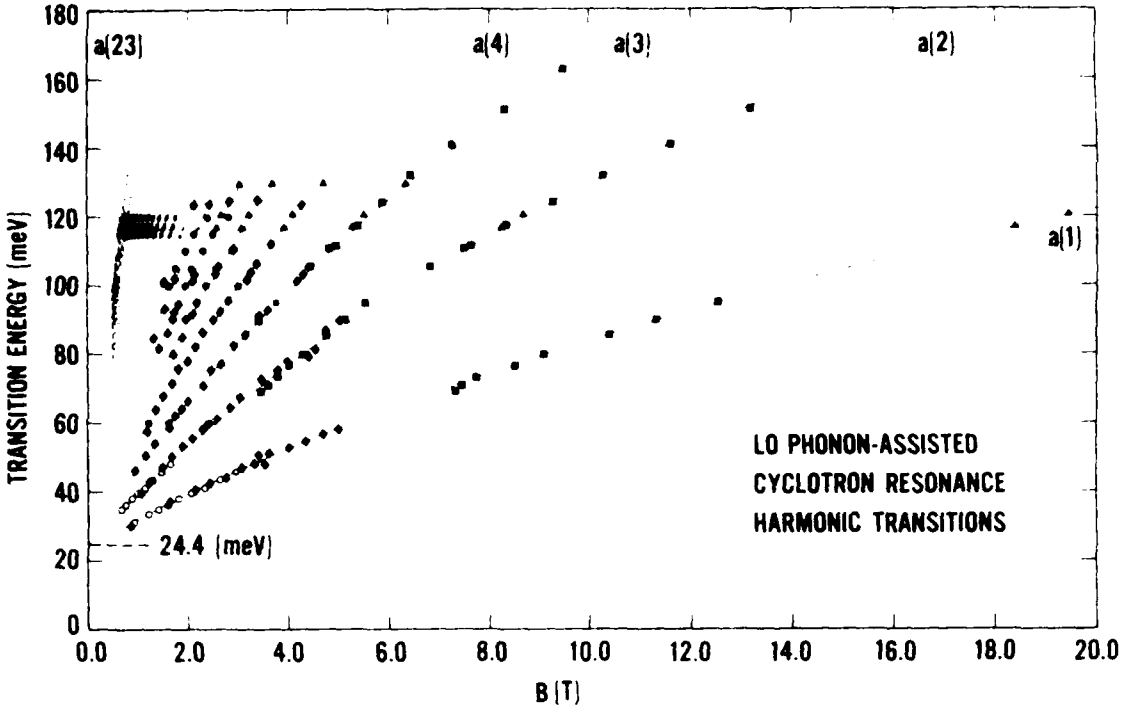

FIG. 4. Fan chart of PACRH for our data and other authors. The labels are the final state of the transition while the initial state is the $a(0)$ Landau level. The intercept corresponds to the LO-phonon energy (24.4 meV). The data points are as follows: ○, Ref. 4; ▲, Ref. 6; ■, Ref. 5; ●, Ref. 13; ◇, Ref. 14; ◆ Ref. 15. The low field ×'s represent our data presented in this paper. An expanded scale of our low-field work is presented in Fig. 6.

Fig. III.17

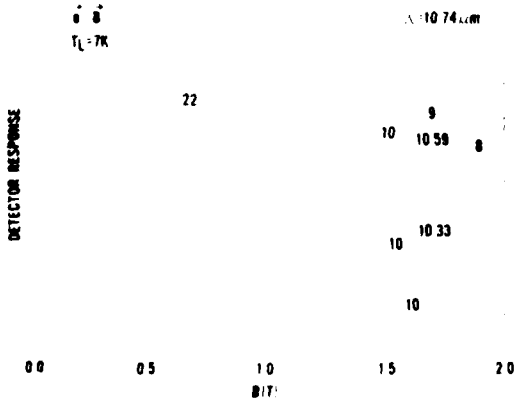

FIG. 5. Wavelength dependence of PACRH. The numbers correspond to distinct experimental transitions.

Fig. III.18

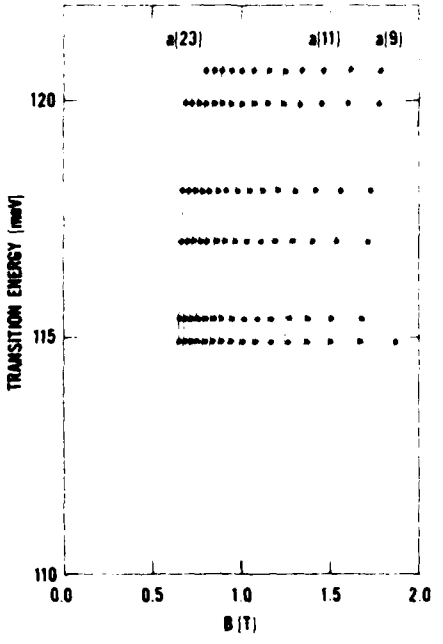

FIG. 6. Expanded scale of the fan chart for PACRH (Fig. 4) with present data. The labels are the final state of the transitions.

Fig. III.19

III-19

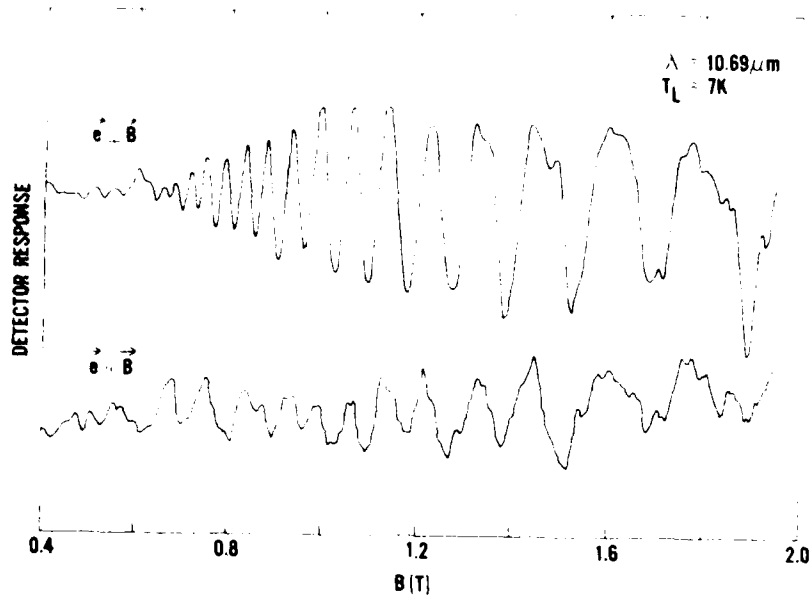

FIG. 7. Polarization dependence of PACRH for $\hat{e} \perp \vec{B}$ and $\hat{e} \parallel \vec{B}$. PACRH is strong for $\hat{e} \perp \vec{B}$ and very weak for $\hat{e} \parallel \vec{B}$

Fig. III .20

tions between any Landau levels n and n' are allowed, because there are no selection rules for the electron-phonon interaction. The same types of virtual transitions to and from the intermediate states are also possible for σ_R. PACRH should not be observed for $\hat{e} \parallel \vec{B}$, because then the photon transitions are between states of opposite spin.

The minimum positions of the PACRH structure at each photon energy for new data presented in this paper and the data of other previous work are plotted in Fig. 4. With the set of band parameters determined in this investigation, transition energies for PACRH were also calculated (lines) and compared with the data. In addition to the band parameters already discussed, the LO-phonon energy (the energy intercept at $B = 0$) was also used as an adjustable parameter in the computer minimization program. With a fit to all the data shown in Fig. 4, the value

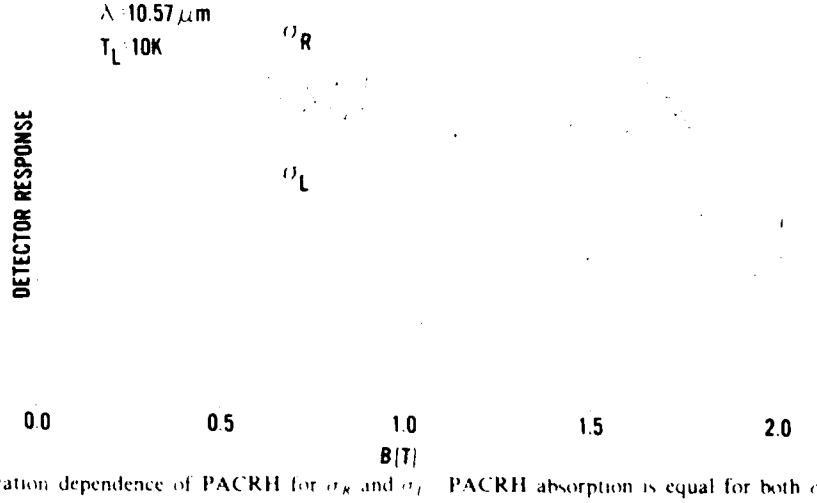

FIG. 8. Polarization dependence of PACRH for σ_R and σ_L. PACRH absorption is equal for both σ_R and σ_L with equal incident powers

Fig. III .21

for the LO-phonon energy $\hbar\omega_0$ was found to be 24.4 ± 0.2 meV. Johnson and Dickey[4] also determined the LO-phonon energy from their measurements to be 24.4 ± 0.3 meV. Over the full range of magnetic fields and photon energies there is thus excellent agreement of theory with a wide variety of data using the band parameter set determined in this investigation.

Present results of PACRH

Experiments on PACRH were also performed in this study for n-type-InSb with the free-carrier concentration $\sim 9 \times 10^{13}$ cm^{-3}. Figure 5 shows the wavelength dependence of PACRH that we obtained with the sampling and lock-in technique for three representative wavelengths. The PACRH resonances are associated with the minimum structure because the minima correspond to maxima in the conductivity. With the sampling and lock-in technique the detector response is proportional to the second derivative of the photoinduced magnetoresistance. Thus changes in the resistance of the sample are inversely proportional to changes in the conductivity. For PACRH the light induces changes in the mobility of the free electrons in the conduction band, which causes changes in the conductivity of the sample. At a resonance, the light will excite carriers at the bottom of the band to very high energies in the band where the mobility of the carriers is larger, thus increasing the conductivity or decreasing the magnetoresistance. The structure could only be resolved for wavelengths greater than 10.33 μm because two-photon magnetoabsorption[2,3] dominated the spectra for high photon energies and therefore masked any intra-conduction-band process below that wavelength. The numbers correspond to the Landau-level number of the final state of the transition.

An expanded scale of our low-field data is shown in Fig. 6. The lines represent theoretical calculations using our same set of band parameters, and $\hbar\omega_0 = 24.4$ meV. With the sensitive sampling and lock-in amplifier technique, transitions to the 23rd harmonic of PACRH can be resolved. Even to these high harmonics of PACRH, our new set of band parameters is still quite valid for describing the observed transition energies.

The polarization dependence of PACRH is shown in Fig. 7 for $\vec{\epsilon} \perp \vec{B}$ and $\vec{\epsilon} \parallel \vec{B}$. As indicated, PACRH is much stronger for $\vec{\epsilon} \perp \vec{B}$ than for $\vec{\epsilon} \parallel \vec{B}$. The fact that small resonances are even observed for $\vec{\epsilon} \parallel \vec{B}$ is probably due to a small admixture of $\vec{\epsilon} \perp \vec{B}$ polarization in the $\vec{\epsilon} \parallel \vec{B}$ trace. In addition to $\vec{\epsilon} \perp \vec{B}$ and $\vec{\epsilon} \parallel \vec{B}$ we have also obtained spectra for the circular polarizations σ_R and σ_L, shown in Fig. 8, by propagating the beam through a ZnSe Fresnel rhomb. For both σ_R and σ_L the PACRH resonances appear to have equal strengths. To our knowledge this has not been observed before. However, for the transitions with final states $n = 9-23$ in the range of magnetic fields shown here, the transition rate for both σ_R and σ_L are expected to become approximately equal as shown by the following simple argument. For the large harmonics observed here ($n = 9-23$) the second sum over t' in the transition probability given in Eq. (9) will dominate, rather than the first sum over t. Thus we consider second-order transitions proceeding by the phonon interaction H_L first and then by the photon interaction for either σ_L or σ_R polarized light. Choosing an intermediate state of Landau-level number $n+1$ for both polarizations allows us to write the transition probability ratio

$$\frac{T^{\sigma_R}_{0,n}(\omega,\omega_c)}{T^{\sigma_L}_{0,n+2}(\omega,\omega_c)} \approx \frac{|\langle n \mid H_R^{\sigma_R} \mid n+1\rangle|^2}{|\langle n+2 \mid H_R^{\sigma_L} \mid n+1\rangle|^2} \frac{|\langle n+1 \mid H_L^{\sigma_R} \mid 0\rangle|^2}{|\langle n+1 \mid H_L^{\sigma_L} \mid 0\rangle|^2}. \tag{10}$$

The use of Eq. (9) of Ref. 13 to evaluate the photon matrix elements and approximating the ratio of the phonon matrix elements for large n as ~ 1 allows us to write the ratio as $(n+1)/(n+2)$ for a fixed ω. Thus, for large n, the absorption strengths for σ_R and σ_L would not be expected to differ much, as shown in Fig. 8.

CONCLUSIONS

In conclusion we have been able to characterize the conduction band of InSb to much greater accuracy that has previously been reported. With the following set of band parameters, $E_g = 235.2$ meV, $E_p = 23.2$ eV, $\Delta = 0.803$ eV, $\gamma_1 = 3.25$, $\gamma_2 = -0.2$, $\gamma_3 = 0.9$, $\kappa = -1.3$, $F = -0.2$, $q = 0.0$, $N_1 = -0.55$, and a modified Pidgeon and Brown Hamiltonian model of the Landau levels, we are able to calculate transition energies for most of the important intra-conduction-band magneto-optical processes. These include cyclotron resonance, combined resonance, cyclotron-resonance harmonics, combined resonance harmonics, electron spin resonance, and phonon-assisted cyclotron-resonance harmonics (PACRH). In addition, the magnetic field dependence of the conduction-band g_c^* factor is calculated from these band parameters and is found to agree very well with the experimental spin-resonance results.[10,11,27]

III -21

It should also be noted that these band parameters can also be used to calculate transition energies that are also in excellent agreement with recent intra-valence-band[29] and two-photon-interband[28] magneto-optical data. Except for the value of E_g, these band parameters are in good agreement with those obtained by Weiler[5] from analyzing one-photon-interband data, including exciton contributions. Thus with one band-parameter set more magneto-optical processes can now be explained, making this the most accurate set for InSb so far.

In addition to the band-parameter studies we also present new experimental results of PACRH. With a sensitive photoconductivity technique PACRH transitions up to the 23rd harmonic have been resolved, extending previous observations of PACRH to much lower magnetic fields ($B \sim 6$ kG). From polarization studies PACRH is shown to be present for $\vec{\epsilon} \perp \vec{B}$, but almost absent for $\vec{\epsilon} \parallel \vec{B}$, as expected. However, polarization measurements with circularly polarized light (σ_R and σ_L) indicate that, at least in the magnetic field range of our experiments PACRH absorption is approximately equal for both σ_R and σ_L, in agreement with simple predictions.

ACKNOWLEDGMENTS

This work was supported in part by the U.S. Office of Naval Research and a Faculty Research Grant from North Texas State University. We gratefully acknowledge the help and support of M. W. Weiler, whose energy-band model was used extensively in this study.

[*]Present address: Texas Instruments, Inc., Dallas, Texas 75265.

[1]C. R. Pidgeon and R. N. Brown, Phys. Rev. 146, 575 (1966).

[2]B. D. McCombe, S. G. Bishop, and R. Kaplan, Phys. Rev. Lett. 18, 748 (1967).

[3]B. D. McCombe, Phys. Rev. 181, 1206 (1969).

[4]E. J. Johnson and D. H. Dickey, Phys. Rev. B 1, 2676 (1970).

[5]K. Lee, B.S. thesis, Massachusetts Institute of Technology, 1970 (unpublished).

[6]R. Grisar, H. Wachernig, G. Bauer, J. Wlasak, J. Kowalski, and W. Zawadzki, Phys. Rev. B 18, 4355 (1978).

[7]H. Wachernig, R. Grisar, G. Bauer, and S. Hayashi, Physica 89B, 290 (1977).

[8]M. H. Weiler, R. L. Aggarwal, and B. Lax, Solid State Commun. 14, 299 (1974).

[9]M. H. Weiler, R. L. Aggarwal, and B. Lax, Phys. Rev. B 17, 3269 (1978).

[10]B. D. McCombe and R. J. Wagner, Phys. Rev. B 4, 1285 (1971).

[11]F. Kuchar, R. Meisels, and M. Kriechbaum, in the *Proceedings of the Physics of Narrow Gap Semiconductors, Linz, Austria, 1981*, edited by F. Gornik, H. Heinrich, and L. Palmetshofer (Springer, New York, 1982), p. 197.

[12]G. Bemski, Phys. Rev. Lett. 4, 62 (1960).

[13]R. C. Enck, A. I. Saleh, and H. Y. Fan, Phys. Rev. 182, 790 (1969).

[14]S. Narita, S. Takano, and H. Kawamura, J. Phys. Soc. Jpn. 39, 1040 (1975).

[15]V. I. Ivanov-Omskii, K. I. Korovin, and F. M. Shereghii, Phys. Status Solidi B 90, 11 (1978).

[16]C. R. Pidgeon and S. H. Groves, Phys. Rev. 186, 824 (1969).

[17]M. H. Weiler, Ph.D. thesis, Massachusetts Institute of Technology, 1977 (unpublished).

[18]G. Dresselhaus, A. F. Kip, and C. Kittel, Phys. Rev. 98, 368 (1955).

[19]G. Dresselhaus, A. F. Kip, C. Kittel, and G. Wagoner, Phys. Rev. 98, 556 (1955).

[20]E. Burstein, G. S. Picus, and H. A. Gebbie, Phys. Rev. 103, 825 (1956).

[21]R. J. Keyes, S. Zwerdling, S. Foner, H. H. Kolm, and B. Lax, Phys. Rev. 104, 1804 (1956).

[22]H. Lipson, S. Zwerdling, and B. Lax, Bull. Am. Phys. Soc. 3, 218 (1958).

[23]E. D. Palik, G. S. Pikus, S. Teitler, and R. F. Wallis, Phys. Rev. 122, 475 (1961).

[24]R. L. Bell and K. T. Rogers, Phys. Rev. 152, 746 (1966).

[25]R. B. Dennis, R. A. Wood, C. R. Pidgeon, S. D. Smith, and J. W. Smith, J. Phys. C 5, 1173 (1972).

[26]G. Favrot, R. L. Aggarwal, and B. Lax, Solid State Commun. 18, 577 (1976).

[27]R. A. Isaacson, Phys. Rev. 169, 312 (1968).

[28]M. W. Goodwin, D. G. Seiler, and M. H. Weiler, Phys. Rev. B 15, 6300 (1982).

[29]C. Littler, D. G. Seiler, R. Kaplan, and R. J. Wagner (unpublished).

[30]R. L. Aggarwal, in *Semiconductors and Semimetals*, edited by R. K. Willardson and A. C. Beer (Academic, New York, 1972), Vol. 9, p. 151.

[31]J. Apel, T. Poehler, and C. Westgate, Appl. Phys. Lett. 14, 161 (1969).

[32]C. Summers, R. Dennis, B. Wherrett, P. Harper, and S. Smith, Phys. Rev. 170, 755 (1968).

[33]B. McCombe, Solid State Commun. 6, 533 (1968).

[34]C. R. Pidgeon, D. L. Mitchell, and R. N. Brown, Phys. Rev. 154, 737 (1967).

[35]M. H. Weiler, J. Magn. Magn. Mater. 11, 131 (1979).

[36]F. G. Bass and I. B. Levinson, Zh. Eksp. Teor. Fiz. 49, 914 (1965) [Sov. Phys. JETP 22, 635 (1966)].

[37]W. Zawadski, in *Proceedings of the Narrow Gap Semiconductors Physics and Applications, Nimes 1979*, Vol. 133 of *Lecture Notes in Physics*, edited by W. Zawadzki (Springer, New York, 1980), p. 85.

IV. INTERACTION OF CO LASER RADIATION WITH n-InSb

The optical properties of InSb such as absorption and refractive index have been shown to be strongly dependent upon the creation of even a small number of free electrons or holes. Particularly large and interesting nonlinear effects are seen near the bandgap wavelengths because of resonant enhancement near the sharp band edge. In "dynamic" nonlinear optics, the changes in optical effects depend upon the dynamics of the relaxation of the excitation (i.e., how long does it take for the electron and/or hole to relax) back to an equilibrium situation. Needless to say, this is a very complex subject because many different physical processes can take place either simultaneously during the photon absorption or subsequently after the absorption.

Here we have investigated absorption processes at CO laser wavelengths both below the fundamental gap energy and above it. Photoconductive responses are observed and identified as arising from (1) impurity or defect level transitions to conduction band Landau levels and (2) interband transitions originating from valence to conduction band Landau levels by one-photon interband magneto-absorption (exciton effects must be taken into account).

We have already reported on deep level transitions using the CO_2 laser in Section III. One reprint there contained a short section of transitions from a deep level to the conduction band Landau levels using the CO laser. This deep level was found to originate at an energy of 170 meV below the conduction band edge (or about 65-66 meV above the valence band edge). This level may correspond to an excited state of a gold acceptor.

Figure IV.1 shows unpublished reproductions of the photoconductive response of a high purity sample of n-InSb. The numerals 1-6 correspond to one-photon interband magneto-optical transitions between the valence band and the conduction band. Of course, the role of excitons is important and must be taken into

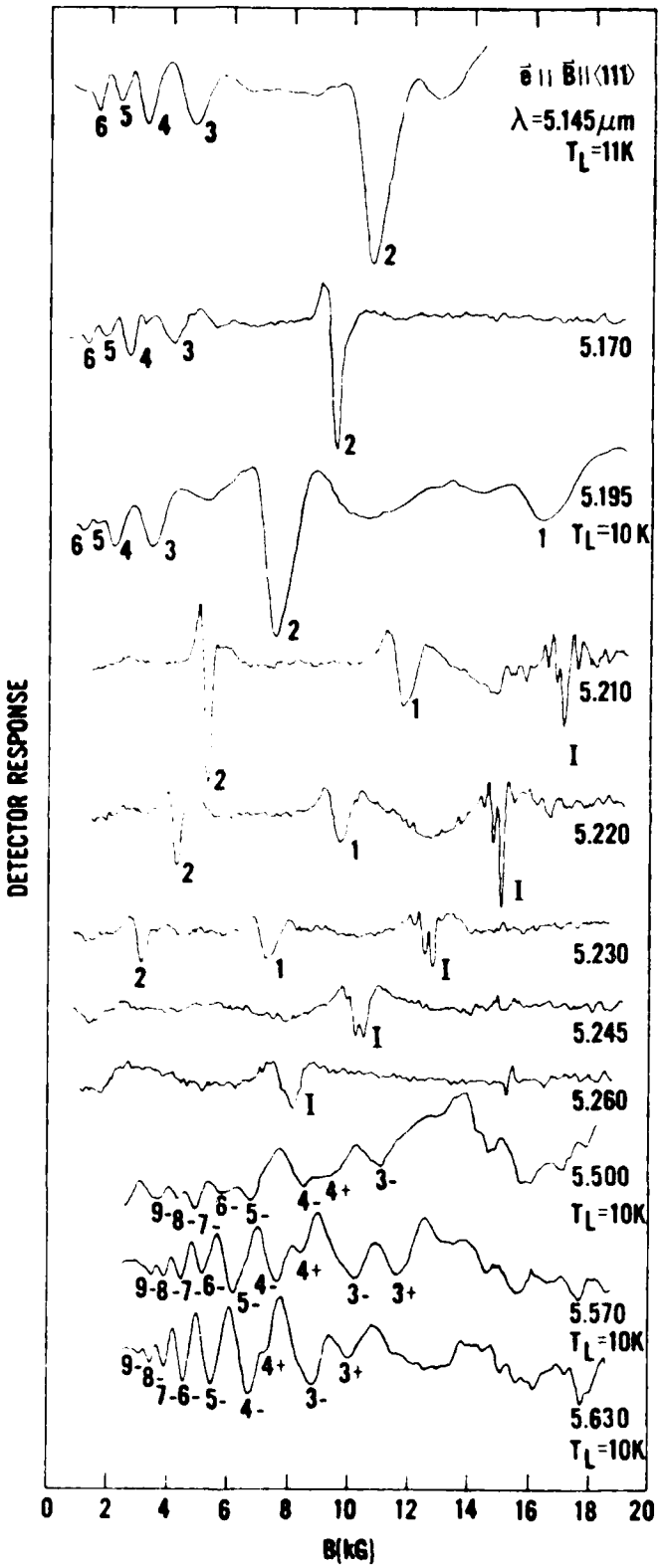
e ⊥ B ∥ ⟨111⟩
λ=5.145μm
T_L=11K
6 5 4 3
2
5.170
5.195
T_L=10 K
1
5.210
I
5.220
5.230
5.245
5.260
5.500
T_L=10K
9-8-7-6-5-4-4+3-3+
5.570
T_L=10K
5.630
T_L=10K
DETECTOR RESPONSE
0 2 4 6 8 10 12 14 16 18 20
B(kG)

Fig. IV.1

account in the quantitative interpretation of this data. Transition energies can be calculated from an 8 x 8 Pidgeon-Brown energy band model and compared to the data. The major unresolved question is to investigate the quantitative role of the excitons. This work is being pursued with the theoretical help of Dr. R. F. Wallis.

The structure labeled 1 in figure IV.1 is a transition which we have identified as a valence-to-shallow impurity level process. The fine structure splitting may be due to central cell splitting of this shallow donor ground state. The observed magnetic field splittings correspond to fractions of an meV in energy and are in reasonable agreement with the expected central cell splittings.

At much lower energies one sees a series of structures which is related to electron transitions from deep levels to the conduction band Landau levels. This deep level is different from the one reported earlier in the reprint in Section III. Different samples of n-InSb were used which accounts for the different activation energies. This sample has an activation energy value of $\simeq$ 38 meV above the valence band edge which is in reasonable agreement with the ground state of a gold acceptor.

V. INVESTIGATION OF NONLINEAR OPTICAL PROPERTIES OF SEMICONDUCTORS

A. Indium Antimonide

Here we present some of our results of an investigation of the nonlinear optical properties of n-InSb using two-photon spectroscopy techniques and only cw CO_2 lasers. Our two-photon experiments were the first to be carried out in solids using only cw lasers. Some very high magnetic field work (up to 15 T) was carried out at the Francis Bitter National Magnet Laboratory on the MIT campus. Most of the experimental work was carried out at NTSU at much lower fields (< 2 T). More extensive details than can be presented here are contained in a Ph.D. thesis of Dr. M. W. Goodwin. In what follows we reproduce several of our published papers.

V-2

PHYSICAL REVIEW B VOLUME 23, NUMBER 12 15 JUNE 1981

High-resolution two-photon spectroscopy in InSb at milliwatt cw powers in a magnetic field

D. G. Seiler* and M. W. Goodwin
Department of Physics, North Texas State University, Denton, Texas 76203

M. H. Weiler
Department of Physics, Massachusetts Institute of Technology, Cambridge, Massachusetts 02139

(Received 1 December 1980)

Resonant structure in the magnetophotoconductivity of *n*-InSb is shown to arise from two-photon absorption of cw CO_2 laser radiation. This is the first time that two-photon experiments in solids have been carried out with only cw lasers.

Weak magneto-optical transitions in high-purity *n*-InSb induced by a CO_2 laser have been recently observed by photoconductivity measurements for $\vec{e} \parallel \vec{B}$ in the Voigt configuration for magnetic fields up to 1.2 T.[1-3] This resonant structure was first attributed to multiple LO phonon emission from high-energy photoexcited electrons created by intraband absorption.[1,2] Later, it was proposed that the structure instead originates from midgap deep defect levels that are known to be present in InSb.[3] Two-photon resonant magneto-absorption was not suspected because of the use of cw lasers and the very low intensities ($\simeq 1$ W/cm^2) where the structure can first be observed. In this paper we present new experimental results on this resonant structure for $\vec{e} \perp \vec{B}$ and for fields up to 2 T. The simultaneous use of two CO_2 lasers has enabled us to identify unambiguously the physical origin of these resonant transitions as two-photon absorption rather than either of the two previous interpretations. This is a surprising and important result since two-photon effects (in any material) have only been previously observable with the help of at least one high-power pulsed laser which produces the high photon fluxes that were previously thought to be necessary. The use of cw lasers for two-photon absorption opens up new opportunities in spectroscopy by allowing high-resolution studies of new transitions with selection rules and exciton effects which are different from one-photon transitions.

The evidence for the two-photon-absorption interpretation which we present in this paper consists of (1) the change in conductivity induced by two cw CO_2 lasers simultaneously incident on the sample, (2) the amplitude of the structure which varies as the square of the intensity, and (3) the good agreement between theoretical and experimental two-photon transition energies. Our new experimental results cannot be explained by the multiple-phonon or deep-level models since neither model is consistent with the two-laser results or the intensity dependence of the amplitudes.

In our experiments, a constant dc electrical current is applied to the sample (of concentration 9×10^{13} cm^{-3}) while a small ac magnetic field modulates the sample conductivity at a frequency of 43 Hz. The photoconductive signal produced by the chopped laser (~ 20-μsec pulse width and 1700-Hz repetition rate) is fed into a sampling oscilloscope, the output of which is fed into a lock-in detector with response proportional to the second derivative of the photoconductive signal. All experiments were done in the Voigt configuration with either $\vec{e} \perp \vec{B}$ or $\vec{e} \parallel \vec{B}$ and the current parallel to $\vec{B}$ with $\vec{B}$ parallel to a (110) crystallographic direction.

The crucial experiment that clearly shows that the observed resonant structure in the photoconductivity is due to two-photon processes is illustrated in Fig. 1. The top curve shows a photoconductive trace ob-

V-3

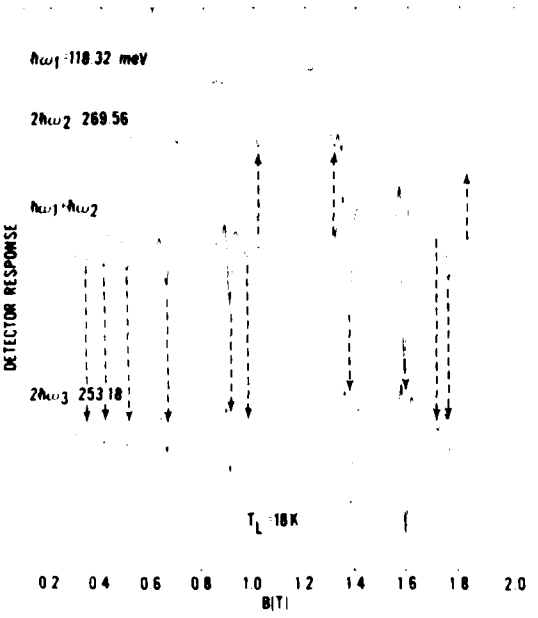

FIG. 1. Photoconductive spectra with $\vec{e} \perp \vec{B}$ at $T_l = 18$ K using various combinations of two-photon energies $2\hbar\omega_1 = 236.64$ meV, $2\hbar\omega_2 = 269.56$ meV, $\hbar\omega_1 + \hbar\omega_2 = 253.10$ meV, and $2\hbar\omega_3 = 253.18$ meV. The spectrum with $\hbar\omega_1 + \hbar\omega_2$ was obtained with two separate laser beams simultaneously incident upon the sample.

Fig. V.A.1

tained from a single 10.48-μm ($\hbar\omega_1 = 118.32$ meV) laser operating with a large peak incident power of 1.8 W. The sharp resonant structure is absent, and only one-LO phonon-assisted cyclotron harmonic transitions within the conduction band can be seen.[4] The next trace shows the resonant structure obtained with a single 9.20-μm line ($\hbar\omega_2 = 134.78$ meV) at a lower power of 0.2 W from another laser. The two-beam experimental results are shown in the next trace where completely different structure is seen, with only traces of the structure due to the weak 9.20-μm laser. Clearly this new structure arises only because of the presence of the two photons $\hbar\omega_1$ and $\hbar\omega_2$. As a final check, if two-photon processes are the origin of this new structure, the positions are determined by $\hbar\omega_1 + \hbar\omega_2$. Consequently, the same structure should be observed with only one laser, but at a different photon energy $\hbar\omega_3$ such that $2\hbar\omega_3 = \hbar\omega_1 + \hbar\omega_2$; the last trace shows that this is in fact the case using only one laser operating at 9.795 μm ($2\hbar\omega_3 = 253.18$ meV).

The only other possible interpretation of these data, aside from two-photon absorption, could be absorption of second-harmonic intensity produced when the incident radiation is polarized along a ⟨110⟩ crystal axis. However, we have also observed these same resonant effects for light polarized along a ⟨100⟩ axis. Consequently, we conclude that second-harmonic effects are negligible and that we are observing pure two-photon resonant transitions.

The amplitude of the resonant structure, which is directly related to the number of photoexcited carriers, was found to vary approximately as the square of the intensity. This is additional confirmation of the involvement of two-photon absorption. The number of photoexcited carriers n created by two-photon absorption is given by

$$\frac{dn}{dt} = A_2 I^2 - r_2 n(n + n_0) \quad . \tag{1}$$

where A_2 is the coefficient of two-photon absorption,[5] r_2 is the coefficient of quadratic or direct recombination,[6] I is the light intensity incident on the sample, and n_0 is the electron density when $I = 0$. For the small intensities of our experiments where $n << n_0$, we then have for steady state $n \simeq (A_2/r_2 n_0) I^2$, which explains the observed intensity dependence of the amplitude.

For the purpose of obtaining a value for A_2, we repeated our experiments using a boxcar integrator with no field modulation. From the photoconductivity voltage at resonance we estimate that $n \approx 1 \times 10^{13}$ cm^{-3} at a peak intensity of ~ 130 W/cm^2 for a peak observed at $\lambda = 9.59$ μm at $B \approx 1.2$ T. Averaging over a Gaussian intensity distribution and using a value of $r_2 \approx 1 \times 10^{-9}$ cm^3/sec,[6] and $n_0 \simeq 9 \times 10^{13}$ cm^{-3}, gives $A = 0.7$ cm sec/erg^2 in reasonable agreement with the experimental results of 1.6 cm sec/erg^2 measured by Nguyen *et al.*[5] for the same line observed in absorption. This value is also consistent with their theoretical estimate. A more detailed analysis of the intensity will be published later.

There have only been a few previous observations of multiphoton absorption in InSb in a magnetic field, first by Button *et al.*[7] This work was extended by Weiler *et al.*,[8] who interpreted the data using a tunneling theory of multiphoton absorption[9] which, like the zero-magnetic-field theory of Keldysh,[10] was later shown to be incorrect for two- (or even-) photon absorption.[11,12] Manlief and Pakık[13] explained most of their experimental results using the selection rules from perturbation theory, which were later also given by Zawadzki and Wlasak[14] with the absorption for polarizations $\vec{e} \parallel \vec{B}$ also observed and explained by Favrot *et al.*[15] Nguyen and co-workers[5] also explained their observation of two-photon absorption for $\vec{e} \perp \vec{B}$ with transition strengths calculated from perturbation theory using nonparabolic wave functions. The most recent study of two-photon absorption in InSb, in zero magnetic field, is that of Pidgeon and co-workers,[16] who give references to other work, and show that a perturbation-theory treatment, taking into account the exact nonparabolic wave functions and neglecting exciton effects, gave good agreement with their experimental results. Their conclusions

should also be valid for experiments in a magnetic field.

Comparison of our data shown in Fig. 1 with the two-photon data of Ref. 13 (Fig. 1) using a transversely excited atmosphere (TEA) CO_2 laser and of Ref. 5 (Fig. 1) using a q-switched CO_2 laser clearly illustrates the high resolution of our measurements where structure is seen at fields as low as ~ 2 kG. Also, an apparent doublet structure is resolved in some lines which has not previously been observed. We have observed two-photon structure using a single laser with peak incident powers as low as 14 mW in a beam of 1.5-mm $1/e^2$ intensity diameter.

Further confirmation of the identification of the resonant structure with two-photon absorption is provided in Fig. 2, where the resonance positions, from experiments with a single laser, are compared with a theoretical calculation. The theoretical transition energies were calculated using a refinement[17] of the Pidgeon and Brown 8×8 model[18] with parameters adjusted to give excellent agreement with interband and intra-conduction-band magneto-optical experiments. A value of $E_g = 236.6$ meV gave the best overall fit, with the other band parameters as given in Ref. 17. In Ref. 17 the observed one-photon interband transition peaks were identified with the exciton ground state associated with each transition by reducing the calculated interband transition energy by an approximate exciton binding energy.[19,20] For comparison with the present experiments we have used a numerical approximation[21] to the calculated exciton binding energy which is valid for the range of magnetic field values in Fig. 2.

The theoretical curves in Fig. 2 were calculated using the two-photon perturbation theory selection rule $\Delta n = 0, \pm 2$.[5,14,15] The positions are quite different from those with the single-photon selection rule $\Delta n = \pm 1$, differing essentially by a hole or electron cyclotron resonance energy. The high resolution of the present data provides an opportunity for identification of individual two-photon transitions, as opposed to unresolved groups of transitions. The fact that new transitions are observed is a general characteristic of two-photon spectroscopy, and provides a further test and opportunity for refinement of the theoretical model.

It is clear from an examination of Figs. 1 and 2 that the experimental resolution of 0.2 meV is sufficient to resolve not only the exciton ground-state peaks, but also excited-state peaks, associated with the different interband transitions. In Fig. 2 only the exciton ground-state transitions are plotted. Although the exciton correction is quite crude, we are satisfied with the good overall fit with the data. In future work we will attempt a better identification of the observed lines using an improved exciton correction, taking into account the possibility of excited exciton states. This will also allow a more accurate

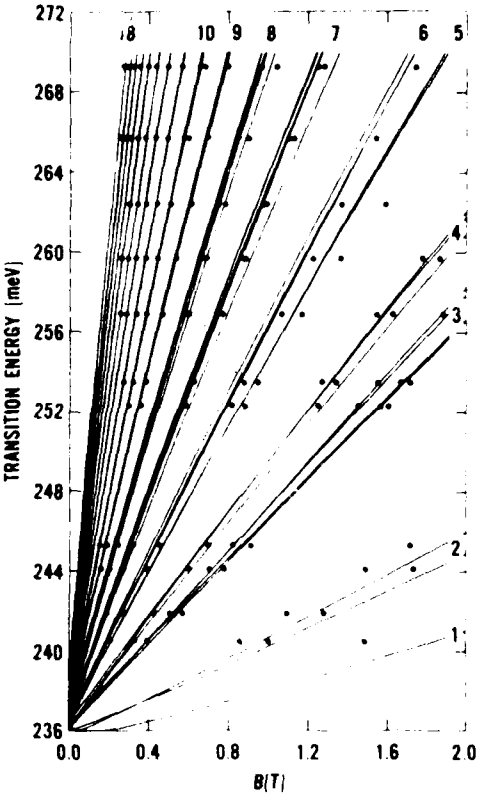

FIG. 2. Transition energies vs magnetic field. The dots represent the experimental data while the curves are the transition energies calculated for the strongest allowed two-photon transitions $\Delta n = 0, \pm 2$. We give below, in the notation of Ref. 17, the strongest transitions corresponding to each group of curves. 1. $a^-(2) \rightarrow a^c(0)$, 2. $a^+(0) \rightarrow a^c(0)$, $b^-(2) \rightarrow b^c(0)$, 3. $a^+(-1), a^-(3) \rightarrow a^c(1)$ $b^+(0) \rightarrow b^c(0)$, 4. $b^+(-1), b^-(1), b^-(3) \rightarrow b^c(1)$, 5. $a^+(2) \rightarrow a^c(0)$, 6. $a^+(1) \rightarrow a^c(1)$, $a^-(4) \rightarrow a^c(2)$, $b^-(2) \rightarrow b^c(2)$, 7. $a^-(5) \rightarrow a^c(3)$, $b^-(1), b^-(3) \rightarrow b^c(3)$, $b^+(1) \rightarrow b^c(1)$, $b^+(0) \rightarrow b^c(2)$, 8. $a^-(6) \rightarrow a^c(4)$, $b^-(4) \rightarrow b^c(4)$, $a^+(2) \rightarrow a^c(2)$, $a^+(3) \rightarrow a^c(1)$, 9. $a^-(7) \rightarrow a^c(5)$, $b^-(3), b^-(5) \rightarrow b^c(5)$, $b^+(2) \rightarrow b^c(2)$, $b^+(1) \rightarrow b^c(3)$, 10. $a^-(8) \rightarrow a^c(6)$, $b^-(6) \rightarrow a^c(6)$, $a^+(3) \rightarrow a^c(3)$, $a^+(4) \rightarrow a^c(2)$, etc.

Fig. V.A.2

determination of the band parameters from this complex set of two-photon data.

In summary, we have carried out the first two-photon experiments in solids using only cw lasers. A new dimension for two-photon spectroscopy has now been created with the distinct advantages that use of cw lasers has to offer. (1) better long- and short-term amplitude stability than pulsed lasers; (2) enhancement of signal-to-noise with the use of modulation and lock-in amplifier techniques. Other semiconductors with different band gaps will undoubtedly be studied with the appropriate cw lasers in the near future.

V-5

ACKNOWLEDGMENTS

The authors gratefully acknowledge the partial support of the research by the U.S. Office of Naval Research and a Faculty Research Grant from North Texas University. We also thank D. Heiman and D. Larson for their helpful comments.

---

*Present address: Francis Bitter National Magnet Laboratory, Massachusetts Institute of Technology, Cambridge, Mass. 02139.

[1]D. G. Seiler and M. W. Goodwin, in *Theoretical Aspects and New Developments in Magneto-Optics*, edited by J. Devreese (Plenum, New York, 1980), p. 569.

[2]D. G. Seiler, M. W. Goodwin, and K. Ngai, Opt. Commun. 31, 340 (1979).

[3]D. G. Seiler, M. W. Goodwin, and A. Miller, Phys. Rev. Lett. 44, 807 (1980).

[4]M. W. Goodwin, D. G. Seiler, and M. H. Weiler (unpublished).

[5]V. T. Nguyen and A. R. Strnad, Opt. Commun. 3, 25 (1971), V. T. Nguyen, A. R. Strnad, and Y. Yafet, Phys. Rev. Lett. 26, 1170 (1971).

[6]H. J. Fossum and B. Ancker-Johnson, Phys. Rev. B 8, 2850 (1973).

[7]K. J. Button, B. Lax, M. H. Weiler, and M. Reine, Phys. Rev. Lett. 17, 1005 (1966).

[8]M. H. Weiler, R. Bierig, and B. Lax, Phys. Rev. 184, 709 (1969).

[9]M. H. Weiler, M. Reine, and B. Lax, Phys. Rev. 171, 949 (1968).

[10]L. V. Keldysh, Zh. Eksp. Teor. Fiz. 47, 1946 (1964) [Sov. Phys. JETP 20, 1037 (1951)].

[11]M. H. Weiler, Phys. Rev. B 7, 5403 (1973).

[12]Y. A. Bychkov and A. M. Dykhne, Zh. Eksp. Teor. Fiz. 58, 1734 (1970) [Sov. Phys. JETP 31, 928 (1970)].

[13]S. K. Manlief and E. D. Palik, Solid State Commun. 12, 1071 (1973).

[14]*W. Zawadzki and J. Wlasak, J. Phys. C 9, L663 (1976).*

[15]G. Favrot, R. L. Aggarwal, and B. Lax, in *Proceedings of the 13th International Conference on Physics of Semiconductors, Rome*, edited by F. G. Fumi (North-Holland, Amsterdam, 1976), p. 1035.

[16]C. R. Pidgeon, B. S. Wherrett, A. M. Johnston, J. Dempsey, and A. Miller, Phys. Rev. Lett. 42, 1785 (1979), A. M. Johnston, C. R. Pidgeon, and J. Dempsey, Phys. Rev. B 22, 825 (1980).

[17]M. H. Weiler, J. Magn. Magn. Mater. 11, 131 (1979).

[18]C. R. Pidgeon and R. N. Brown, Phys. Rev. 146, 575 (1966).

[19]E. J. Johnson, Phys. Rev. Lett. 19, 352 (1967).

[20]Q. H. F. Vrehen, J. Phys. Chem. Solids 29, 129 (1968).

[21]K. Alavi (private communication).

V-6

PHYSICAL REVIEW B VOLUME 25, NUMBER 10 15 MAY 1982

Two-photon magnetoabsorption spectroscopy in n-InSb with cw CO_2 lasers

M. W. Goodwin and D. G. Seiler
Center for Applied Quantum Electronics, North Texas State University, Denton, Texas 76203

M. H. Weiler
Department of Physics, Massachusetts Institute of Technology, Cambridge, Massachusetts 02139

(Received 22 December 1981)

High-resolution two-photon magnetoabsorption (TPMA) spectra are obtained for $\vec{e}\perp\vec{B}$ and $\vec{e}\parallel\vec{B}$ polarizations in the Voigt geometry. The use of cw CO_2 lasers and a sensitive photoconductivity technique have allowed the observation of many new TPMA transitions. A modified Pidgeon-Brown energy-band model, along with the usual spherical two-photon selection rules, explains most of the observed transitions. The temperature dependence of the energy gap is deduced from an analysis of the TPMA spectra at various temperatures.

I. INTRODUCTION

Magneto-optical investigations of two-photon processes are particularly valuable for studying nonlinear absorption in semiconductors. The selection rules for two-photon magnetoabsorption (TPMA) allow completely different transitions to occur than for one-photon magnetoabsorption. In previous experiments of TPMA in InSb, pulsed lasers were used because it was believed that high intensities were necessary to observe two-photon transitions. However, we have recently shown that for the first time in solids, cw lasers operating at even milliwatt powers can be used in the study of TPMA if a sensitive enough detection method like photoconductivity (pc) is used.[1] Derivative TPMA spectroscopy with sampling and magnetic field modulation techniques applied to the pc signal further allows the observation of weak transitions in the TPMA pc spectra that would otherwise be unobservable.

In this paper we present comprehensive results on the TPMA spectra for both $\vec{e}\perp\vec{B}$ and $\vec{e}\parallel\vec{B}$ in the Voigt geometry for various lattice temperatures from 1.8 to 100 K. Most of the observed transitions are adequately explained by the spherical selection rules $\Delta s=0$, $\Delta n=0,\pm 2$, and a Pidgeon-Brown model calculation for the Landau-level energies. For the first time, we determine a set of band parameters for InSb from our TPMA experiments. By observing the resonant structure at different temperatures, we determine the variation of the energy gap with lattice temperature and compare it to previous experiments and theoretical results. From measurements of the number of two-photon-produced carriers as a function of laser intensity, we estimate TPMA coefficients for some of the stronger transitions. To our knowledge this is the first time that TPMA coefficients have been calculated from magnetophotoconductivity experiments.

The first TPMA experiments in InSb were carried out by Button *et al.*[2] using a Q-switched CO_2 laser simultaneously oscillating on two lines. They observed resonant structure in the photoconductivity caused by two-photon absorption between Landau levels in the valence and conduction bands. Zawadzki, Hanamura, and Lax[3] were the first to develop a set of two-photon selection rules using a *time-dependent perturbation-theory approach*. Later, Weiler *et al.*[4] extended Keldysh's[5] tunneling theory to the magnetic field case to try to explain the observed[6] polarization dependence ($\vec{e}\perp\vec{B}$ and $\vec{e}\parallel\vec{B}$). However, this theory was later found to be incorrect for two- (or even-) photon absorption and was shown to reduce to the perturbation-theory result.[7,8] Perturbation theory was again used by Bassani and Girlanda[9] to calculate explicit expressions for the two-photon transition rate in a magnetic field. TPMA experiments on InSb were continued by Nguyen and Strnad[10] and Nguyen *et al.*[11] who studied the absorption by free holes created by the two-photon processes using a Q-switched CO_2 laser pulse. Both linearly polarized light with $\vec{e}\parallel\vec{B}$ and $\vec{e}\perp\vec{B}$ and left (σ_L) and right (σ_R) circularly polarized light were used. They compared the experimental absorption strengths of the two-photon transitions for $\vec{e}\perp\vec{B}$ ($\sigma_L,\sigma_R,\sigma_L+\sigma_R$) with a

theoretical calculation based on the perturbation-theory approach and found reasonably good agreement. However, only a small number of transitions were observed and only one-photon energy was used. Manlief and Palik[12] extended the TPMA experiments to investigate the differences between the light polarizations $\vec{e}\perp\vec{B}$ and $\vec{e}\|\vec{B}$ in the Voigt configuration. The light source was a transversely excited atmospheric (TEA) CO_2 laser with an intracavity grating which allowed the photon-energy dependence of the TPMf_- transition to be studied. Their use of the photoconductivity technique enabled more transitions to be observed than were found by Nguyen *et al.* However, their transition assignments were somewhat ambiguous because of the uncertainty of both their measurements and the one-photon-interband Landau-energy data that was used to obtain the transition energies for their two-photon case. Nevertheless, they found several transitions in their studies which were not adequately explained by the usual spherical selection rules obtained from ordinary perturbation theory. In this paper we give transition assignments that are more unambiguous because (1) the higher resolution of our data allows more transitions to be seen, and (2) the data are compared with two-photon transition energies actually calculated from a Pidgeon-Brown model with band parameters adjusted to give a best fit.

Selection rules are extremely important for a good description of the two-photon magnetoabsorption process. The most complete summary of the two-photon selection rules for the different light polarizations (σ_L, σ_R, σ, and π) was given by Zawadzki and Wlasak, but only for the case of $\vec{B}\|[001]$.[13] Extra transitions were shown to occur because of warping and inversion-asymmetry effects. In this paper we give more complete two-photon selection rules for the different light polarizations and for $\vec{B}\|[111]$ and [110] directions, as well as the [001] direction.

II. EXPERIMENT

The samples of high-purity n-InSb ($\sim 9\times 10^{13}$ cm^{-3}) were mounted in the Voigt configuration with the current parallel to the magnetic field $\vec{B}$ and $\vec{B}$ parallel to [110] [100] and [111] crystallographic directions. Light from a grating-tunable cw CO_2 laser was mechanically chopped by a rotating slotted wheel to produce optical pulses of approximately 20-μsec width at a repetition rate of 1700 Hz. This minimized heating of the sample which was either immersed in liquid helium or surrounded by flowing helium gas for the higher temperature measurements. To vary the intensity of the laser we placed CaF_2 attenuators in the beam path. Beam profile measurements at the sample location showed that the beam was Gaussian with a typical $1/e$ intensity diameter of approximately 0.5 mm. A boxcar integrator was used to measure directly the photoconductive voltage, which at low powers is related to the number of two-photon-produced photocarriers. Field positions, amplitudes, and line widths can then be directly measured and studied as a function of laser intensity, lattice temperature, etc. The addition of modulation techniques significantly improves the sensitivity and resolution of photoconductivity experiments allowing a more accurate determination of the resonant field positions and resolution of weak structure.

A variation of the sampling and magnetic field modulation technique developed by Kahlert and Seiler,[14] for hot-electron quantum transport measurements is used to improve greatly the signal-to-noise ratio in photoconductivity measurements. A constant dc electrical current is applied to the sample while an ac magnetic field B_m of amplitude up to 200 G modulates the sample conductivity at a freqency of 43 Hz. The photoconductive signal produced by the laser pulse and the field modulation is amplified by a high-impedance differential amplifier, the output of which is connected to a sampling oscilloscope and lock-in amplifier combination.

In Fig. 1 we demonstrate how powerful the photoresistance-derivative technique is by comparing traces obtained with the sampling oscilloscope and lock-in amplifier combination (d^2R/dB^2, dR/dB) to that obtained with a boxcar averager (R). As can be seen, the TPMA structure in the d^2R/dB^2 trace is much sharper and more pronounced than in the R trace, making determination of magnetic field positions for the transitions not only easier but more accurate. The field positions of the resonant structure are not changed by the modulation technique. In addition, and most importantly, the second-derivative technique is able to resolve very weak structure that is marginally or not at all observable in the R trace (note the dotted lines). This is one reason we are able to observe more TPMA transitions than have previously been reported. The use of stable cw lasers also reduces the pulse-to-pulse amplitude variation usually present from pulsed lasers. The resulting enhanced

V-8

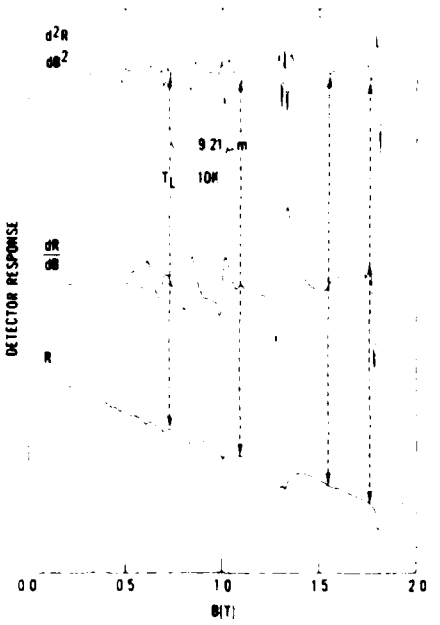

FIG. 1. Comparison of TPMA data using our high-resolution technique and that obtained with a boxcar averager. The d^2R/dB^2 and dR/dB curves are the second and first derivative of the magnetophotoresistance R with respect to magnetic field B using the sampling and magnetic-field modulation system. R is the magnetophotoresistance of the sample obtained with a boxcar averager commonly used on other experiments. The dashed lines point to weak transitions in d^2R/dB^2 not found in the R traces. ($B_m = 200$ G.)

Fig. V.A.3

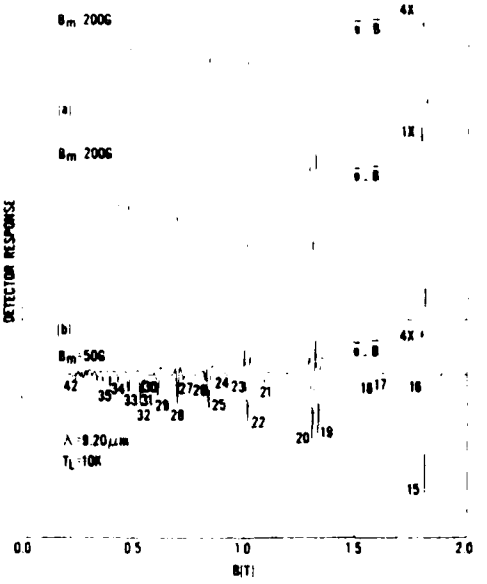

FIG. 2. (a) Comparison of TPMA structure for $\vec{e}\|\vec{B}$ and $\vec{e}\perp\vec{B}$ with $B_m = 200$ G. (b) Increased resolution of structure for $\vec{e}\perp\vec{B}$ using $B_m = 50$ G.

Fig. V.A.4

signal-to-noise ratio thus allows more TPMA transitions to be seen at low fields where the TPMA transition strength is weak.

III. RESULTS

A. Transition energies

An interesting aspect of two-photon magnetoabsorption and one that has been the subject of much controversy is the effect of different polarizations of the light on the TPMA spectra. Such effects are a consequence of the selection rules, which are different for different polarizations. In Fig. 2(a) the resonant structure caused by the polarizations $\vec{e}\perp\vec{B}$ and $\vec{e}\|\vec{B}$ in the Voigt configuration is shown. The structure is labeled with numbers corresponding to distinct sets of transitions. Two major observations about these transitions are apparent: (1) those for $\vec{e}\|\vec{B}$ are much weaker than those for $\vec{e}\perp\vec{B}$ and (2) for $\vec{e}\perp\vec{B}$, more complex structure is seen. Previous studies[10,12] of TPMA with pulsed lasers also showed this. The complexity of the $\vec{e}\perp\vec{B}$ structure is much more evident in Fig. 2(b) where a lower modulation field $B_m \simeq 50$ G results in small resonant amplitudes but allows resolution of fine structure down to very low magnetic fields. For example, we have complete resolution of a "double nature" to lines 19,20,22,23,25 – 32, while evidence for doublets from the line shape can still be seen in lines 33 – 35. Previous TPMA experiments did not have the resolution to detect this nature of the actual TPMA structure.

In Table I we have listed the two-photon magnetoabsorption selection rules derived from the usual spherical approximation and additional selection rules which are allowed because of warping and inversion-asymmetry effects. We have included the selection rules for the case of $\vec{B}\|[111]$ and $\vec{B}\|[110]$ by extending the one-photon selection rules of Weiler *et al.*[15] to the two-photon absorption case. Transitions within the a and b set of solutions are denoted by $\Delta s = 0$, while $\Delta s = -1$ denotes transitions from a to b and $\Delta s = +1$, b to a. Also given is the corresponding change in Landau-level number Δn from the initial valence-band state to the final conduction-band state using the unrenumbered valence-band-state notation. In

Table V A.1

TABLE I. Selection rules for two-photon transitions in zinc-blende semiconductors, for a magnetic field $\vec{B}$ [001], [110], and [111] crystal axes, both allowed (A) and induced by warping (W) and inversion asymmetry (I)

		$\vec{B}\|\|[001]$						$\vec{B}\|\|[110]$				$\vec{B}\|\|[111]$			
		A		W		I		W		I		W		I	
Polarization		Δs	Δn	Δs	Δn	Δs	Δn	Δs	Δn	Δs	Δn	Δs	Δn	Δs	Δn
	σ_L	0	+2	0	−2, +6	−1	+1, +5	0	0, 2, +4, +6	0	+1, +3, +5	1	0, +6	0	1 + 5
														1	+3
						+1	−1, +3					+1	−2, +4	+1	+1
$\vec{E}\perp\vec{B}$	σ_R	0	−2	0	+2, −6	−1	+1, −3	0	0, +2, −4, −6	0	±1,	1	+2, −4	0	+1, −5
														−1	−1
						+1	−1, −5					+1	0, −6	+1	−3
	σ	0	0	0	±4	−1	±1, ±3	0	±2, ±4	0	±1, ±3	−1	−2, +4	0	±3
														−1	+1
						+1	±1, ±3					+1	+2, −4	+1	−1
$\vec{E}\|\|\vec{B}$	π	0	0	0	±4	−1	±1, ±3	0	±2, ±4	0	±1, ±3	−1	−2, +4	0	±3
														−1	+1
						+1	±1, ±3					+1	+2, −4	+1	−1

agreement with the data (1) the spherical approximation rules predict more transitions for $\vec{e}\perp\vec{B}$ than for $\vec{e}\|\|\vec{B}$ and (2) some of the transitions should be the same for both light polarizations (i.e., $\Delta n=0, \Delta s=0$).

Quantitative results of transition energies (twice the photon energy) versus resonant magnetic field positions are shown in Fig. 3 for both (a) $\vec{e}\perp\vec{B}$ and (b) $\vec{e}\|\vec{B}$ along with theoretically calculated results with $\vec{B}\|[110]$. There are many more transitions plotted than have been found from the earlier studies using pulsed lasers.[2,6,10–12] We have added several weaker transitions to the $\vec{e}\perp\vec{B}$ set reported earlier by us.[1] In Table II, we give the theoretical assignments of the intial and final states to the experimentally observed two-photon transitions. The experimental positions of our two-photon structure are in good agreement with those published in Refs. 10–12. In addition, it is interesting to note that our identification of the transitions 4, 5, 7, 9, 10, 12, 15, and 20 is the same as that in Refs. 10 and 11, whereas the identification in Ref. 12 is the same for only transitions 4, 7, 10, 11, and 15. The Landau levels were calculated from an 8×8 Pidgeon-Brown model which includes only the warping terms in the diagonal part of the Hamiltonian and no inversion asymmetry terms.[15,16] Transitions involved in magnetoabsorption experiments are usually considered as being to exciton levels rather than being between the Landau levels. However, there is at present no adequate exciton theory for TPMA in semiconductors with complex coupled energy bands. In our earlier approach[1] we reduced the calculated interband transition energy by an approximate exciton ground-state binding energy. This is the standard exciton correction used in one-photon spectroscopy. Here we adopt the approach of not correcting for exciton effects and of treating the Landau-level theory as accurately as possible in calculating transition energies. We then look for differences between the calculated and observed energies for the lowest transitions where exciton effects should be most important. The theortically calculated *solid lines* shown in Fig. 3 result from using only the spherical selection rules given in Table I. It appears that most of the experimental data can be adequately described (but with a new set of band parameters) with these rules without using exciton corrections even for the low-energy high-field transitions. A good fit of these theoretical transitions to the data results from using the following band parameters: $E_g=235.2$ meV, $E_p=23.0$ eV, $\Delta=0.803$ eV, $\gamma_1=3.0$, $\gamma_2=-0.2$, $\gamma_3=1.0$, $\kappa=-1.2$, $q=0.55$, $F=-0.5$, and $N_1=-0.4$. No attempt was made to determine a value of Δ from our two-photon data. Instead we have used the stress-modulated magnetoreflectance results of $\Delta=0.803\pm0.005$ eV obtained by Aggarwal.[17] Our results for the rest of the band parameters are compared in Table III

V-10

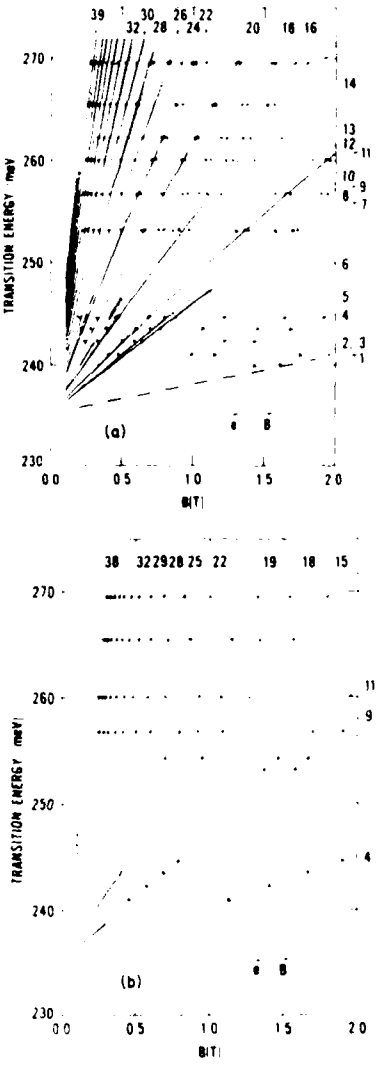

FIG. 3. (a) Fan chart of TPMA transition energies ($\vec{\epsilon} \perp \vec{B}$ [110]). Solid lines represent theoretical calculations with selection rules $\Delta s = 0$, $\Delta n = 0, \pm 2$. Dotted lines used other selection rules explained in the text. Dots are the data. (b) Fan chart for $\vec{\epsilon} \parallel \vec{B}$.

Fig. V.A.5

with previously published one-photon results of Grisar *et al.*,[18] Ranvaud *et al.*,[19] Weiler,[20] Pidgeon and Brown,[16] and Pidgeon and Groves.[21] We have used this same set of parameters in also fitting intra-conduction-band (combined resonance, cyclotron resonance, and LO phonon-assisted resonances)[22] and intra-valence-band (both bound and free-hole transitions)[23] data. An excellent fit in both cases is achieved.

Additional weaker structure labeled (1,3), (6), (17,18), and (24) in Fig. 3 appears not to be explainable by the spherical selection rules. We find that lines 1,3 may be explained by spin-flip transitions $b^-(1) \rightarrow a^c(0)$ ($\Delta s = +1$, $\Delta n = -1$) and $b^+(-1) \rightarrow a^c(0)$ ($\Delta s = +1$, $\Delta n = +1$). These are shown by the dashed lines in Fig. 3. According to Table I these transitions are allowed because of inversion-asymmetry effects but only for $\vec{B} \parallel$ [100] or [111]. Transition 6 was also observed by Manlief and Palik for $\vec{B} \parallel$ [100] at higher magnetic fields and higher photon energies and was identified with an $a^+(0) \rightarrow b^c(0)$ ($\Delta s = -1$, $\Delta n = 0$) transition. Using this transition we calculate an additional line passing exactly through our data points in set 6 (as shown by the dashed line) confirming this identification. Transitions in set 17, 18, and 24 have not been previously reported. They are very weak resonances which can only be observed using the modulation technique. Our calculations support the identification for an $a^+(2) \rightarrow b^c(0)$ transition with $\Delta s = -1$ and $\Delta n = -2$ for 17 and $a^+(1) \rightarrow b^c(1)$ and $a^+(2) \rightarrow b^c(2)$ transitions with $\Delta s = -1$ and $\Delta n = 0$ for 18 and 24, respectively. According to Table I $\Delta s = -1$, $\Delta n = 0$ transitions can occur for $\vec{B} \parallel$ [111] because of warping effects. However, these transitions are also present for $\vec{B} \parallel$ [100] and [110] is not presently understood.

B. Effect of lattice temperature

TPMA experiments provide an accurate means of determining the variation of the fundamental energy gap E_g with lattice temperature T_L. Figure 4 shows how the TPMA spectra at $\lambda = 9.33$ μm is affected by increasing T_L for $T_L \leq 100$ K. The shift in magnetic field positions of the resonant structure is quite noticeable for $T_L \geq 30$ K and is directly related to the decrease in energy gap with increasing temperature. At each value of T_L, fan charts of transition energies versus magnetic field were determined and analyzed assuming that all parameters except E_g were constant. The results are shown in Fig. 5 where a comparison with theoretical calculations of Tsay *et al.*[24] and Camassel and Auvergne[25] is also given. These theoretical results were normalized to our experimental band gap of 235.2 meV at $T_L \leq 10$ K. Also shown are the experimental results of Roberts and Quarrington[26] and Auvergne *et al.*[27] There is good agreement between our data and the results of Cammassel and Auvergne who directly calculated the temperature dependence using a pseudopotential approach. With increasing T_L one increases both the lattice constant and the electron-phonon

V-11

Table V.A.2

TABLE II. Theoretical two-photon transition assignments for each distinct experimentally observed series of resonant structure in the photoconductivity for $\vec{e}\perp\vec{B}$ polarization in the Voigt geometry. The * marks indicate those transitions which can only be explained by the nonspherical or extra transitions.

Experimental transition no.	Theoretical assignment	Experimental transition no.	Theoretical assignment
*1,3	$a^-(1)\,a^c(0)$	20	$b^+(0)\,b^c(2)$
	$a^+(-1)\,a^c(0)$	21	$a^+(3)\,a^c(1)$
	$b^-(2)\,a^c(0)$	22	$a^-(6)\,a^c(4)$
	$b^-(1)\,a^c(0)$		$a^+(2)\,a^c(2)$
	$b^+(-1)\,a^c(0)$	23	$b^-(6)\,b^c(4)$
2	$a^-(2)\,a^c(0)$	*24	$a^+(2)\,b^c(2)$
4	$a^+(0)\,a^c(0)$	25	$a^-(7)\,a^c(5)$
5	$b^-(2)\,b^c(0)$		$b^+(2)\,b^c(2)$
*6	$a^+(0)\,b^c(0)$	26	$b^+(1)\,b^c(3)$
7	$a^+(-1)\,a^c(1)$	27	$a^+(4)\,a^c(2)$
8	$a^-(1)\,a^c(1)$	28	$a^-(8)\,a^c(6)$
9	$b^+(0)\,b^c(0)$		$a^+(3)\,a^c(3)$
10	$a^-(3)\,a^c(1)$	29	$a^-(9)\,a^c(7)$
11	$b^-(1)\,b^c(1)$		$b^+(3)\,b^c(3)$
12	$b^+(-1)\,b^c(1)$	30	$b^+(2)\,b^c(4)$
13	$b^-(3)\,b^c(1)$	31	$a^+(5)\,a^c(3)$
14	$a^+(2)\,a^c(0)$	32	$a^-(10)\,a^c(8)$
15	$a^-(4)\,a^c(2)$		$a^+(4)\,a^c(4)$
	$a^+(1)\,a^c(1)$	33	$b^+(3)\,b^c(5)$
16	$b^-(4)\,b^c(2)$		$a^-(11)\,a^c(9)$
*17	$a^+(2)\,b^c(0)$		$b^+(4)\,b^c(4)$
	$a^-(4)\,b^c(2)$	34	$a^+(6)\,a^c(4)$
*18	$a^+(1)\,b^c(1)$		$a^-(12)\,a^c(10)$
	$a^+(0)\,b^c(2)$		$a^+(5)\,a^c(5)$
	$b^+(2)\,b^c(0)$	35	$b^+(4)\,b^c(6)$
19	$a^-(5)\,a^c(3)$		$a^-(13)\,a^c(11)$
	$b^+(1)\,b^c(1)$		$b^+(5)\,b^c(5)$

Table V.A.3

TABLE III. Energy-band parameter sets for InSb from various experiments.

Parameter	Grisar *et al.* (Ref. 18)	Ranvaud *et al.* (Ref. 19)	Weiler (Ref. 20)	Pidgeon and Brown (Ref. 16)	Pidgeon and Groves (Ref. 21)	This paper
E_g (eV)	0.2355	0.235	0.2329	0.2355 ±0.0005	0.2366	0.2352
E_p (eV)	21.6	26.1	23.5±0.5	21.9	21.2	23.0
γ_1	0.5	3.1	3.4	1.5	3.6	3.0
γ_2	−1.0	−0.4	−0.3	−1.2	−0.5	−0.2
γ_3	0.1	0.7	0.9	−0.1	0.7	1.0
$\gamma_2-\gamma_3$	−1.1	−1.1	−1.2	−1.1	−1.2	−1.2
κ	−1.4	−1.5	−1.2	−2.1	−1.47	−1.2
q	0	0.39	0	0	0.39	0.55
N_1	0	0	−0.3	0	0	−0.4
F	0	0	−1.0	0	0	−0.5

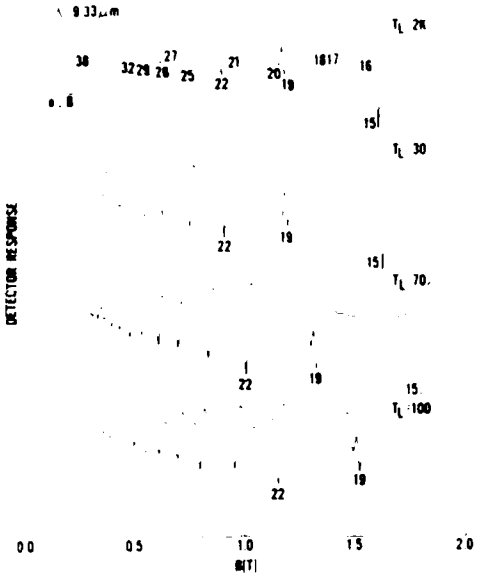

FIG. 4. Temperature dependence of TPMA structure for $\lambda = 9.33\ \mu m$.

Fig. V.A.6

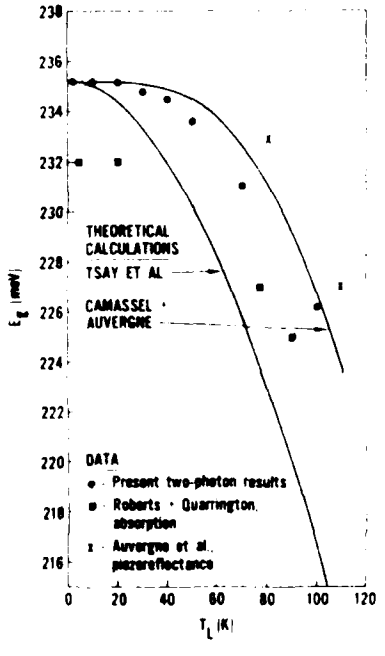

FIG. 5. Plot of energy gap vs temperature from our TPMA measurements and other results. The lines are theoretical calculations of Tsay *et al* (Ref. 24) and of Cammassel and Auvergne (Ref. 25) normalized to $E_g = 235.2$ meV.

Fig. V.A.7

interaction. Their contributions to the gap change are of opposite sign leading to only slight decreases in band gap for $T_L \leq 25$ K. The gap at 77 K is thus approximately 230 meV.

C. Intensity dependence

Figure 6 shows the TPMA structure for the "low-intensity" case using a cw CO_2 laser and for that obtained using a rotating mirror Q-switched CO_2 laser operating at 200 Hz with a pulsewidth of full width at half maximum of 100 nsec. There is good agreement between the observed structures. Since no additional structure is observed in the rotating mirror case, one concludes that this is additional confirmation of the correct identification of the cw laser-induced structure as indeed arising from TPMA effects. It is also apparent that in the cw case we have really reached the "high-intensity" limit where TPMA effects can be observed at rather low powers.

Two-phonon absorption is a nonlinear process which has a nonlinear dependence on the incident intensity. The two-photon absorption coefficient K_2, which is a parameter of the semiconductor and

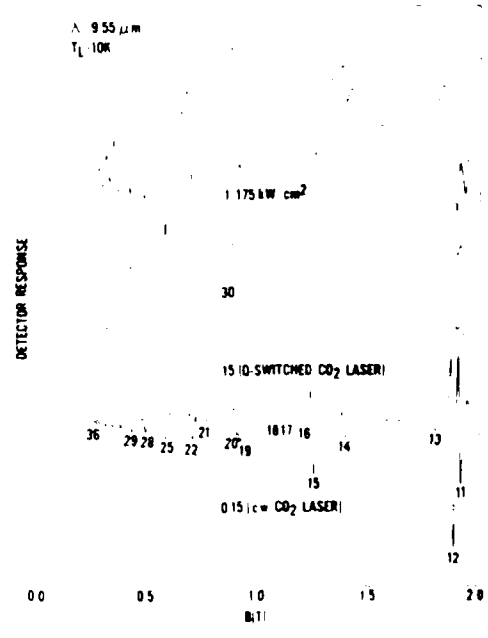

FIG. 6. TPMA structure obtained with a Q-switched CO_2 laser (top 3 traces) and with a cw CO_2 laser for $\lambda = 9.55\ \mu m$.

Fig V.A.8

V-13

describes the rate of two-photon-produced free carriers, has been the subject of intense experimental studies.[28-34] However, these results are not consistent. For this reason we have determined two-photon absorption coefficients for some of the stronger transitions in our pc data.

The standard approach for describing the rate of two-photon-generated carriers is to assume that an electron in the valence band is excited into the conduction band via two-photon absorption and then decays by the bimolecular process of radiative recombination. A suitable rate equation can then be written

$$\frac{dn}{dt} = \frac{K_2}{2\hbar\omega} I^2 - rn(n + n_0) , \tag{1}$$

where n is the photon-created carrier density, K_2 the two-photon magnetoabsorption coefficient, $\hbar\omega$ the photon energy, I the incident intensity, r the recombination rate, and n_0 the equilibrium carrier density without light. The time duration of our optical pulses is sufffficiently long enough (20 μsec) that a steady state occurs at the time of our measurements, usually 10 μsec after the beginning of the pulse. For steady state $dn/dt = 0$, simplifying Eq. (1) tremendously. For the low laser intensities (< 200 W/cm^2) of our study the photon-created carrier density n is small (i.e., $n << n_0$). With these assumptions Eq. (1) is reduced to the following:

$$n = \frac{K_2}{2\hbar\omega r n_0} I^2 , \tag{2}$$

which shows that the number of free carriers produced by TPMA is proportional to I^2. Also considered in many TPMA experiments is the depletion of the laser intensity as it propagates through the crystal. For our sample thickness of approximately 100 micrometers we estimate that the change in intensity of the beam from the front to the back surface is roughly 0.01% for the highest intensities reported here. We therefore neglect the change in intensity of the laser beam and assume a uniform constant Gaussian optical flux throughout the sample.

In Fig. 7 we have plotted n vs I^2 for five different laser intensities for the strong transition labeled 12 ($\vec{e} \perp \vec{B}$) of Fig. 3. Assuming a negligible change in mobility, the photocreated carrier densities were determined from the amplitude of the resonant resistance structure obtained with a boxcar averager (an example of the structure for a different wavelength is trace R of Fig. 1). Thus n is seen to vary approximately as I^2 in agreement with Eq. (2). At higher intensities the amplitude of the resonant structure is observed to depart significantly from a square-law behavior because of hot-electron and free-hole absorption effects. Also plotted in Fig. 7 is a fit of Eq. (2) to the data using K_2 as an adjustable parameter. The value of the other parameters are $\hbar\omega = 128.14$ meV, $r = 1 \times 10^{-9}$ cm^3/sec,[35] $n_0 = 9 \times 10^{13}$ cm^{-3}, giving a value of K_2 of 5.6 cm/MW. For the same transition above at a slightly higher magnitude field (1.92 T) and higher photon energy (129.8 meV) Nguyen *et al.*[10] obtained a value for K_2 of 16.6 cm/MW. Their somewhat larger value of K_2 is partly due to that fact that a higher magnetic field will increase the magnitude of K_2 for a particular transition. However, it must be pointed out that our K_2 is sensitive to a proper choice of the recombination rate r. Another problem that arises when trying to extract information about an individual transition is that a minimum in the structure may actually be a combination of two or more transitions. The large number of transitions (theory and experiment) evident in Fig. 3 certainly seem to indicate this. Therefore, K_2 was calculated and measured only for a strong transition which was minimally influenced by a presence of other closely-spaced weak transitions.

IV. CONCLUSIONS

High-resolution TPMA spectra in InSb for $\vec{e} \perp \vec{B}$ and $\vec{e} \parallel \vec{B}$ polarizations in the Voigt geometry have been investigated using cw CO_2 lasers. A highly

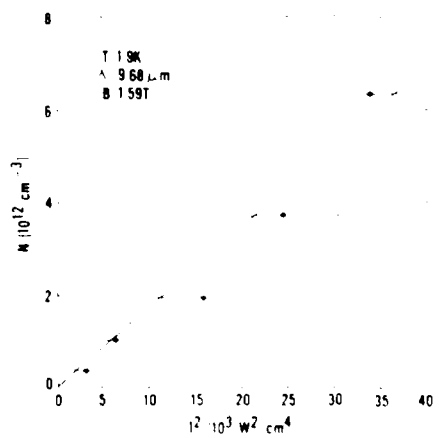

FIG. 7. Two-photon-produced free-carrier density as a function of intensity for transition 12. The line represents the variation of Eq. (2) with $K_2 = 5.7$ cm/MW.

Fig. V A.9

V-14

sensitive photoconductivity technique in conjuction with a stable cw laser have allowed the observation of many new TPMA transitions. Previous TPMA experiments have not been able to show how complicated the two-photon spectra really is. Many of the previously observed transitions are shown to be combinations of two or more transitions. A minimum of 42 distinct transitions are observed and identified for $\vec{\epsilon} \perp \vec{B}$, most of which can be explained by the usual spherical two-photon selection rules $\Delta n = 0, \pm 2$, $\Delta s = 0$. For $\vec{\epsilon} \parallel \vec{B}$ the structure is less complicated and can be explained by the spherical rule $\Delta n = 0$, $\Delta s = 0$. A modified Pidgeon-Brown energy-band model, along with these spherical selection rules explain most of the observed transitions using the following set of band parameters: $E_g = 235.2$ meV, $E_p = 23.0$ eV, $\Delta = 0.803$ eV, $\gamma_1 = 3.0$, $\gamma_2 = -0.2$, $\gamma_3 = 1.0$, $\kappa = -1.2$, $F = -0.5$, $q = 0.55$, and $N_1 = -0.4$. Additional weaker TPMA transitions appear to result from warping and inversion-asymmetry effects. The variation of the fundamental energy gap with lattice temperature is deduced from an analysis of the temperature-dependent TPMA spectra. Our results give a gap of ~ 230 meV at 77 K and compare favorably with the pseudopotential calculations of Camassel and Auvergne. At low intensities the number of photoexcited electrons varies approximately as the square of the incident intensity, as predicted by a simple rate equation model.

Note added in proof. Band-gap renormalization caused by many-body effects of the laser-created electron-hole plasma would be expected to decrease the energy gap. The amount of decrease depends upon the laser intensity which also controls the number of electron-hole pairs. However, the magnetic field positions of the resonances shown in Fig. 6 do not appear to shift even at the high intensities from the Q-switched laser. Thus the band-gap change with these high intensities must be much less than 1 meV. Recently Koch *et al.*[36] calculated the change in band gap as a function of electron-hole pair density for InSb. Since the number of created electron-hole pairs at the large intensities is estimated to be at least $10^{14} - 10^{15}$ cm^{-3} their results indicate a much larger band-gap renormalization effect when we observe (at 10^{15} cm^{-3}) their calculated decrease is approximately 2.5 meV).

[1] D. G. Seiler, M. W. Goodwin, and M. H. Weiler, Phys. Rev. B 23, 6806 (1981).

[2] K. J. Button, B. Lax, M. H. Weiler, and M. Reine, Phys. Rev. Lett. 17, 1055 (1966).

[3] W. Zawadzki, F. Hanamuara, and B. Lax, Bull. Amer. Phys. Soc. 12, 100 (1967).

[4] M. H. Weiler, M. Reine, and B. Lax, Phys. Rev. 171, 949 (1968).

[5] L. V. Keldysh, Zh. Eksp. Teor. Fiz. 47, 1945 (1964) [Sov. Phys.—JETP 20, 1307 (1965)].

[6] M. H. Weiler, R. Bierig, and B. Lax, Phys. Rev. 184, 709 (1969).

[7] M. H. Weiler, Phys. Rev. B 7, 5403 (1973).

[8] Y. N. Bychkov and A. M. Dykhne, Zh. Eksp. Teor. Fiz. 58, 1734 (1970) [Sov. Phys.—JETP 31, 928 (1970)].

[9] F. Bassani and R. Girlanda, Opt. Commun. 1, 359 (1970).

[10] V. T. Nguyen and A. R. Strnad, Opt. Commun. 3, 25 (1971).

[11] V. T. Nguyen, A. R. Strnad, and Y. Yafet, Phys. Rev. Lett. 26, 1170 (1971).

[12] S. K. Manlief and D. E. Palik, Solid State Commun. 12, 1071 (1973).

[13] W. Zawadzki and J. Wlasak, J. Phys. C 9, L663 (1976).

[14] H. Kahlert and D. G. Seiler, Rev. Sci. Instrum. 48, 1017 (1977).

[15] M. Weiler, R. L. Aggarwal, and B. Lax, Phys. Rev. B 17, 3269 (1978).

[16] C. R. Pidgeon and R. N. Brown, Phys. Rev. 146, 575 (1966).

[17] R. L. Aggarwal, in *Semiconductors and Semimetals*, edited by R. K. Willardson and A. C. Beer (Academic, New York, 1972), Vol. 9, p. 151.

[18] R. Grisar, H. Wachernig, G. Bauer, J. Wlask, J. Kowalski, and W. Zawadzki, Phys. Rev. B 18, 4355 (1978).

[19] R. Ranvaud, H.-R. Trebin, U. Rossler, and F. H. Pollak, Phys. Rev. B 20, 701 (1979).

[20] M. H. Weiler, J. Magn. Magn. Mater. 11, 131 (1979).

[21] C. R. Pidgeon and S. H. Groves, Phys. Rev. 186, 824 (1969).

[22] M. W. Goodwin and D. G. Seiler (unpublished).

[23] C. L. Littler, D. G. Seiler, R. Kaplan, and R. J. Wagner (unpublished).

[24] Y. F. Tsay, B. Gong, S. S. Mitra, and J. F. Vetelino, Phys. Rev. B 6, 2330 (1972).

[25] J. Camassel and D. Auvergne, Phys. Rev. B 12, 3258 (1975).

[26] V. Roberts and J. E. Quarrington, J. Electron. 1, 152 (1955).

[27] D. Auvergne, J. Camassel, H. Mathieu, and M. Cardo-

na, Phys. Rev. B 9, 5168 (1974).
[28]A. F. Gibson, M. J. Kent, and M. F. Kimmitt, Brit. J. Appl. Phys. 1, 149 (1968).
[29]A. M. Danishevskii, A. A. Patrin, S. M. Ryvkin, and J. D. Yaroshetskii, Zh. Eksp. Teor. Fiz. 56, 1459 (1969) [Sov. Phys.—JETP 29, 781 (1969)].
[30]J. M. Doviak, A. F. Gibson, M. F. Kimmitt, and A. C. Walker, J. Phys. C 6, 593 (1973).
[31]H. J. Fossum and D. B. Chang, Phys. Rev. B 8, 2842 (1973).
[32]C. C. Lee and H. Y. Fan, Phys. Rev. B 9, 3502 (1974).
[33]A. F. Gibson, C. B. Hatch, P. N. D. Maggs, D. R. Tilley, and A. C. Walker, J. Phys. C 9, 3529 (1976).
[34]A. Miller, A. Johnston, J. Dempsey, J. Smith, C. R. Pidgeon, and G. D. Holah, J. Phys. C 12, 4839 (1979).
[35]H. J. Fossum and B. Ancker-Johnson, Phys. Rev. B 8, 2850 (1973).
[36]S. W. Koch, S. Schmitt-Rink, and H. Haug, Phys. Status Solidi B 106, 135 (1981).

Preprint of an Invited Paper Presented at the International Conference
"The Application of High Magnetic Fields in Semiconductor Physics"
Grenoble, France, September 13-17, 1982

Two-Photon Spectroscopy in InSb at High Magnetic Fields*

D. G. Seiler, M. W. Goodwin†, and S. W. McClure
Center for Applied Quantum Electronics
Department of Physics
North Texas State University
Denton, Texas 76203

and

L. A. Veilleux††
Francis Bitter National Magnet Laboratory
Massachusetts Institute of Technology
Cambridge, MA 02139

ABSTRACT

High resolution two-photon magneto-absorption (TPMA) spectra for n-InSb have been investigated for magnetic fields up to 15 T using cw CO_2 lasers and photoconductivity techniques. A modified Pidgeon-Brown energy band model using spherical and nonspherical selection rules is used to interpret the data. Anisotropic effects are observed for the first time in the TPMA photoconductive spectra. TPMA structure is also observed for the first time in the photovoltaic response.

INTRODUCTION

Magneto-optical studies have proven capable of determining energy band parameters of semiconductors because of the optical transitions that occur between magnetically quantized electronic or impurity states. Many studies during the past 30 years have used one-photon absorption (OPA) techniques with conventional photon sources. However, the increasing availability of laser sources now opens the possibility of carrying out nonlinear magneto-optical studies in semiconductors. In particular, two-photon absorption (TPA) techniques offer unique spectroscopic advantages over the traditional OPA techniques. TPA has a small cross section for absorption in many semiconductors and therefore has a large penetration depth resulting in uniform bulk absorption. This reduces problems associated with surface effects often encountered in OPA measurements (OPA has a large absorption cross section and thus a small penetration depth, usually on the order of a micron). Another advantage of TPA is that different states of the energy bands can be accessed. For an applied magnetic field not only different but more selection rules between Landau levels are allowed. Thus, TPA and TPMA (two-photon magneto-absorption) measurements can yield significantly more information about the eigenstates of a material. Recently[1], we have shown that TPMA is easily observable in n-InSb using only cw CO_2 lasers operating at even milliwatt powers. This result opens up a new dimension for two-photon spectroscopy using cw lasers only.

Two-photon absorption experiments on InSb divide basically into two categories; those without an applied magnetic field and those with an applied magnetic field. Although TPA in a magnetic field is the main subject of this paper much of the concepts and theories developed for the no magnetic field case are extremely relevant.

The purpose of this investigation was to examine the TPMA process in more detail than has previously been possible (The historical background on TPMA effects in InSb was recently reviewed by Goodwin et al.[2]). With high resolution experimental techniques many transitions in the TPMA spectra have been observed. In past studies there has been much ambiguity in the identification of the TPMA transitions. However, with more observable transitions and better resolution, a systematic investigation of this complex process has now been performed using polarized light and high magnetic fields. Most of the transitions can be

explained by the usual spherical approximation two-photon selection rules. However, there are some transitions which can not be described with these selection rules. Possible explanations for these transitions are warping and inversion asymmetry-induced effects due to the band structure of InSb. For the first time anisotropic effects are observed and shown to be related to the anisotropy of the initial hole states.

THEORY

The interpretation of results of any magneto-optical experiment depends strongly on the model used for the energy band structure of the material. One of the most useful energy band models was developed by Pidgeon and Brown.[3] Their 8 x 8 Hamiltonian gives the energies of the Γ_6 conduction band, Γ_8 light and heavy hole valence bands, and the Γ_7 spin-orbit split-off band and includes the effects of higher bands to order k^2. They also extended their results to yield the Landau level energies when a magnetic field B is applied.

The most recent extensive calculations of the energy bands of InSb have come from Weiler.[4,5] The double group representation of the intermediate states in the second order matrix elements of the $\vec{k} \cdot \vec{p}$ Hamiltonian were used instead of the single group as in Pidgeon and Brown's. As a result of the spin-orbit splitting of the higher bands, this analysis yields other parameters N_1, N_2, and N_3 (in Weiler's notation). These results were used to explain the presence of certain anamolous magneto-optical effects in InSb, such as spin-flip and cyclotron harmonic transitions. By neglecting the contributions of small terms and certain parameters, but including the presence of a magnetic field, the 8 x 8 Hamiltonian was reduced to two 4 x 4 matrices, one for the a-set (spin-up, +1/2) and one for the b-set (spin-down, -1/2) energies, which can then be solved numerically. However, calculations of the eigenvalues and eigenvectors are not sufficient for a good description of TPMA processes; a proper choice of selection rules is also extremely important.

Zawadzki and Wlasak[6] gave a summary of the two-photon selection rules for the different light polarizations (σ_L, σ_R, σ, and π) for the case of $\vec{B} \parallel$ <001>. Extra transitions were shown to occur because of warping and inversion-asymmetry effects. More recently, Goodwin et al.[2] gave more complete two-photon selection rules for the same light polarizations and for $\vec{B} \parallel$ <111> and <110> directions, as well as the <001> direction. The selection rules in the spherical approximation governing transitions between initial and final states for the different light polarizations are for σ_L: $\Delta n = 2$, $\Delta s = 0$; σ_R: $\Delta n = -2$, $\Delta s = 0$; σ: $\Delta n = 0$, $\Delta s = 0$; π: $\Delta n = 0$, $\Delta s = 0$. Here Δn is the final minus initial state Landau level number and Δs is the final minus the initial state spin number (a-set spin up +1/2 and b-set spin-down -1/2). In some of the previous papers the authors renumbered the valence band Landau levels (to eliminate $n = -1$ states) which caused their selection rules for n to differ from ours by 1.

Once the matrix elements have been calculated and the selection rules are known, the two photon magneto-absorption coefficients are straight forward to calculate. Following second-order perturbation theory, the transition rate[7,8] for a two-photon process in c.g.s. units is

$$T = \frac{2\pi}{\hbar} \frac{4\pi^2 e^4 I^2}{n_p^2 c^2 m^4 \omega^4} \sum_f \int \left| \sum_t \frac{\langle f|\vec{\epsilon} \cdot \vec{p}|t\rangle\langle t|\vec{\epsilon} \cdot \vec{p}|i\rangle}{E_t - E_i - \hbar\omega} \right|^2 \delta(E_f - E_i - 2\hbar\omega) \frac{d\vec{k}}{(2\pi)^3} \quad (1)$$

for both magnetic field and no magnetic field cases. The symbols in this equation are n_p which is the index of refraction, I is the incident intensity, $\vec{\epsilon}$ is the polarization vector in the direction of the electric field, and i, t, and f, are the initial, intermediate, and final states, respectively. The delta function

is a statement of energy conservation between the initial and final states and the two photons. The two-photon absorption coefficient is

$$K_2 = (2\hbar\omega/I^2)T \ . \qquad (2)$$

Although [illegible] were derived for two-photon absorption in the absence of a magnetic field, they can be easily adapted to the magnetic field case. The principal differences between the two cases are in the matrix elements and the integration over $\vec{k}$, which is related to the joint density of states. In general the magnetic field density of states in the parabolic approximation[9] has the form

$$g(E) = \frac{1}{\pi^2}\left(\frac{2m^*}{\hbar^2}\right)^{3/2} \sum_{n=0}^{n_{max}} \frac{\hbar\omega_c}{\left[E - (n + 1/2)\hbar\omega_c\right]^{1/2}} \qquad (3)$$

where n_{max} is the largest positive integer for which the summand is real, m^* is the cyclotron effective mass, and ω_c is the cyclotron frequency ($= eB/m^*$). Immediately one sees that the density of states diverges whenever the energy E equals the energy of a Landau level. This is completely different from the case without a magnetic field where the density of states is proportional to $\sqrt{E}$ and no divergence is observed. This divergence in $g(E)$ is responsible for the two-photon resonances observed in the conductivity. To remove the infinite divergence whenever $E = (n + 1/2)\hbar\omega_c$, it has been customary to introduce a broadening term Γ into the energy of the Landau levels.[10] This broadening factor is a result of collisions of electrons with other particles (i.e. other electrons, phonons, or impurities). Kubo et al.[11] has shown that Γ can be expressed as $\Gamma = \hbar/(2\tau)$ where τ is a characteristic lifetime of the state.

Including broadening into the transition rate and assuming all transitions occur at $k_z = 0$, we can write a general expression for the two-photon magneto-absorption coefficient as follows:

$$K_2^{i,f} = \frac{e^2\hbar 4\pi^2}{n_p^2 c^2 m^2}\left(\frac{B}{(\hbar\omega)^3}\right)\left(\frac{2\mu}{\hbar}\right)^{1/2}\left|\sum_t \frac{\langle f|\hat{\epsilon}\cdot\vec{p}|t\rangle\langle t|\hat{\epsilon}\cdot\vec{p}|i\rangle}{E_t - E_i - \hbar\omega}\right|^2 \qquad (4)$$

where μ is an effective mass for an electron and light or heavy hole system ($1/\mu = 1/m_e + 1/m_h$). The final state is some Landau level in the conduction band and the initial state is a Landau level of either the light or heavy hole band. The intermediate state t can be a Landau level in any one of the four bands (conduction, heavy or light hole, or spin-orbit split-off band). Notice that $K_2^{i,f}$ is dependent on the initial and final states. Therefore each transition between specific Landau levels in the valence and conduction bands has a characteristic two-photon absorption coefficient, which depends upon magnetic field B and photon energy $\hbar\omega$. We have restricted the sum over intermediate states to the four bands just mentioned; the contribution of higher bands is expected to be small, because of the large energy difference in the denominators. The prescription for calculating $K_2^{i,f}$ is to numerically solve for the eigenvectors of the two 4×4 Hamiltonians and then use these eigenvectors to calculate the matrix elements. In Figure 1 the splitting of the bands into Landau levels is shown along with a representative two-photon transition for σ_L. Figure 2 schematically shows the two-photon transitions for the different light polarizations according to the spherical selection rules.

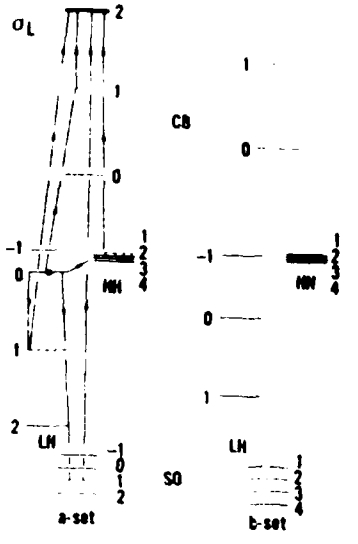

Figure 1. Splitting of the bands into Landau levels. a-set are the spin up levels (+1/2) and b-set are the spin down levels (-1/2). (CB-conduction band, HH-heavy hole band, LH-light hole band, SO-spin orbit split off band). A two-photon transition ($a^+(0) \rightarrow a^C(2)$ for σ_L) is shown with all the intermediate states. (——●—— initial state, ----- intermediate state, ——— final state).

Fig. V.A.10

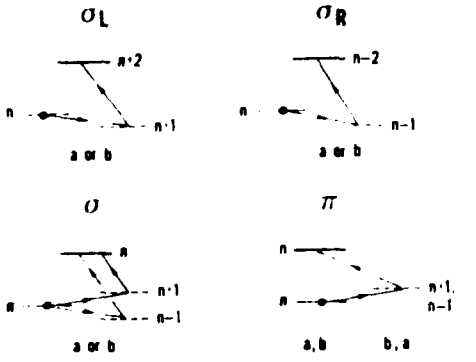

Figure 2. Schematic diagram of the initial, intermediate and final states of the two-photon process for the different light polarizations. For $\vec{e} \perp \vec{B}$ (σ_R, σ_L, σ) all transitions are within the a or b set. For $\vec{e} \parallel \vec{B}$ (π) the initial and final states are of the same spin while the intermediate state is of opposite spin.

Fig. V.A.11

Although there has been extensive theoretical work on TPA in the absence of a magnetic field, there has been only two major attempts to calculate TPMA coefficients. The first attempt was by Bassani and Girlanda.[12] Using second-order perturbation theory, they considered the absorption of two photons each with different energies and different polarizations. They also used the parabolic approximation to the Landau levels and considered both inter-inter and inter-intra band transitions between one valence band and two conduction bands. In addition broadening was not included in their model; K_2 therefore exhibited infinite divergences at the resonance points. No comparison with experiment was ever made with their results. The other major attempt was by Nguyen, Strnad and Yafet,[13] who also used second-order perturbation theory. In the sum over intermediate states they included the conduction, light, and heavy hole bands and did not include the spin-orbit split-off band, which is usually only a small contribution. However, they were able to obtain analytical expressions for K_2, because they used first-order perturbation wave functions in calculating the matrix elements. Their theoretical results compared favorably with their experiment.

EXPERIMENTAL WORK

Oriented samples of high purity n-InSb (9×10^{13} cm^{-3}) were mounted in a variable temperature dewar for the lower magnetic field work (0 - 2 T) carried out at NTSU using a Varian electromagnet. High field (0 - 15 T) studies were carried

out at the Francis Bitter National Magnet Laboratory with the samples immersed directly in pumped liquid helium. Light from grating tunable cw CO_2 lasers was mechanically chopped by a rotating slotted wheel with a small duty cycle to minimize sample heating effects. In the low field region the photoconductive measurements were carried out using either boxcar integrator techniques or a combination of sampling oscilloscope and magnetic field modulation techniques. At high fields only the boxcar was used. Field positions, amplitudes and line widths could then be directly measured and studied as a function of laser intensity, lattice temperature, etc. The addition of modulation techniques significantly improves the sensitivity and resolution of these magneto-optical experiments allowing a more accurate determination of the resonant field positions and observation of weak structure or resolution of closely spaced doublets.

Figure 3 shows a reproduction of the output of the lock-in detector versus magnetic field for sample dc bias currents of I = 1 mA (photoconductive response) and I = 0 mA (photovoltaic response). The detector response is proportional to the second derivative of the photo-induced magnetoresistance or photovoltaic effect. The observed amplitude of the resonant structure contains the effects of the modulation method. To our knowledge this is the first time that two-photon absorption effects have been observed in the photovoltaic response of a semiconductor. In all subsequent experiments the photovoltaic response was minimized by keeping the laser beam spot positioned between the sample contacts. Thus, in most cases two-photon effects were not discernible in the photovoltaic response, while the photoconductive response showed excellent two-photon resonances.

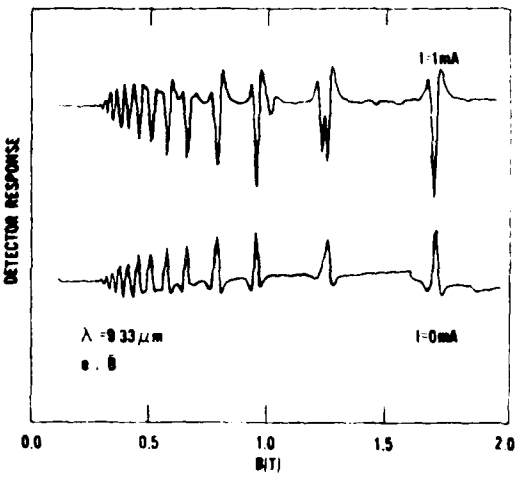

Figure 4. TPMA effects in the photo-voltaic response (I = 0 mA trace). The top trace contains both the photoconductivity and the photovoltaic signals.

Fig. VI.A.12

RESULTS

Experiments were performed in two principal magnetic field ranges: 0 - 2 T and 0 - 15 T. Most of the results, analysis, and interpretation are focused on the 0 - 2 T range. However, the higher magnetic fields are important for the observation of certain transitions near the TPMA band edge, which are not predicted by the spherical selection rules. In addition, at the higher fields the hole Landau levels are split further apart allowing clear resolution of unresolved transitions at the lower magnetic fields.

Figure 4 shows the wavelength dependence of the TPMA structure. The numbers correspond to distinct transitions that have been identified from all the data that has been taken and not just this figure. For TPMA each transition corresponds to an increase in the conductivity or a decrease in the magnetoresistance. That is, as the magnetic field is increased to some value where the energy between two allowed Landau levels equal twice the photon energy, electrons in the initial valence band Landau level will be photo-excited to the final conduction band Landau level. Transitions can originate from either the light or heavy hole Landau level. This process is repeated at every magnetic field where a two-photon transition is allowed. The increase in amplitude of the structure with higher magnetic fields is partly due to the increase with field of the joint density of states. In addition, the sampling and lock-in technique produces a Bessel function envelope to the amplitudes. Figure 5 dramatically illustrates the movement of the TPMA structure towards lower magnetic fields as the wavelength is increased. The usefulness of the CO_2 laser in studying TPMA in InSb is also demonstrated in that its spectral output can be tuned below the TPMA threshold (the energy gap equal to twice the photon energy) or to higher photon energies where much complex structure can be observed since electrons can now be excited high into the conduction band. To resolve the transitions close to the TPMA band edge, these experiments were extended to 15.0 T using the boxcar averager technique. Figure 5 shows the results of those experiments where the TPMA band edge transitions (1, 2, and 3) are clearly resolved. The detector response in this figure is proportional to the photo-induced change in magnetoresistance. At the higher fields, transitions 2 and 3 are well resolved, whereas at the lower magnetic fields, they are not resolved even

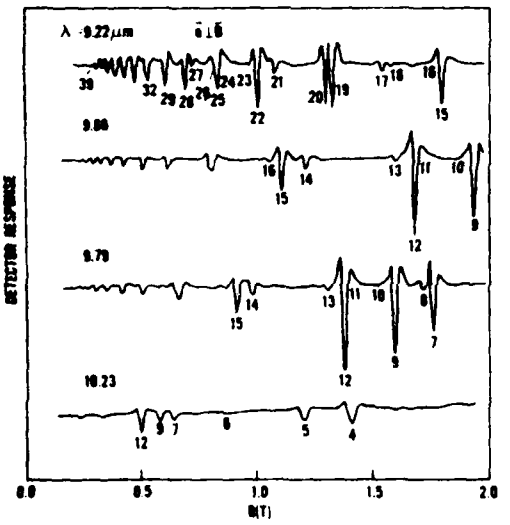

Figure 4. Wavelength dependence of the TPMA structure for $\vec{B} \parallel$ <110> and for 0 - 2 T using sampling oscilloscope and field modulation techniques. The numbers correspond to distinct transitions.

Fig. V. A.13

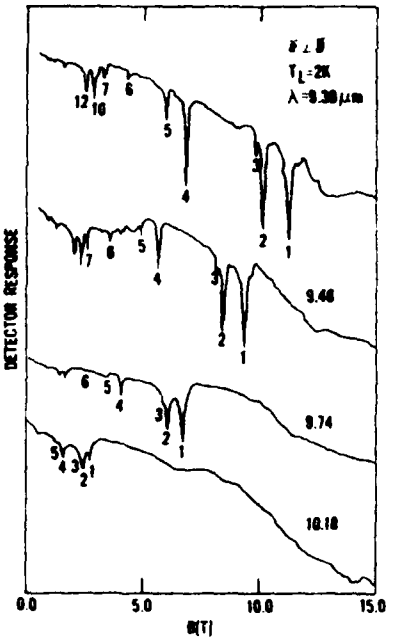

Figure 5. Wavelength dependence of TPMA for $\vec{B} \parallel$ <211> and for 0 - 15 T. The data were taken with the boxcar averager technique and shows directly the TPMA band edge.

Fig. V. A. 14

with the sampling and lock-in technique. Figure 5 also shows the growth in amplitude of the structure as it moves toward higher magnetic fields with higher photon energies. Although use of the boxcar averager technique eliminates the Bessel function envelope to the structure, there is present a background photo-induced magnetoresistance due to non-resonant absorption processes. For our experiments TPMA was not observed for wavelengths above 10.5 μm.

The results of polarization studies for $\vec{e} \perp \vec{B}$ and $\vec{e} \parallel \vec{B}$ in the Voigt configuration have recently been presented.[1] Here we present additional results using circularly polarized light (obtained by using a Fresnel Rhomb) in the Faraday geometry. The TPMA structure obtained for σ_R, σ_L, and $\pi(\vec{e} \parallel \vec{B})$ polarizations are shown in Figure 6. The magnetic field positions of the structures for σ_R and σ_L are basically the same. Figure 6 also shows additional structure between transitions 16 and 17 in the σ_R polarization which have not been labeled. However, there are some noticeable differences in the strengths of some of the transitions. For instance, transitions 13, 15, 16, 17, and 21 appear to be stronger for σ_R, while transitions 12, 16, and 22 appear to be dominant for σ_L. Some transitions such as 15, 19, and those higher than 22 have no significant difference between σ_R and σ_L. These transitions are the result of π polarization, which is the sum of σ_R and σ_L. The reason why these transitions are present in both σ_R and σ_L is that each polarization, σ_R or σ_L, contains some residual polarization of the opposite circularly polarized wave. That is, rather than having pure circular polarization, the wave is slightly elliptical. We estimate from a polarization analysis of the beam that perhaps as much as 10 percent of the opposite circular polarized electric field is present for either of the σ_R or σ_L polarizations. The transitions in the π polarization should match magnetic field positions for the σ transitions, because they both obey the same selection rules for transitions between initial and final states. However, the strengths of the σ transitions are different from those of the π transitions, because the intermedite states are different.

Specific transitions are assigned to the structure in Figure 7 by comparing theoretical calculations of K_2, the TPMA coefficient, from Eq. (4) with the amplitude and magnetic field positions for the structure obtained using σ_L and σ_R polarizations. Each line for K_2 represents the strength of a specific transition. The magnetic field position of each transition was estimated from an energy band calculation of the Landau levels. Only those transitions which obey the spherical selection rules are plotted. The amplitude of the structure can only be compared qualitatively with the calculations for K_2 because (1) the detector response signal is a second-derivative which may be slightly different from the actual signal and (2) the detector response signal contains a Bessel function type envelope to the transitions. As can be seen, some of the structure, certainly at the lower magnetic fields, are actually the sum of several transitions which are not resolved. The observed resonant structure in Figure 7 was identified with only the strongest calculated transitions. The results of the identification are given in Table I. We have only made comparisons of the $\vec{e} \perp \vec{B}$ transitions with the calculated K_2 values. In principle the same method can be applied for the $\vec{e} \parallel \vec{B}$ or π transitions. However, the structure is much less complicated making the identification of the transitions easier. Therefore for the purpose of identification of transitions K_2 values were not calculated.

After the structure in the data has been tentatively identified, the energy band Landau level calculations can be used to determine a set of band parameters. This involves a considerable amount of computer usage in fitting the theoretical calculations to the data. The two-photon transition energies as a function of magnetic field are plotted in the usual "fan chart" method and compared to the experimental data. The results of our fitting procedure for both $\vec{e} \perp \vec{B}$ and $\vec{e} \parallel \vec{B}$, are shown in Figures 8-10, where the data are the experimental transition energies (twice the photon energy) versus resonant magnetic field positions and the lines (solid and dashed) are the calculated results for $\vec{B} \parallel \langle 110 \rangle$. There are many more transitions plotted than have been found from the earlier studies using pulsed lasers. Interband transitions involved in magneto-absorption experiments are usually considered as being to exciton levels. However, there is at present no

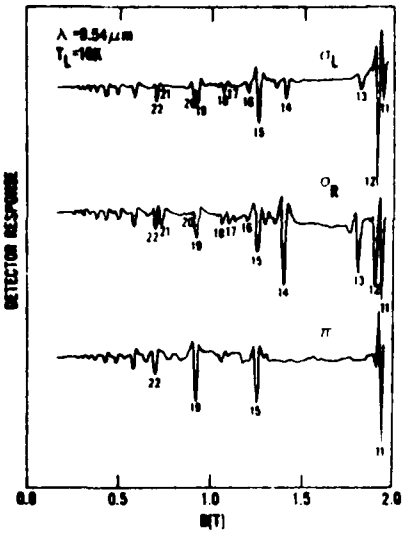

Figure 6. Polarization dependence of TPMA for $\vec{B} \parallel$<110>.

Fig. V.A.15

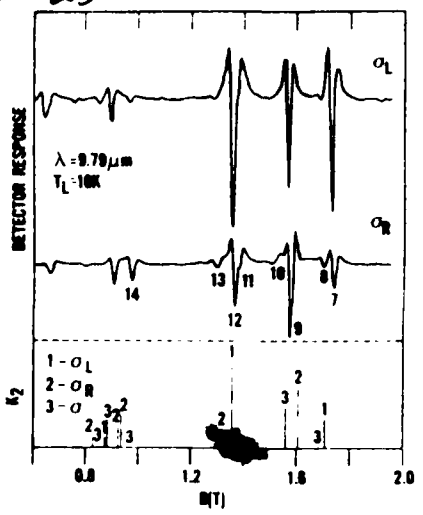

Figure 7. Comparison of the amplitude of the TPMA structure for σ_L and σ_R and for $\vec{B} \parallel$ <110> with theoretically calculated values of the TPMA coefficient for the possible two-photon transitions.

Fig. V.A.16

adequate exciton theory for TPMA in semiconductors with complex coupled energy bands. Here we adopt the approach of not correcting for exciton effects and of treating the Landau-level theory as accurately as possible in calculating transition energies. We then look for differences between the calculated and observed energies for the lowest transitions where exciton effects should be most important. The theoretically calculated solid lines shown in Figures 8-10 result from using only the spherical selection rules. It appears that most of the low field experimental data can be adequately described (but with a new set of band parameters) with these rules without using exciton corrections. A good fit of these theoretical transitions to the low field data results from using the following band parameters: E_g = 235.2 meV, E_p = 23.2 eV, Δ = 0.803 eV, γ_1 = 3.25, γ_2 = -0.2, γ_3 = 0.9, κ = -1.3, F = -0.2, q = 0.0, N_1 = -0.55. No attempt was made to determine a value of Δ from our two-photon data. Instead we have used the stress modulated magnetoreflectance results of Δ = 0.803 ± 0.005 eV obtained by Aggarval.[14] There are some noticeable differences, however, between the theory and data in Figure 10 where the transitions have been plotted out to 15 T. If excitons are present, the transition energies would be slightly altered from the no-exciton case, which the data clearly indicates for transitions 7 and lower. The deviation between the exciton and no-exciton theories should also be more evident with increasing magnetic fields. An adequate TPMA exciton theory is thus needed to improve the fit for these transitions.

Additional structure labeled (1,2), (6), (17,18), and (24) in Figure 8, (1,2) and (6) in Figure 10, and (18) in Figure 9, appears not to be explainable by the spherical selection rules. These transitions could be described by nonspherical selection rules allowed because of inversion asymmetry and warping effects.

Table II. A.4

Table I. Theoretical two-photon transition assignments for each distinct experimental transition number (Exp. Trans. No.) of the observed resonant structure in the photoconductivity for $\vec{e} \perp \vec{B}$ polarization (σ_R, σ_L, $\sigma_R + \sigma_L = 0$) in the Voigt geometry. The * marks indicate those transitions which can only be explained by nonspherical or extra transitions.

Exp. Trans. No.	Polarization	Theoretical Assignment	Exp. Trans. No.	Polarization	Theoretical Assignment
*1,*2		$a^-(1)\ a^c(0)$	28	σ_R	$a^-(7)\ a^c(5)$
		$a^+(-1)\ a^c(0)$			$b^+(2)\ b^c(2)$
		$b^-(2)\ a^c(0)$	30	σ_L	$b^+(1)\ b^c(3)$
		$b^-(1)\ a^c(0)$	31	σ_R	$a^+(4)\ a^c(2)$
		$b^+(-1)\ a^c(0)$	32	σ_R	$a^-(8)\ a^c(6)$
3	σ_R	$a^-(2)\ a^c(0)$			$a^+(3)\ a^c(3)$
4	σ	$a^+(0)\ a^c(0)$	29	σ_R	$a^-(9)\ a^c(7)$
5	σ_R	$b^-(2)\ b^c(0)$			$b^+(3)\ b^c(3)$
*6		$a^+(0)\ b^c(0)$	30	σ_L	$b^+(2)\ b^c(4)$
7	σ_L	$a^+(-1)\ a^c(1)$	33	σ_R	$a^+(5)\ a^c(3)$
8	σ	$a^-(1)\ a^c(1)$	37	σ_R	$a^-(10)\ a^c(8)$
9	σ	$b^+(0)\ b^c(0)$			$a^+(4)\ a^c(4)$
10	σ_R	$a^-(3)\ a^c(1)$	33	σ_L	$b^+(3)\ b^c(5)$
11	σ	$b^-(1)\ b^c(1)$		σ_R	$a^-(11)\ a^c(9)$
12	σ_L	$b^+(-1)\ b^c(1)$			$b^+(4)\ b^c(4)$
13	σ_R	$b^-(3)\ b^c(1)$	34	σ_R	$a^+(6)\ a^c(4)$
14	σ_R	$a^+(2)\ a^c(0)$		σ_R	$a^-(12)\ a^c(10)$
15	σ_R	$a^-(4)\ a^c(2)$			$a^+(5)\ a^c(5)$
	σ	$a^+(1)\ a^c(1)$	35	σ_L	$b^+(4)\ b^c(6)$
16	σ_R	$b^-(4)\ b^c(2)$		σ_R	$a^-(13)\ a^c(11)$
*17		$a^+(2)\ b^c(0)$	36	σ	$b^+(5)\ b^c(5)$
		$a^-(4)\ b^c(2)$		σ_R	$a^+(7)\ a^c(5)$
*18		$a^+(1)\ b^c(1)$		σ_R	$a^-(14)\ a^c(12)$
		$a^+(0)\ b^c(2)$			$a^+(6)\ a^c(6)$
	σ_R	$b^+(2)\ b^c(0)$	37	σ_L	$b^+(5)\ b^c(7)$
19	σ_R	$a^-(5)\ a^c(3)$		σ_R	$a^-(15)\ a^c(13)$
	σ	$b^+(1)\ b^c(1)$		σ	$b^+(6)\ b^c(6)$
20	σ_L	$b^+(0)\ b^c(2)$	38	σ_R	$a^+(8)\ a^c(6)$
21	σ_R	$a^+(3)\ a^c(1)$		σ_R	$a^-(16)\ a^c(14)$
22	σ_R	$a^-(6)\ a^c(4)$		σ	$a^+(7)\ a^c(7)$
	σ	$a^+(2)\ a^c(2)$	39	σ_L	$b^+(6)\ b^c(8)$
23	σ_R	$b^-(6)\ b^c(4)$		σ_R	$a^-(17)\ a^c(15)$
*24		$a^+(2)\ b^c(2)$		σ	$b^+(7)\ b^c(7)$

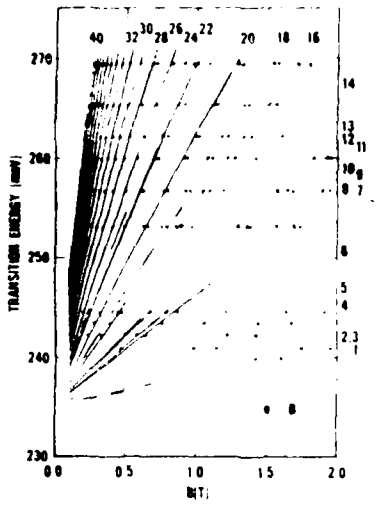

Figure 8. Fan chart of TPMA transitions energies ($\hat{e} \perp \hat{B} \parallel$<110>). Solid lines represent theoretical calculations with selection rules $\Delta s = 0$, $\Delta n = 0, \pm 2$. Dashed lines, nonspherical selection rules. Dots are the data.

Fig V.A.17

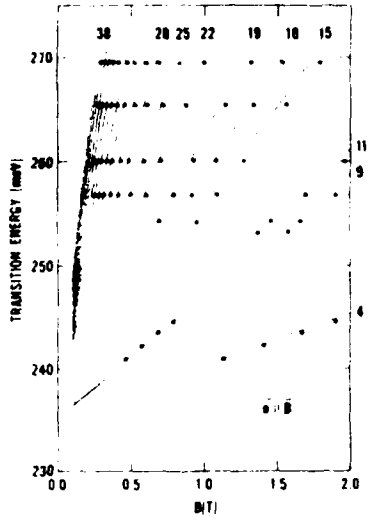

Figure 9. Fan chart of TPMA transition energies $\hat{e} \parallel \hat{B} \parallel$<110>.

Fig. V.A.18

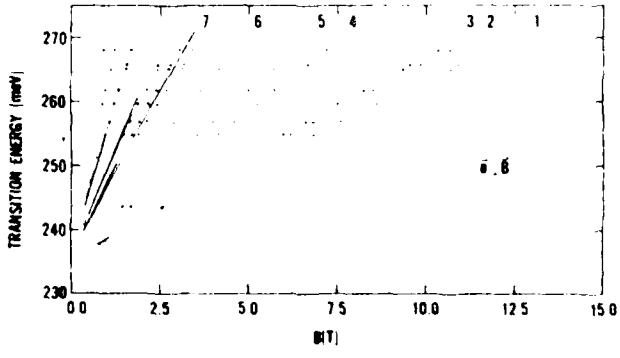

Figure 10. Fan chart of TPMA transition energies $\hat{e} \perp \hat{B} \parallel$<211> for the magnetic field range 0 - 15 T.

Fig. V.A.19

In Figure 11 TPMA spectra are shown for the major crystal directions. Manlief and Palik[15] reported that they observed no difference in the TPMA spectra for the three crystal directions. From Figure 11 one can see that for much of the structure, there is no appreciable differences in the spectra between the three crystal directions. However, one striking feature seen is the clear resolution of the doublet nature to transitions 11 and 12 for $\hat{B} \parallel$ <111>. This has not been previously reported in any TPMA study. There are also some definite magnetic field

shifts for some of the weaker transitions (8, 10, 11, 13) observable at the higher magnetic fields for $\lambda = 9.79$ μm. The observed shift in these structures is due to the difference in energy of the heavy hole Landau levels for the three crystal directions. Calculations of the heavy hole Landau level energies give good agreement with the observed shifts. This is further proof for our heavy hole identification of these transitions. From cyclotron resonance measurements of the heavy hole masses the heavy hole mass $m^-[111]$ is the largest, while the $m^-[100]$ mass is the smallest ($m^-[111] > m^-[110] > m^-[100]$). Since the Landau level energies are inversely proportional to the effective masses of a particular band ($E \sim neB/m^*$ in the parabolic approximation), the heavy hole energies will be somewhat smaller for the <111> direction than the <100> direction, thus causing a shift in the heavy hole transitions toward higher magnetic fields for the <111> direction. The light hole transitions do not show a significant shift in magnetic field position, because there is not a large anisotropy associated with the light holes.

We have calculated the TPMA spectra as a function of magnetic field. In Figure 12 we show an experimental spectrum (top curve) and a calculated spectrum (bottom curve). The experimental trace was obtained using the boxcar averager technique and is proportional to the photo-induced magnetoresistance. The theoretical spectrum was calculated assuming a parabolic magnetic field dependent joint density of states function, similar to Eq. (7), for each transition with broadening of the energy levels included. The energy of the Landau levels as a function of magnetic field in the joint density of states function was calculated from the nonparabolic 8 x 8 Hamiltonian matrix. The spectrum at each magnetic field point was obtained by summing the contributions of all the transitions in the spectrum at that point. Thus, transitions in close proximity will be significantly influenced by each other, while transitions further away in magnetic field will have a much less influence, depending on the strength of the transitions. The theoretical spectrum is plotted as $1/K_2$ since the experimental spectrum is $\propto 1/n$ or $1/K_2$.

The theoretical spectrum is in qualitative agreement with the experimental spectrum. The two high field sets of transitions (9, 10, and 11, 12) show a sharp rise on the high magnetic field side of a transition while a much more gradual decrease is evident on the low field side of a transition because of the density of states. The magnetic field width of a transition depends on the amount of broadening of the energy levels. For this spectrum an energy width of $\Gamma = 0.1$ meV was used corresponding to a collision broadening time $\tau = 1 \times 10^{-12}$ sec. Although the two large transitions at the high magnetic fields are at a slightly lower magnetic field than the experimental ones, the theoretical spectrum reproduces transitions 9-12 of the experimental spectrum very well. However, the theoretical spectrum in the vicinity of transitions 14 and 15 shows a complex multiplet of structure while the experimental shows one seemingly large transition. Either certain transitions are stronger and dominate the spectrum or a slightly different set of band parameters would perhaps reproduce the spectra more accurately. The theoretical spectrum does show however, that some of the transitions, certainly at the lower magnetic fields, are actually the sum of several unresolved transitions. Also the experimental spectrum contains a noticeable magnetic field background in addition to the resonant structure.

CONCLUSIONS

The TPMA spectra in InSb is shown to be very complex, exhibiting characteristic polarization, crystalline anisotropy, and magnetic field dependences. Many aspects of these spectral features are presently understood with calculations using a modified Pidgeon-Brown energy band model and the appropriate selection rules. However, a real quantitative understanding of the role of excitons in the TPMA spectra is lacking at the present time.

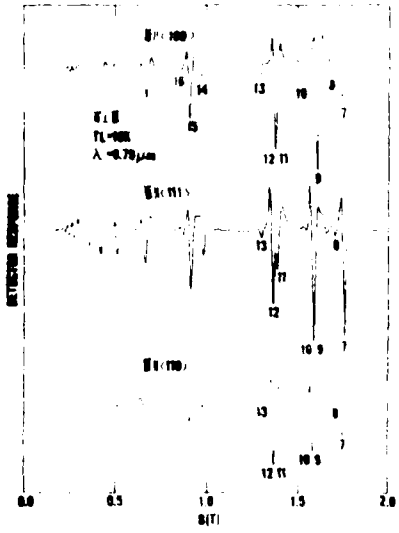

Figure 11. Crystal orientation dependence of TPMA.

Fig. V.A.20

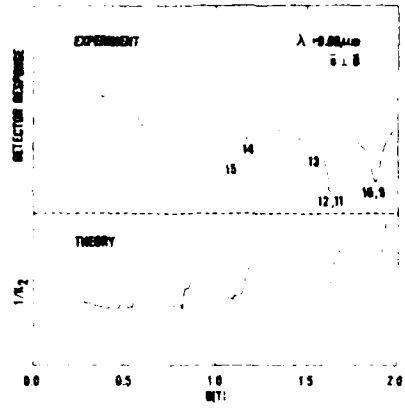

Figure 12. Comparison of an experimental TPMA spectrum with a theoretically calculated value of $1/K_2$.

Fig. V.A.21

REFERENCES

*Work supported in part by the Office of Naval Research and a Faculty Research Grant from North Texas State University.
†Present address: Texas Instruments, Inc., Dallas, Texas 75265.
††Also, Department of Electrical Engineering.

1. D. G. Seiler, M. W. Goodwin, and M. H. Weiler, Phys. Rev. B 23, 6806 (1981).
2. M. W. Goodwin, D. G. Seiler, and M. H. Weiler, Phys. Rev. B 25, 6300 (1982).
3. C. R. Pidgeon and R. N. Brown, Phys. Rev. 146, 575 (1966).
4. M. H. Weiler, R. L. Aggarwal, and B. Lax, Phys. Rev. B 17, 3269 (1978).
5. M. H. Weiler, Ph.D. Thesis, Massachusetts Institute of Technology (1977).
6. W. Zawadzki and J. Wlasak, J. Phys. C: Solid State Physics 9, L663 (1976).
7. C. C. Lee and H. Y. Fan, Phys. Rev. B 9, 3502 (1974).
8. C. R. Pidgeon, in Theoretical Aspects and New Developments in Magneto-Optics, edited by J. T. Devresse (Plenum Press, New York, 1980), p. 255.
9. A. H. Kahn and H. P. R. Frederikse, in Solid State Physics, edited by F. Seitz and D. Turnbull (Academic Press, New York, 1959), Vol. 9, p. 257.
10. L. M. Roth and P. N. Argyres, in Semiconductors and Semimetals, edited by R. K. Willardson and A. C. Beer (Academic Press, New York, 1966), Vol. 1, . 159.
11. R. Kubo, N. Hasitsume, and S. J. Miyake, in Solid State Physics, edited by F. Seitz and D. Turnbull (Academic Press, New York, 1965), Vol. 17, p. 269.
12. F. Bassani and R. Girlanda, Opt. Comm. 1, 359 (1970).
13. Van-Tran Nguyen, A. R. Strnad, and Y. Yafet, Phys. Rev. Lett. 26, 1170 (1971).
14. R. L. Aggarwal, in Semiconductors and Semimetals, edited by R. K. Willardson and A. C. Beer, (Academic Press, New York, 1972), Vol. 9, p. 151.
15. S. K. Manlief and E. D. Palik, Sol. State Commun. 12, 1071 (1973).

AD-A139 227 INVESTIGATION OF NONLINEAR OPTICAL PROPERTIES OF SEMICONDUCTORS(U) NORTH TEXAS STATE UNIV DENTON CENTER FOR APPLIED QUANTUM ELECTRONICS D G SEILER 23 FEB 84

1/2

UNCLASSIFIED N00014-82-C-0545 F/G 20/12 NL

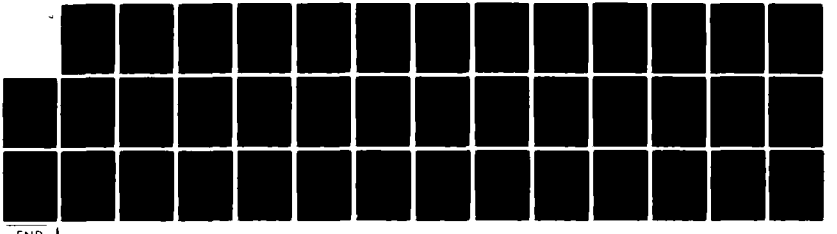

END

DATE FILMED

DTIC

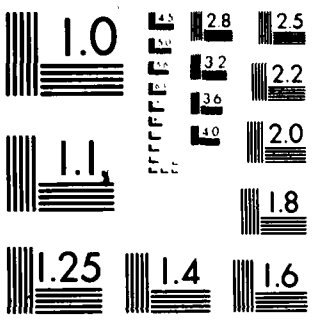

Solid State Communicaitons, Vol.47,No.1, pp.17-21, 1983.
Printed in Great Britain.

0038-1098/83 $3.00 + .00
Pergamon Press Ltd.

ANISOTROPIC TWO-PHOTON MAGNETO-ABSORPTION IN n-InSb*

D. G. Seiler and S. W. McClure

Center for Applied Quantum Electronics, Department of Physics, North Texas State University
Denton, Texas 76203

(Received 10 February 1983 by J. Tauc)

High resolution two-photon magneto-absorption spectra have been obtained for $\vec{B}$|| <100>, <111>, and <110> crystallographic directions. Anisotropic effects are observed for the first time in InSb and are shown to be related to the anisotropy of the initial hole states.

Detailed information on energy band structure of semiconductors comes directly from magneto-optical experiments such as intravalence and intra-conduction band studies and one- (OPMA) and two-photon magneto-absorption (TPMA) studies. The resonant structure observed in such experiments can be qualitatively understood by Landau-level and density-of-states models. For a fixed magnetic field, the density of states exhibits singularities at the energy corresponding to the bottom of each Landau-level. When two Landau-levels are resonant with the photon energy of the laser there is an increase in the absorption. For small absorption coefficients any direct measurement of the changes in transmission are extremely difficult to detect. However, photoconductivity measurements on pure samples are capable of detecting even weak magneto-optical transitions. In this study we have measured the photoconductive response of n-InSb samples using magnetic field modulation and sampling oscilloscope techniques (derivative techniques) in order to obtain high resolution TMPA spectra that show effects caused by crystalline anisotropy.

Two-photon processes are related to the imaginary part of the third order non-linear electric dipole susceptibility tensor $\chi^{(3)}$ which has certain crystalline symmetry properties. Van der Ziel[1] has observed a crystalline anisotropy in the two-photon luminescence intensity in GaAs without a magnetic field. He attributes this dependence to the anisotropy of $\chi^{(3)}$. In contrast, our anisotropies in the TPMA spectra are observed in the resonant magnetic field positions and not in the strength of the signals. The two-photon second order transition probability depends upon the delta function $\delta(E_f-E_i-2\hbar\omega)$ where simultaneous absorption of two photons causes a transition between an initial E_i and final E_f energy levels whose positions (or values) depend upon magnetic field. Thus, the slight differences in the initial light- and heavy-hole valence band level energies for the different crystal orientations shift the TPMA resonant spectra. Hereafter, we only refer to anisotropy in this manner.

Several reports[2-6] on TPMA in n-InSb using pulsed and Q-switched CO_2 lasers did not report any anisotropy, even though in one case[6] they were explicity looked for. The observation of anisotropic TPMA effects in this study is a direct result of the increased resolution that comes from using only cw CO_2 lasers in conjunction with derivative techniques.[7,8]

Until now, valence band anisotropy in InSb has usually only been studied using cyclotron resonance,[9-11] combined resonance,[12] or one-photon interband[13-17] measurements. For cyclotron and combined resonance both the energy levels of the initial and final states vary as a function of crystalline direction, thus making it somewhat difficult to accurately determine the anisotropy of individual valence band levels. For interband absorption the anisotropy observed must be due to the anisotropy of the initial hole states since the conduction band Landau levels are essentially isotropic. However, since radiation for OPMA is almost completely absorbed in the first few microns of the crystal, very thin samples are necessary.[18] In contrast, TPMA is a bulk process, thereby eliminating the difficulty in handling thin samples. TPMA also has different selection rules from OPMA, thus more information can be gained about the energy band structure because more transitions are observed. Most of the transitions observed have been identified and explained using the usual spherical two-photon selection rules.[8] All of the anisotropic TPMA structure studied here is explained using these spherical selection rules.

The experiments were performed on InSb crystals grown by Cominco with $N_d-N_a \approx 10^{14}cm^{-3}$. A constant dc electrical current is applied to the sample while a small ac magnetic field modulates the sample conductivity at a frequency of 43Hz. The photoconductive signal ($\approx$ 20 μsec wide and at a 1500 Hz repetition rate) is fed into a sampling oscilloscope, the output of which is fed into a lock-in amplifier. The resulting signal is proportional to the second derivative of the photoconductive

*Work supported in part by the Office of Naval Research and a Faculty Research Grant from North Texas State University.

signal. Magnetic fields up to 2T were obtained from a Varian electromagnet calibrated by NMR techniques. All experiments were done in the Voigt configuration with either $\vec{e} \parallel \vec{B}$ or $\vec{e} \perp \vec{B}$ and the current parallel to $\vec{B}$, with $\vec{B}$ parallel to either the <100>, <111> or <110> crystallographic directions.

A comparison of TPMA photoconductive data taken with a boxcar averager and with the sampling and field modulation system (which produces a second-derivative-like spectra) is given in Fig. 1 of Ref. 8. Thus, much sharper and more pronounced structure can be observed which is useful in determining accurate magnetic field positions and in identifying weak or closely spaced structure. This is extremely advantageous for measurements of small anisotropic effects such as reported in this paper.

Fig. 1 shows photoconductive TPMA spectra for the major crystallographic directions. The minima in the structure correspond to minima in the magnetoresistance or maxima in the photoconductivity. The labels correspond to distinct transition assignments which have been made using circular and plane polarized light.[8] Looking at Fig. 1, one sees that for much of the structure no appreciable differences in the spectra exist for the three crystal directions.

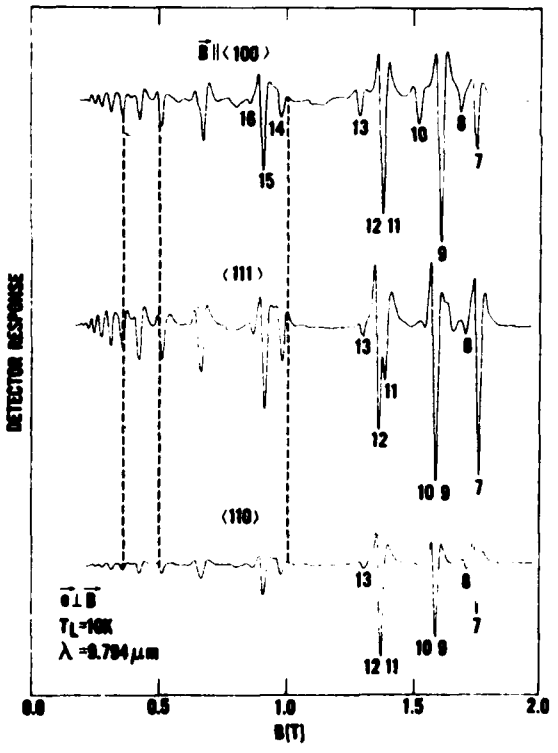

Fig. 1 Crystal orientation dependence of the TPMA resonant structure. The dashed lines show the near isotropy of the resonant field positions. These are second-derivative like spectra obtained with the field modulation and sampling oscilloscope techniques.

Fig. V.A.22

However, one striking feature observed is the clear resolution of the doublet nature of transitions 11 and 12 for $\vec{B} \parallel$ <111>. This has not been previously reported in any TPMA study. There are also some definite magnetic field shifts for some of the weaker transitions (8,10,11,13) observable at the high magnetic fields. We now investigate the detailed nature of the anisotropy of the TPMA structure and show that it is a direct consequence of the anisotropy of the hole Landau levels, which produces an anisotropy in the TMPA transition energies.

Since the structure for the weaker fields (<1T) does not exhibit any observable anisotropy, we concentrate our analysis on the structure at fields greater than 1T. Consequently, in Fig. 2 we reproduce TPMA spectra on an expanded scale which is capable of showing the small shifts in field positions caused by the anisotropy. Transition assignments for each of these processes is given in Table I. The usual spherical selection rules (giving the change in Landau level number n) describe these transitions; for $\vec{e} \perp \vec{B}$, we have $\sigma_L(\Delta n = +2)$, $\sigma_R(\Delta n = -2)$, and $\sigma(\Delta n = 0)$ transitions; for $\vec{e} \parallel \vec{B}$, we have $\pi(\Delta n = 0)$ transitions. In all cases $\Delta s = 0$, i.e., spin is conserved between the initial and final states.

The theoretical description of interband magneto-absorption transitions should take into account exciton effects. However, there is at present no adequate exciton theory for TPMA in

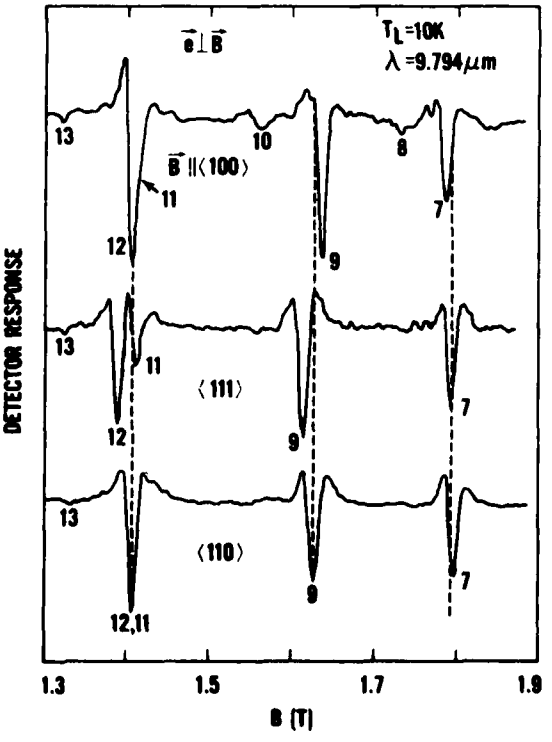

Fig. 2 TPMA anisotropic spectra of high fields showing slight shifts in field position.

Fig. V.A.23

semiconductors with complex coupled bands. Hence we adopt the approach of not correcting for exciton effects, but do treat the Landau-level theory as accurately as possible in calculating transition energies. We then determine differences in TPMA magnetic field positions. These differences should be relatively insensitive to shifts in positions due to exciton corrections. We also point out that the TPMA exciton corrections are much smaller than those that must be applied to one-photon data. Thus, even though exciton corrections must be used to explain the absolute field positions, differences in field positions because of crystalline anisotropy should be relatively insensitive to exciton corrections for the same transition.

In Table I we give the difference in observed magnetic field positions (expressed as values for B(100) - B(110) and B(111) - B(110)) of the resonant structure for the major crystallographic directions. These differences can be seen directly from the TPMA spectra, as shown in plots such as Fig. 2. These observed differences are a direct consequence of the anisotropy of the energy band structure which results in slight changes in the heavy- and light-hole Landau level energies for the different orientations of the magnetic field. Since the conduction band is isotropic,[18] any anisotropies in the TPMA transition energies should result directly from anisotropies in the initial hole states. The Landau level energies are calculated using a modified Pidgeon-Brown model which includes only the warping terms in the diagonal part of the Hamiltonian and no inversion asymmetry terms. Thus, the transition energies versus resonant magnetic field positions are calculated and then used to determine the theoretical differences in field positions for a constant transition energy (shown in Table I). We use the following set of band parameters which has been shown to be able to explain a wide variety of magneto-optical data including intra-conduction,[18] intra-valence band,[12] and TPMA interband[8] data: E_g = 235.2 meV, E_p = 23.2 eV, Δ = 0.803 eV, γ_1 = 3.25, γ_2 = -0.2, γ_3 = 0.9, κ = -1.3, F = -0.2, q = 0, and N_1 = -0.55. Most of the data shown agree remarkably well with the theoretical calculations confirming that the identification of the states has been properly made and that a correct set of band parameters has been used. The calculated anisotropy depends on the choice of the valence band parameters γ_1, γ_2, γ_3, κ and q. This study does not attempt to calculate these parameters, but to verify that they also describe the crystalline anisotropy of InSb. Further comparisons using TPMA exciton corrections and a refined energy band model would undoubtedly lead to even better agreement.

The anisotropic nature of the light- and heavy-hole Landau levels is directly shown in Fig. 3 for B = 1.8T, where we present our calculated results for several of the levels given in Table I. We now show how Fig. 3 can be directly used to explain the observed anisotropic features of specific TPMA transitions like those shown in Figs. 4(a), 4(b), and 4(c). For $\vec{e} \perp \vec{B}$ polarization both transitions 19 and 20 are present as shown in Fig 4(a). For $\vec{e} \parallel \vec{B}$ polarization, transition 20 is absent as theoretically expected. The initial hole state for transition 19 is a light-hole spin down $b^+(1)$ level whose theoretical anisotropy is shown in

Table. V. A.5

Two-photon transition assignments for some observed resonant structure in the Voigt geometry (for $\vec{e} \perp \vec{B}$, we have σ_L, σ_R, and $\sigma_L + \sigma_R = \sigma$ transitions; for $\vec{e} \parallel \vec{B}$ we have π transitions). The anisotropy of the resonant structure is expressed as the differences in field positions for the given two-photon transition energies. The maximum experimental uncertainties are ± 20 G.

Exp. Trans. Number	Polarization	Theoretical Assignment	Transition Energy $2\hbar\omega$(meV)	B(100) – B(110) Experimental (G)	B(100) – B(110) Theoretical (G)	B(111) – B(110) Experimental (G)	B(111) – B(110) Theoretical (G)
7	σ_L	$a^+(-1) \rightarrow a^c(1)$	253.19	-160	- 78	- 10	+33
8	σ or π	$a^-(1) \rightarrow a^c(1)$	255.27	-190	-278		
9	σ or π	$b^+(0) \rightarrow b^c(0)$	253.19	+160	+176	-100	-57
			255.27	+160	+199	-110	-65
			256.76	+170	+218	-130	-70
11	σ or π	$b^-(1) \rightarrow b^c(1)$	253.19	- 60	- 53	+ 40	+16
			255.27	- 90	- 61	+ 20	+21
			256.76	- 70	- 68	+ 20	+25
12	σ_L	$b^+(-1) \rightarrow b^c(1)$	253.19	+ 60	+ 35	-110	-12
			253.72	+ 30	+ 37		
			255.27	+ 40	+ 40	-140	-11
			256.76	+ 40	+ 39	-150	-16
			259.14	+ 40	+ 40	-150	-16
15	σ or π	$a^+(1) \rightarrow a^c(1)$	268.08	- 40	- 50	+ 40	+13
19	σ or π	$b^+(1) \rightarrow b^c(1)$	268.08	+ 90	+ 98	- 40	-32
20	σ_L	$b^+(0) \rightarrow b^c(2)$	268.08	+ 50	+ 54	- 10	-20

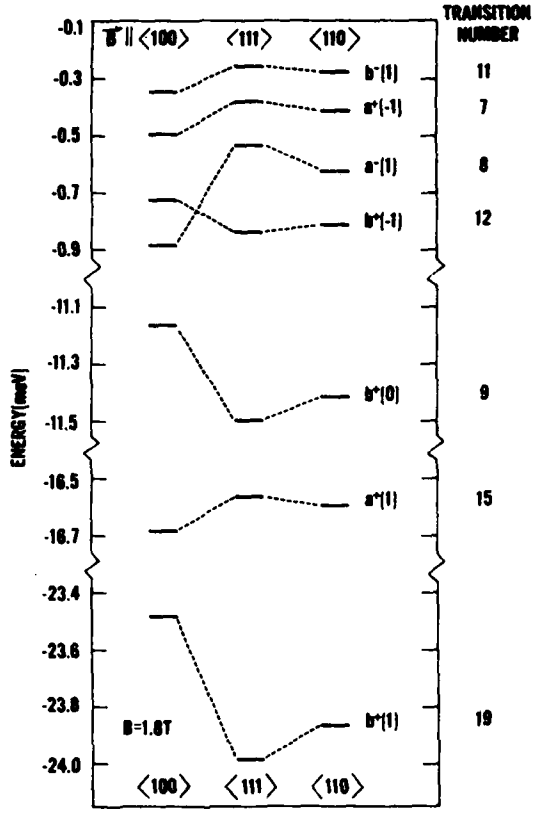

Fig. 3 Hole Landau level energies calculated from a modified Pidgeon-Brown energy band model for B = 1.8 T. The anisotropy present in this figure explains the anisotropy in the TPMA spectra. Spin-up (spin-down) levels are denoted by a (b), while the superscript + (-) signifies a light- (heavy-) hole level.

Fig. V. A.24

Fig. 3. Since the magnitude of the <100> light-hole Landau level energy is less than that for the <110> energy for a constant magnetic field, this means that the <100> TPMA resonant field position will be shifted to a higher magnetic field than that for the <110> position at the fixed transition energy of Fig. 4(a). Likewise, one can see that the TPMA resonant field position for the <111> direction should be shifted to a lower field than for the case of the <110> direction. In contrast the opposite anisotropy is predicted from Fig. 3 and observed in Fig. 4(b) for transition 15 (dealing with an initial light-hole spin up $a^+(1)$ state). In addition, the degree of the anisotropy for the $a^+(1)$ levels is much smaller than for the $b^+(1)$ levels as shown in Fig. 3. Figure 4(c) shows that both transitions 11 and 12 are present and unresolved for $\vec{e} \perp \vec{B}$, with the strongest component arising from transition #12. Thus, use of the $\vec{e} \| \vec{B}$ polarization is necessary to demonstrate the true nature of the anisotropy of the weaker transition 11 which is explained by the anisotropy of the $b^-(1)$ (heavy-hole spin down initial state) level shown in Fig. 3. Thus, the b^+ or a^- levels are more anisotropic than the b^- or a^+ hole levels, in agreement with the intravalence band data of Littler et al.[12]

In conclusion, we have shown for the first time that the TPMA spectra in InSb are anisotropic and that the anisotropy is quantitatively related to the light- and heavy-hole anisotropy. Consequently, TPMA appears to be a powerful approach to investigating the valence band in semiconductors, which have usually only been studied with cyclotron resonance, combined resonance, or one-photon interband techniques.

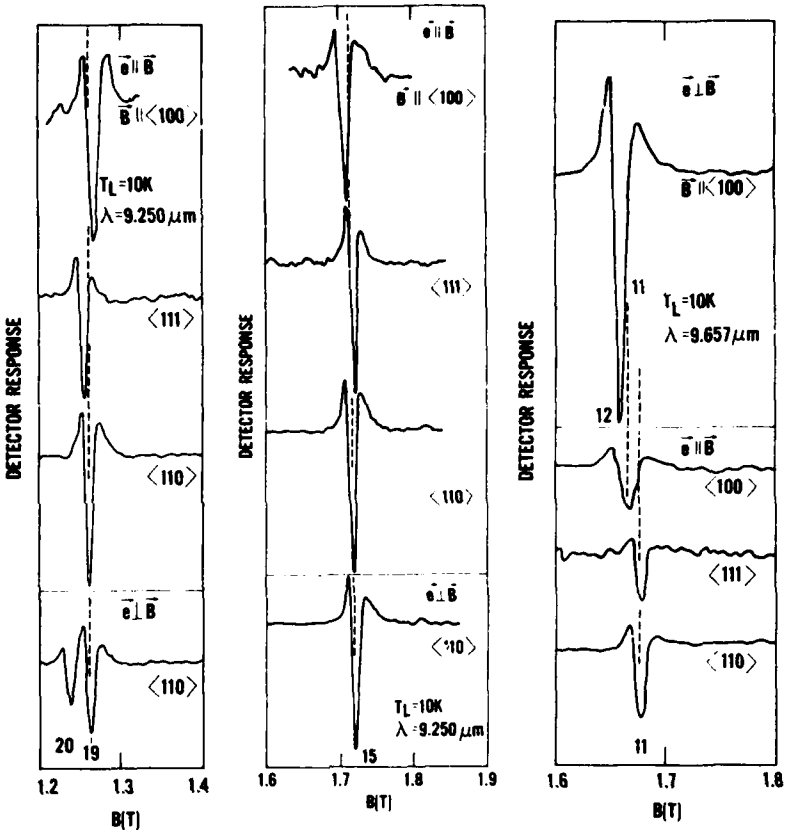

Fig. 4 TPMA spectra showing polarization and anisotropy for:
(a) transitions 19 ($b^+(1) \rightarrow b^c(1)$) and 20($b^+(0) \rightarrow b^c(2)$)
(b) transition 15 ($a^+(1) \rightarrow a^c(1)$)
(c) transition 11 ($b^-(1) \rightarrow b^c(1)$)

Fig. V.A.25

Acknowledgements--We thank M. H. Weiler, whose energy band model was used in this study, and M. W. Goodwin, C. L. Littler, and E. W. Van Stryland for helpful discussions.

References

1. J. P. van der Ziel, Phys. Rev. B 16, 2775 (1977).
2. K. J. Button, B. Lax, M. H. Weiler, and M. Reine, Phys. Rev. Lett. 17, 1005 (1966).
3. M. H. Weiler, R. W. Bierig, and B. Lax, Phys. Rev. 184, 709 (1969).
4. V. T. Nguyen and A. R. Strnad, Opt. Commun. 3, 25 (1971).
5. V. T. Nguyen, A. R. Strnad, and Y. Yafet, Phys. Rev. Lett. 26, 1170 (1971).
6. S. K. Manlief and E. D. Palik, Solid State Commun. 12, 1071 (1973).
7. D. G. Seiler, M. W. Goodwin, and M. H. Weiler, Phys. Rev. B 23, 5806 (1981).
8. M. W. Goodwin, D. G. Seiler, and M. H. Weiler, Phys. Rev. B 25, 6300 (1982).
9. D. M. S. Bagguley, M. L. A. Robinson, and R. A. Stradling, Phys. Lett. 6, 143 (1963).
10. M. L. A. Robinson, Phys. Rev. Lett. 17, 963 (1966).
11. R. Ranvaud, H. R. Trebin, U. Rossler, and F. H. Pollak, Phys. Rev. B 20, 686 (1979).
12. C. L. Littler, D. G. Seiler, R. Kaplan, and R. J. Wagner, to be published in Phys. Rev. B.
13. C. R. Pidgeon and R. N. Brown, Phys. Rev. 146, 575 (1966).
14. C. R. Pidgeon and S. H. Groves, Phys. Rev. 188, 824 (1969).
15. M. H. Weiler, J. Mag. and Mag. Mat. 11, 131 (1979).
16. A. L. Efros, L. M. Kanskaya, S. I. Kokhanouskiu, and R. P. Seysyan, Solid State Commun. 43, 613 (1982).
17. A. P. Roth and E. Fortin, Phys. Rev. B 18, 4200 (1978).
18. M. W. Goodwin and D. G. Seiler, Phys. Rev. B 27, 3451 (1983).

B. Cadmium Sulfide

In this subsection we present the results of an investigation of nonlinear optical properties of CdS using two photon spectroscopy techniques. All of the major experimental work was carried out at the Francis Bitter National Magnet Laboratory on the MIT campus in Boston. D. G. Seiler spent one year there carrying out research during September 1, 1980, to August 31, 1981. Extensive analysis and computations were also carried out later at NTSU. In what follows several papers are reproduced: one dealing with A-excitons and one with B-excitons. In addition, a reprint of a paper (given at the XIIth International Quantum Electronics Conference held in Munich, West Germany, during 1982) is also reproduced.

PHYSICAL REVIEW B VOLUME 25, NUMBER 12 15 JUNE 1982

Two-photon magnetospectroscopy of A-exciton states in CdS

D. G. Seiler
Francis Bitter National Magnet Laboratory, Massachusetts Institute of Technology, Cambridge, Massachusetts 02139
and Department of Physics, North Texas State University, Denton, Texas 76203

D. Heiman
Francis Bitter National Magnet Laboratory, Massachusetts Institute of Technology, Cambridge, Massachusetts 02139

R. Feigenblatt
Francis Bitter National Magnet Laboratory, Massachusetts Institute of Technology, Cambridge, Massachusetts 02139
and Department of Electrical Engineering, Massachusetts Institute of Technology, Cambridge, Massachusetts 02139

R. L. Aggarwal and B. Lax
Francis Bitter National Magnet Laboratory, Massachusetts Institute of Technology, Cambridge, Massachusetts 02139
and Department of Physics, Massachusetts Insititute of Technology, Cambridge, Massachusetts 02139
(Received 22 December 1981)

High-resolution spectra are obtained for the free A excitons in CdS by two-photon absorption using photoconductivity techniques. At zero applied magnetic field the anisotropy splitting of the $2P$ and $3P$ exciton states is observed and interpreted with an anisotropic effective-mass Hamiltonian. The energies of these states are measured as a function of magnetic field up to $B \simeq 10$ T. The magnetic field dependences are analyzed in terms of linear Zeeman splitting and diamagnetic interactions. At low fields the diamagnetic contribution gives the usual quadratic field dependence but deviates significantly at higher fields. At a given field, the deviation is found to increase dramatically with increasing quantum number n. This deviation is fitted by variational calculations developed by Larsen, which take into account the interaction of states through the diamagnetic term in the Hamiltonian. The magnetic field dependence of these states allow us to determine the masses as $m_e^{\perp}=(0.210\pm0.003)m_0$ and $m_h^{\perp}=(0.64\pm0.2)m_0$. At $B=0$ the narrow laser linewidths (0.05 meV) allow an accurate determination of the A-exciton binding energy of 27.4 ± 0.8 meV and the anisotropy parameter of 0.797 ± 0.013 from which the energy gap $E_g^A=2582.5\pm0.2$ meV at $T=1.8$ K is calculated. Finally, the temperature dependence of the A gap is determined.

I. INTRODUCTION

Excited states ($n \geq 2$) of the free exciton in CdS have been studied previously by linear absorption[1-3] and two-photon absorption (TPA).[4-8] Magnetic field effects on these excitons were studied up to $B=3$ T by Hopfield and Thomas[1] in high resolution and up to $B=10$ T by Shah and Daman[2] with moderate resolution using one-photon techniques. Daman *et al.*[7] studied $2P$ exciton states by two-photon magnetoabsorption (TPMA) techniques for a magnetic field of 5 T parallel to the hexagonal c axis. Through polarization studies they were able to understand the Zeeman splitting of the $2P_{\pm1}$ states and fine structure splitting of the $2P_{+1}$, $2P_{-1}$, and $2P_z$ states. We present here the results of high-resolution, TPA magneto-optical experiments on the free-exciton excited states in CdS up to $B \simeq 10$ T. Both Zeeman splitting and diamagnetic shifts of the $n=2$ and $n=3$ exciton states are investigated. At these fields the higher-lying exciton states show considerable deviation from quadratic diamagnetic behavior. This deviation is explained by considering level interactions or state mixing using variational calculations due to Larsen.[9] The high reso-

lution obtained in the present experiment enables us to determine some material parameters of CdS more accurately than in previous studies.

CdS has a hexagonal wurtzite structure.[10] This structural anisotropy causes crystal-field splitting, which interacts with the spin-orbit coupling to split the valence band into three bands, A, B, C, each twofold degenerate with spin considered. The lowest band gap is due to the A-valence band and is at the Brillouin-zone center at $E_g^A \simeq 2.582$ eV. The conduction band with electron mass $m_e \simeq 0.2 m_0$ produces free excitons associated with each valence band having an effective Rydberg of $\simeq 27$ meV and a ground-state radius of $\simeq 30$ Å. The pioneering work of Hopfield and Thomas[1] utilized a magnetic field to study these excitons using one-photon absorption. They determined values for the exciton binding energy, electron and hole masses, the electron and hole spin g factors and analyzed the Zeeman splitting and diamagnetic shifts up to $B = 3$ T. At these fields the magnetic perturbation on the wave functions is weak in comparison to the Coulomb interaction, while at higher magnetic fields the Lorentz force on the exciton becomes comparable to the Coulomb force. As a result, the wave functions contract to such an extent that deviations from quadratic diamagnetic behavior occur. The magnetic field causes mixing of the $B = 0$ wave functions through the ordinary diamagnetic perturbation. This interaction is known to couple states having $\Delta l = 0, \pm 2$ and $\Delta m_l = 0$ for all principal quantum numbers ($\Delta n \neq 0$ or $\Delta n = 0$). Higher-lying energy levels tend to repel lower states down in energy. This effect reduces the quadratic dependence of the levels and eventually causes it to once again approach a linearlike dependence. This departure from the low-field behavior is expected to occur at lower fields for excited-state excitons. This occurs because the wave functions are much larger and hence have a smaller Coulomb interaction to overcome. Thus, we expect to see $n = 3$ exciton states deviate much more from a quadratic dependence than $n = 2$ states at a given field.

The energy-level spectra of the free excitons are produced in the present study by two-photon absorption. In this particular experiment two photons are simultaneously absorbed, where one is fixed in energy and the other is tunable and their sum is made equal to the exciton level. Since both photon energies are below the gap, the absorption occurs throughout the bulk of the sample, which places less importance on the sample surface. The absorption is monitored by the photoconductivity of the samples and the spectral resolution is determined by the linewidth of the laser which is less than 0.05 meV. To our knowledge this is the first time that the photoconductivity technique has been used to obtain the TPA spectra of free excitons in semiconductors.

II. EXPERIMENTAL WORK

The single-crystal samples of CdS were high-purity platelets of 10^{-3}-cm thickness grown from the vapor phase. The crystals used were all in the as-grown condition. Overall sizes were approximately 1×5 mm^2 with the hexagonal c axis lying in the platelet plane parallel to the longest side. Indium electrodes were attached to the surface by melting pure indium onto the samples at 410 °C while in a nitrogen environment. 6-μm-thick indium-gold ribbon was used for the contact wires. Patterns obtained on a Tektronix I-V curve tracer at both very low and very high voltages were symmetric, indicating good Ohmic contacts. To minimize any possible external strain on the crystals, the samples themselves were not epoxied or glued directly to any base. Instead, all samples were placed on polished sapphire substrates and only the flexible ribbon wire was carefully glued to the sapphire. Typical room-temperature resistivities of "good" crystals were $\simeq 10^3$ Ω cm in the light, while dark resistivities were $\geq 10^6$ Ω cm. [Good crystals showed clear resolution of the $A(2P_0)$ line from the $A(2P_{\pm 1})$ line at $B = 0$ with full width at half-maximum (FWHM) linewidths $\simeq 0.3$ meV.] We expect that $N_d - N_a < 10^{16}$ cm^{-3}, indicating some degree of compensation. Voltages up to 45 V were applied across the sample ($E \lesssim 100$ V/cm) without affecting the spectra. Of the half-dozen samples tried only one half showed the narrow $B = 0$ spectral linewidths; the others had $A(2P)$ linewidths approximately twice as wide.

The spectrum of the exciton states was taken by observing the increase in light absorption as monitored by the increase in sample conductivity as a function of photon energy. This method has been used previously by Button *et al.*[11] and more recently by Seiler *et al.*[12] in studying two-photon-induced photoconductivity in InSb using CO_2 lasers. Photoconductive structure using one-photon spectroscopy has been observed at the positions of the free excitons.[13] The exact mechanism causing breakup of the excitons into free electrons and holes is a

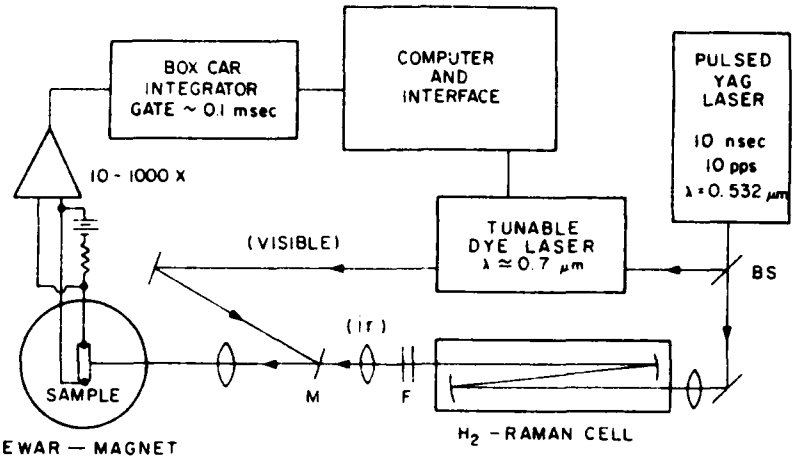

FIG. 1. Schematic diagram of two-photon magnetoabsorption spectroscopy equipment. The doubled-YAG laser output is divided by a beam splitter (BS) in order to pump a tunable dye laser and triple-pass stimulated-Raman-shifting cell. The unwanted Stokes and anti-Stokes outputs of the cell are attenuated by filters (F). The infrared and visible beams are combined by a dielectric mirror (M). The absorption as a function of total photon energy was monitored by measuring the photoinduced conductivity change.

Fig. V.B.1

matter of conjecture; presumably it occurs through interaction with defect or impurity centers.[14]

A Q-switched yttrium aluminum garnet (YAG) laser was used to produce two light beams as seen in Fig. 1, one tunable at $\hbar\omega_v \simeq 1.8$ eV from a dye laser and the other fixed at $\hbar\omega_{ir} = 0.7840$ eV produced by stimulated Raman scattering.[15] The YAG second harmonic at $\lambda = 0.532$ μm was divided by a beam splitter in order to simultaneously pump the tunable dye laser using LD688 dye and a Raman-shifting cell. The 50-cm-long cell contained hydrogen gas at 450 psi. The pump beam was focused three times inside the cell by initially using a 50-cm focal-length lens placed outside the cell and two concave mirrors (25-cm radius of curvature) mounted inside the cell. Triple passing the cell allowed lower threshold power, approximately one half that obtainable with a single pass. The third-Stokes-shifted ir light was selected by blocking the unwanted Stokes and anti-Stokes light by a long pass filter (0.57 μm) and a 1-mm-thick silicon window. After the visible and ir beams were made to overlap in time they were combined collinearly using a dielectric mirror that reflected the red light while transmitting the ir. The beams were then focused onto the sample using a 30-cm focal-length spherical lens. The peak power of the ir beam was about 5 kW while the visible beam was the order of 10—100 W. The sample was mounted in a variable temperature Dewar containing pumped liquid He at 1.8 K or flowing He gas for higher temperatures. The optical Dewar tail was mounted in a 2-in. bore Bitter magnet solenoid having radial access to the light in a Voigt configuration. The applied current, c axis, and B field were all parallel. A 10-MΩ resistor in series with a battery was placed across the sample. The photoinduced voltage change across the sample was extracted by a low-pass—high-pass filter combination, then amplified between 10 and 1000 times. This output was sampled by a boxcar integrator of gatewidth 0.1 msec. The spectral scans were taken via a computer that read the boxcar output with an analog-to-digital converter while scanning the tunable dye laser through a stepping-motor-shaft-encoder combination. Fluctuations in the photoconductivity signal at 60 Hz were eliminated by locking the laser pulses to a subharmonic of the 60-Hz line frequency.

Spectra were also taken in a single-beam experimental configuration, where $\hbar\omega_{ir}$ was one half the exciton energy. With additional pump power, the dye laser output could be directed into the Raman cell producing "tunable," near-infrared light. The single-beam setup was found to give spectra without the flat background present in the two-beam spectra. Also alignment was much easier since the overlap of two beams is not necessary.

III. THEORY

A. Free-exciton energy levels

The energy-level spectrum of the free excitons in CdS can be conveniently calculated within the

effective-mass approximation. The basic Hamiltonian appropriate to this anisotropic situation has been derived in detail by several authors using slightly different parameter notations suitable for perturbation or variational solutions. Using a center-of-mass coordinate system where the center-of-mass motion is set equal to zero, the effective one-particle Schrödinger equation for an electron-hole pair interacting with each other by the Coulomb field in a wurtzite-type material such as CdS can be written as[16]

$$\left[\frac{-\hbar^2}{2\mu_\perp}\left(\frac{\partial^2}{\partial x^2}+\frac{\partial^2}{\partial y^2}\right)-\frac{\hbar^2}{2\mu_\parallel}\frac{\partial^2}{\partial z^2}-\frac{e^2}{\{K_\perp K_\parallel[x^2+y^2+(K_\perp/K_\parallel)z^2]\}^{1/2}}\right]F(\vec{r})=EF(\vec{r})\ . \tag{1}$$

Here z is parallel to the c axis, $F(\vec{r})$ is the exciton envelope function, $E=E_{ex}-E_g$, $K_\perp$ and $K_\parallel$ are components of the dielectric tensor, and $\mu_\perp$ and $\mu_\parallel$ are components of the effective reduced-mass tensor of the exciton, i.e.,

$$\frac{1}{\mu_\perp}=\frac{1}{m_e^\perp}+\frac{1}{m_h^\perp},\quad \frac{1}{\mu_\parallel}=\frac{1}{m_e^\parallel}+\frac{1}{m_h^\parallel}\ . \tag{2}$$

Making the substitution

$$x'=x,\quad y'=y,\quad z'=\frac{K_\perp}{K_\parallel}z\ ,$$

Eq. (1) becomes

$$\left[-\frac{\hbar^2}{2\mu_\perp}\left(\frac{\partial^2}{\partial x'^2}+\frac{\partial^2}{\partial y'^2}\right)-\frac{\hbar^2}{2\mu_\parallel}\frac{K_\perp}{K_\parallel}\frac{\partial^2}{\partial z'^2}-\frac{e^2}{K(x'^2+y'^2+z'^2)^{1/2}}\right]F(\vec{r}')=EF(\vec{r}')\ . \tag{3}$$

It is convenient to write Eq. (3) in the dimensionless form

$$\left[-\left(\frac{\partial^2}{\partial x^2}+\frac{\partial^2}{\partial y^2}+\frac{\partial^2}{\partial z^2}\right)-\frac{2}{r}\right]F(\vec{r})=EF(\vec{r})\ , \tag{4}$$

where we have dropped the primes, and the units of length and energy are given by

$$a_B=\frac{\hbar^2K}{\mu_\perp e^2},\quad \mathcal{R}^*=\frac{\mu_\perp e^4}{2\hbar^2K^2}\ , \tag{5}$$

and are, respectively, the reduced Bohr radius and the effective Rydberg binding energy. The anisotropy parameter $\gamma=(\mu_\perp K_\perp)/(\mu_\parallel K_\parallel)$. This same equation was given by Faulkner for solving the donor impurity-level case in silicon and germanium at zero magnetic field.[17]

In the presence of a uniform external magnetic field parallel to the c axis and using a cylindrical gauge where the vector potential $\vec{A}=(\vec{B}\times\vec{r})/2$ results in the addition of several terms to the one-particle Hamiltonian of Eq. (3):

$$\frac{m_h^\perp-m_e^\perp}{m_h^\perp+m_e^\perp}\eta L_z+\eta^2(x^2+y^2)/4+g_zS_z\eta/2\ , \tag{6}$$

where $\eta=\mu_B^*B/\mathcal{R}^*$ is a dimensionless measure of the strength of the magnetic field B, the effective Bohr magneton $\mu_B=e\hbar/2\mu_\perp c$, L_z is the z component of the orbital angular momentum operator, g_z is the parallel component of the exciton g factor, and S_z is the z component of the exciton spin angular momentum. The first term linear in B is due to the ordinary Zeeman effect arising from the $\vec{A}\cdot\vec{P}$ terms for the electron and hole, while the last term, also linear in B, is due to the interaction of the electron and hole spins with the magnetic field. The middle term represents the diamagnetic effect arising from the A^2 term which is usually considered to be quadratic in B; at high enough magnetic fields and/or for higher excited exciton states considerable deviation from a quadratic behavior can be expected as a result of the strong mixing of states of different principle quantum number.

In order to calculate the eigenvalues of the Hamiltonian in Eq. (4) for the $2P$ levels at $B=0$ and the diamagnetic part of the Hamiltonian in Eq. (6) we employ the following variational trial functions[9]:

$$\psi_{2P_\pm}=\rho e^{-A_1\rho^2-A_2\bar{r}}\ ,$$

$$\psi_{2P_0}=ze^{-A_1\rho^2-A_2\bar{r}}\ ,$$

TABLE I. Calculated energy levels of the A excitons in CdS. Variational calculations of the binding energy, in units of $\mathscr{R}^*$, are compared with those of Faulkner (Ref. 17) and Praddaude (Ref. 19). $B=0$ at $\eta=0$ and $B\simeq 7.5$ T at $\eta=0.1$.

Anisotropic model	$\eta=0$ $[\gamma^{1/3}=(0.729)^{1/3}=0.900]$		$\eta=0.1$ Spherical model ($\gamma=1$)	
Energy level	This paper	Faulkner	This paper	Praddaude
$2P_0$	0.3010	0.3009	0.3239	0.3248
$2P_-$	0.2656	0.2656	0.3995	0.4017
$3P_0$	0.1342	0.1342	0.1381	0.1398
$3P_-$	0.1183	0.1184	0.1583	0.1624

Table V.B.1

where $\tilde{r}=(\rho^2+\alpha z^2+\beta^2)^{1/2}$, $\rho^2=x^2+y^2$. The variational parameters[9] A_1, A_2, α, and β are optimized for each state and magnetic field of interest by minimizing

$$\langle\psi_{2P}|H|\psi_{2P}\rangle/\langle\psi_{2P}|\psi_{2P}\rangle\ .$$

The $3P$ eigenvalues are computed by using the trial functions[18]

$$\psi_{3P_\pm}=\rho(2-\xi\tilde{\tilde{r}})e^{-D\rho^2-E(\rho^2+\xi z^2)^{1/2}}+C_\pm\psi_{2P_\pm}\ ,$$

$$\psi_{3P_0}=z(2-\xi\tilde{\tilde{r}})e^{-D\rho^2-E(\rho^2+\xi z^2)^{1/2}}+C_0\psi_{2P_0}\ ,$$

where $\tilde{\tilde{r}}=(\rho^2+\delta z^2+\theta^2)^{1/2}$. The variational parameters D, E, ξ, δ, and θ are optimized in a fashion similar to the $2P$ case. The C parameters were determined by forcing orthogonality between $3P_\pm$ and $2P_\pm$, and between $3P_0$ and $2P_0$ for each choice of the other parameters.

The accuracy of these $2P$ and $3P$ variational calculations can be seen from the results given in Table I for both $\eta=0$ and $\eta=0.1$. At zero field we compare our results with those of Faulkner[17] who used the Rayleigh-Ritz approach to determine the values of $\mathscr{R}^*$ for certain values of γ. Using a value of $\gamma=0.729$ which corresponds to his tabulated $\gamma^{1/3}=0.900$ gives excellent agreement for the various energy levels shown in Table I. Solutions in a magnetic field ($\gamma=0.1$) are compared to the more accurate spherical results of Praddaude[19] obtained by expansion of the wave function in Laguerre polynomials for hydrogenlike atoms in a magnetic field. Our calculated binding energies, in units of $\mathscr{R}^*$, are lower than Praddaude's by 0.0009, 0.0022, 0.0017, and 0.0041 for the $2P_0$, $2P_-$, $3P_0$, and $3P_-$ states, respectively. This is to be expected from a variational calculation. However, the relative spacings of the energy levels $E(2P_-)-E(2P_0)$, $E(3P_0)-E(2P_0)$, and $E(3P_-)-E(2P_0)$ levels are generally in closer agreement: Praddaude's, $+0.0769$, -0.1850, -0.1624; our results, $+0.0756$, -0.1858, and -0.1656, respectively. As we shall see later, these errors are approximately the same as the uncertainties in field-dependent energy shifts of each of the respective levels. Consequently, we expect our variational calculations to adequately explain the data.

B. Two-photon absorption

The basic theory of two-photon processes was formulated by Göppert-Mayer in 1931.[20] Using second-order perturbation theory and making the dipole approximation gives the probability per unit time per unit volume $W^{(2)}(E)$ that the system makes a transition from an initial state i to a final state f of energy $E=\hbar(\omega_1+\omega_2)$ above the ground state, while the field loses one quantum each of energy $\hbar\omega_1$ and $\hbar\omega_2$.[21] Thus,

$$W^{(2)}(E)=\frac{2\pi}{\hbar}\left|\frac{eA_{01}}{mc}\right|^2\left|\frac{eA_{02}}{mc}\right|^2|A_{fi}^{(2)}|^2\times\delta(E_f-E_i-\hbar\omega_1-\hbar\omega_2)\ , \tag{7}$$

where A_{01} and A_{02} are the magnitude of the vector potentials of the radiation beams polarized in the fixed directions $\hat{\epsilon}_1$ and $\hat{\epsilon}_2$, and $A_{fi}^{(2)}$ is the composite matrix element given by

$$A_{fi}^{(2)}=\sum_I\left|\frac{(\vec{P}_{fI}\cdot\hat{\epsilon}_1)(\vec{P}_{Ii}\cdot\hat{\epsilon}_2)}{E_I-E_i-\hbar\omega_2}+\frac{(\vec{P}_{fI}\cdot\hat{\epsilon}_2)(\vec{P}_{Ii}\cdot\hat{\epsilon}_1)}{E_I-E_i-\hbar\omega_1}\right|\ . \tag{8}$$

Here P_{fI} and P_{Ii} are matrix elements of the dipole operator and the sum is over all possible intermediate states I. The quantity usually measured in a TPA experiment is β which is related to the transition rate per unit volume by the expression

$$\beta=(\hbar\omega_1+\hbar\omega_2)\frac{W^{(2)}(E)}{I_1 I_2}\ .$$

A knowledge of the laser beam properties both in space and time is needed to determine β and a lack of complete beam characterization can lead to large uncertainties. As pointed out by Bechtel and Smith,[22] the absorption may depend upon the laser pulsewidth because absorption by two-photon-created excess carriers is not negligible.

For the purposes of this study we are interested in the two-photon resonance condition given in the δ function of Eq. (7). Thus whenever $E_f-E_i=\hbar\omega_1+\hbar\omega_2$ we expect to observe a maximum in the two-photon absorption and hence the greatest photoconductive response. The complications just mentioned should not affect this resonance condition.

The transition probabilities depend upon the light polarization as seen in Eq. (8). There have been several calculations and tabulations of the form of these angular dependences in order that they might be readily available for the analysis of experimental data. Inoue and Toyozawa[23] gave the angular dependence of two-photon transitions in which either the initial or final state transforms according to the totally symmetric representation of the point group. This work was subsequently extended by Bader and Gold[24] to (1) the allowed transitions between states belonging to all irreducible representations of the point group and (2) the double-group representations encountered when spin-orbit coupling is included. Both Stafford and Sondergeld[6] and Nguyen *et al.*[4] found no evidence for TPA to final S-exciton states, in contrast to the work of Pradere and Mysyrowicz.[5] The polarization dependence of these matrix elements was used by Nguyen *et al.* to show that the $1S$-exciton ground state is an effective intermediate state when one photon from a dye laser is nearly resonant with the $1S$ exciton energy, while the other photon is produced by a CO_2 laser.

The allowed TPA selection rules at the Γ point can be determined from group theory applied to the C_{6v} symmetry of CdS-type crystals. The symmetries of the A excitons are then a result of the Γ_7 conduction band and Γ_9 valence-band symmetries along with the symmetries of the hydrogenic states of the exciton in the center-of-mass coordinate system. We summarize the results in Table II where various exciton states, their decomposition into various symmetries, and the allowed one- and two-photon transitions are given. For $\vec{E}\|c$, the dipole radiation representation is Γ_1 and for $\vec{E}\perp c$, it is Γ_5. A magnetic field parallel to the hexagonal axis of the crystal represents a perturbation of symmetry Γ_2. Group theory can then be used to calculate g values for all the exciton states as shown in Table II.

IV. RESULTS AND CONCLUSIONS

The TPA spectra near the A exciton region are shown in Fig. 2. The lowest observable exciton states are the $2P$ levels. Even though a Γ_6 $1S$ or $2S$ transition is allowed in TPA, no evidence for their existence was found. These observations were first made by Stafford and Sondergeld[6] and later by Nguyen *et al.*[4] using TPA. Evidently the oscillator strength for this Γ_6 state is very small. At

TABLE II. CdS exciton states and their symmetries. The allowed one- and two-photon transitions and their polarizations are shown for $\vec{E}\perp c$ ($\perp$) and $\vec{E}\|c$ ($\|$). The corresponding g values for $\vec{B}\|c$ are also given.

State	Possible symmetries	One-photon allowed	Two-photon allowed	g values
$1S,2S$	Γ_5,Γ_6	$\Gamma_5(\perp)$		$\lvert g_{e\|\|}-g_{h\|\|}\rvert$
			$\Gamma_6(\perp,\perp)$	$\lvert g_{e\|\|}+g_{h\|\|}\rvert$
$2P_0$	Γ_5,Γ_6	$\Gamma_5(\perp)$		$\lvert g_{e\|\|}-g_{h\|\|}\rvert$
			$\Gamma_6(\perp,\perp)$	$\lvert g_{e\|\|}+g_{h\|\|}\rvert$
$2P_{\pm1}$	$\Gamma_1,\Gamma_2,\Gamma_3,\Gamma_4,\Gamma_5,\Gamma_6$	$\Gamma_5(\perp)$		$\lvert 2g_{\mu\|\|}-g_{e\|\|}-g_{h\|\|}\rvert$
		$\Gamma_1,\Gamma_2(\|\|)$		$\lvert 2g_{\mu\perp}+g_{e\|\|}-g_{h\|\|}\rvert$
			$\Gamma_1,\Gamma_2(\perp,\perp$ or $\|\|,\|\|)$	$\lvert 2g_{\mu\|\|}+g_{e\|\|}-g_{h\|\|}\rvert$
			$\Gamma_6(\perp,\perp)$	$\lvert 2g_{\mu\perp}-g_{e\|\|}+g_{h\|\|}\rvert$

Table V.B.2

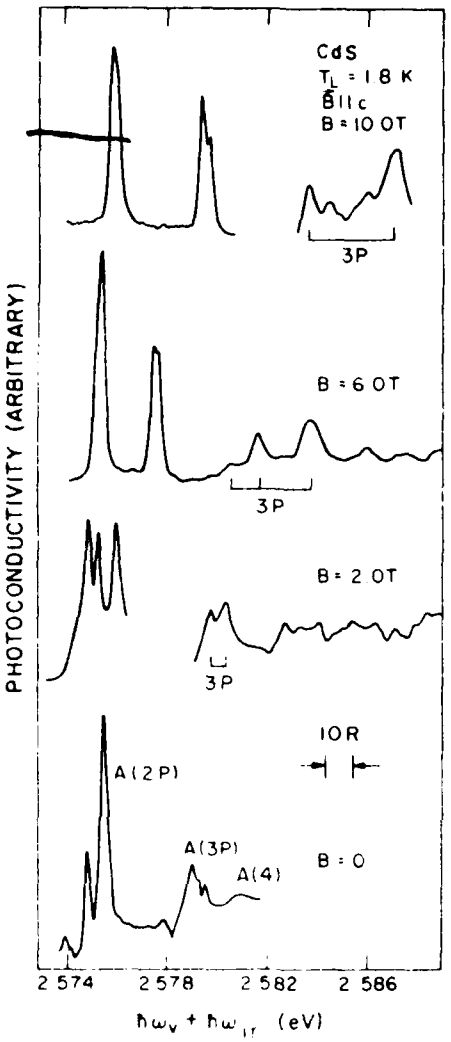

FIG. 2. Photoconductivity vs total photon energy $\hbar\omega_v + \hbar\omega_{1r}$ near the A-exciton region in CdS platelets for various magnetic fields. The magnetic field was parallel to the hexagonal c axis in a Voigt configuration with $\vec{E}$ perpendicular to c for the two photons at a lattice temperature of $T_L = 1.8$ K. The instrumental resolution $R = 0.1$ meV is narrower than the intrinsic linewidths.

Fig. V.B.2

$B = 0$ the $2P$ states clearly show the expected anisotropy splitting corresponding to $2P_0$ ($m_l = 0$) and $2P_\pm$ ($m_l = \pm 1$). The $2P$ structure has allowed contributions from both the Γ_1, Γ_2 and the Γ_6 symmetry states which lie close in energy so that one cannot resolve them at $B = 0$. At $B = 10$ T, there is fine-structure splitting observable in the $2P_+$ state which is caused by the slightly different g factors for the $\Gamma_1 + \Gamma_2$ and the Γ_6 states. Similar splitting at $B = 0$ has been seen by Hopfield and Thomas[1] and Nguyen *et al.*[4] For the $3P$ states the signal-to-noise ratio at $B = 0$ was lower, resulting in poor resolution. In order to extract the peak positions many scans were taken on several samples. Zero-field results of the $3P_0$ and $3P_\pm$ states reported here are averages of these scans. This is the first experiment with enough resolution to resolve this anisotropy splitting of the $3P$ states. Zero-field positions of the observed A-exciton states in CdS are given in Table III where a comparison is also given with the one-photon results of Hopfield and Thomas[1] and Litton *et al.*[3] and the two-photon results of Stafford and Sondergeld[6] and Nguyen *et al.*[4] There is in general very good agreement.

The result of fitting our variational calculations to our data gives values for the effective Rydberg $\mathscr{R}^* = 27.4 \pm 0.8$ meV and the anisotropy parameter, $\gamma = 0.797 \pm 0.013$. Using our data and the less-accurate first-order perturbation approach of Hopfield and Thomas, whose state energies involve a mean Rydberg $\bar{\mathscr{R}}^*$ and a different anisotropy parameter γ', gives $\bar{\mathscr{R}}^* = 29.5$ meV and $\gamma' = 0.234$. This may be compared with Hopfield and Thomas's results of 28 ± 1 meV. Using $\mathscr{R}^* = 27.4$ meV and the energy levels for the anisotropic situation puts the energy gap for the A valence band at $E_g^A = 2582.5 \pm 0.2$ meV at $T = 1.8$ K. When a magnetic field is applied, the $n \geq 2$ peaks show both Zeeman splitting and diamagnetic shifting to higher energies. Although the $n = 3$ peaks shift to larger energy more rapidly, their splitting is seen to be nearly the same as for the $n = 2$ peaks. At higher fields, substructure in the $2P_\pm$ state and additional structure in the region of the $3P$ states are observed.

The energy positions of these peaks are plotted as a function of magnetic field in Fig. 3. The six states $2P_0$, $2P_\pm$, $3P_0$, and $3P_\pm$ are clearly observed with the exception of $2P_0$ and $2P_-$ at high fields, which appear to have merged together. This is the first time that the $3P$ states of CdS have been investigated in a magnetic field. An important result immediately apparent from Fig. 3 is that the $3P$-exciton states become linear in B at relatively low fields in agreement with the theoretical calculations of Praddaude.[19] Thus, the linear slopes of the exciton states become "Landau-like."[25,26]

The linear Zeeman splitting between P_+ and P_- pairs is shown in Fig. 4 for both the $n = 2$ and $n = 3$ states. The straight line is a best fit to the $2P_\pm$ states and results in $g_{\rm eff}^{2P} = 6.39 \pm 0.08$, where the energy splitting is defined by $\Delta E \equiv g_{\rm eff} \mu_B B$.

TABLE III. Experimental values of the zero-field A-exciton energies in CdS. All energies given in eV.

	Transition energy				
	One-photon results		Two-photon results		
Energy level	Hopfield and Thomas (Ref. 1)	Litton *et al.* (Ref. 3)	Stafford and Sondergeld (Ref. 6)	Nguyen *et al.* (Ref. 4)	This paper
$1S\Gamma_6$	2.5524	2.5537			
$1S_L$	2.554 55	2.554 55			
$2S$		2.574 58			
$2P_0$	2.575 08			2.5754	2.574 64
		2.575 21	2.5745		
$2P_{\pm 1}$	2.575 75			2.5762	2.575 33
$3S$		2.578 41			
$3P_0$					2.5789
		2.578 91		2.5815	
$3P_{\pm 1}$					2.5793
$3D_{\pm 2}$	2.579 77	2.579 23			
$n=4$	2.580 94	2.580 18			2.5809

Table V.B.3

The splitting of the $3P_{\pm}$ states gives the slightly smaller value of $g_{\rm eff}^{3P}=6.09\pm0.20$. According to Table II the $2P_0\Gamma_6$ state should have a g factor of $|g_{e\parallel}+g_{h\parallel}|$. However, splitting of this line is not observed. If somehow the two-photon selection rule for this state allowed transitions to a Γ_5 symmetry level, then a g factor of $|g_{e\parallel}-g_{h\parallel}|$ would be predicted. Using $g_{e\parallel}=-1.78$ and $g_{h\parallel}=-1.15$ gives $g_{\rm eff}=0.63$ which is small enough such that the splitting would not be observed at the low fields where the P_0 state is clearly resolved from the P_- state. We identify the observed fine-structure splitting of the $2P_+$ state with the $\Gamma_1+\Gamma_2$ and the Γ_6 states. Thus the average g value of these two lines from Table II is $g_{\rm eff}=|2g_{\mu\parallel}|=|2(1/m_h^{\perp}-1/m_e^{\perp})|=6.39\pm0.08$. The energy difference of the fine-structure splitting of the $2P_+$ states is $(\frac{1}{2}|2g_{\mu\parallel}+g_{e\parallel}-g_{h\parallel}|-\frac{1}{2}|2g_{\mu\parallel}-g_{e\parallel}+g_{h\parallel}|)\mu_B B=|g_{e\parallel}-g_{h\parallel}|\mu_B B$. Thus at $B=10$ T, the observed splitting of 0.29 meV gives $|g_{e\parallel}-g_{h\parallel}|=0.50$. This compares favorably with the results of Venghaus *et al.*[27] of $|g_{e\parallel}-g_{h\parallel}|=0.56\pm0.05$, with $g_{e\parallel}=1.79\pm0.1$ and $g_{h\parallel}=1.23\pm0.1$ and the results of Damen *et al.*,[7] $|g_{e\parallel}-g_{g\parallel}|=0.55\pm0.05$.

In order to extract the quadratic diamagnetic contribution to the experimental energy shifts,

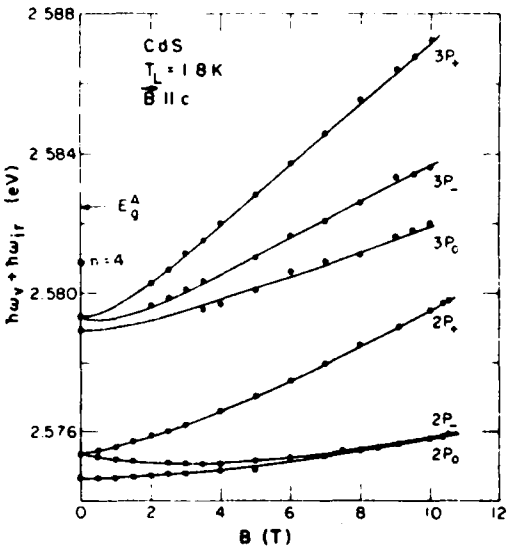

Fig. V.B.3

FIG. 3. Peak positions, in total photon energy $\hbar\omega_{ir}+\hbar\omega_{ir}$, for the $2P$ and $3P$ A excitons in CdS platelets as a function of applied B field. The solid points were determined experimentally and the solid curves are theoretically obtained from variational calculations of the diamagnetic shifts along with use of the experimental g factors.

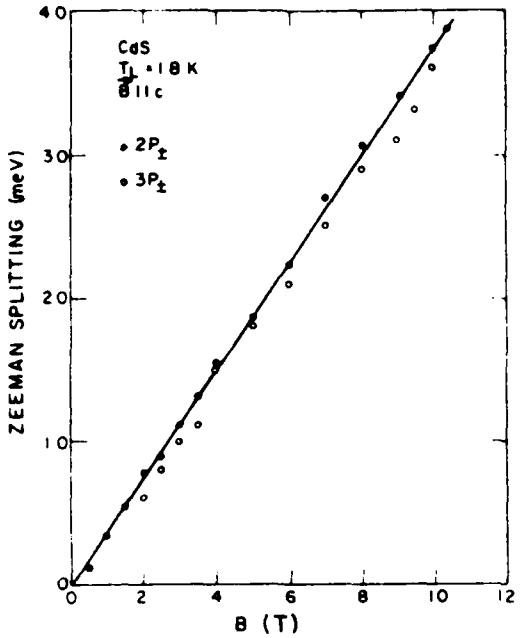

FIG. 4. Zeeman splitting of the $2P$ and $3P$ A excitons ($m_l = \pm 1$) in CdS as a function of magnetic field. The solid points represent the doublet splitting of the $2P_+$ and $2P_-$ pair, while the open circles are splittings of the $3P_+$ and $3P_-$ pair. The solid line is a linear fit to $2P$ with $g_{\text{eff}}(2P_\pm) = 6.39 \pm 0.08$.

Fig. V.B.4

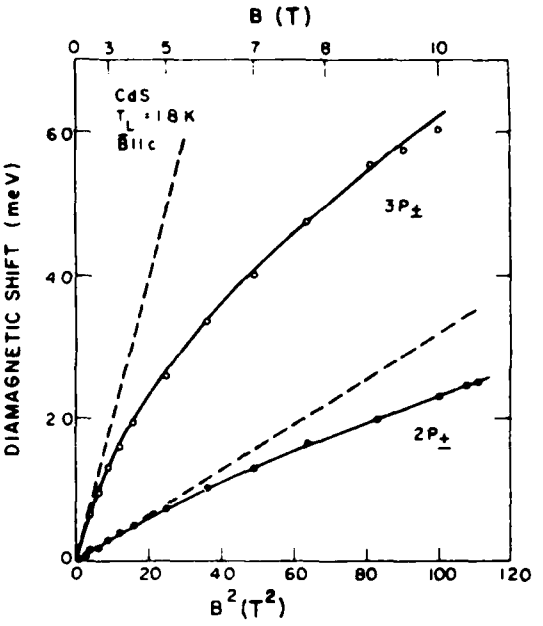

FIG. 5. Diamagnetic shift of the $2P_\pm$ and $3P_\pm$ A-exciton peaks in CdS as a function of applied B field squared. The solid points represent the $2P$ shift and the open circles are for $3P$. The diamagnetic shift is determined by subtracting one-half the Zeeman splitting from the total magnetic-field-induced shift. The lower dashed straight line is a fit to the $2P$ excitons at low fields. The solid curves are theoretical values determined from a variational calculation which includes level interactions. The upper dashed curve is a straight line with six times the slope of the lower dashed curve.

Fig. V.B.5

one-half of the Zeeman splitting is subtracted from the P_+ state and added to the P_- state. The results for both $2P_\pm$ and $3P_\pm$ are plotted as a function of B^2 in Fig. 5. The lower dashed curve is a straight-line fit to the experimental $2P_\pm$ points at low fields, $B < 3$ T. For $B > 3$ T the points deviate significantly; at $B = 10$ T the separation is 28%. The deviation from quadratic behavior of the $3P_\pm$ states is even much more pronounced. The slope at $B = 0$ gives the coefficient of the diamagnetic term from simple theory.[1] The upper dashed straight line near the $3P_\pm$ states has a slope 6 times that for the $2P_\pm$ as expected from this theory.

The diamagnetic shifts for the $2P$ and $3P$ states were calculated using the variational method described in the theory section. The solid lines in Fig. 5 show the results of these calculations. The fit is quite good. In Fig. 6 the diamagnetic shifts versus B are shown for all the exciton states. Excellent agreement is found between the experiment and theory. We note here that only *one* adjustable parameter $\mu_\perp$ was used to fit the field dependence of all six exciton states simultaneously. The best value was found to be $\mu_\perp = 0.158 \pm 0.002$, using $\mathcal{R}^* = 27.4$ meV and $\gamma = 0.797$, which were determined previously from the $B = 0$ energies. As a final test, the sum of the diamagnetic contribution from the theory and the experimentally determined Zeeman splitting is shown in Fig. 3 for all $2P$ and $3P$ states. Again, very good agreement is seen between the experimental points and the theory.

Using our experimentally determined values for $\mathcal{R}^*$ and $\mu_\perp$ in Eq. (2) gives a value of the mean dielectric constant $K = 8.9 \pm 0.2$. This and other material parameters are listed in Table IV along with values determined by other experiments.

Individual values for the electron and hole masses will now be extracted from our data in the most self-consistent manner. Two methods give results for both $m_e^\perp$ and $m_h^\perp$: (a) using our values for $\mu_\perp$ and $g_{\mu_\perp}$, and (b) using our values for $\mu_\perp$ and the exciton translational mass determined from resonant Brillouin scattering experiments.[28] These

TABLE IV. Material parameters for CdS. The values given are for low temperature ($T = 1.8$ K) and for the A valence band.

Parameter	Definition	Present results	Other results	Reference	Comments
$\mathcal{R}^*$	$\frac{\mu_\perp e^4}{2\hbar^2 K^2}$	27.4±0.8 meV			from $B=0$ energies
			28±1	1	
γ	$\frac{(\mu_\perp K_\perp)}{(\mu_\parallel K_\parallel)}$	0.797±0.013			
	$\left\lvert\frac{3-2\gamma'}{\gamma'+3}\right\rvert$		0.793	1	from $\gamma'=0.222$ of Ref. 1
	in terms of anisotropy γ' in Ref. 1				
E_g^A		2.5825±0.0002 eV			
			2.582 eV	31	
$\mu_\perp$	$\left\lvert\frac{1}{m_e^\perp}+\frac{1}{m_h^\perp}\right\rvert^{-1}$	(0.158±0.002)m_0			from diamagnetic shifts and fit to variational calculations
			(0.16)m_0	1	
			(0.16±0.03)m_0	27	
$K=(K_\perp K_\parallel)^{1/2}$	$\frac{\mu_\perp e^4}{2\hbar^2 \mathcal{R}^*}$	8.9±0.2			
			8.5	10	
			8.7	29	unpublished results of Barker and Summers mentioned in Ref. 29
$\lvert g_{e\parallel}-g_{h\parallel}\rvert$		0.50±0.15	0.62±0.06	1	
			0.56±0.05	27	
			0.55±0.05	7	
$\lvert 2g_{\mu_\parallel}\rvert$	$2\left\lvert\frac{1}{m_h^\perp}-\frac{1}{m_e^\perp}\right\rvert$	6.39±0.08			
			6.60	1	
$m_e^\perp$		(0.210±0.003)m_0			from $\mu_\perp$ and $g_{\mu_\parallel}$
			(0.205±0.003)m_0	28	from $\mu_\perp$ and exciton mass of (0.89±0.1)m_0 given in Ref. 28
			(0.204±0.010)m_0	1	
			(0.190±0.002)m_0	29	
$m_h^\perp$		(0.64±0.02)m_0			from $\mu_\perp$ and $g_{\mu_\parallel}$
			(0.685±0.013)m_0	28	from $\mu_\perp$ and exciton mass of (0.89±0.01)m_0 given in Ref. 28
			(0.7±0.1)m_0	1	

Table V.B.4

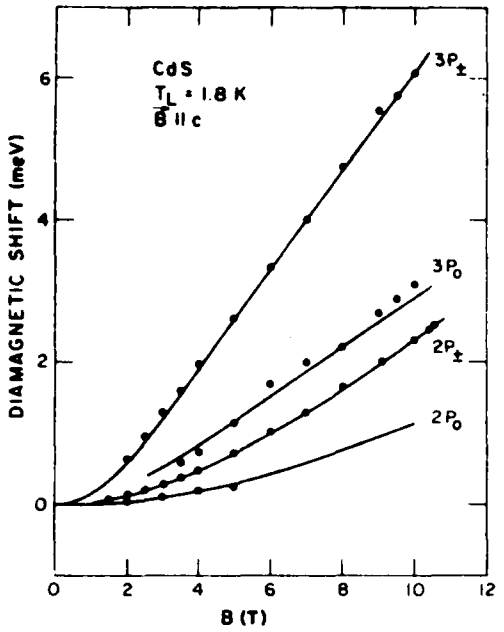

FIG. 6. Diamagnetic shift of the $2P$ and $3P$ A excitons in CdS as a function of applied B field. The experimental points for the P_0 states are the field-induced shifts, and the points for $P_\pm$ are obtained by taking the average of the P_+ and P_- field-induced shifts. The solid curves were determined from Larsen's variational calculations as described in the text. Only one adjustable parameter $\mu_\perp = (0.158 \pm 0.002) m_0$ was needed to simultaneously fit all curves.

Fig. V.B.6

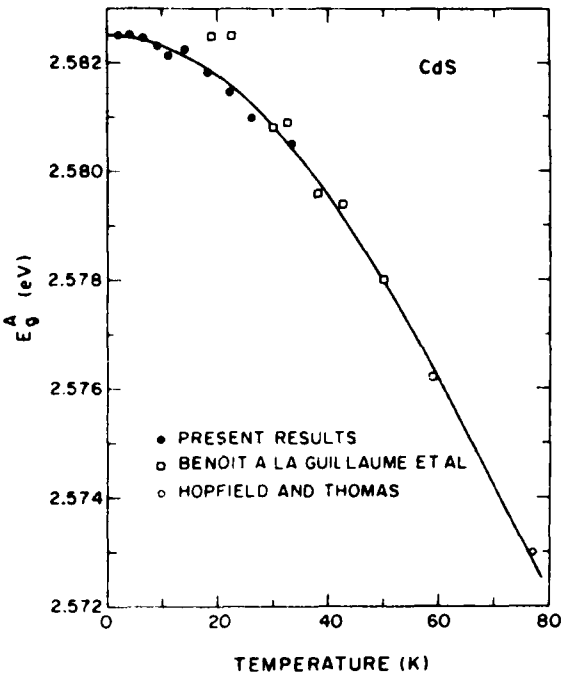

FIG. 7. Temperature dependence of the A energy gap in CdS. The solid points for E_g^A were derived from the positions of the $A(2P_\pm)$ exciton peaks by subtracting a constant binding energy (assuming a temperature-independent effective Rydberg). The open squares are from luminescence studies of Benoit à la Guillaume *et al.* (Ref. 30) and the open circle is from the reflectivity measurements of Thomas and Hopfield (Ref. 31).

Fig. V.B.7

results are tabulated in Table IV along with previously published results, including those of Henry and Nassau[29] for $m_e^\perp$.

The temperature dependence of the A gap is shown in Fig. 7. The low-temperature data points were determined from the energy of the $2P_\pm$ level at $B = 0$ as a function of temperature. Above $T = 35$ K the peak could not be observed above the noise level. Our data smoothly connects with results from luminescence by Benoit à la Guillaume *et al.*[30] and reflectivity by Thomas and Hopfield.[31]

In summary, we have shown that high-resolution two-photon-induced photoconductivity spectra are useful in studying absorption processes in semiconductors. The chief advantage of two-photon absorption is that it is a bulk process, and for strong absorption does not demand micrometer-thick samples or special attention to sample surfaces. The high resolution allows us to determine the anisotropy splitting of the $2P$ and $3P$ free-exciton states at zero magnetic field. These states show the expected linear Zeeman and quadratic diamagnetic dependence at low field. At higher fields the energy levels show a departure from the quadratic diamagnetism. This is especially striking for the higher quantum level $3P$ states. At these fields ($B \geq 2$ T) the $3P$ states show a linear field dependence similar to the Landau-level behavior. These effects are due to the mixing of states via the diamagnetic interaction. The magnitude of the deviation is fitted quite well by a variational method due to Larsen. Also, at the higher fields ($B \geq 6$ T) we see evidence of fine-structure splitting of the levels due to the small difference of the electron and hole spin g values. Finally, accurate values for the effective Rydberg and energy gap are determined by the zero-field exciton levels, as well as the effective electron and hole masses from the Zeeman splitting and diamagnetic interactions.

ACKNOWLEDGMENTS

We sincerely appreciate many useful conversations with D. M. Larsen, B. Wherrett, and H. C. Praddaude. D. M. Larsen is gratefully acknowledged for use of his computer programs for the variational calculations. We also thank D. Reynolds and C. Litton for supplying the excellent crystals and to D. Spears of Lincoln Laboratory for his help in making electrical contacts on the samples. The work of one of us (D.G.S.) was supported in part by the Office of Naval Research and NTSU and experimentally carried out of the Francis Bitter National Magnet Laboratory, which is supported by the National Science Foundation.

---

[1]J. J. Hopfield and D. G. Thomas, Phys. Rev. 122, 35 (1961).
[2]J. Shah and T. C. Damen, Solid State Commun. 9, 1285 (1971).
[3]C. W. Litton, D. C. Reynolds, and T. C. Collins, Phys. Rev. B 6, 2269 (1972).
[4]V. T. Nguyen, T. C. Damen, and E. Gornik, Appl. Phys. Lett. 30, 33 (1977).
[5]F. Pradere and A. Mysyrowicz, in *Proceedings of the Tenth International Conference on the Physics of Semiconductors,* edited by S. P. Keller, J. C. Hensel, and F. Stern (U. S. AEC, Washington, D. C., 1970), p. 101.
[6]R. G. Stafford and M. Sondergeld, Phys. Rev. B 10, 3471 (1974).
[7]T. C. Damen, V. T. Nguyen, and E. Gornik, Solid State Commun. 24, 179 (1977).
[8]V. T. Nguyen, T. C. Damen, E. Gornik, and C. K. N. Patel, Appl. Phys. Lett. 31, 603 (1977).
[9]D. M. Larsen, J. Phys. Chem. Solids 29, 271 (1968).
[10]B. Segall and D. T. F. Marple, in *Physics and Chemistry of II-VI Compounds,* edited by M. Aven and J. J. Prener (North-Holland, Amsterdam, 1967), Chap. 7.
[11]K. J. Button, B. Lax, M. Weiler, and M. Reine, Phys. Rev. Lett. 17, 1005 (1966).
[12]D. G. Seiler, M. W. Goodwin, and M. H. Weiler, Phys. Rev. B 23, 6806 (1981).
[13]Y. S. Park and D. W. Langer, Phys. Rev. Lett. 13, 392 (1964).
[14]Y. S. Park and D. C. Reynolds, Phys. Rev. 132, 2450 (1963).
[15]R. L. Byer, Electro-Opt. Syst. Des. 12, 24 (1980).
[16]F. Bassani and G. Pastori Parravicini, *Electronic States and Optical Transitions in Solids* (Pergamon, New York, 1975), p. 189.
[17]R. A. Faulkner, Phys. Rev. 184, 713 (1969).
[18]D. M. Larsen, private communication. These wave functions are analogous to the 2*S* trial functions described in G. E. Stillman, D. M. Larsen, and C. M. Wolfe, Phys. Rev. Lett. 27, 989 (1971).
[19]H. C. Praddaude, Phys. Rev. A 6, 1321 (1972).
[20]M. Göppert-Mayer, Ann. Phys. (Leipzig) 9, 273 (1931).
[21]F. Bassani and G. Pastori Parravicini, *Electronic States and Optical Transitions in Solids* (Pergamon, New York, 1975), p. 165.
[22]J. H. Bechtel and W. L. Smith, Phys. Rev. B 8, 3515 (1976).
[23]M. Inoue and Y. Toyozawa, J. Phys. Soc. Jpn. 20, 363 (1965).
[24]T. R. Bader and A. Gold, Phys. Rev. 171, 997 (1968).
[25]B. Lax and S. Zwerdling, Prog. Semicond. 15, 221 (1960).
[26]R. L. Aggarwal, Semicond. Semimet. 9, 151 (1972).
[27]H. Venghaus, S. Suga, and K. Cho, Phys. Rev. B 16, 4419 (1977).
[28]E. S. Koteles, in *Excitons,* edited by E. I. Rashba and M. D. Sturge (North-Holland, Amsterdam, 1982).
[29]C. H. Henry and K. Nassau, Phys. Rev. B 2, 997 (1970).
[30]C. Benoit à la Guillaume, J.-M. Debever, and F. Salvan, Phys. Rev. 177, 567 (1969).
[31]D. G. Thomas and J. J. Hopfield, Phys. Rev. 116, 573 (1959).

PHYSICAL REVIEW B VOLUME 27, NUMBER 4 15 FEBRUARY 1983

Two-photon spectroscopy of B excitons in CdS

D. G. Seiler
Center for Applied Quantum Electronics, Department of Physics, North Texas State University, Denton, Texas 76203

D. Heiman
Francis Bitter National Magnet Laboratory, Massachusetts Institute of Technology, Cambridge, Massachusetts 02139

B. S. Wherrett
Department of Physics, Heriot-Watt University, Edinburgh, Scotland
(Received 13 October 1982)

High-resolution spectra are obtained for the free A and B excitons in CdS by two-photon absorption photoconductivity techniques at 1.8 K. At zero applied magnetic field, spectra are shown which indicate for the first time the presence of anisotropy splitting of the $B(2P)$ exciton states. The first observation of the $B(3P)$ exciton state at $B=0$ T then allows the conclusion that both the effective Rydberg and the anisotropy parameter of the A and B excitons are the same. This further indicates that the A and B valence-band masses are equal. These conclusions are confirmed by the first observation of the Zeeman splitting of the $B(2P_{\pm 1})$ and $B(3P_{\pm 1})$ exciton states at fields up to 10 T. Fine-structure splitting of the $B(2P_{+1})$ and $B(2P_{-1})$ states results from an effective g factor for the B valence band of $g_h^B = 0.7 \pm 0.3$.

INTRODUCTION AND BACKGROUND

There have been a number of studies over the past 20 years that have provided detailed information about the nature of the free A exciton in CdS and its behavior in a magnetic field. Linear spectroscopy using one-photon absorption, one-photon emission or luminescence, or one-photon reflectance techniques allowed various features of the magneto-optical effects in the A-exciton spectrum to be investigated.[1-7] The primary features were Zeeman splittings and diamagnetic shifts from which effective masses and g factors for the conduction band and A valence band were extracted. The A-exciton spectra of cadmium sulfide has also been extensively investigated using two-photon absorption (TPA) techniques.[8-14] This form of nonlinear spectroscopy has several advantages over one-photon spectroscopy: (1) less sensitivity to crystal surface quality and crystal thickness (since TPA is a bulk effect); (2) different selection rules allowing different eigenstates to be investigated; and (3) more transitions are possible because of the flexibility of using two photons of different polarization.

The A valence band as well as the conduction band have been well characterized in previous studies (see Table IV of Ref. 14). In contrast, little information is available about the B valence band. This is due to the difficulty in obtaining well-resolved free-exciton spectra. In this paper we investigate free excitons associated with the B valence band using two-photon spectroscopy techniques. Application of a magnetic field allows Zeeman splittings and diamagnetic shifts of the B—free-exciton states to be observed. The results and analysis provide new, quantitative information about the B valence band.

High-purity, single-crystal platelets of CdS were used in the as-grown condition. "Good" crystals [those showing clear resolution of the $A(2P_0)$ lines at $B=0$ with full width at half maximum (FWHM) linewidths ~ 0.3 meV] had dark-room-temperature resistivities $>10^6$ Ω cm. The free-exciton spectra were taken by observing the increase in light absorption as monitored by the increase in sample conductivity as a function of photon energy. This has previously been shown to be a sensitive method of investigating TPA effects in InSb (Refs. 15 and 16) with cw lasers and in CdS (Ref. 14) with pulsed lasers.

A Q-switched yttrium aluminum garnet laser was used to produce two light beams, one tunable ($1700 < \hbar\omega_v < 1834$ meV) from a dye laser and the other fixed at $\hbar\omega_{ir} = 784$ meV produced by stimulated Raman scattering.[17] The visible and infrared (ir) beams were made to overlap in time and were com-

bined collinearly before being focused onto the sample. The samples were mounted in a Dewar containing pumped liquid He at 1.8 K. The optical Dewar tail was mounted in a 2-in. Bitter magnet solenoid having radial access to the light in a Voigt configuration. The applied current, c axis, and B field were all parallel. Spectral scans were taken via a computer that read the photoinduced voltage from a boxcar integrator with an analog-to-digital converter while scanning the tunable dye laser through a stepping-motor-shaft-encoder combination.

From the group theory of the C_{6v} double group one can determine both the radiation selection rules for the excitonic states of CdS and the nature of the magnetic field splittings of the various levels. A full analysis for the A-exciton problem was summarized by Seiler *et al.*[14] for Γ-point transitions. Specific results pertaining to one-photon absorption of the B *excitons* are given by Mahan and Hopfield[18] and for two-photon absorption (in ZnO) by Dinges *et al.*[19] The symmetries of the B exciton at the Γ point, are obtained from the direct product of the Γ_7 conduction-band symmetry, the Γ_7 (B) valence-band symmetry, and the symmetry of the hydrogenic functions (Γ_1 for S or P_0 functions, Γ_5 for the pair of $P_\pm$ functions).

Radiation selection rules for both one- and two-photon absorption follow from this while recognizing that the radiation-matter interaction has symmetry Γ_1 for the electric field parallel to the crystal c axis ($\vec{E}||c$) and Γ_5 for $\vec{E}\perp c$. Two-photon interactions thus have the symmetries Γ_1, Γ_5 and $(\Gamma_1+\Gamma_2+\Gamma_6)$, respectively, for the configurations $(\|,\|)$, $(\|,\perp)$, and $(\perp,\perp)$. The allowed radiative transitions ($\Gamma_{\text{exciton}}\times\Gamma_{\text{interactions}}$ containing the symmetric irreducible representation) are summarized in Table I, for the zero magnetic field case.

To obtain expressions for the magnetic field splittings of either transitions requires the forms of the exciton eigenfunctions. The presence of splitting can alternatively be deduced from consideration of the symmetry of the field itself, either as a perturbation in the C_{6v} symmetry group, or as the cause of symmetry reduction to C_6. For all but the $2\Gamma_5(P_{\pm1})$ states, the eigenfunctions are easy to find. They are just the symmetry adapted basis functions based upon the Γ_7 conduction, Γ_7 valence, and hydrogenic functions. The valence-band eigenfunctions are discussed by Mahan and Hopfield.[18] Ignoring the $\vec{k}\cdot\vec{p}$ mixing of the bands, and omitting the relatively small spin-orbit mixing of the Z states into the B levels the essential form of the eigenfunctions is given by $(X+iY)\downarrow_h$ and $(X-iY)\uparrow_h$. The conduction states we term $\uparrow_e$ and $\downarrow_e$. Symmetry adapted exciton functions are included in Table I. The Γ_5 pair are degenerate in the absence of an applied magnetic field. The Γ_1,Γ_2 states are, strictly speaking, the antisymmetric and symmetric combinations of the functions shown. When the field splitting is larger than the crystal-field splitting of the excitonic levels, then the eigenfunctions will be those Γ_1,Γ_2 combinations of specific spins (the functions written out). Only the $2\Gamma_5(P_{\pm1})$ states are not uniquely specified by group-theoretical analysis; they are appropriate linear combinations of the four functions shown. We will not consider this case any further since the $(\|,\perp)$ geometry was not used in the present experiment.

For states other than $\Gamma_5(P_{\pm1})$ we obtain the magnitude of the g value by defining the conduction-band spin-splitting, $\uparrow_e-\downarrow_e$, to be $g_e\mu_B B$, the valence splitting,

$$(X+iY)\downarrow_h-(X-iY)\uparrow_h\ ,$$

TABLE I. CdS B-exciton states and their symmetries. The allowed one- and two-photon transitions and their polarizations are shown for $\vec{E}\perp\vec{c}$ and $\vec{E}||\vec{c}$. The corresponding eigenfunctions and g values in the presence of a magnetic field $\vec{B}||\vec{c}$ are also given.

State	Symmetries	Polarization: One-photon	Polarization: Two-photon	Eigenfunctions	g values
S,P_0	Γ_5	$\perp$	$(\|,\perp)$	$(X+iY)\downarrow_h\uparrow_e S,P_0$ $(X-iY)\uparrow_h\downarrow_e S,P_0$	$\lvert g_h^B+g_e\rvert$
	Γ_2		$(\perp,\perp)$	$(X+iY)\downarrow_h\downarrow_e S,P_0$	$\lvert g_h^B+g_e\rvert$
	Γ_1	$\|$	$(\|,\|)$ or $(\perp,\perp)$	$(X-iY)\uparrow_h\uparrow_e S,P_0$	
P_+	Γ_6		$(\perp,\perp)$	$(X+iY)\downarrow_h\uparrow_e P_+$ $(X-iY)\uparrow_h\downarrow_e P_-$	$\lvert 2g_\mu^B+g_h^B+g_e\rvert$
	$2\Gamma_5$	$\perp$	$(\|,\perp)$	$(X+iY)\downarrow_h\downarrow_e P_\pm$ $(X-iY)\uparrow_h\uparrow_e P_\pm$	
	Γ_2		$(\perp,\perp)$	$(X+iY)\downarrow_h\uparrow_e P_-$	$\lvert 2g_\mu^B-g_h^B-g_e\rvert$
	Γ_1	$\|$	$(\|,\|)$ or $(\perp,\perp)$	$(X-iY)\uparrow_h\downarrow_e P_+$	

Table V.B.5

to be given by g_t^B and the hydrogenic orbital splitting, $P_+ - P_-$, by $2g_\mu^B$. The tabulated g values follow from the forms of the eigenfunctions. A further consequence of the field is that the selection rules for the Γ_1, Γ_2 states become mixed; thus, for both states one-photon absorption is allowed for $\vec{E}||c$ and two-photon absorption for either $(||,||)$ or $(\perp,\perp)$ configurations.

RESULTS

B=0

TPA results for the free *B* excitons at zero magnetic field are shown in Fig. 1 in the upper three traces. Also shown for direct comparison is a high-resolution TPA spectra for the *A* excitons. Several conclusions can be drawn from this figure. (1) The quality of these CdS crystals is "good" because there is a clear resolution of the splitting between the

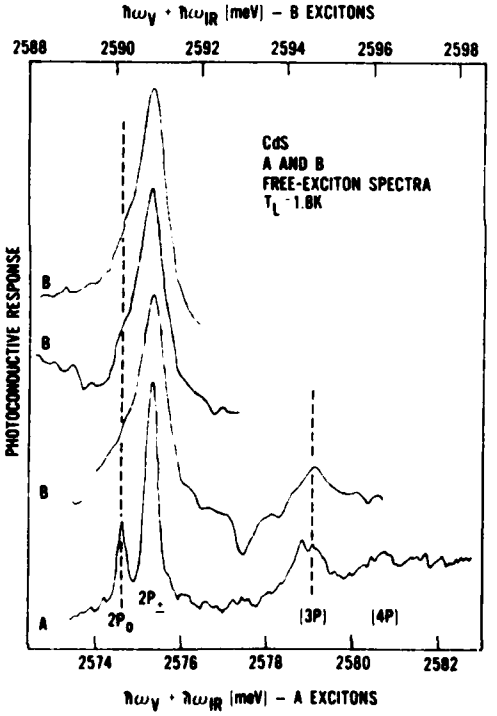

FIG. 1. Two-photon photoconductivity spectra for the *A* and *B* free excitons in CdS at $B=0$ T. The bottom trace *A* shows the high resolution of the *A* excitons with the $A(2P_0)$-$A(2P_{\pm 1})$ anisotropy splitting clearly resolved. The three upper traces show spectra of the *B* excitons which have a much larger linewidth. The presence of a $B(2P_0)$ component is indicated by the asymmetric lineshape in the vicinity of the dashed line near the $2P_0$ state. The instrumental resolution of 0.1 meV is narrower than the intrinsic linewidth of the excitons.

Fig. V.B.8

$A(2P_0)$ and $A(2P_{\pm 1})$ spectral positions. The FWHM linewidth for the $A(2P_{\pm 1})$ state is 0.3 meV. The signal-to-noise ratio is also sufficient to resolve the $n=3$ and $n=4$ *A* excitons at $B=0$ T. A more detailed analysis of these $A(2P)$ and $A(3P)$ excitons was presented earlier by Seiler *et al.*[14] Clearly, the *B* excitons have a much larger FWHM linewidth (values from $\sim 0.7 \rightarrow 1.1$ meV have been observed in "good" crystals, with an average over five spectral runs equal to ~ 0.9 meV). The *B*-exciton lines are broader because their lifetimes are shorter than those of the *A* excitons. (2) Since the *B* excitons have larger linewidths, it has been difficult to observe the anisotropy splitting between the $B(2P_0)$ and $B(2P_{\pm 1})$ states. However, we show in Fig. 1 three spectral scans of the $B(2P)$ region that consistently show strong evidence for the presence of the $B(2P_0)$ component as indicated by the asymmetry in the line shape. Although the $B(2P_0)$ state is not clearly resolved, we estimate that its position is at 2590.2 ± 0.2 meV. In spectra where a good baseline could be established, subtracting off a large symmetric $B(2P_{\pm 1})$ peak, resulted in a peak at this position. This is *the first* observation of this state. The anisotropy splitting of the $B(2P)$ state is thus estimated to be

$$B(2P_{\pm 1}) - B(2P_0) = 0.6 \pm 0.2 \text{ meV} ,$$

compared to that of the $A(2P)$,

$$A(2P_{\pm 1}) - A(2P_0) = 0.69 \pm 0.02 \text{ meV} .$$

(3) The energy separations between the $3P_{\pm 1}$ and $2P_{\pm 1}$ states are also the same within the uncertainties. For the *A* exciton, this splitting is 3.97 ± 0.11 meV and for the *B* exciton 3.8 ± 0.2 meV. This also represents the *first time* that the $B(3P)$-exciton state has been observed. See also Fig. 2 at $B=0$ for a clear resolution of the $B(3P)$-exciton state.

Several important conclusions can now be made from these observations. Points (2) and (3) give strong support that the effective Rydberg R_y^* $(=\mu_\perp e^4/2\hbar^2 K^2)$ and the anisotropy parameter γ $(=\mu_\perp K_\perp/\mu_{||}K_{||})$ of the *B* excitons are equal to those of the *A* excitons. Thus

$$R_y^{*B} = R_y^{*A} = 27.4 \pm 0.8 \text{ meV}$$

and

$$\gamma^B = \gamma^A = 0.797 \pm 0.013$$

(see Ref. 14 for the *A*-exciton values). Assuming $K_\perp$ and $K_{||}$ are the same for both the *A*- and *B*-exciton regions implies that

(i) $\mu_\perp^B = \mu_\perp^A = (0.158 \pm 0.002) m_0$

and

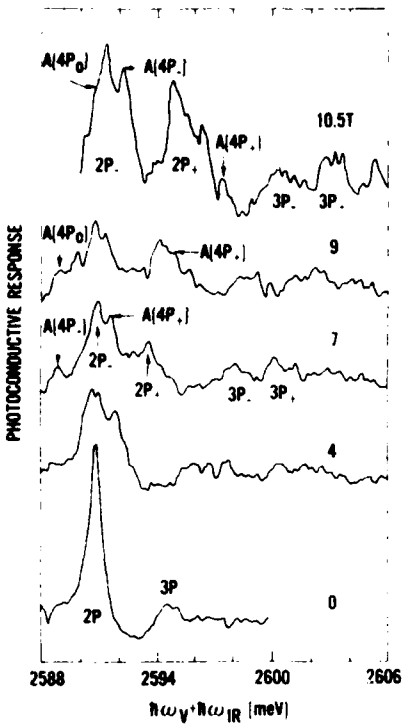

FIG. 2. Photoconductive response vs total photon energy $\hbar\omega_v + \hbar\omega_{ir}$ near the B-exciton region for various magnetic fields. The magnetic field $\vec{B}$ was parallel to the hexagonal c axis in a Voigt configuration with $\vec{E}$ perpendicular to c for the two photons at a lattice temperature of $T_L = 1.8$ K. The presence of the overlapping $A(4P)$ excitons is indicated.

Fig. V.B.9

$$m^B_{h\perp} = m^A_{h\perp} = (0.64 \pm 0.02) m_0$$

[using $m_e = (0.210 \pm 0.003)\ m_0$] and (ii) $\mu^B_{\parallel} = \mu^A_{\parallel}$ or $m^B_{h\parallel} = m^A_{h\parallel}$.

Table II shows the results of previously measured values of the excited B-exciton states and the results of this study. Our position for the $B(2P_{+1})$ state is in excellent agreement with the TPA studies of Stafford and Sondergeld[9] and Jackel and Mahr.[13] Taking into account the anisotropy by using Faulkner's analysis as was done for the A exciton[14] determines the B energy gap to be

$$E_g^B = 2598.0 \pm 0.2 \text{ meV} .$$

Hopfield and Thomas[2] determined the position of a $B(n=2)$ state to be 2590.8 eV, which is in excellent agreement with our $B(2P_{+1})$ level [presumably their state was a $B(2S)$ level because they used one-photon spectroscopy].

B≠0

The application of a magnetic field allows shifts and Zeeman splittings of individual exciton states to be measured. In fact, magneto-optical studies allow determination of exciton parameters and the corresponding energy-band parameters of the semiconductor. Figure 2 shows the effect of the magnetic field on the B–free-exciton spectra. At $B=0$ T both the $B(2P)$ and the $B(3P)$ are clearly seen. A study of Fig. 2 shows one major feature: the $B(2P)$ state splits into two parts, presumably $2P_{+1}$ and $2P_{-1}$ states. At fields >7 T, there also appears to be a fine structure splitting to these $2P_{\pm 1}$ states. We shall return to this feature later. At fields >6 T, the $B(2P)$ spectral region becomes very complex due to the overlapping of the $A(4P_0, 4P_{\pm 1})$-exciton states. The energy positions of these photoconductive peaks are plotted in Fig. 3 as a function of magnetic field. This shows the complex nature of the exciton structure and can be used to identify the spectral features shown in Fig. 2. We also point out that this is *the first time* the magnetic field dependence of the $A(4P)$ excitons has been determined. The $B(2P_0)$ state could not be identified in any of the spectral features present at finite magnetic fields.

According to Table I for $(1,1)$ polarization two exciton states of symmetry $\Gamma_1 + \Gamma_2$ and Γ_6 can be observed with effective g factors of $|2g^B_\mu - g_e - g^B_h|$

TABLE II. Measured values of excited B-exciton states (in meV).

Energy level	One-photon emission [Litton *et al.* (Ref. 4)]	Two-photon absorption: Nguyen *et al.* (Ref. 10)	Two-photon absorption: Stafford and Sondergeld (Ref. 9)	Two-photon absorption: Jackel and Mahr (Ref. 13)	Present work
$2S$	2585.2				
$2P_0$					2590.26±0.2
$2P_{\pm 1}$		2593.5	2590.5	2590.8	2590.86±0.05
$3S$	2589.2				
$3P_0$					
$3P_{\pm 1}$					2594.6±0.1
$4S$	2590.7				

Table V.B.6

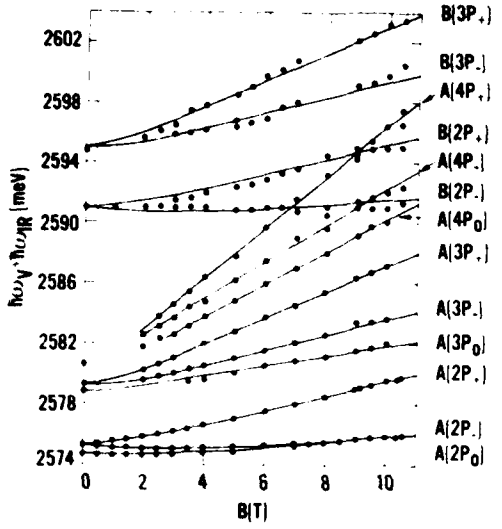

FIG. 3. Peak positions in total photon energy $\hbar\omega_v + \hbar\omega_{ir}$, for the $A(2P)$, $A(3P)$, $A(4P)$, $B(2P)$, and $B(3P)$ excitons as a function of applied magnetic field B. The solid points were determined experimentally while the lines for the $A(2P)$ and $A(3P)$ represent the variational calculations done in Ref. 14. Straight lines are drawn through the $A(4P)$ levels. The lines drawn through the $B(2P_\pm)$ and $B(3P_\pm)$ points are the same as the theoretical variations of the $A(2P_\pm)$ and $A(3P_\pm)$ levels.

Fig. V.B.10

and $|2g_\mu^B + g_e + g_h^B|$, respectively. The Zeeman splittings are given by $\Delta E = g_{\rm eff}\mu_B B$, where μ_B is the Bohr magneton. Thus the average splitting of these two symmetry states is given by

$$|2g_\mu^B| = 6.4 \pm 0.4$$

from our data. Using the definition of

$$g_\mu^B = m_0(1/m_{h\perp}^B - 1/m_{e\perp})$$

and

$$m_{e\perp} = 0.210 \pm 0.003 m_0$$

gives $m_{h\perp}^B = 0.64 \pm 0.17 m_0$. This mass value is the same as that of the A band which agrees with the conclusions of the zero magnetic field results discussed earlier.

The fine-structure splitting of the $B(2P_\pm)$ states can be used to determine g_h^B from $g_{\rm eff} = |g_e + g_h^B|$. For fields ≥ 7 T, the fine-structure splitting of these states does appear to be evident in Fig. 4, indicated by the down-pointing arrows. From the experimental splitting, $g_{\rm eff} = 1.1 \pm 0.3$, which along with $g_e = -1.78$ gives $g_h^B = 0.7 \pm 0.3$. Also shown by dashed arrows are the $A(4P_0, 4P_\pm)$ exciton states. At 9 T the region around the $B(2P_\pm)$ is rather complex making identification of the spectral features

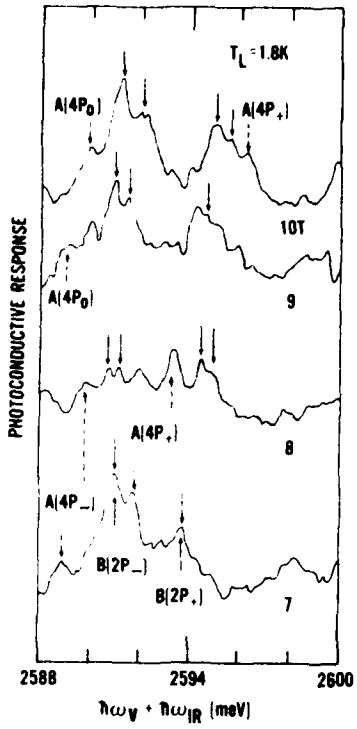

FIG. 4. High-resolution photoconductive spectral scans in the region of the $B(2P)$ exciton at various magnetic fields. The dashed lines show the overlapping $A(4P)$ excitons, while the solid arrows pointing down indicate the fine-structure splitting.

Fig. V.B.11

difficult. We point out that these spectral features are *reproducible from run to run.*

The high resolution obtainable by the two-photon spectroscopy technique is illustrated in Fig. 5, where a spectral scan over both the A- and B-exciton regions at $B = 10$ T reveals a wealth of structure. Principal features that can be clearly identified are shown. Additional structure is present which has not been identified as yet. Again we point out that the photoconductive spectral features are reproducible, so that each peak no matter how small is physically meaningful. The dominant spectral features arise from the excitons and not just transitions between Landau levels. This conclusion is in contrast to an earlier conclusion by Shah and Damen[3] that excitonic effects are apparently not important for $N \geq 2$, where N is the Landau-level number.

The lines plotted in Fig. 3 for the $A(2P)$ and $A(3P)$ excitons represent the theoretical dependence obtained from variational calculations as explained in Ref. 14. Straight lines are drawn through the data points representing the $A(4P)$ states; no attempt was made to calculate their dependence on

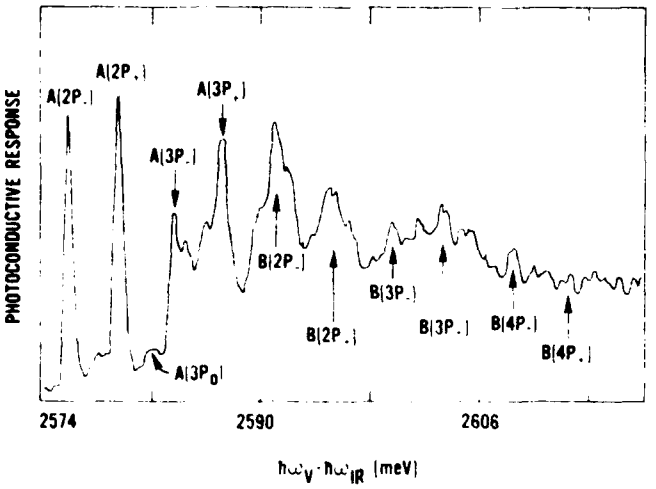

FIG. 5. High-resolution two-photon spectra for $B = 10$ T, showing the complexity of the A- and B-exciton struture.

Fig. V.B.12

field because of the difficulty of carrying out variational calculations for the higher excited states. The lines shown for the $B(2P)$ and $B(3P)$ states are the shifted replicas of the theoretical variation of the $A(2P_{\pm 1})$ and $A(3P_{\pm 1})$ states with magnetic field. Consequently, the good correspondence shown in Fig. 3 reflects the fact that the parameters of the B exciton are very similar to those of the A exciton.

SUMMARY AND CONCLUSIONS

The results of our two-photon spectroscopy measurements and analysis are shown in Table III along with the few values determined by other experiments and the theoretical results of Mahan and Hopfield.[18] Our results for γ, $m_{h\perp}^B$, and g_h^B differ most significantly from the values estimated previously as shown in Table III. We believe that our measurements represent the most direct and hence most accurate means of determining these values at present.

In summary, we have for the *first time* (1) shown evidence for the anisotropy of the B valence band by giving evidence for the presence of the $B(2P_0)$ exciton at $B=0$ T, (2) observed the $B(3P)$ exciton at $B=0$ T, (3) determined the magnetic field dependence of the $A(4P_0,4P_{\pm 1})$ excitons, (4) observed Zeeman splitting of the $B(2P_{\pm 1})$- and $B(3P_{\pm 1})$-exciton levels, and finally (5) given evidence for the fine-structure splitting of the $B(2P_{+1})$- and $B(2P_{-1})$-exciton states. Consequently, we can conclude that two-photon spectroscopy is a valuable technique of investigating semiconductor energy-band structures.

ACKNOWLEDGMENTS

We thank D. Reynolds and C. Litton for supplying the excellent quality CdS crystals and D. Spears

TABLE III. CdS B-exciton and B-band parameters.

Reference	R_y^* (meV)	γ	$\mu_\perp$ (m_0)	$m_{h\perp}^B$ (m_0)	E_g^B (eV)	g_h^B
This paper	27.4	0.797	0.158	0.64±0.17	2598.0±0.2	0.7±0.3
Blattner *et al.* (Ref. 7)				1.1		1.8
Koteles and Winterling (Ref. 20)				1.0±0.1		
Broser and Rosenzweig (Ref. 21)				1.1		
Mahan and Hopfield (Ref. 18)		$\sim 10^{-2}$	0.17	1.0 - 1.2		
Segall and Marple (spherical-band approximation) (Ref. 22)			0.156		2598.1	

Table V.B.7

IV - 52

of Lincoln Laboratory for his help in making electrical contacts on the samples. The work of one of us (D. G. S.) was supported in part by the U. S. Office of Naval Research and experimentally carried out at the Francis Bitter National Magnet Laboratory, which is supported by the National Science Foundation.

[1]D. G. Thomas and J. J. Hopfield, Phys. Rev. 116, 573 (1959).
[2]J. J. Hopfield and D. G. Thomas, Phys. Rev. 122, 35 (1961).
[3]J. Shah and T. C. Damen, Solid State Commun. 9, 1285 (1971).
[4]C. W. Litton, D. C. Reynolds, and T. C. Collins, Phys. Rev. B 6, 2269 (1972).
[5]H. Venghaus, S. Suga, and K. Cho, Phys. Rev. B 16, 4419 (1977).
[6]I. Broser and M. Rosenzweig, Phys. Rev. B 22, 2000 (1980).
[7]C. Blattner, G. Kurtze, G. Schmeider, and C. Klingshirn, Phys. Rev. B 25, 7413 (1982).
[8]F. Pradere and A. Mysyrowicz, in *Proceedings of the Tenth International Conference on the Physics of Semiconductors*, edited by S. P. Keller, J. C. Hensel, and F. Stern (U. S. Atomic Energy Commission, Washington, D.C., 1970), p. 101.
[9]R. G. Stafford and M. Sondergeld, Phys. Rev. B 10, 3471 (1974).
[10]V. T. Nguyen, T. C. Damen, and E. Gornik, Appl. Phys. Lett. 30, 33 (1977).
[11]T. C. Damen, V. T. Nguyen, and E. Gornik, Solid State Commun. 24, 179 (1977).
[12]V. T. Nguyen, T. C. Damen, E. Gornik, and C. K. N. Patel, Appl. Phys. Lett. 31, 603 (1977).
[13]J. Jackel and H. Mahr, Phys. Rev. B 17, 3387 (1978).
[14]D. G. Seiler, D. Heiman, R. Feigenblatt, R. L. Aggarwal, and B. Lax, Phys. Rev. B 25, 7666 (1982).
[15]D. G. Seiler, M. W. Goodwin, and M. H. Weiler, Phys. Rev. B 23, 6806 (1981).
[16]M. W. Goodwin, D. G. Seiler, and M. H. Weiler, Phys. Rev. B 25, 6300 (1982).
[17]R. L. Byer, Electro-Opt. Syst. Des. 12, 24 (1980).
[18]G. D. Mahan and J. J. Hopfield, Phys. Rev. 135, A428 (1964).
[19]R. Dinges, D. Frohlich, B. Staginnus, and W. Staude, Phys. Rev. Lett. 25, 922 (1970).
[20]E. S. Koteles and G. Winterling, Phys. Rev. Lett. 44, 948 (1980).
[21]I. Broser and M. Rosenzweig, Phys. Status Solidi B 95, 141 (1979).
[22]B. Segall and D. T. F. Marple, in *Physics and Chemistry of II-VI Compounds*, edited by M. Aven and J. J. Prener (North-Holland, Amsterdam, 1967), Chap. 7, p. 344.

XIIth International Quantum Electronics Conference,
1982, Munich, West Germany, June 22-25, 1982

Two-Photon Spectroscopy of the A-and B-Excited Free-Exciton States in CdS

D. G. Seiler, (817-788-2626), Center for Applied Quantum Electronics,
North Texas State University, Denton, Texas 76203 and D. Heiman,
R. Feigenblatt, R. L. Aggarwal, and B. Lax (617-253-1753),
M.I.T. Francis Bitter National Magnet Laboratory,
Cambridge, Massachusetts 02139

High resolution two-photon photoconductive spectra of CdS obtained using a tunable dye laser and Raman cell exhibit a wealth of structure from excited-exciton states. Zeeman splittings and diamagnetic shifts are observed and analyzed.

XIIth International Quantum Electronics Conference,
1982, Munich, West Germany, June 22-25, 1982

Two-Photon Spectroscopy of the A-and B-Excited Free-Exciton States in CdS

D. G. Seiler*, Center for Applied Quantum Electronics,
North Texas State University, Denton, Texas 76203
and D. Heiman, R. Feigenblatt, R. L. Aggarwal, and B. Lax,
M.I.T. Francis Bitter National Magnet Laboratory,†
Cambridge, Massachusetts 02139

High resolution two-photon absorption (TPA) spectra are obtained for the free A-and B- exciton excited states in CdS using photoconductivity techniques. To our knowledge this is the first time that the potoconductivity technique has been used to obtain the TPA spectra of free excitons in semiconductors. At zero magnetic field, anisotropy splittings of the exciton states are observed and analyzed. Application of magnetic fields up to 10 T result in linear Zeeman splittings and diamagnetic shifts of the exciton states.

The single crystal samples of CdS were high purity platelets grown from the vapor phase and had thicknesses of $\approx 10^{-3}$ cm.[1] Good crystals showed clear resolution of the $A(2P_0)$ line from the $A(2P_{\pm 1})$ line at B = 0 T with FWHM linewidths ≈ 0.3 meV. The two-photon spectra of the exciton states were taken by observing the increase in conductivity from the light absorption as a function of photon energy. This method has been used recently by Seiler et al.[2] in studying two-photon effects in InSb using only cw CO_2 lasers. Here a Q-switched YAG laser was used to produce the two light beams; one tunable at ≈ 1.8 eV from a dye laser and the other fixed at 0.784 eV produced by stimulated Raman scattering. The two photons are simultaneously absorbed when their sum is made equal to the exciton level. Since both photon energies are below the gap the absorption occurs throughout the bulk of the sample which places less importance on the sample surface. The spectra resolution is determined by the linewidth of the laser which is less than 0.05 meV. Spectral scans were taken via a computer that read a boxcar integrator output with an analog-to-digital converter while scanning the tunable dye laser through a stepping motor/shaft encoder combination. At zero magnetic field, the A(2P), (3P), and (4P) and B(2P) and (3P) free exciton states can be seen. The anisotropy splitting of the A(2P) and (3P) states is observed and interpreted with an anisotropic effective mass Hamiltonian which is solved with variational

calculations originally developed by Larsen.[3] At B = 0 the narrow laser linewidths (0.05 meV) allow an accurate determination of the A-exciton binding energy of 27.4 ± 0.8 meV and the anisotropy parameter of 0.797 ± 0.013 from which the energy gap E_g^A = 2582.5 ± 0.2 meV at T = 1.8 K is calculated.

The energies of the A(2P) and (3P) states are measured as a function of magnetic field up to B = 10 T. The magnetic field dependences are analyzed in terms of linear Zeeman splitting and diamagnetic interactions. Fine structure splitting of the $A(2P_+)$ states is observed and identified as arising from the $\Gamma_1 + \Gamma_2$ and Γ_6 symmetry states with slightly different g factors. At B = 10 T, the observed splitting of = 0.29 meV gives $|g_{e\parallel} - g_{h\parallel}| = 0.50 \pm 0.15$. The average g-values of these two lines is given by $|2g_{\mu\parallel}| = |2\,(1/m_h^{\perp} - 1/m_e^{\perp})|$ = 0.39 ± 0.08. At low fields the diamagnetic contribution gives the usual quadratic field dependence but deviates significantly at higher fields. At a given field, the deviation is found to increase dramatically with increasing quantum number n. At these high magnetic fields, the Lorentz force on the exciton becomes comparable to the Coulomb forces. As a result, the wave functions contract to such an extent that deviations from quadratic diamagnetic behavior occur. The magnetic field causes mixing of the B = 0 wavefunctions through the ordinary diamagnetic perturbation. This deviation is fit by variational calculations developed by Larsen which take into account the interaction of states through the diamagnetic term in the Hamiltonian. The magnetic field dependence of these states allows us to determine the reduced exciton mass $\mu_{\perp} = (0.158 \pm 0.002)m_0$ and the individual masses as $m_e^{\perp} = (0.210 \pm 0.003)m_0$ and $m_h^{\perp} = (0.64 \pm 0.2)m_0$. Finally the temperature dependence of the A-gap is determined from the energy of the $2P_{\pm 1}$ level at B = 0 as a function of temperature.

*Visiting scientist at the Francis Bitter National Magnet Laboratory. Work supported in part by NTSC and the Office of Naval Research.

†Supported by the National Science Foundation.

1. We thank D. Reynolds and C. Litton for the crystals of CdS
2. D. G. Seiler, M. W. Goodwin, M. H. Weiler, Phys. Rev. B 23, 6806 (1981).
3. We thank D. M. Larsen for his help with the variational calculations.

C. Gallium Arsenide

This part of the nonlinear project was experimentally carried out at the Francis Bitter National Magnet Laboratory in collaboration with Dr. Don Heiman. Analysis of the data subsequently has taken place at NTSU. In this section we summarize our findings. A paper on this work has been submitted for consideration to the XIIIth International Quantum Electronics Conference, 1984, Anaheim, California, June 18-21. We reproduce a copy of the short abstract and the extended summary that was submitted at the end of this section.

Magneto-absorption experiments are a useful way to measure the effective mass band parameters of semiconductors.[10] In direct-gap materials the absorption is usually large necessitating very thin samples, the order of microns. An alternative method is to use modulated reflectivity.[11] This works well when the modulation configuration does not perturb the sample appreciably. Magneto-absorption experiments by Vrehen[12] were used to determine the mass parameters of a 4 μ thick sample of bulk-grown GaAs. Reine[13] attempted to determine the masses in high-purity epitaxial GaAs by stress-modulated magneto-reflectivity but found that dc strain prohibited a meaningful analysis. In the present study it is shown that high-resolution magneto-absorption spectra of high-purity epitaxial GaAs can be obtained using the two-photon absorption technique. This experiment is the first two-photon absorption spectroscopy of GaAs in a magnetic field.

The GaAs sample was a high-purity epitaxial layer (77°K mobility of 10^5 cm^2/V-sec) with surface perpendicular to [100]. Leads were attached by soldering with indium. The sample was immersed in pumped liquid He at the end of a dewar tail which was inserted in a radial access Bitter solenoid magnet. The laser light was focused on the sample surface using a 30 cm focal length lens in the Voigt configuration.

Absorption spectra were taken by monitoring the change in conductivity

(resistivity) induced by a near-IR light beam. The light was produced by the second-Stokes, Raman-shifted output of hydrogen gas which was pumped by the output of a tunable dye laser with LD688 dye. The dye laser was, in turn, pumped by the second harmonic of a doubled-YAG laser producing 10 pulses per second of 10 nsec duration. The light intensity at the sample was $\gtrsim 10^7$ W/cm^2. A small current was supplied to the sample parallel to B by an applied voltage of a few tenths of a volt. (Above one volt, impact ionization occurs.) The output voltage signal was amplified by $\gtrsim 10^2$ before being fed into a boxcar integrator. The best signal-to-noise ratio was obtained by pre-smoothing with a three-laser-shot time constant on the boxcar, then averaging ten shots with a computer, and finally adding five repeated spectral scans. The last feature was needed to average out long term fluctuations of the laser intensity.

The two-photon magneto-absorption spectrum, above the bandgap, in GaAs is shown in Figure 1 for B = 10.0 T. The direct gap at this temperature is at E_g = 1.519 eV in zero magnetic field. The structure is seen to be quite sharp with large peak-to-background ratios at low energies. This spectrum was taken with light polarization $\vec{E} \perp \vec{B}$, but the spectral features were found to be nearly independent of polarization. Higher resolution scans clearly resolve the peaks at 1.529 and 1.547 eV and show the feature at 1.542 to be a doublet.

Positions of the various absorption peaks are plotted in Figure 2 as a function of magnetic field. Fifteen distinct Landau transitions show an approximate linear behavior which extrapolates to the bandgap at B = 0.

Analysis of this data is a complicated problem; Coulomb binding of the electrons and holes (exciton effects) must be taken into account, as well as the nonparabolicity of the conduction band and the complex nature of the degenerate valence bands. Work is in progress to evaluate the effective mass parameters using these corrections. The high resolution of the present experiment combined

with the high-purity sample will allow a more accurate determination of these parameters than previous studies.

M. N. Afsar and D. M. Larsen are gratefully acknowledged for supplying the excellent quality sample.

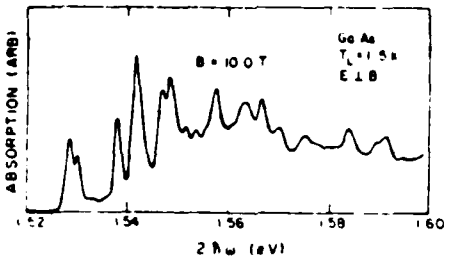

Fig. V.C.1

Figure 1. Photoconductive signal (absorption) versus twice the laser photon energy $2\hbar\omega$ near the fundamental gap in epitaxial GaAs in a magnetic field. The light was polarized perpendicular to B and the lattice temperature was T_L = 1.5 K. The spectrum is uncorrected for intrument response.

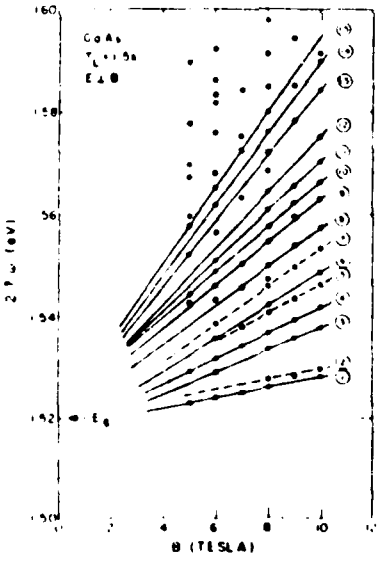

Fig. V.C. 2

Figure 2. Absorption peak energies versus B in epitaxial GaAs at T = 1.5K. Linear Landau level behavior is seen by the straight lines connecting the experimental points which intersect B = 0 near the energy gap.

XIIIth International Quantum Electronics Conference,
1984, Anaheim, California, June 18-21, 1984

Two-Photon Spectroscopy of GaAs*

D. G. Seiler (817-565-3262, P.O. Box 5368) and C. L. Littler,
Center for Applied Quantum Electronics, North Texas State
University, Denton, Texas 76203 and D. Heiman, M.I.T.
Francis Bitter National Magnet Laboratory,†
Cambridge, Massachusetts 02139

Two-photon absorption spectra of high purity GaAs, obtained at 1.8 K using a tunable dye laser and a Raman cell, show resonant structure in high magnetic fields related to exciton and Landau level behavior.

*Work performed at the Francis Bitter National Magnet Laboratory and supported by the National Science Foundation, Office of Naval Research, and North Texas State University.

†Supported by the National Science Foundation.

XIIIth International Quantum Electronics Conference,
1984, Anaheim, California, June 18-21, 1984

Two-Photon Spectroscopy of GaAs*

D. G. Seiler (817-565-3262, P.O. Box 5368) and C. L. Littler,
Center for Applied Quantum Electronics, North Texas State
University, Denton, Texas 76203 and D. Heiman, M.I.T.
Francis Bitter National Magnet Laboratory,†
Cambridge, Massachusetts 02139

Nonlinear spectroscopy is an interesting and increasingly useful method in the study and characterization of semiconductors.[1,2] As a result it has now become an active and rapidly growing field of spectroscopy. In this paper we present high resolution two-photon absorption (TPA) spectra obtained at 1.8 K for high purity epitaxial GaAs using photoconductivity (PC) techniques. The TPA spectra was studied from energies below to well above the free exciton and band gap region. At zero magnetic field, the PC response has a $(2\hbar\omega - E_g)^{3/2}$ dependence just above the band gap. Application of magnetic fields up to 10 T produced resonances in the PC response which are quantitatively interpreted in terms of exciton and Landau level behavior. To our knowledge these are the first two-photon absorption spectra for GaAs in a magnetic field.

The single crystal samples of n-GaAs were high purity (77 K mobility of 10^5 cm^2/V-sec) epitaxial layers of ≈ 50 μm thickness with (112) surface orientations. The sample was immersed in pumped liquid He at 1.8 K in a dewar tail which was inserted in a radial access Bitter solenoid magnet. The Voigt configuration was used with the field along the [110] crystallographic direction and the photoconductive signals were analyzed by a boxcar integrator and computer. The TPA spectra were obtained by monitoring the change in resistance (or conductivity) of the sample induced by tunable 1.6 μm

radiation from a hydrogen Raman shifting cell. The cell was pumped by the output of a tunable dye laser with a 5 nsec pulse length. The two-photon magneto-absorption spectra exhibited well defined structure for fields above 5 T and were investigated for incident light polarizations with $\vec{e} \perp \vec{B}$ and $\vec{e} \parallel \vec{B}$.

Theoretical transition energies were calculated using a modified Pidgeon-Brown 8 x 8 energy band model and two-photon selection rules. Comparison of these calculations to the data gives good agreement, and indicates that the final states of the TPA transitions are "P excitons" rather than "S excitons" as in the one-photon absorption (OPA) case. The energy band parameters that describe our TPA spectra are E_g = 1.519 eV, E_p = 22.7 eV, γ_1 = 1.87, γ_2 = -0.39, γ_3 = 0.4, κ = -1.29, F = 0, q = 0.04, and N_1 =0.0. The influence of exciton contributions to the TPA spectra will also be discussed. Finally, we will compare our TPA results to the OPA experiments of Ulbrich and Fehrenbach[3] at B=0, and of Vrehen[4] and Reine[5] at B≠0.

*David G. Seiler was a visiting scientist at the Francis Bitter National Magnet Laboratory. Work supported in part by NTSU and the Office of Naval Research. M. N. Afsar and D. M. Larsen are gratefully acknowledged for supplying the samples.

+Supported by the National Science Foundation.

1. M. D. Levenson, Introduction to Nonlinear Laser Spectroscopy (Academic Press, New York, 1982).

2. D. S. Chemla and J. Jerphagnon in Handbook on Semiconductors (North-Holland Publishing Co., New York, 1980), edited by M. Balkanski, Vol. 2, p. 545.

3. R. G. Ulbrich and G. W. Fehrenbach, Phys. Rev. Lett. 43, 963 (1979).

4. Q. H. F. Vrehen, J. Phys. Chem. Solids 29, 129 (1968).

5. M. B. Reine, Ph.D. Thesis, Massachusetts Institute of Technology, 1970.

VI. REFERENCES

1. J. M. Worlock, in Laser Handbook, edited by F. T. Arecchi and E. O. Schulz - Dubois (North Holland Publishing Co., Amsterdam, 1972), pp. 1323-1369.

2. V. I. Bredikhin, M. D. Galanuim, and V. N. Genkin, Sov. Phys. - Usp. 16, (1974), pp. 299-321.

3. H. Mahr, in Quantum Electronics, edited by H. Rabin and C. L. Tang (Academic Press, New York, 1975), Vol. 1, pp. 285-360.

4. D. G. Seiler, M. W. Goodwin, and M. H. Weiler, Phys. Rev. B 23, 6806 (1981).

5. Laser Focus 17, 14 (April, 1981).

6. M. W. Goodwin, D. G. Seiler, and M. H. Weiler, Phys. Rev. B 25, 6300 (1982).

7. D. G. Seiler, D. Heiman, R. Feigenblatt, R. L. Aggarwal, and B. Lax, Phys. Rev. B 25, 7666 (1982).

8. D. G. Seiler, D. Heiman, R. Feigenblatt, R. L. Aggarwal, and B. Lax, Applied Physics B 28, 147 (1982).

9. D. G. Seiler, D. Heiman, and B. Wherrett, Phys. Rev. B 27, 2355 (1983).

10. B. Lax and S. Zwerdling, Progr. in Semicond. 15, 221 (1960).

11. R. L. Aggarwal, in Semiconductors and Semimetals (Academic Press, New York), 1972), Vol. 9, 151.

12. Q. H. F. Vrehen, J. Phys. Chem. Solids 29, 129 (1968).

13. M. B. Reine, Ph.D. Thesis, Massachusetts Institute of Technology, 1970.

APPENDIX: PROFESSIONAL ACCOMPLISHMENTS

1. Papers Published

1. "High Resolution Magneto-Optical Studies of p-InSb", C. L. Littler, D. G. Seiler, R. Kaplan, R. J. Wagner, and W. Zawadzki, Solid State Commun. 37, 783 (1981).

2. "High Resolution Two-Photon Spectroscopy in InSb at Milliwatt cw Powers in a Magnetic Field", D. G. Seiler, M. W. Goodwin, and M. H. Weiler, Phys. Rev. B 23, 6806 (1981).

3. "High Resolution Magneto-Optical Studies of Free and Bound Hole Excitations in InSb", R. Kaplan, R. J. Wagner, D. G. Seiler, C. L. Littler, M. H. Weiler, and W. Zawadzki, in Physics of Narrow Gap Semiconductors, Proceedings, Linz, Austria, 1982 (Springer-Verlag, New York, 1982), edited by E. Gornik, H. Heinrich, and L. Palmetshafer, p. 188.

4. "Two-Photon Spectroscopy in InSb with cw CO_2 Lasers", D. G. Seiler, M. W. Goodwin, and M. H. Weiler, in Physics of Narrow Gap Semiconductors, Proceedings, Linz, Austria, 1981 (Springer-Verlag, New York, 1982), edited by E. Gornik, H. Heinrich, and L. Palmetshafer, p. 192.

5. "Two-Photon Magnetoabsorption Spectroscopy in n-InSb with cw CO_2 Lasers", M. W. Goodwin, D. G. Seiler, and M. H. Weiler, Phys. Rev. B 25, 6300 (1982).

6. "Two-Photon Magnetospectroscopy of A-exciton states in CdS", D. G. Seiler, D. Heiman, R. Feigenblatt, R. L. Aggarwal, and B. Lax, Phys. Rev. B 25, 7666 (1982).

7. "Two-Photon Spectroscopy of the A- and B-Excited Free-Exciton States in CdS", D. G. Seiler, D. Heiman, R. Feigenblatt, R. L. Aggarwal, and B. Lax, Applied Physics B 28, 147 (1982).

8. "Magneto-optical Detection of Deep Acceptor Impurities in p-InSb", C. L. Littler, D. G. Seiler, R. Kaplan, and R. J. Wagner, Appl. Phys. Lett. 41, 880 (1982).

9. "Laser-Induced Magneto-optical Transitions from Deep Levels in n-InSb", D. G. Seiler and M. W. Goodwin, J. Appl. Phys. 53, 7505 (1982).

10. "Two-Photon Spectrosccopy in InSb at High Magnetic Fields", D. G. Seiler, M. W. Goodwin, S. W. McClure, and L. A. Veilleux, in Application of High Magnetic Fields in Semiconductor Physics, Proceedings, Grenoble, France 1982 (Springer-Verlag, New York, 1983), G. Landwehr, editor, p. 297.

11. "Laser-Induced Magneto-Optical Transitions from Deep Levels in n-InSb", D. G. Seiler, M. W. Goodwin, and K. H. Littler, in Proceedings of the 16th Int. Conf. on the Physics of Semiconductors, Montpellier, France, 1982, (North-Holland, Amsterdam, 1983), M. Averous, editor, p. 167.

12. "Laser Induced Magneto-Optical Transitions from Deep Levels in n-InSb", D. G. Seiler, M. W. Goodwin, and K. H. Littler, Physica 117B, 167 (1983).

13. "Two-Photon Spectroscopy of B Excitons in CdS", D. G. Seiler, D. Heiman, and B. Wherrett, Phys. Rev. B 27, 2355 (1983).

14. "Intra-Conduction Band Magneto-Optical Studies of InSb", M. W. Goodwin and D. G. Seiler, Phys. Rev. B 27, 3451 (1983).

15. "High Resolution Magneto-Optical Studies of Free and Bound Holes in p-InSb", C. L. Littler, D. G. Seiler, R. Kaplan, and R. J. Wagner, Phys. Rev. B 27, 7473 (1983).

16. "Anisotropic Two-Photon Magneto-Absorption in n-InSb", D. G. Seiler and S. W. McClure, Solid State Commun. 47, 17 (1983).

2. Contributed Talks
a. National Meetings

1. M. H. Weiler, D. G. Seiler, and M. W. Goodwin, "High Resolution Two-Photon Magneto-Spectroscopy in InSb", Bull. Am. Phys. Soc. 26, 354 (1981).

2. D. Heiman, D. G. Seiler, R. Feigenblatt, R. L. Aggarwal, and B. Lax, "Two-Photon Magneto-Spectroscopy of Excitons in CdS", Bull. Am. Phys. Soc. 26, 795 (1981).

3. D. Heiman, D. G. Seiler, R. Feigenblatt, R. L. Aggarwal, and B. Lax, "Magnetic Field Dependence of Free Excitons in CdS by Two-Photon Absorption Spectroscopy", Bull. Am. Phys. Soc. 27, 144 (1982).

4. C. L. Littler, D. G. Seiler, R. Kaplan, and R. J. Wagner, "High Resolution Magneto-Optical Studies of Bound and Free Hole Excitations in p-InSb", Bull. Am. Phys. Soc. 27, 144 (1982).

5. M. W. Goodwin and D. G. Seiler, "Two-Photon Magneto-Absorption in n-InSb", Bull. Am. Phys. Soc. 27, 145 (1982).

6. S. W. McClure and D. G. Seiler, "Anisotropic Two-Photon Magneto-Absorption Effects in n-InSb", Optics New 8, 57 (1982).

7. C. L. Littler, D. G. Seiler, R. Kaplan, and R. J. Wagner, "Magneto-optical Detection of Deep Acceptor Impurities in p-InSb", Optics News 8, 39 (1982).

8. C. L. Littler, D. G. Seiler, and S. W. McClure, "Two-Photon Induced Photo-Hall Effect in n-InSb", Bull. Am. Phys. Soc. 28, 338 (1983).

9. S. W. McClure, D. G. Seiler, and C. L. Littler, "CO_2 Laser-Induced Photoexcited Carrier Lifetimes in n-InSb", Bull. Am. Phys. Soc. 28, 338 (1983).

b. International Meetings

1. D. G. Seiler, M. W. Goodwin, and M. H. Weiler, "High Resolution Two-Photon Magnetospectroscopy in InSb at Milliwatt CO_2 cw Powers", presented at the International Conference on Excited States and Multiresonant Nonlinear Optical Processes in Solids, Aussois, France, March 1981.

2. R. Kaplan, R. J. Wagner, D. G. Seiler, C. L. Littler, M. H. Weiler, and W. Zawadzki, "High Resolution Magneto-Optical Studies of Free and Bound Hole Excitations in InSb", presented at the 4th International Conference on the Physics of Narrow Gap Semiconductors, Linz, Austria, September 1981.

3. D. G. Seiler, M. W. Goodwin, and M. H. Weiler, "Two-Photon Spectroscopy in InSb with cw CO_2 Lasers" presented at the 4th International Conference on the Physics of Narrow Gap Semiconductors, Linz, Austria, September 1981.

4. D. G. Seiler, D. Heiman, R. Feigenblatt, R. L. Aggarwal, and B. Lax, "Two-Photon Spectroscopy of the A- and B-Excited Free-Exciton in CdS", presented at the 12th International Quantum Electronics Conference, Munich, Germany, June 1982.

5. D. G. Seiler, M. W. Goodwin, K. E. Littler, "Laser-Induced Resonant Magneto-Optical Transitions from Deep Levels in n-InSb", presented at the 16th International Conference on the Physics of Semiconductors, Montpellier, France, September, 1982.

3. Invited Talks

a. National

"Two-Photon Absorption Spectroscopy of Semiconductors", D. G. Seiler, invited talk at the Southeastern Section of the American Physical Society, Lexington, Kentucky, October 1982. Bull. Am. Phys. Soc. 27, 739 (1982).

b. International

D. G. Seiler, M. W. Goodwin, S. W. McClure, and L. A. Veilleux, "Two-Photon Spectroscopy in InSb at High Magnetic Fields", invited paper presented at the International Conference on the Application of High Magnetic Fields in Semiconductor Physics, Grenoble, France, September, 1982.

4. Seminars Given

1. Spring, 1981, Solid State Seminar, Minneapolis Honeywell, Inc., Lexington, Massachusetts

2. Spring, 1981, Solid State Seminar, Heriot-Watt University, Edinburgh, Scotland

3. Spring, 1981, Solid State Seminar, St. Andrews University, St. Andrews, Scotland

4. Spring, 1981, Solid State Seminar, Royal Signals and Radar Establishment, Malvern, England

5. Spring, 1981, Solid State Seminar, University of Toronto, Toronto, Canada

6. Summer, 1981, Solid State Seminar, GTE Laboratories, Waltham Massachusetts

7. Fall, 1981, Quantum Electronics Seminar, NTSU, Denton, Texas

8. Fall, 1981, Solid State Seminar, Technical University of Munich, Munich, West Germany

9. Summer, 1982, Solid State Seminar, Montanuniversitat, Leoben, Austria.

10. Summer, 1982, Solid State Seminar, Ludwig Boltzmann, Institute fur Festkorperphysik, Vienna, Austria

11. Fall, 1982, General Colloquium, North Texas State University, Denton, Texas

5. Participation in Professional Organizations

Chairman of Session on Optical Properties of Semiconductors at the March American Physical Society Meeting, see Bull. Am. Phys. Soc. 27, 173 (1982).

Member of the local arrangements committee for the American Physical Society Meeting in Dallas, March 1982.

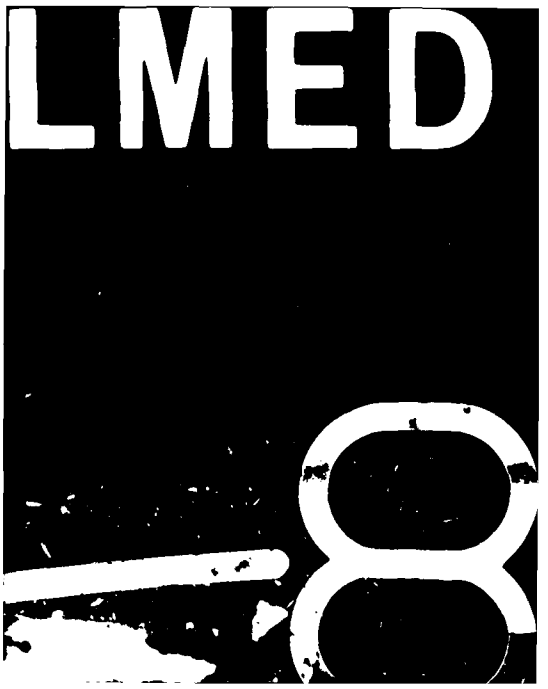
LMED